TOWARDS A BETTER UNDERSTANDING OF VACCINE STABILITY AS APPLIED TO PHARMACEUTICAL DEVELOPMENT OF VARIOUS RECOMBINANT PROTEIN VACCINE CANDIDATES

By

© 2018

Vishal M. Toprani

M.S., Pharmaceutical Chemistry, 2015, The University of Kansas, Lawrence, KS

M.S., Pharmaceutical Analysis, 2011, Campbell University, Buies Creek, NC

B.Pharm., Pharmacy, 2009, Gujarat University, Ahmedabad, India

Submitted to the graduate degree program in Pharmaceutical Chemistry and the Graduate Faculty of the University of Kansas in partial fulfillment of the requirements for the degree of Doctor of Philosophy.

_____

Chair: David B. Volkin, Ph.D.

_____

C. Russell Middaugh, Ph.D.

_____

Michael J. Hageman, Ph.D.

_____

Teruna J. Siahaan, Ph.D.

_____

Prajnaparamita Dhar, Ph.D.

Date Defended: 19 February 2018

The dissertation Committee for Vishal M. Toprani certifies that this is the approved version of the following dissertation:

TOWARDS A BETTER UNDERSTANDING OF VACCINE STABILITY AS APPLIED TO PHARMACEUTICAL DEVELOPMENT OF VARIOUS RECOMBINANT PROTEIN VACCINE CANDIDATES

_____

Chair: David B. Volkin, Ph.D.

Date Approved: 19 February 2018

ABSTRACT

Protein based vaccine antigens and adjuvants offer several advantages over inactivated or live attenuated viruses and bacteria including ease to manufacture and improved safety. Due to the structural complexity and inherent marginal stability of protein based antigens and adjuvants, however, extensive analytical characterization and robust formulation development approaches are required to develop a stable, potent and safe vaccine dosage form for use in patients. In addition, the elucidation of physical and chemical instability pathways of protein antigens plays a key role in their formulation design, and are generally studied using numerous biophysical and analytical techniques, during forced degradation as well as accelerated and real-time stability studies. Furthermore, analytical comparability assessments form a cornerstone for assessing vaccine quality (including stability) between pre-change versus post-change drug products during development and scale-up of manufacturing processes. This Ph.D. thesis research work is aimed to better understand vaccine stability from three different pharmaceutical development aspects including analytical characterization, formulation development and comparability assessments. In addition, this work contributes towards the ongoing efforts to discern interrelationships of a protein antigen's physicochemical properties to critical quality attributes of various vaccine candidates.

As a part of this work, we developed and utilized improved analytical tools for formulation development and comparability assessments. For example, a scaled down micro-polyethylene glycol (PEG) induced precipitation assay was developed to determine apparent solubility of proteins using less than a milligram of material (as described in Chapter 2). This assay will be helpful in apparent solubility measurements during pharmaceutical development of proteins, especially, in early stages where limited material is available. In addition, analytical

characterization of three different protein virus-like particle antigens (equine encephalitis virus-like particles, EEV) and a protein adjuvant (double mutant heat labile toxin, dmLT) by various biophysical and biochemical techniques was performed. The analytical characterization of the physical stability profile of the VLPs and physicochemical stability profile of dmLT, along with the role of pharmaceutical excipients in stabilizing their respective formulations, was evaluated. Lastly, an analytical comparability assessment involving five CRM_{197} carrier protein molecules was performed to better understand the effect of different manufacturing processes on the physicochemical and *in vitro* antigenic properties of the carrier protein.

Currently, the protein adjuvant dmLT is an oral vaccine candidate for enterotoxigenic *E.coli* (ETEC) and is under clinical development. For this project, the primary and higher-order structures, physicochemical and conformational stability profiles of dmLT were assessed as described in Chapter 3. The physicochemical degradation pathways of dmLT included protein aggregation, glycation and oxidation. By identifying the physicochemical degradation pathways of dmLT using newly developed stability-indicating analytical methods, a more stable candidate bulk formulation of dmLT was developed that protected dmLT against conformational destabilization, freeze-thaw stress, aggregation/particle formation and chemical degradation.

As described in Chapter 4, this work contributed to ongoing efforts to develop a vaccine against three strains of equine encephalitis (Eastern, Western and Venezuelan). Here, analytical characterization of three different monovalent VLPs was performed to identify structural alterations induced by thermal and pH stress. A candidate formulation mitigating thermal and aggregation instabilities of the VLPs was also developed. The candidate formulation showed a good maintenance of stability at all storage temperatures (40 to -80^{o}C), with the exception of a distinct instability at -20°C; the mechanism of which is discussed in detail in Chapter 4. The

interaction of both monovalent and trivalent VLP formulation with aluminum salt adjuvants was also studied to better understand the binding interactions of the VLPs with the adjuvant and its implications on future drug product development are discussed.

Lastly, a comprehensive and detailed analytical characterization of CRM_{197} molecules from different manufacturers and expression hosts was executed as described in Chapter 5. This work provides an initial basis to eventually develop global manufacturing specifications to ensure the quality of the bulk CRM_{197} proteins from a variety of manufacturers. Furthermore, the high similarities between five different recombinant CRM_{197} expressed in the native host (*C.diptheriae)* vs. alternative hosts (*E.coli* or *P.fluorescens),* as demonstrated in this work, is a first step that will help facilitate lower cost CRM_{197} bulk production, with the long term goal to develop lower-cost polysaccharide conjugate vaccines for the developing world.

Dedicated to:

My parents

Mahendra and Kiran Toprani

and

my sisters

Sweety and Shilpa Toprani

ACKNOWLEDGEMENTS

The work accomplished in this dissertation wouldn't have been possible without the unyielding support and guidance of many individuals and entities. First, I want to thank my research advisor, Professor David Volkin, without whom I wouldn't be the scientist I am today. He has been a constant source of encouragement, support, guidance and immense knowledge. I am grateful to him for giving me an opportunity to work on different projects, believing in me and pushing me to do my best. Along with the scientific research and presentation skills, he has also taught me to how to mentor other people, and be an effective team player. Thank you for grooming me to be a sound scientist and I will always be thankful for your mentorship and kindness.

I would like to thank Drs. Michael Hageman, Teruna Siahaan and Prajnaparamita Dhar for serving as members on my thesis committee and providing their valuable time and insightful feedback on my research. I would like to offer special thanks to Dr. Hageman for his valuable assistance during my job search. I truly appreciate the support and networking contacts that he provided during this time.

My sincere thanks to Dr. Russ Middaugh for being a part of my thesis committee as well as for his coursework on protein biophysics and pharmaceutical equilibrium. I have learned a lot about proteins through his courses along with his scientific feedback on my manuscripts. I want to say a special word of thanks to Dr. Sangeeta Joshi for her support, scientific inputs, friendship and guidance throughout my time in MVSC. It has been an absolute pleasure to work with her.

I would like to thank Drs. Apurva More and Neha Sahni (former members) for their scientific help, instrument training and friendship. I will truly miss our social gatherings and fun-filled conversations. I would like to thank Dr. John Hickey for his scientific guidance and valuable feedback on my manuscripts. I thank all the present and past MVSC members for their direct or

indirect contributions to my great time in the laboratory. I acknowledge the financial support from Bill and Melinda Gates Foundation and National Institutes of Health for my projects. I would also like to acknowledge financial support from Gilead Sciences Graduate fellowship and Gretta Jean & Gerry D Goetsch fellowship towards my tuition and stipend.

I would like to thank Department of Pharmaceutical Chemistry and MVSC for their support and providing resources for the graduate program. My friends Dr. Ishan Shah (former member, Tolbert Lab) and Manan Vaghela offered immense support throughout my graduate school in the form of scientific discussions and a great friendship. Lastly, the most important contributors of my achievements are my family; especially my sisters and my ninety seven year old grandmother who showered tremendous encouragement and support. I miss my parents, Mahendra and Kiran Toprani today, who made me who I am, and know that my debt to them is beyond measure. I dedicate this dissertation to them.

TABLE OF CONTENTS

LIST OF TABLES

LIST OF SUPPLEMENTARY TABLES

LIST OF FIGURES

LIST OF SUPPLEMENTARY FIGURES

This page intentionally left blank.

Chapter 1 Introduction

1.1 Vaccines

Vaccines are considered as one of the greatest inventions of mankind in controlling, and in some cases, eliminating infectious diseases. The historic innovations of both Edward Jenner and Louis Pasteur are widely recognized in the field of vaccinology[1]. Their original methods of vaccination with alternative or attenuated versions of virulent viruses have undergone medical and technological advances in the past century, and have resulted in development of numerous successful vaccines. The implementation of these vaccines along with public health efforts have been successful in both reducing the prevalence of many diseases such as measles, mumps, rubella etc., as well as completely eradicating small pox[2] and eliminating polio by 99 % globally[3]. This remarkable achievement has been made possible due to the massive efforts of several entities such as academic and industrial scientists, pharmaceutical companies, public health officials, World Health Organization (WHO), non-profit organizations such as Bill and Melinda Gates Foundation, Global Alliance for Vaccines and Immunization (GAVI) and governments of various countries worldwide.

With the advent of recombinant DNA technology and whole genome sequencing, the field of vaccinology has greatly advanced in the past 50 years, and has resulted in effective vaccines for the prevention cervical cancer caused by human papilloma virus, liver infections including hepatitis A and B viruses as well as bacterial infections such as meningitis. These new technological advances have also resulted in increased efforts to develop novel vaccine candidates against fighting many diseases such as malaria, Ebola, AIDS, cancer and enteric diseases causing diarrhea. However, the development of a vaccine from early discovery to regulatory approval for use in humans is very challenging since vaccines are the most complex products of the pharmaceutical industry[4]. This introduction chapter provides a brief overview of

the components of a vaccine, different types of vaccines, and some aspects of the pharmaceutical development of a vaccine by treating them as molecules with well-defined physical and chemical properties[5]. This work contributes towards better understanding of the inter-relationships between vaccine's structural integrity, pharmaceutical stability and critical quality attributes including immunological activity.

1.2 Components of Vaccines

There are three major components of a vaccine dosage form namely, an antigen, an adjuvant and various pharmaceutical excipients.

1) Antigen (active ingredient): An antigen is a weakened version or subcomponent of a foreign disease causing microorganism such as a virus or bacteria. By being modified from the original infectious form, it no longer causes a disease but still elicits an immune response in the body[6]. The antigen is often made from weakened or killed forms of the entire microbe, or from components such as its toxins or one of its surface proteins or polysaccharides.

2) Adjuvant: Vaccine adjuvants include any substance that primarily enhances the immune response of the antigen or helps shape antigen-specific immune responses[7,8]. Currently, the licensed adjuvants include aluminum salts, adjuvant systems (AS03, AS04), virosomes, a TLR9 agonist and the oil in water emulsion MF-59®[9]. Numerous novel adjuvants such as CpG oligonucleotides, labile toxin from entertoxigenic E.coli (LT) and its mutants are currently in development to enhance the efficacy of vaccines[7,10].

3) Stabilizers (inactive ingredient): Apart from the antigen and adjuvant, excipients or inactive ingredients such as stabilizers or preservatives are often added to a vaccine either during its manufacturing or as a part of the final drug product. Excipients such as sugars, salts, amino

acids, buffering agents, etc. are added to ensure that the various components remain stable and effective and to ensure appropriate tonicity for parenteral administration[11]. Preservatives such as thiomersal and phenolic compounds prevent contamination and enable multi-dose vaccine formulations.

1.3 Types of Vaccines

The design of a vaccine depends on several factors including type of microbe, pathology of disease, desired immune responses for protection, and geographical location of the world. There are several kinds of vaccines[12-14] which are currently approved or in developmental phases and can be grouped into three main categories as described below:

1) First generation or Traditional Vaccines:

The first generation vaccines consist of whole cell microorganisms (viruses and bacteria) either killed or live, attenuated, forms. These vaccines are still widely in use as outlined below.

a) ***Killed or Inactivated whole-cell vaccines:*** Inactivated vaccines are produced by killing the pathogen with chemicals, heat, or radiation. Majority of inactivated vaccines elicit a weaker immune response than live vaccines and usually require adjuvants and booster doses. However, they are considered safer than live vaccines since they do not contain live viruses or bacteria. Examples include whole-cell pertussis (wP), inactivated polio virus (IPV), hepatitis A, influenza (flu), and rabies vaccines.

b) ***Live attenuated vaccines (LAV):*** These vaccines contain the weakened form of the live pathogen (virus or bacteria), elicit strong cellular and antibody immune responses and often provide lifelong immunity. However, there is a potential risk for the microbe to revert back to a

disease-causing form. Examples include measles, mumps, rubella (MMR vaccine), oral polio vaccine (OPV), rotavirus, shingles, tuberculosis (BCG) and yellow fever vaccines.

2) Second generation or Modern Vaccines:

The modern vaccines do not contain the whole pathogen and in general exhibit a higher level of safety than the traditional vaccines described above. These vaccines are based on subunit design, and consist of only a part of pathogen such as toxins from bacteria or certain proteins/components of pathogens. Modern vaccines can be grouped into three main categories as described below.

a) Toxoid vaccines: These vaccines contain an inactivated or detoxified bacterial protein toxin isolated from the microorganism and are capable of eliciting a neutralizing immune response. They are considered safer because they neither can cause the disease nor revert back to virulent form. Examples include tetanus toxoid (TT) and diphtheria toxoid (DT) vaccines.

b) Subunit vaccines: These contain a define component (antigenic part) from a pathogen such as a protein or a polysaccharide capsule, that elicits a specific immune response that is capable of neutralizing the pathogen so as to prevent actual infection. They are safer than live and inactivated vaccines but elicit a weaker immune response and usually require an adjuvant. Subunit vaccines can be further categorized into:

- Protein-based subunit vaccines: Acellular pertussis (aP), hepatitis B (HepB), human papillomavirus (HPV), influenza
- Polysaccharide vaccines: Pneumococcal and meningococcal
- Conjugate vaccines: Pneumococcal conjugate, heamophilus influenza type b

3) Third generation or Novel Vaccines:

They comprise of approaches to identify and develop vaccine candidates against difficult targets and unmet medical needs for diseases such as HIV/AIDS, cancer, malaria and they attempt to improve the ways of antigen presentation and vaccine delivery[15]. Some of the research and development activities also include structure-based antigen design, synthetic vaccine candidates, genomic analysis, novel nanoparticle delivery systems and novel routes of administration. The main categories of novel vaccines are as follows:

a) Nucleic acid (DNA and mRNA) vaccines: Naked viral or bacterial DNA (plasmids) or mRNA encoding immunogens can be taken up human cells and translated into protein. mRNA represents a promising platform for developing prophylactic and therapeutic vaccines[16]. Some of these vaccines against influenza, zika[17] etc. are still in experimental stages. Recently, an mRNA-based cancer vaccine has entered into Phase I clinical trial[18].

b) Recombinant Vector: The vaccine components (DNA for a surface protein) are introduced into a recombinant vector (usually a virus or bacteria) and then injected into the body. Experimental vaccines include the use of vectors (e.g., adenovirus, CMV, etc.) for vaccine targets against HIV, rabies and measles.

c) Synthetic peptide vaccines: These comprise of peptide sequences of antigen as the vaccine component and are produced using chemical synthetic approaches. Again, these vaccines are under experimental or early clinical development and will need to overcome many challenges[19].

1.4 Pharmaceutical Development of Vaccines

The journey of a vaccine from lab to clinic is long, complex and costly with a high rate of failure of many vaccine candidates in preclinical or Phase I trials. An outline of the different

stages of vaccine development[20] is shown in Figure 1.1. The exploratory stage involves a basic understanding of the disease, its epidemiological data and protective antigen and host responses. The preclinical stage assesses antigen efficacy and safety by conducting animal studies for selection of the best vaccine candidate. As the vaccine candidate moves into human clinical trials the process gets more complex. The clinical stage has three phases (phase I, II and III) and is the longest development phase for a vaccine candidate. Phase I or safety studies are performed by testing the vaccine candidate on a small group of people, Phase II involves larger group of people to assess immune responses and Phase III includes the largest groups of people to evaluate both safety and efficacy. Phase III also involves production of clinical and industrial batches of the vaccine candidate for compliance and regulatory approval. The results from all the preceding stages are collected and submitted to regulatory authorities to obtain an approval for use in humans (regulatory stage). If the vaccine candidate is approved, Phase IV or post-licensure studies continue to gather additional information on the efficacy and safety of the vaccine in various populations. Finally, after the regulatory approval manufacturing process begins; which may take up to 24 months to produce, release and ship a single batch of vaccine. The majority of the production time is spent not only in manufacturing the bulk and drug product, but also on checking the quality of the final vaccine product. This whole process of bringing a vaccine candidate from basic lab research to an approved product for use in humans typically takes on an average 12-15 years[20,21].

In the field of vaccine development, the final product is frequently strictly defined by the manufacturing process[22,23]. The process of manufacturing a vaccine comprises of a diverse production, purification and fill-finish platforms. Traditionally, the manufacturing process of a vaccine has consisted of three stages namely, growing and isolating the microorganism,

sometimes inactivating it, and then vialing (and sometimes lyophilizing) allowing for injecting the pathogen or pathogen component[24]. MMR, diphtheria and tetanus toxoid vaccines are still produced using this technology. Modern vaccine manufacturing as shown in Figure 1.2 consists of recombinant expression of the antigen and viral vectors in cell lines followed by harvesting, purification, and inactivation, addition of other components (adjuvants, stabilizers, etc), formulation, fill-finish, packaging, lot release and distribution[24]. These manufacturing steps present challenges and complexity as vaccines are manufactured from living organisms such as virus, bacteria or cell culture. The complexity is due to the diversity of the complex set of vaccine antigens (live organisms, proteins, etc.) coupled with different production platforms (egg based, cell culture, cell free, VLP etc.). Additionally, since vaccines are administered in healthy population rather than patients, the vaccine must meet an increased number of quality checks throughout the entire manufacturing cycle as well as those of its country of destination. This additional complexity further adds to the manufacturing challenges for vaccines. Thus, due to the complexity of all the different stages of manufacturing a vaccine product, it becomes utmost important to have a thorough knowledge of the vaccine components, the final drug product and process development activities as the vaccine candidate moves from discovery into clinical development phase. This is achieved through a combination of analytical characterization and quality control tests. Furthermore, understanding the critical quality attributes (CQA's) of vaccine antigens and adjuvants is crucial not only for eliciting optimal vaccine immune response but also for reproducibility of vaccine manufacturability, potency and safety[25]. The failure to understand the factors that can affect structural integrity and stability of either the vaccine antigen or adjuvant which in turn can affect its potency and safety, and is one of the primary reasons for the failure of many vaccine candidates in both preclinical and clinical development.

Therefore, there is a need to better characterize and evaluate vaccine antigens and adjuvants to understand the interrelationship of physicochemical properties to critical functional attributes of the molecule.

The focus of this work was to better understand vaccine stability from three different aspects of pharmaceutical development namely, analytical characterization, formulation development and comparability assessments (Figure 1.3) by treating vaccine candidates as well-defined physicochemical entities from an analytical point of view. It is critical that the vaccine maintains stability during all stages of development to ensure the safety and potency of the final vaccine drug product. Analytical methods are needed to monitor vaccine stability at all stages of preclinical and clinical development. Additionally, developing analytical methods that can successfully characterize and discriminate between all the components (multiple antigens, adjuvant, and stabilizers) of a vaccine is essential and is a challenge. An optimized formulation is required to ensure the final vaccine remains stable and potent throughout its desired shelf life. Apart from this, comparability studies are needed during the clinical development and post approval lifecycle management of a vaccine product in order to evaluate the impact of both product and process related changes to the manufacturing process that occur during clinical development that can potentially affect the quality of the final vaccine drug product.

1.5 Vaccine Stability

Protein based vaccine antigens and novel protein adjuvants such as bacterial enterotoxins, like any other therapeutic protein drug, consist of complex, heterogeneous, fragile primary and higher order structures with marginal stability. As a result, structures of these proteins are very sensitive to their environment and are prone to both physical and chemical degradation during

manufacturing, formulation, storage, transport and administration. These degradation pathways can lead to changes in the both primary and higher order structures of proteins that in turn can affect the stability, potency and safety profile of the vaccine drug product during storage. The two main types of degradation pathways observed for protein vaccine antigens are physical and chemical instability.

1.5.1 Physical Instability

Physical instabilities refers to structural changes of the proteins without any changes to their chemical composition[26]. This primarily includes structural alterations, undesirable adsorption to surfaces, and aggregation. The exposure of vaccine antigens to stresses such as pH changes, temperature fluctuations, agitation and light exposure can negatively affect their physical stability and potency[27,28]. Due to the temperature sensitive nature (heat and freezing) of vaccines, cold chain (2-8 ^{o}C) is required during the storage, distribution and administration of the vaccine in various parts of the world. The lack of efficient vaccine cold chain systems, or accidental exposure to freezing or elevated temperatures in both the developed and developing countries, can expose the vaccine to excessive heat or freezing conditions[27,29-31]. These temperature excursions are known to decrease the potency of many vaccines[27,30,32]. For example, HBV vaccine containing hepatitis B surface antigen (HbsAg) is formulated with aluminum salt adjuvant. Freezing of the vaccine causes aggregation of aluminum salt that alters the conformation of antigen, agglomerates the aluminum adjuvants particles and reduces potency[33].

Changes in the structure/conformation of the vaccine antigen could either result in loss of key epitopes or lead to the exposure of additional epitopes potentially causing a competition between neutralizing and non-neutralizing antibody responses.[34-36] Additionally, the exposure of apolar residues resulted in aggregation, precipitation or adsorption to containers in a number of

vaccines[37]. Protein aggregation has been shown to affect potency and reduce the yields of number of vaccine antigens[38-41].

1.5.2 Chemical Instability

Chemical instabilities involve either breaking or formation of covalent bonds in a protein leading to formation of new chemical species[26]. There can be a number of chemical degradation reactions that a protein vaccine can undergo such as deamidation, oxidation, glycation, disulfide scrambling, hydrolysis, fragmentation/proteolysis, racemization, etc. These modified molecules can potentially affect antigen and or adjuvant conformation, stability, efficacy and immunogenicity. For example, deamidation reaction involves conversion of asparagine or glutamine residues to their corresponding acids. Typically, asparagine (Asn) residue is converted into an aspartic or isoaspartic acid under both acidic (pH <3) and basic conditions (pH >6) by direct hydrolysis or via formation of a succinimide intermediate, respectively. Previous studies have shown that Asn deamidation in critical epitopes of the recombinant protective antigen lead to a change in the conformation of epitopes which caused reduction in potency and immunogenicity of a recombinant anthrax vaccine[42,43].

Another major chemical degradation pathway for protein vaccines is oxidation of Met, His, Cys, Trp and Tyr amino acids. Oxidation can be caused by peroxides, light, metal impurities from aluminum adjuvants or excipients such as polysorbates which are frequently used in vaccines. Recently, one study showed that an inactivated Japanese encephalitis vaccine (IXIARO®) adsorbed to aluminum hydroxide adjuvant degraded via a oxidation pathway involving residual metal impurity Cu from aluminum hydroxide[44]. Another study by Estey et.al[45] identified both Met and Trp oxidation (+16 m/z) in rBoNT(H_c) antigens bound to aluminum hydroxide at multiple sites on storage stability at 4 ^{o}C and 30^{o}C for 9 weeks.

Hydrolysis mediated degradation of carbohydrate monomers in polysaccharide based vaccines over time has also been reported[46-48]. The hydrolysis may result in reduction of the molecular size of both the saccharide component and the conjugate, and cause increase in unbound saccharide content. Further, aluminum hydroxide used as an adjuvant in haemophilus influenza type B polysaccharide vaccine was reported to catalyze the depolymerization of polysaccharides and release of oligomers from the conjugate vaccine[46].

1.6 Analytical Characterization of Vaccines

Vaccines are considered as a heterogeneous product of the biopharmaceutical industry, and require extensive clinical testing for market approval[49-51]. The heterogeneity is related to the type of vaccine antigen (e.g., viral or bacterial vaccine versus a subunit protein vaccine) and different components of a vaccine (single or multiple antigens, adjuvants, stabilizers, etc.). In addition, the protective effect of the immune response triggered by a vaccine is not well understood, which in turn makes it difficult to link the *in vivo* potency of vaccine to its quality attributes that can be tested *in vitro*. Therefore it is challenging to develop relevant analytical tests to characterize the vaccine and each vaccine requires product specific set of analytical techniques to monitor product quality at release and during storage. For example, in the case of a live-attenuated viral vaccine, it is critical to measure the degree and stability of infectivity along with the number of infectious particles[52]. For a subunit protein vaccine, analytical techniques may be needed to monitor the physical and chemical stability of the protein antigen. Moreover, an extensive set of analytical tools comprising both physicochemical and potency assays are needed during the development of a vaccine in order to ensure that the vaccines remain stable during storage and hence reducing the risk of failure in clinical trials.

Physicochemical assays comprise of techniques that can monitor the purity, quantity, identity, size, stability and structural integrity of the protein antigen[53]. These techniques are not only used to monitor and quantify both the active components, but to evaluate the level of impurities as well. Potency assays measure a surrogate of the biological immunological activity of the vaccine including immunological binding assays, infectivity assays or animal studies. Potency assays are considered a key vaccine release/stability assay and are frequently a predictor of clinical outcome[24]. The selection of analytical methods and extent of characterization for a particular vaccine depends on several factors including the physicochemical properties of antigen and adjuvant, formulation conditions, degradation pathways and the stage of development[54]. It is possible that sufficient resources and materials may not be available for an extensive analytical characterization during early stages of development. However, it is expected by the regulatory authorities that a recombinant protein antigen containing vaccine should be well characterized before a Biologics Licensing Application (BLA) is filed[55]. An overview of physicochemical and potency assays that can be useful to assess the properties of protein based vaccines (focus of this work) is summarized in Table 1.

The structural complexity and marginal stability of protein-based antigens and adjuvants require extensive analytical characterization to monitor the physical, chemical and biological properties of the molecule and link these properties to critical quality attributes of the vaccine (e.g., ability to generate the appropriate immune response). Analytical methods are needed throughout entire vaccine product lifecycle including preclinical, clinical and commercialization phases. During preclinical development, regulatory compliant analytical tools are needed for cell banks, virus seeds, protein antigens, adjuvants, drug substance, and drug product. These tools

must be able to identify and quantify the active species, structurally related molecules (product related variants) and impurities[24].

Analytical methods are needed to assess protein antigen degradation during preclinical/clinical and commercialization phases. Orthogonal methods are often needed during most stages of vaccine development to evaluate different types of protein degradations (structural changes, charge variants and chemical changes). The stability indicating methods are also essential for monitoring the accelerated and long-term stability testing in order to establish the expiration dating of the vaccine. Further, in comparability studies, analytical tools are required to monitor the vaccine's key structural and functional properties to demonstrate product consistency as a result of both process and product related manufacturing changes,[56] such as changes in fermentation conditions or changes in final vaccine dosage form (e.g., lyophilized to liquid formulation), that may occur during clinical development.

The characterization and quality assessment of the final vaccine drug product requires specialized analytical tools. The quantification of the antigen amounts in the final vaccine formulation may cause some problems since their amounts tend to be relatively low and are adsorbed to adjuvants. Aluminum salts such as aluminum hydroxide and aluminum phosphate are the most commonly used adjuvants in protein based subunit vaccines. It is important to understand antigen-adjuvant interactions to design a stable and efficacious vaccine drug product[57]. The characterization of a protein antigen in presence of aluminum is challenging since aluminum particulates can interfere with common analytical assays such as chromatographic techniques. Therefore, the antigen needs to be desorbed to better characterize the final vaccine drug product for total antigen content, amount of antigen adsorbed, conformational integrity and various *in vitro* bioassays. If not possible, then bioactivity of the aluminum adsorbed vaccine is

often assessed by *in vivo* potency assays in animals[53]. It is now possible to characterize the antigen-adjuvant samples using biophysical techniques such front-face fluorescence, attenuated total reflection fourier transform infrared (ATR-FTIR) and raman spectroscopies, however, often the vaccine dose is low and near the sensitivity limit of such methods.

Historically, the development of vaccines has solely relied on testing in animal models. However, recent advances in analytical techniques have now made it possible to more rapidly monitor the key structural attributes of vaccines and evaluate the effect of process and formulation changes without relying solely on extensive biological testing such as animal potency assays. Many of the analytical techniques mentioned in Table 1 can be used to develop, characterize, and manufacture protein based vaccines. In addition, high resolution techniques such as X-ray crystallography and hydrogen-deuterium exchange mass spectrometry (HX-MS) can aid in development of epitope-based vaccines which may in the long term reduce the cost, complexity, and time of development of new vaccines[58,59]. HX-MS could potentially be an effective and faster way to obtain complete information about epitope structure and relate to functional properties[60]. Various groups have probed the binding between antibodies and antigens using HX-MS and found the results to correlate well with high resolution techniques such as crystallography and electron microscopy[61-64].

1.7 Formulation Development of Vaccines

Traditionally, vaccine formulation development for live and attenuated bacterial and viral vaccines has been an empirical process and focused on studying the temperature stability of the different formulations for various periods of time using *in vitro* antigenicity measurements and/or *in vivo* animal studies[28,65]. This is primarily due to complexity of both the nature of

pathogens and their relationship to generating protective immune responses. On the other hand, recombinant protein vaccines can take advantage of the tremendous improvements in stabilization and formulation of recombinant protein therapeutics to consider more rational formulation design strategies[66]. However, the need for systematic formulation development studies, which can be used to minimize instability and maintain/augment the potency of vaccine, is often poorly recognized in the field of vaccinology [67]. For example, *in vivo* animal studies are often used to monitor antigen-adjuvant structural integrity, while, sensitive biophysical and analytical assays can often help to better understand the structural characteristics and the instabilities of antigens and link them to the key critical quality attributes of a vaccine such as potency[25].

Further, recombinant protein vaccine antigens such as proteins and virus-like particles, as well as whole, inactivated viruses, are often inherently marginally stable and are sensitive to external conditions such as changes in pH and temperature, surface interactions and agitation, light exposure, and even the presence of impurities from excipients[68]. For example, vaccines may be exposed to temperature fluctuations during manufacturing, storage, and transport from the manufacturer to the end user (e.g., clinic site)[69]. The fill finish process can induce mechanical stress on the protein antigen or adjuvant causing aggregation and structural alterations. In addition, the lack of a robust cold chain in developing countries[70], and even in developing countries, can expose vaccines to elevated temperatures, as well as freeze thaw effects, causing degradation and loss of potency. Further, these vaccine dosage forms are multicomponent and inherently complex in nature (e.g., biological antigens, adjuvants, excipients). Hence, it becomes essential as part of their formulation development to study the factors that can affect their stability and potency.

To design a stable and efficacious vaccine for clinical use, formulation development activities include preformulation characterization of the antigen including forced degradation studies to identify stability indicating assays, formulation design and excipient screening to define stabilizing solution conditions, and accelerated and real time stability studies as well as freeze-thaw and potency studies[54,71,72] to ensure that the candidate formulations remain stable and maintain potency over a defined shelf life. Pharmaceutical excipients are added not only to stabilize the vaccine antigen, but also to ensure appropriate interaction with the adjuvant (e.g., binding of antigen to aluminum adjuvant) as well as to maintain appropriate solubility, tonicity, and compatibility with containers and administration procedures[65,71,73].

Another major component of vaccines includes the use of adjuvants such as aluminum salts, oil in water emulsions (e.g., MF-59®), or immunostimulatory molecules (e.g., MPL) in order to boost the immune response. Similar to antigens, adjuvants may also be susceptible to degradation under certain stress conditions. For example, aluminum salts used in recombinant protein vaccines are known to undergo freeze-thaw induced aggregation[74-76] leading to a loss of adjuvant activity[33,77]. It is also well established in literature that certain antigens when adsorbed to aluminum undergo conformational destabilization that may alter the thermal stability of vaccine[45,78,79]. Hence, vaccine formulation should also involve studying the stability of antigen, adjuvant and antigen-adjuvant complex during all stages of vaccine formulation development.

Vaccine formulation also involves identification and testing of suitable container-closure system. The selection of container-closure depends on variety of factors such as product compatibility, route of administration, potential market and regulatory guidelines[28,80]. Injectable vaccines (subQ and IM) are typically formulated in glass vials or prefilled syringes while oral vaccines may be administered using polymer containers (squeeze tubes) and nasal vaccines

through metered devices[28,80,81]. The incompatibility of vaccine components with the container material can cause product instability, loss of potency, loss of market share and safety risks to patients. Lastly, validation of the scale-up of formulation process for commercial manufacturing is also essential in order to ensure that the all the quality attributes of the vaccine product are optimized and do not change at a large scale. Hence, it is critical to have a robust formulation with consideration of scale-up and technology transfer effects.

1.8 Comparability Assessments of Vaccines

During the clinical development and post approval manufacturing of a vaccine, both product and process related changes[56] can occur that may affect the structural and functional properties of protein antigens and adjuvants. For example, alterations in the manufacturing process to increase the yields, scale-up, and introduce new facilities and new manufacturing technologies, as well as changes in formulation or in the final vaccine dosage form (e.g., lyophilized to liquid formulation) may be necessary to meet market demands. These types of process and product changes can potentially affect the identity, strength, purity, quality, and potency of the drug substance (antigen/adjuvant) or the final vaccine drug product. Hence, it becomes essential to have an adequate understanding of both the manufacturing process and the product to design comparability studies to assess the impact of such changes on any critical quality attributes of the vaccine and in turn their impact on safety and potency[82,83]. Comparability assessments requiring an extensive combination of analytical and biological tests[56,84,85], and in some cases, nonclinical and clinical studies are performed to evaluate the impact of such changes with regard to the quality, safety and efficacy of the vaccine product.

Comparability does not necessarily mean that the quality attributes of the pre-change and post-change product are identical, but that they are highly similar and sufficient knowledge is available on the drug product development (early research, stability studies, manufacturing process and validation, early clinical trials etc.) to ensure that any differences in quality attributes have no adverse impact on safety or efficacy of drug product (ICH Q5E Guideline). The key components of a comparability exercise may include impact of manufacturing process changes, physicochemical characterization, impurity profiles, stability profile assessments, and potency assays[84]. Many changes can take place during the manufacturing stages including changes in expression system (prokaryotic vs eukaryotic) and changes in process (raw materials, equipment, downstream processing steps). In such cases, it is essential to have a thorough understanding of how these changes can impact the final vaccine drug product and its potential impact on safety, purity, and efficacy. Furthermore, comparability also needs to be demonstrated to ensure the consistency of production of a vaccine. This means that, each lot of the vaccine is of the same quality and within the same specifications as a lot which has been shown to be safe and efficacious in animal or human trials.

An assessment of the physicochemical properties of the protein antigen including its primary structure, higher-order structure (HOS), post-translational modifications, content, impurity profiles, and biological activity is a critical part of comparability studies[86]. Another important of aspect of comparability studies is to compare product and process related impurity profiles[87] between the pre change and post change product. The impurities in vaccines may include host cell DNA, host cell proteins, cell culture components, endotoxins, adventitious agents and viral contamination. In order to demonstrate comparability, the impurity profiles of the post change product must be either comparable or at lower values than the pre change

product[88]. It is also necessary to conduct forced degradation (elevated temperatures, freeze-thaw, oxidation etc.) and stability studies to assess the impact of process changes on product quality and potency. A comparison between the degradation profiles of pre-change versus post change product using various analytical and functional assays can help to assess comparability and potentially estimate shelf-life, based on the pre-change product[88-90].

A wide set of analytical techniques and bioassays that can be used to characterize the impact of both process and product related changes on the different structural aspects of a protein antigen, impurity profiles, elucidate the degradation mechanisms on both physical and chemical stresses and determine bioactivity using *in vitro* and *in vivo* assessments are summarized in Table 1. High resolution techniques such as HX-MS, NMR and X-ray crystallography can potentially be used to monitor subtle changes in HOS of proteins and vaccines[91-94], however, some of these techniques may not be routinely available, expensive and are time consuming. Therefore, lower resolution biophysical and biochemical techniques such as circular dichroism, fluorescence spectroscopy, differential scanning calorimetry etc. coupled with new data visualization tools such as empirical phase diagram (EPD) and radar plots may be useful in examining the structural alterations in proteins under stress conditions. In fact, the use of both the above-mentioned data visualization tools has been reported to be potentially useful in analytical comparability assessments for proteins[84,95,96]. Although there are many analytical tools available for assessing comparability, however, the major question during any comparability evaluation is the extent of testing needed to answer how the changes affect the safety and efficacy of the drug product. Hence, scientifically sound comparability design and assessment is needed based on target profile of the protein antigen and structure/function relationship[56], leading to reduced testing and minimizing/eliminating clinical studies.

In this Ph.D. thesis work, we utilized state-of-the-art analytical techniques to assess and compare numerous physicochemical properties of different vaccine candidates including (a) a virus-like particle (VLP) antigen against equine encephalitis, (b) double mutant heat labile toxin, dmLT (a protein-based adjuvant), and (c) five CRM_{197} molecules (a carrier protein used in conjugate-polysaccharide vaccines). The VLP candidates and CRM_{197} molecules were extensively characterized in terms of higher order structure (HOS) and physical stability profiles while, for dmLT, apart from the above mentioned studies, chemical stability studies were also executed. In addition, the data from the various biophysical techniques were incorporated into EPD's and radar plots to better understand the stability profiles of these proteins under stress conditions (pH and temperature). We also developed separate candidate formulations for VLPs and dmLT. Additionally, we developed a miniaturized version of polyethylene glycol (PEG) induced solubility assay to determine the apparent solubility of various broadly neutralizing monoclonal antibodies (mAbs) against HIV-1 which are considered as potential candidates for the development of a passive HIV-1 vaccine. The PEG precipitation assay was also utilized to compare the apparent solubility profiles of CRM_{197} molecules as part of the analytical comparability assessment.

The analytical comparability assessment between five CRM_{197} molecules produced by different manufacturer's and expression systems (*E. coli*, *P. fluorescens* and *C. diptheriae*) was performed. Using various analytical techniques, the physicochemical and *in vitro* antigenic properties of the CRM_{197} molecules were compared. Additionally, the readouts from biophysical techniques combined with EPDs and radar plots helped to probe the changes in higher order structure (HOS) and the stability profiles of the CRM_{197} molecules under stress conditions such as pH and temperature. The stability assessment of protein's structural integrity under such stress

conditions is important part of comparability studies. This study contributes towards the importance of in-depth analytical characterization during comparability assessments. It also provides an initial analytical dataset to eventually develop manufacturing specifications and ensuring the quality of the purified carrier protein produced by different manufacturers.

1.9 Chapter Reviews

1.9.1 A Micro-PEG Precipitation Assay as a Relative Solubility Screening Tool for Monoclonal Antibody Design and Formulation Development (Chapter 2)

Adequate protein solubility is an important prerequisite for development and manufacture of protein based drugs and vaccines, and for administration of biotherapeutic drug candidates in high-concentration protein formulations. A previously established method for determining the relative apparent solubility (thermodynamic activity) of proteins using polyethylene glycol (PEG) precipitation is adapted for screening and comparing monoclonal antibody (mAb) candidates where only limited quantities (≤1 mg) are available. This micro-PEG assay is used to evaluate various broadly neutralizing mAb candidates to HIV-1 viral spike (gp120 and gp41 glycoproteins) for potential clinical use as a passive immunization strategy. Using ~1 mg of VRC01-WT mAb per assay, the precision of the micro-PEG assay was established. A series of 7 different broadly neutralizing mAbs to the HIV-1 viral spike proteins were compared by curve shape (%PEG vs. protein concentration), $\%PEG_{midpoint}$ determinations, and extrapolated apparent solubility values. Numerous formulation conditions were then evaluated for their relative effects on the VRC01-WT mAb. The PEG_{midpt} and apparent solubility values of VRC01-WT mAb decreased as the solution pH increased and increased as NaCl and arginine were added. A final optimization of the micro-PEG assay established that amounts as low as 0.1-0.2 mg can be used.

Thus, the micro-PEG assay has significant potential as a relative solubility screening tool during candidate selection and early formulation development.

1.9.2 Structural Characterization, Physicochemcial Stability Profile and Formulation Development of a Double Mutant heat Labile Toxin (dmLT)- A Novel Protein Based Adjuvant Candidate (Chapter 3)

A novel protein adjuvant, a double-mutant *Escherichia coli* heat-labile toxin (R192G/L211A), called dmLT, is in preclinical and early clinical development with various vaccine candidates. Structural characterization and formulation development of dmLT will play a key role in its successful process development, and eventual scale-up/transfer and commercial manufacturing. This work describes extensive analytical characterization of structural integrity and physicochemical stability profile of dmLT from a lyophilized formulation from an early phase clinical lot. Reconstituted dmLT contained a heterogeneous mixture of intact holotoxin (AB_5, ~75%) and free B_5 subunit (~25%) as assessed by analytical ultracentrifugation and hydrophobic interaction chromatography. Intact mass spectrometry (MS) and LC-MS peptide mapping analysis revealed presence of Lys^{84} glycation near the native sugar-binding site in dmLT. Forced degradation studies using LC-MS peptide mapping also demonstrated specific Asn deamidation and Met oxidation sites in dmLT. Using multiple biophysical measurements, dmLT was found most conformationally stable between pH 6.5 and 7.5 and at temperatures ≤50°C. Upon shake stress, soluble aggregates and particle formation were observed with the reconstituted dmLT solution. By identifying the physicochemical degradation pathways of dmLT using newly developed stability-indicating analytical methods, a more stable candidate bulk formulation of dmLT was developed. The new candidate formulation containing phosphate, sucrose, sodium chloride, methionine and polysorbate-80 protected dmLT against

conformational destabilization, freeze-thaw stress, aggregation/particle formation and chemical degradation (e.g., Met oxidation and Lys glycation). In addition, the new bulk formulation of the dmLT adjuvant also provides flexibility for future use in combination with a variety of different vaccine dosage forms with different antigens.

1.9.3 Structural Characterization and Formulation Development of a Trivalent Equine Encephalitis Virus-Like Particle Vaccine Candidate (Chapter 4)

The zoonotic equine encephalitis viruses (EEV) can cause debilitating and life-threatening disease, leading to ongoing vaccine development efforts for an effective virus-like particle (VLP) vaccine based on three strains of EEV (Eastern, Western and Venezuelan or EEE, WEE and VEE VLPs, respectively). In this work, TEM and light scattering studies showed enveloped, spherical, and ~70 nm sized VLPs. Biophysical studies demonstrated optimal VLP physical stability in the pH range of 7.5-8.5 and at temperatures below ~50^{o}C. Interestingly, the individual stability profiles differed notably between the three VLPs. Numerous pharmaceutical excipients were screened for their VLP stabilizing effects against thermal stress. Sucrose, sorbitol, sodium chloride and pluronic F-68 were identified as promising stabilizers and the concentrations and combinations of these additives were optimized. Candidate monovalent VLP bulk formulations were incubated at temperatures ranging from -80^{o}C to 40^{o}C to establish freeze-thaw, long-term (2-8°C) and accelerated stability trends. Good VLP stability was observed at each storage temperature, except for a distinct instability observed at -20°C. The interaction of monovalent and trivalent VLP formulations with aluminum adjuvants was examined, both in terms of antigen adsorption and desorption over time. The implications of these findings on future vaccine formulation development of EEV VLPs are discussed.

1.9.4 Analytical Comparability Assessments of Five recombinant CRM_{197} Proteins from Different Manufacturers and Expression Systems (Chapter 5)

CRM_{197}, a single amino acid mutant of diphtheria toxoid, is a commonly used carrier protein in commercial polysaccharide-protein conjugate vaccines. In this study, CRM_{197} proteins from three different expression systems and five different manufacturers were obtained for an analytical comparability assessment using a wide variety of physicochemical and *in vitro* antigenic binding assays. A comprehensive analysis of the five CRM_{197} molecules demonstrate that recombinant CRM_{197}'s expressed in heterologous systems (*E. coli* and *Pseudomonas fluorescens*) are overall highly similar (if not better in some cases) to those expressed in the traditional system (*Corynebacterium diphtheriae*) in terms of primary sequence/post translational modifications, higher-order structural integrity, apparent solubility, physical stability profile (vs. pH and temperature) and *in vitro* antigenicity. These results are an encouraging step to demonstrate that recombinant CRM_{197} expressed in alternative sources have the potential to replace CRM_{197} expressed in *C. diphtheriae* as a source of immunogenic carrier protein for lower-cost polysaccharide conjugate vaccines. The physicochemical assays established in this work to monitor the key structural attributes of CRM_{197} should also prove useful as complementary characterization methods (to routine quality control assays) to support future process and formulation development of lower-cost CRM_{197} carrier proteins for use in various conjugate vaccines.

1.10 Conclusions and Future Work (Chapter 6)

This final chapter of this thesis summarizes the findings about the structural integrity, solubility, physicochemical properties and formulation development of four different types of proteins namely, mAbs, dmLT, EEV VLPs and CRM_{197}. The results from Chapters 2-5 provide a better understanding of the pharmaceutical development of protein containing vaccines by considering analytical characterization, formulation development and comparability assessments with vaccine stability profiles being a common theme. In addition, the final chapter provides recommendations for future experimental work, and possible future implications of this work are also discussed.

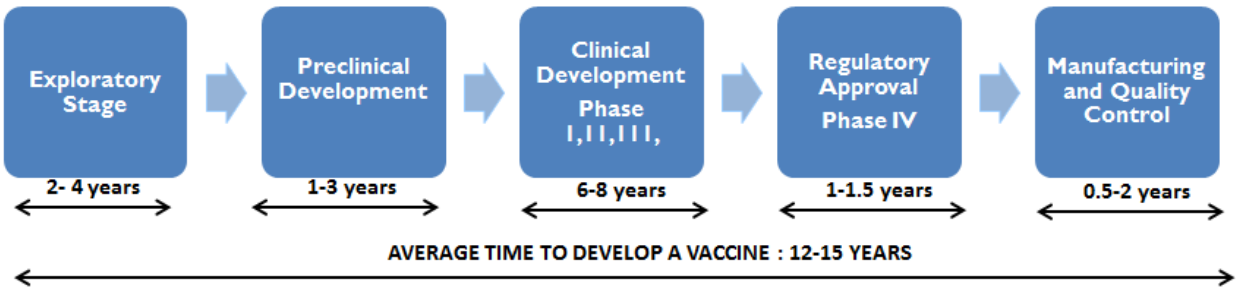

Figure 1.1 Preclinical and clinical development stages of a vaccine candidate[20,21].

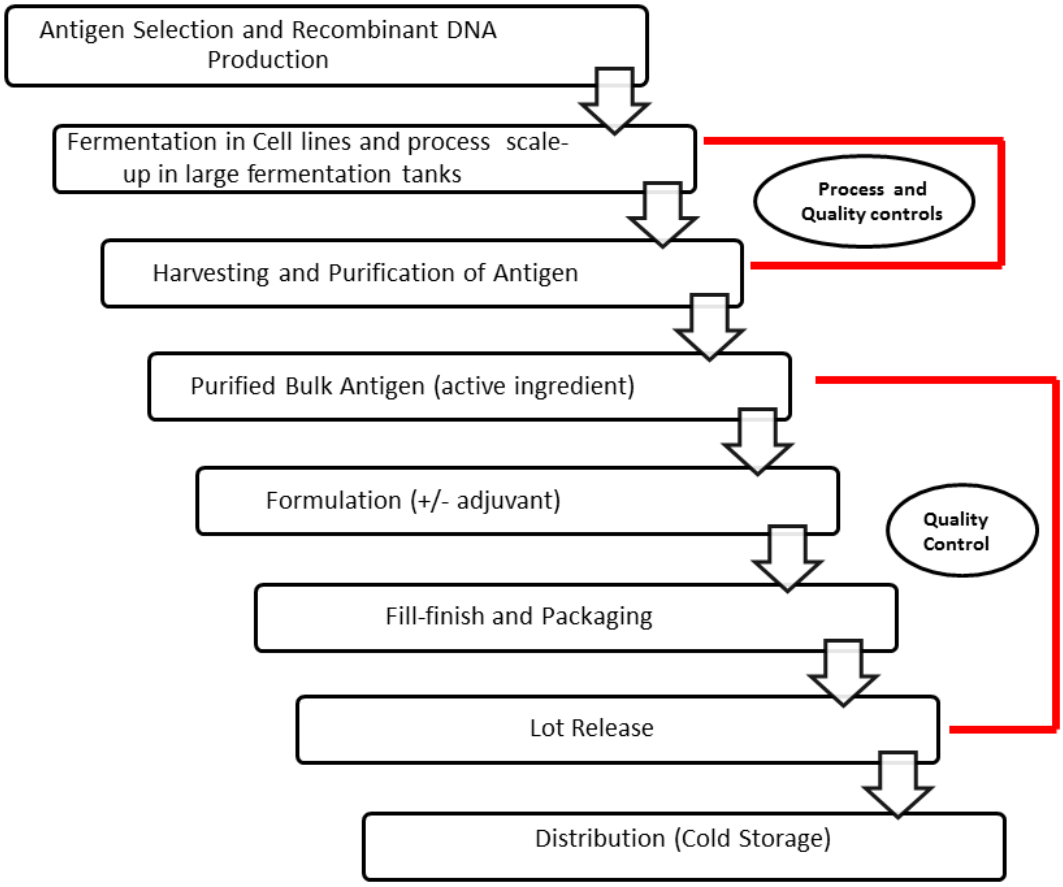

Figure 1.2. Overview of a representative manufacturing process scheme for a recombinant protein vaccine[20,24].

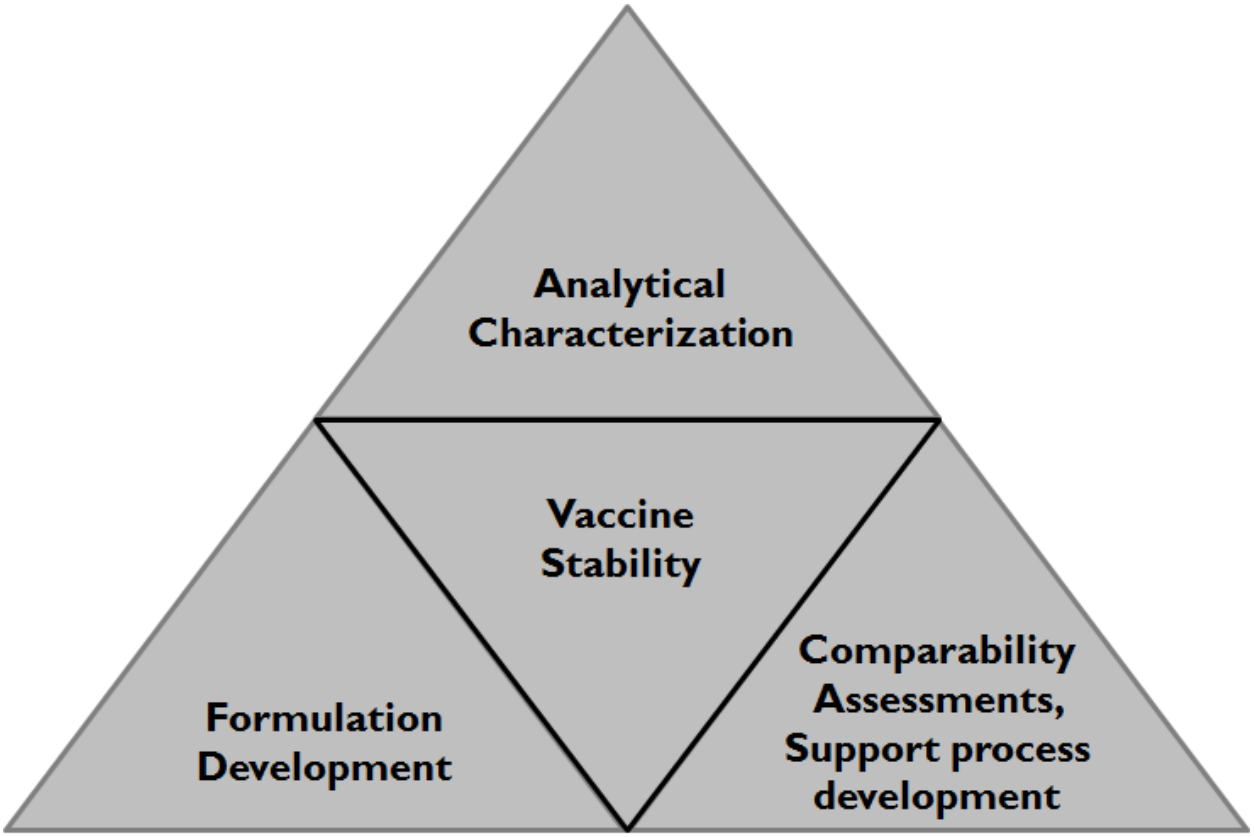

Figure 1.3. Essential elements of vaccine stability as applied to the pharmaceutical development of a protein antigen vaccine candidate.

Table 1.1 Overview of various analytical tools for characterization of protein-based vaccines

Parameter Measured	Analytical Method
Quantitation of protein	UV-Visible Spectroscopy (A280)
	Bradford/BCA assay
	Enzyme-Linked Immunosorbent Assay (ELISA)
Host-cell DNA	DNA hybridization and dot blot analysis
	Quantitative polymerase chain reaction (qPCR)
Host-cell proteins (HCP)	Enzyme-Linked Immunosorbent Assay (ELISA)
Purity	Native or SDS-PAGE
	Isoelectric focusing (IEF) gels
	Capillary isoelectric focusing (cIEF)
	Reverse phase chromatography (RP-HPLC)
	Hydrophobic interaction chromatography (HIC)
	Ion exchange chromatography (IEX)
Identity	Mass spectrometry
	Peptide mapping
Primary Structure/Post translational modifications (PTMs)	Mass spectrometry
Secondary Structure	Far UV circular dichroism
	Fourier Transform Infrared Spectroscopy
Tertiary Structure	Near UV circular dichroism
	Intrinsic Trp fluorescence spectroscopy
	Intrinsic ANS fluorescence spectroscopy
Overall conformational stability	Differential scanning calorimetry (DSC)
Mass/Size	Size-exclusion chromatography (SEC)
	Analytical ultracentrifugation (AUC)
	Field-flow fractionation
	Light scattering (static, dynamic and multi angle)
	Electron microscopy
	Light obscuration
	Flow imaging microscopy
In vitro potency	Enzyme-Linked Immunosorbent Assay (ELISA)
	Biolayer Inferometry (BLI)
	Surface Plasmon Resonance (SPR)
	Cell-based assays
In vivo potency	Animal models
Antigen-aluminum adjuvant assays	Front-face fluorescence
	Attenuated total reflection Fourier transform infrared (ATR-FTIR) spectroscopy
	Raman spectroscopy
	Isothermal titration calorimetry (ITC)
	Differential scanning calorimetry (DSC)
	Electron microscopy
	Flow cytometry

1.11 References:

1. Philadelphia TCoPo. 2017. The History of Vaccines. ed. p The History of Vaccines https://www.historyofvaccines.org/timeline (accessed 5 Oct 2017).

2. Finco O, Rappuoli R 2014. Designing Vaccines for the Twenty-First Century Society. Frontiers in Immunology 5:12.

3. Organization WH 2017. 10 Facts on Polio Eradication http://www.who.int/features/factfiles/polio/en/ (accessed 5 Oct 2017).

4. Rosini R, Barocchi MA, Rappuoli R. 2011. Microbial Vaccine Design: The Reverse Vaccinology Approach. Development of Vaccines, ed.: John Wiley & Sons, Inc. p 1-18.

5. Volkin DB, Middaugh CR 2010. Vaccines as physically and chemically well-defined pharmaceutical dosage forms. Expert review of vaccines 9(7):689-691.

6. Siegrist C-A 2008. Vaccine immunology. Vaccines 5:17-36.

7. Lee S, Nguyen MT 2015. Recent Advances of Vaccine Adjuvants for Infectious Diseases. Immune Network 15(2):51-57.

8. Petrovsky N, Aguilar JC 2004. Vaccine adjuvants: Current state and future trends. Immunology And Cell Biology 82:488.

9. Di Pasquale A, Preiss S, Tavares Da Silva F, Garçon N 2015. Vaccine Adjuvants: from 1920 to 2015 and Beyond. Vaccines 3(2):320-343.

10. Brunner R, Jensen-Jarolim E, Pali-Schöll I 2010. The ABC of clinical and experimental adjuvants—A brief overview. Immunology letters 128(1):29-35.

11. Kamerzell TJ, Esfandiary R, Joshi SB, Middaugh CR, Volkin DB 2011. Protein-excipient interactions: mechanisms and biophysical characterization applied to protein formulation development. Advanced drug delivery reviews 63(13):1118-1159.

12. Philadelphia TCoPo 2017. Different Types of Vaccines https://www.historyofvaccines.org/content/articles/different-types-vaccines (accessed 12 Oct 2017).

13. Services USDoHH 2017. Types of Vaccines https://www.vaccines.gov/basics/types/index.html (accessed 12 Oct 2017).

14. Leitner WW, Ying H, Restifo NP 1999. DNA and RNA-based vaccines: principles, progress and prospects. Vaccine 18(9-10):765-777.

15. Rappuoli R, Bagnoli F. 2011. Vaccine Design: Innovative Approaches and Novel Strategies. ed.: Caister Academic.

16. Schlake T, Thess A, Fotin-Mleczek M, Kallen K-J 2012. Developing mRNA-vaccine technologies. RNA Biology 9(11):1319-1330.

17. Richner JM, Himansu S, Dowd KA, Butler SL, Salazar V, Fox JM, Julander JG, Tang WW, Shresta S, Pierson TC, Ciaramella G, Diamond MS Modified mRNA Vaccines Protect against Zika Virus Infection. Cell 168(6):1114-1125.e1110.

18. Moderna Announces First-in-Human Dosing for Phase 1 Study (KEYNOTE-603) of mRNA-4157, a Personalized Cancer Vaccine, for the Treatment of Solid Tumors [Press release]. (2017, November 15). Retrieved January 1, 2018, from https://www.modernatx.com/newsroom/press-releases/moderna-announces-first-human-dosing-phase-1-study-keynote-603-mrna-4157. ed.

19. Skwarczynski M, Toth I 2016. Peptide-based synthetic vaccines. Chemical Science 7(2):842-854.

20. Pasteur S 2017 Development of Vaccines http://www.sanofipasteur.us/essentials/development (accessed 14 Oct 2017).

21. Bregu M, Draper SJ, Hill AVS, Greenwood BM 2011. Accelerating vaccine development and deployment: report of a Royal Society satellite meeting. Philosophical Transactions of the Royal Society B: Biological Sciences 366(1579):2841-2849.

22. Ball P, Brown C, Lindström K 2009. 21st century vaccine manufacturing. BioProcess Int 7(4).

23. Marshall V, Baylor NW 2011. Food and Drug Administration Regulation and Evaluation of Vaccines. Pediatrics 127(Supplement 1):S23-S30.

24. Josefsberg JO, Buckland B 2012. Vaccine process technology. Biotechnology and bioengineering 109(6):1443-1460.

25. Dey AK, Malyala P, Singh M 2014. Physicochemical and functional characterization of vaccine antigens and adjuvants. Expert review of vaccines 13(5):671-685.

26. Manning MC, Chou DK, Murphy BM, Payne RW, Katayama DS 2010. Stability of Protein Pharmaceuticals: An Update. Pharmaceutical Research 27(4):544-575.

27. Kumru OS, Joshi SB, Smith DE, Middaugh CR, Prusik T, Volkin DB 2014. Vaccine instability in the cold chain: mechanisms, analysis and formulation strategies. Biologicals 42(5):237-259.

28. Burke CJ 1999. Formulation, stability, and delivery of live attenuated vaccines for human use. Critical reviews in therapeutic drug carrier systems 16(1):1-83.

29. Matthias DM, Robertson J, Garrison MM, Newland S, Nelson C 2007. Freezing temperatures in the vaccine cold chain: A systematic literature review. Vaccine 25(20):3980-3986.

30. Chen D, Kristensen D 2009. Opportunities and challenges of developing thermostable vaccines. Expert review of vaccines 8:547+.

31. Kristensen DD, Lorenson T, Bartholomew K, Villadiego S 2016. Can thermostable vaccines help address cold-chain challenges? Results from stakeholder interviews in six low- and middle-income countries. Vaccine 34(7):899-904.

32. Milstien JB, Galazka AM, Kartoglu Um, Zaffran M, Organization WH 2006. Temperature sensitivity of vaccines.

33. Chen D, Tyagi A, Carpenter J, Perkins S, Sylvester D, Guy M, Kristensen DD, Braun LJ 2009. Characterization of the freeze sensitivity of a hepatitis B vaccine. Human vaccines 5(1):26-32.

34. Karthigesu VD, Allison LMC, Ferguson M, Howard CR 1999. A hepatitis B virus variant found in the sera of immunised children induces a conformational change in the HbsAG “a” determinant. Journal of Medical Virology 58(4):346-352.

35. Oggioni MR, Medaglini D, Romano L, Peruzzi F, Maggi T, Lozzi L, Bracci L, Zazzi M, Manca F, Valensin PE, Pozzi G 1999. Antigenicity and immunogenicity of the V3 domain of HIV type 1 glycoprotein 120 expressed on the surface of Streptococcus gordonii. AIDS Res Hum Retroviruses 15(5):451-459.

36. Manivel V, Ramesh R, Panda SK, Rao KV 1992. A synthetic peptide spontaneously self-assembles to reconstruct a group-specific, conformational determinant of hepatitis B surface antigen. The Journal of Immunology 148(12):4006-4011.

37. Brandau DT, Jones LS, Wiethoff CM, Rexroad J, Middaugh CR 2003. Thermal Stability of Vaccines. Journal of Pharmaceutical Sciences 92(2):218-231.

38. Diminsky D, Moav N, Gorecki M, Barenholz Y 1999. Physical, chemical and immunological stability of CHO-derived hepatitis B surface antigen (HBsAg) particles. Vaccine 18(1):3-17.

39. Amador-Molina JC, Valerdi-Madrigal ED, Domínguez-Castillo RI, Sirota LA, Arciniega JL 2016. Temperature-mediated recombinant anthrax protective antigen aggregate development: Implications for toxin formation and immunogenicity. Vaccine 34(35):4188-4195.

40. Chen Y, Zhang Y, Quan C, Luo J, Yang Y, Yu M, Kong Y, Ma G, Su Z 2015. Aggregation and antigenicity of virus like particle in salt solution—A case study with hepatitis B surface antigen. Vaccine 33(35):4300-4306.

41. Volkin DB, Burke CJ, Marfia KE, Oswald CB, Wolanski B, Middaugh CR 1997. Size and Conformational Stability of the Hepatitis a Virus used to Prepare VAQTA⊥, a Highly Purified Inactivated Vaccine. Journal of Pharmaceutical Sciences 86(6):666-673.

42. Verma A, Ngundi MM, Burns DL 2016. Mechanistic Analysis of the Effect of Deamidation on the Immunogenicity of Anthrax Protective Antigen. Clinical and Vaccine Immunology : CVI 23(5):396-402.

43. D'Souza AJM, Mar KD, Huang J, Majumdar S, Ford BM, Dyas B, Ulrich RG, Sullivan VJ 2013. Rapid Deamidation of Recombinant Protective Antigen when Adsorbed on Aluminum Hydroxide Gel Correlates with Reduced Potency of Vaccine. Journal of Pharmaceutical Sciences 102(2):454-461.

44. Schlegl R, Weber M, Wruss J, Low D, Queen K, Stilwell S, Lindblad EB, Möhlen M 2015. Influence of elemental impurities in aluminum hydroxide adjuvant on the stability of inactivated Japanese Encephalitis vaccine, IXIARO®. Vaccine 33(44):5989-5996.

45. Estey T, Vessely C, Randolph TW, Henderson I, Braun LJ, Nayar R, Carpenter JF 2009. Evaluation of chemical degradation of a trivalent recombinant protein vaccine against botulinum neurotoxin by LysC peptide mapping and MALDI-TOF mass spectrometry. Journal of Pharmaceutical Sciences 98(9):2994-3012.

46. Sturgess AW, Rush K, Charbonneau RJ, Lee JI, West DJ, Sitrin RD, Hennessey JP 1999. Haemophilus influenzae type b conjugate vaccine stability: catalytic depolymerization of PRP in the presence of aluminum hydroxide. Vaccine 17(9):1169-1178.

47. Cintra FdO, Takagi M 2015. Study of the chemical stability of the capsular polysaccharide produced by Haemophilus influenzae type b. Carbohydrate Polymers 116(Supplement C):167-172.

48. Sweeney JA 2000. Simultaneous evaluation of molecular size and antigenic stability of PNEUMOVAX 23, a multivalent pneumococcal polysaccharide vaccine. Developments in biologicals 103:11-26.

49. Lebron JA, Wolf JJ, Kaplanski CV, Ledwith BJ 2005. Ensuring the quality, potency and safety of vaccines during preclinical development. Expert review of vaccines 4(6):855-866.

50. Buckland BC 2005. The process development challenge for a new vaccine. Nature Medicine 11:S16.

51. Metz B, van den Dobbelsteen G, van Els C, van der Gun J, Levels L, van der Pol L, Rots N, Kersten G 2009. Quality-control issues and approaches in vaccine development. Expert review of vaccines 8(2):227-238.

52. Plitnick LM. 2013. Chapter 9 - Global Regulatory Guidelines for Vaccines. Nonclinical Development of Novel Biologics, Biosimilars, Vaccines and Specialty Biologics, ed., San Diego: Academic Press. p 225-241.

53. Dey AK, Malyala P, Singh M 2014. Physicochemical and functional characterization of vaccine antigens and adjuvants. Expert review of vaccines 13(5):671-685.

54. Filipe V, Hawe A, Carpenter JF, Jiskoot W 2013. Analytical approaches to assess the degradation of therapeutic proteins. TrAC Trends in Analytical Chemistry 49(Supplement C):118-125.

55. Wang YJ, Hosken B. 2010. Analytical Characterization of Proteins and Peptides. Pharmaceutical Sciences Encyclopedia, ed.: John Wiley & Sons, Inc.

56. Chirino AJ, Mire-Sluis A 2004. Characterizing biological products and assessing comparability following manufacturing changes. Nat Biotech 22(11):1383-1391.

57. Christopher BF, Ryan MK, Lucien Barnes V, Quinton MD, Thomas SV 2013. Working together: interactions between vaccine antigens and adjuvants. Therapeutic Advances in Vaccines 1(1):7-20.

58. Ahmad TA, Eweida AE, Sheweita SA 2016. B-cell epitope mapping for the design of vaccines and effective diagnostics. Trials in Vaccinology 5(Supplement C):71-83.

59. Gershoni JM, Roitburd-Berman A, Siman-Tov DD, Freund NT, Weiss Y 2007. Epitope Mapping: The First Step in Developing Epitope-Based Vaccines. BioDrugs 21(3):145-156.

60. Donnarumma D, Faleri A, Costantino P, Rappuoli R, Norais N 2016. The role of structural proteomics in vaccine development: recent advances and future prospects. Expert Review of Proteomics 13(1):55-68.

61. Malito E, Faleri A, Lo Surdo P, Veggi D, Maruggi G, Grassi E, Cartocci E, Bertoldi I, Genovese A, Santini L, Romagnoli G, Borgogni E, Brier S, Lo Passo C, Domina M, Castellino F, Felici F, van der Veen S, Johnson S, Lea SM, Tang CM, Pizza M, Savino S, Norais N, Rappuoli R, Bottomley MJ, Masignani V 2013. Defining a protective epitope on factor H binding protein, a key meningococcal virulence factor and vaccine antigen. Proceedings of the National Academy of Sciences 110(9):3304-3309.

62. Ciferri C, Chandramouli S, Donnarumma D, Nikitin PA, Cianfrocco MA, Gerrein R, Feire AL, Barnett SW, Lilja AE, Rappuoli R, Norais N, Settembre EC, Carfi A 2015. Structural and biochemical studies of HCMV gH/gL/gO and Pentamer reveal mutually exclusive cell entry complexes. Proceedings of the National Academy of Sciences 112(6):1767-1772.

63. Ciferri C, Chandramouli S, Leitner A, Donnarumma D, Cianfrocco MA, Gerrein R, Friedrich K, Aggarwal Y, Palladino G, Aebersold R, Norais N, Settembre EC, Carfi A 2015. Antigenic Characterization of the HCMV gH/gL/gO and Pentamer Cell Entry Complexes Reveals Binding Sites for Potently Neutralizing Human Antibodies. PLoS Pathogens 11(10):e1005230.

64. Bazzoli A, Vance DJ, Rudolph MJ, Rong Y, Angalakurthi SK, Toth RT, Middaugh CR, Volkin DB, Weis DD, Karanicolas J, Mantis NJ 2017. Using homology modeling to interrogate binding affinity in neutralization of ricin toxin by a family of single domain antibodies. Proteins: Structure, Function, and Bioinformatics 85(11):1994-2008.

65. Jain NK, Sahni N, Kumru OS, Joshi SB, Volkin DB, Russell Middaugh C 2015. Formulation and stabilization of recombinant protein based virus-like particle vaccines. Advanced drug delivery reviews 93(Supplement C):42-55.

66. Hem SL, HogenEsch H, Middaugh CR, Volkin DB 2010. Preformulation studies—The next advance in aluminum adjuvant-containing vaccines. Vaccine 28(31):4868-4870.

67. Brito LA, Malyala P, O'Hagan DT 2013. Vaccine adjuvant formulations: A pharmaceutical perspective. Seminars in immunology 25(2):130-145.

68. Frokjaer S, Otzen DE 2005. Protein drug stability: a formulation challenge. 4:298.

69. Kartoglu U, Milstien J 2014. Tools and approaches to ensure quality of vaccines throughout the cold chain. Expert Review of Vaccines 13(7):843-854.

70. Kumru OS, Joshi SB, Smith DE, Middaugh CR, Prusik T, Volkin DB 2014. Vaccine instability in the cold chain: Mechanisms, analysis and formulation strategies. Biologicals 42(5):237-259.

71. Kamerzell TJ, Esfandiary R, Joshi SB, Middaugh CR, Volkin DB 2011. Protein–excipient interactions: Mechanisms and biophysical characterization applied to protein formulation development. Advanced Drug Delivery Reviews 63(13):1118-1159.

72. Morefield GL 2011. A Rational, Systematic Approach for the Development of Vaccine Formulations. The AAPS Journal 13(2):191-200.

73. Ohtake S, Kita Y, Arakawa T 2011. Interactions of formulation excipients with proteins in solution and in the dried state. Advanced drug delivery reviews 63(13):1053-1073.

74. Salnikova MS, Davis H, Mensch C, Celano L, Thiriot DS Influence of Formulation pH and Suspension State on Freezing-Induced Agglomeration of Aluminum Adjuvants. Journal of Pharmaceutical Sciences 101(3):1050-1062.

75. Kurzątkowski W, Kartoğlu Ü, Staniszewska M, Górska P, Krause A, Wysocki MJ 2013. Structural damages in adsorbed vaccines affected by freezing. Biologicals 41(2):71-76.

76. Clausi AL, Morin A, Carpenter JF, Randolph TW Influence of protein conformation and adjuvant aggregation on the effectiveness of aluminum hydroxide adjuvant in a model alkaline phosphatase vaccine. Journal of Pharmaceutical Sciences 98(1):114-121.

77. Braun LJ, Tyagi A, Perkins S, Carpenter J, Sylvester D, Guy M, Kristensen D, Chen D 2009. Development of a freeze-stable formulation for vaccines containing aluminum salt adjuvants. Vaccine 27(1):72-79.

78. Vessely C, Estey T, Randolph TW, Henderson I, Cooper J, Nayar R, Braun LJ, Carpenter JF Stability of a Trivalent Recombinant Protein Vaccine Formulation Against Botulinum Neurotoxin During Storage in Aqueous Solution. Journal of Pharmaceutical Sciences 98(9):2970-2993.

79. Peek LJ, Martin TT, Elk Nation C, Pegram SA, Middaugh CR Effects of Stabilizers on the Destabilization of Proteins upon Adsorption to Aluminum Salt Adjuvants. Journal of Pharmaceutical Sciences 96(3):547-557.

80. Baez L, Distler A. 2011. Selection of Final Product Containers. Development of Vaccines, ed.: John Wiley & Sons, Inc. p 415-435.

81. Lal M, Jarrahian C 2017. Presentation matters: Buffers, packaging, and delivery devices for new, oral enteric vaccines for infants. Human Vaccines & Immunotherapeutics 13(1):46-49.

82. Food, Administration D 1996. FDA guidance concerning demonstration of comparability of human biological products including therapeutic biotechnology-derived products. Rockville, MD: US Food and Drug Administration.

83. Guideline IHT. 2013. Comparability of biotechnological/biological products subject to changes in their manufacturing process Q5E. ed.

84. Alsenaidy M, Jain NK, Kim J, Middaugh C, Volkin D 2014. Protein comparability assessments and potential applicability of high throughput biophysical methods and data visualization tools to compare physical stability profiles. Frontiers in Pharmacology 5(39).

85. Kirkitadze M Comparability of biotherapeutics: characterization of protein vaccine antigens. Pharmaceutical bioprocessing 1(4):373-380.

86. Federici M, Lubiniecki A, Manikwar P, Volkin DB 2013. Analytical lessons learned from selected therapeutic protein drug comparability studies. Biologicals 41(3):131-147.

87. Specifications IG. International Conference on Harmonization of Technical Requirements for Registration of Pharmaceuticals for Human Use, 1999.

88. Kirkitadze M, Arunachalam A, Carpick B 2013. Comparability of biotherapeutics: characterization of protein vaccine antigens. Pharmaceutical Bioprocessing 1(4):373-380.

89. Lubiniecki A, Volkin DB, Federici M, Bond MD, Nedved ML, Hendricks L, Mehndiratta P, Bruner M, Burman S, DalMonte P, Kline J, Ni A, Panek ME, Pikounis B, Powers G, Vafa O, Siegel R 2011. Comparability assessments of process and product changes made during development of two different monoclonal antibodies. Biologicals 39(1):9-22.

90. Alsenaidy MA, Jain NK, Kim JH, Middaugh CR, Volkin DB 2014. Protein comparability assessments and potential applicability of high throughput biophysical methods and data visualization tools to compare physical stability profiles. Frontiers in Pharmacology 5:39.

91. Wei H, Mo J, Tao L, Russell RJ, Tymiak AA, Chen G, Iacob RE, Engen JR 2014. Hydrogen/Deuterium Exchange Mass Spectrometry for Probing Higher Order Structure of Protein Therapeutics: Methodology and Applications. Drug discovery today 19(1):95-102.

92. Jones C 2005. NMR assays for carbohydrate-based vaccines. Journal of Pharmaceutical and Biomedical Analysis 38(5):840-850.

93. Berti F, Ravenscroft N. 2015. Characterization of Carbohydrate Vaccines by NMR Spectroscopy. In Lepenies B, editor Carbohydrate-Based Vaccines: Methods and Protocols, ed., New York, NY: Springer New York. p 189-209.

94. Malito E, Carfi A, Bottomley MJ 2015. Protein Crystallography in Vaccine Research and Development. International Journal of Molecular Sciences 16(6):13106-13140.

95. More AS, Toprani VM, Okbazghi SZ, Kim JH, Joshi SB, Middaugh CR, Tolbert TJ, Volkin DB 2016. Correlating the Impact of Well-Defined Oligosaccharide Structures on Physical Stability Profiles of IgG1-Fc Glycoforms. Journal of Pharmaceutical Sciences 105(2):588-601.

96. Kim JH, Joshi SB, Tolbert TJ, Middaugh CR, Volkin DB, Smalter Hall A 2016. Biosimilarity Assessments of Model IgG1-Fc Glycoforms Using a Machine Learning Approach. Journal of Pharmaceutical Sciences 105(2):602-612.

Chapter 2 A Micro-PEG Precipitation Assay as a Relative Solubility Screening Tool for Monoclonal Antibody Design and Formulation Development

2.1 Introduction

Protein solubility is a key physical parameter not only for chemistry, manufacturing and control (CMC) bulk development activities, but also for formulation development including long term stability and facile administration of protein based drugs[1-3]. In particular, monoclonal antibodies have emerged as a key class of protein drugs, administered either IV by medical professionals or by subcutaneous (SC) administration by patients[4]. The latter typically requires the development of high protein concentration, stable liquid formulations that can deliver >100 mg per one mL injection[3]. In addition, as part of biopharmaceutical lead identification, *in vitro* and *in vivo* solubility is considered a critical "drug-like" property. Solubility measurements can be used not only to identify potential protein drug candidates, but to rank order them in terms of potential manufacturing, storage or *in vivo* potency issues[5].

There are many methods available for determining protein solubility including ultrafiltration, dialysis/concentration or lyophilization/reconstitution[2,6]. These measurements, however, are often not practical or easily attainable either due to excessive amounts of protein required (several hundred mgs) and/or experimental difficulties such as gel formation and aggregation[1]. An alternative approach to measure apparent protein solubility (apparent thermodynamic activity) is by addition of polyethylene glycol (PEG) that precipitates the protein primarily by exclusion volume effects[7-9]. As described in detail elsewhere, a linear relationship between the log of protein concentration vs. the weight percent PEG in solution, under certain conditions, allows calculation of the apparent solubility (i.e., thermodynamic activity) of proteins by extrapolation of experimental results to zero PEG concentration[7,8]. It should be noted that this extrapolated activity value may contain thermodynamic non-ideality terms and hence the measured solubility is referred to as apparent protein solubility. PEG precipitation method has

been successfully used to determine the apparent solubility of multiple proteins[7,10-14] and also as a formulation screening tool[15]. Recently, Gibson et al. have used a high throughput version of the PEG precipitation method to determine the apparent solubility and PEG_{midpt} values for an IgG1 mAb produced from different cell lines and formulated in different pH and buffer solutions[15]. However, this methodology still requires relatively large amounts of protein (5-10 mgs per sample per experimental condition) which may not be available during early stages of drug development.

In the past decade, in addition to the current antiretroviral drugs, new therapeutics are being developed to reduce and cure HIV-1 infections[16]. Broadly neutralizing monoclonal antibodies (mAbs) against HIV-1 are considered as potential candidates for the development of a passive HIV-1 vaccine and have shown promise in the prevention and treatment of HIV-1 infection[16-23]. These broadly neutralizing mAbs offer several advantages over the current antiretroviral drugs such as virus neutralization and cell killing of the HIV infected cells by Fc receptor-mediated effector mechanisms[16]. A major subset of these antibodies designated as the VRC01 class, target the CD4-binding site on the gp-120 core of the virus and neutralize ~90% of diverse strains of the HIV virus[16,22-24]. Apart from the VRC01 class, there are several other categories of mAbs currently under development including the 10E8 and PGT classes which target the membrane proximal external region on gp41 and recognize epitopes such as the N-linked glycan at Asn 332 on gp120 respectively[22,24]. The low solubility of the majority of these mAbs, however, remains a key challenge during their development as candidates for a HIV-therapy[25,26].

In this work, we have developed a micro-PEG precipitation method requiring between ~0.1-1.0 mg of protein using the VRC01-WT mAb. The relative apparent solubility profile of

VRC01-WT mAb was established as measured by a combination of the curve shape (PEG vs protein concentrations), PEG_{midpt} determinations, and extrapolated apparent solubility values. The micro-PEG method was then used as relative solubility screening tool for a developability assessment of small amounts of multiple mAbs being evaluated as possible neutralizing mAb candidates for HIV-1. We also demonstrate the utility of the micro-PEG method as an early formulation screening tool to evaluate various solution conditions (pH, buffers, salt concentration, and excipients) for their effect on the solubility profile of the VRC01-WT mAb.

2.2 Materials and Methods

2.2.1 Materials

A total of seven mAbs (10E8-WT, 10E8v5, PGT121, 10E8v4, 35O22, VRC13, and VRC01-WT)[19,27-29] were provided by the National Institutes of Allergy and Infectious Disease (NIH) in phosphate buffered saline (PBS) at pH 7.4, except for VRC01-WT which was formulated in 25 mM sodium citrate, 50 mM sodium chloride, and 150 mM L-arginine hydrochloride at pH 5.8. The PGT antibodies were originally identified by the International AIDS Vaccine Initiative (IAVI) and published, (Walker, et al, Nature, 2011) [29] Protein concentrations were determined by UV spectroscopy at 280 nm with an extinction coefficient of $\varepsilon^{0.1\%}$=1.6 $(g/100\ mL)^{-1}cm^{-1}$. All formulation reagents (sodium phosphate, sodium chloride, citric acid, sodium citrate, L-histidine, arginine and PEG-10,000) for preparing different buffer systems namely phosphate, citrate and histidine were purchased from Sigma-Aldrich (St Louis, MO), and were high purity grade (>99%).

2.2.2 Methods

The protocol of the micro-PEG assay for assessing relative apparent solubility of mAbs was adapted from Gibson et al. (2011)[15]. Stock solutions of phosphate buffered saline (PBS), pH

7.4 and PBS containing 40% w/v PEG-10,000 at pH 7.4 were mixed to prepare various concentrations of PEG solutions ranging from 0 to 40% w/v PEG. A volume of 200 µL of twenty two different PEG-10,000 solutions was added in triplicate to wells of a 96-well polystyrene filter plate (Corning #3504, Corning Life Sciences, Corning, NY). The stock solution of VRC01-WT was diluted to 1 mg/mL with PBS buffer, pH 7.4. Fifty microliters (50 µL) of the protein stock solution (1 mg/mL) was then added to each well to a final protein concentration of 0.2 mg/mL. The plates were incubated overnight at room temperature and then centrifuged at 1,233g for 15 min; the filtrate was then collected in a clear 96 well collection plate (Greiner Bio-One#655001, Greiner Bio-One North America Inc., Monroe, NC). Thereafter, 200 µL of filtrate was transferred into a 96 well UV Star microplate (Grenier#655801). The filtrate was measured on a SpectraMax M5 UV-Visible plate reader at 280 nm to determine the protein concentration based on the extinction coefficient of $\varepsilon^{0.1\%}$=1.6 $(g/100\ mL)^{-1}cm^{-1}$ (provided by Vaccine Research Center). This assay is referred to as the standard PEG precipitation assay in this paper.

To further scale down the standard PEG assay, a Nanodrop spectrophotometer (NanoDrop Products, Wilmington, DE) was used as the UV detector for measuring protein concentration. The same procedure was followed for determining the protein concentration as described for the plate reader method, but with lower amounts and smaller volumes of protein. Forty microliters of various PEG-10,000 solutions were added to wells of a 96-well polystyrene filter plate and 10 µL of the resulting protein solution (1 mg/mL) was added to the wells containing various levels of PEG to a final protein concentration of 0.2 mg/mL. Two microliters of the filtrate was measured with the Nanodrop spectrometer at 280 nm to determine the protein concentration using an extinction coefficient of 16 at 280 nm for a 1% (10 mg/mL) mAb solution. This version of PEG assay is referred to as the micro-PEG assay.

The micro-PEG assay was used to evaluate the relative solubility profiles of various monoclonal antibodies (mAbs) that target the HIV-1 viral spike (gp120 envelope glycoprotein and gp41 transmembrane glycoprotein) and to compare the relative solubility profiles of VRC01-WT under different formulation conditions (pH, buffer, salt and arginine). For the additional scaled down version of the micro-PEG assay using 0.1-0.2 mg of protein, experiments with VRC01-WT containing different concentrations of arginine (0, 17, 50 and 150 mM) in 50 mM citrate buffer, pH 6.0 were first performed using ten different % PEG concentrations, followed by repeating at 0 % and 8.3% w/v PEG-10,000 for five replicates and calculating the % VRC01-WT soluble at 8.3% w/v PEG-10,000.

The absorbance at 280 nm (protein concentration) vs. PEG-10,000 (% w/v) data were fit to a standard four-parameter, modified Hill-slope sigmoidal curve equation (Eq.1 as described in Gibson et al, 2011)[15], using Python (x,y) v.2.7.6.0, an open source scientific and engineering software based on the python language. The % PEG_{midpt} (x-axis midpoint) was calculated from the resulting curve fit using equation (1) and the apparent solubility was calculated by fitting the data points from the transition region (i.e., points of partially soluble and partially precipitated protein) using equation (2) as described previously by Middaugh et al, 1979.[7]

$$y = b + \left(\frac{t-b}{1+ e^{\,s(mid-x)}}\right) \qquad (1)$$

where t= top plateau, b= bottom plateau, mid= x-axis midpoint, and s=slope.

$$\log Sp = \log a_o - A_{12}[PEG] \qquad (2)$$

where Sp is the concentration of soluble protein in a solution containing PEG-precipitated protein in equilibrium with soluble protein, a_0 is the activity of the protein in a saturated PEG-free environment, A_{12} is a virial coefficient (primarily corresponding to excluded volume effects) and [PEG] is the % w/v PEG concentration.

For statistical comparisons, the p values for all the above experiments were determined using the student t-test in Microsoft Excel 2010 software and a p value of <0.05 was accepted as significant.

2.3 Results

2.3.1 Comparison of Standard vs. Micro PEG precipitation assay and determination of assay precision

The PEG precipitation assay was performed with VRC01-WT mAb at a final protein concentration of 0.2 mg/mL using two different UV-Visible spectrophotometers, a SpectraMax M5 plate reader and a Nanodrop instrument. The standard PEG assay required larger volumes and thus higher amounts of protein (~5X) compared to the micro PEG assay. As shown in Figure 2.1, PEG precipitation assays run in the two formats resulted in similar shapes of the precipitation curves ($PEG_{curves,}$, i.e., protein concentration in A280 units vs. amount of added PEG) as well as similar results for the VRC01-WT mAb in terms of experimentally determined PEG_{midpt} and relative apparent solubility values (for the latter, well within the relative standard deviation of this extrapolation method as described elsewhere and below)[7,15].

The precision of the % PEG_{midpt} and apparent solubility values by the micro PEG assay were determined for nine replicates of the VRC01-WT mAb sample. As shown in Table 2.1, the precision of the method was determined from the mean % PEG_{midpt} and apparent solubility values of VRC01-WT mAb which were 8.2% w/v (range 8.2-8.3 % w/v) and 19 mg/mL (range 13-29 mg/mL), respectively. Table 2.1 also summarizes the statistical parameters for the precision of % PEG_{midpt} and apparent solubility values in terms of SD (standard deviation) and RSD (relative standard deviation) results. The % PEG_{midpt} values had lower levels of variability (% RSD =0.7) compared to the relative apparent solubility values (% RSD =29 %). These assay

qualification results with the micro-PEG assay format are in good agreement with previous studies using the standard assay format (with a different IgG1 mAb) where the variability in the relative apparent solubility value is primarily due to subtle changes in the slope of the linear fit over the transition region[15].

2.3.2 Evaluation and rank ordering of various mAbs based on their relative solubility profile in PBS buffer, pH 7.4

The micro PEG assay was utilized to rank order and compare the relative solubility profiles of VRC01-WT mAb with six additional mAb candidates that bind different epitopes on HIV-1 virus (gp120 envelope glycoprotein and gp41 transmembrane glycoprotein)[22,24]. The mAbs were all prepared in PBS buffer at pH 7.4 to assess the solubility profiles of these proteins under physiological-like conditions. As a first comparison, differences in the overall shapes of their PEG_{curves} (protein vs. PEG concentration) for each of the six additional mAbs were evaluated by visual comparison to the VRC01-WT mAb (Figure 2.2). It can be seen that the six mAbs varied dramatically in terms of their profiles. For example, the VRC13 mAb closely overlaps the VRC01-WT mAb, while the 10E8-WT mAb precipitates from solution at much lower concentrations of PEG-10,000 (Figure 2.2). The PEG_{curves} provide a qualitative way to compare the protein vs. PEG concentration profiles between protein samples, whereas; % PEG_{midpt} and the apparent solubility values are quantitative parameters for measuring and comparing apparent protein solubility of different samples.

The data in Figure 2.2 were then analyzed to determine the % PEG_{midpt} values (Figure 2.3A) and the relative apparent solubility values (Figure 2.3B) of the different mAbs (as described in the Methods section). Compared to the VRC01-WT mAb, the % PEG_{midpt} and apparent solubility values of the mAbs showed trends of increased values in the order 10E8-WT

< 10E8v5 < PGT121 < 10E8v4 < 35O22 <VRC13 <VRC01-WT. Significant differences ($p < 0.05$) in % PEG_{midpt} values between VRC01-WT and the six mAbs were observed. In terms of relative apparent solubility values, which showed much higher RSD values due to the extrapolation, significant differences ($p < 0.05$) in the relative apparent solubility values were observed between VRC01-WT and three mAbs, namely, 10E8WT, 10Ev5 and PGT121. The individual values and overall rank ordering of the various mAbs, via evaluation of PEG_{curves}, PEG_{midpt}, and apparent solubility values, compared to VRC01-WT are also summarized in the supplemental section (see supplemental Table 2.1).

2.3.3 Evaluation and rank ordering of relative solubility profile of VRC01-WT mAb under various formulation conditions

The effect of solution pH (pH 5.0-8.0) on the PEG_{curves} (protein vs. PEG concentration) of the VRC01 WT mAb, formulated in 50 mM phosphate buffer, is shown in Figure 2.4A. The overall curves shifted to the left (as the pH increases from 5.0-8.0), indicating less PEG-10,000 is required to cause mAb precipitation. Additional analysis of these data showed decreases in the PEG_{midpt} and relative apparent solubility values of VRC01-WT mAb were observed as the pH is increased from 5.0 to 8.0 (See Figure 2.5A and Figure 2.5B for trends and Supplemental Table 2.2 for individual values). These decreases in PEG_{midpt} and apparent solubility values with increases in solution pH are consistent with the pI range of the VRC01-WT mAb (~9.0-9.6) as observed by cIEF (See Supplemental Figure 2.1). As solution pH approaches the pI of the mAb, it is commonly observed that solubility decreases, presumably due to loss of overall charge, and thus loss of charge repulsion between mAbs molecules in solution[30].

Different solution conditions were evaluated for their effect on the VRC01-WT mAb solubility profile including (1) different buffering agents including citrate, phosphate and

histidine with and without sodium chloride (buffer strength = 50 mM, +/- 0.15 M NaCl, pH 6.0), (2) different concentrations of arginine in 50 mM citrate pH 6.0 (17 mM, 50 mM and 150 mM arginine), and (3) an initial formulation buffer identified for VRC01-WT mAb (25 mM Na citrate, 50 mM NaCl, 150 mM arginine, pH 5.8). These formulation conditions were evaluated for their effect on the PEG_{curves}, % PEG_{midpt} and relative apparent solubility values of VRC01-WT mAb. The PEG_{curves} (protein vs. PEG concentration) were similar for the mAb in histidine and citrate buffer but required more PEG for mAb precipitation in phosphate buffer (Figure 2.4B). Interestingly, the addition 150 mM NaCl to each of these buffers (Figure 2.4C) shifted the curves to the right compared to the PEG_{curves} without salt, and also showed that the mAb in histidine buffer+NaCl required more PEG for precipitation compared to the mAb in phosphate buffer+NaCl. In addition, increasing arginine concentrations (0 to 150 mM) (Figure 2.4D) caused the curves to shift to the right (i.e., required more PEG for mAb precipitation) compared to the PEG_{curves} without arginine.

For ease of statistical comparisons of each of these formulation conditions, the mAb in each of the solution conditions (buffer, salt and arginine) was compared with the 50 mM citrate formulation. The % PEG_{midpt} and relative apparent solubility values varied with different formulation conditions as shown in Figure 2.5C and 2.5D, respectively. In terms of general trends, the mAb in 50 mM citrate had the lowest values and the addition of arginine, and to a lesser extent NaCl, greatly increased the values. Combinations of excipients were also effective. For example, VRC01-WT mAb formulated in 25 mM citrate, 50 mM NaCl, 150 mM arginine pH 5.8 showed the highest % PEG_{midpt} and relative apparent solubility (thermodynamic activity) values. Differences in % PEG_{midpt} and relative apparent solubility values between the 50 mM citrate versus all the other formulation conditions were statistically significant ($p<0.05$) with a

few exceptions (e.g., mAb formulated in 50 mM citrate + 17 mM arginine and 50 mM histidine showed no statistically significant differences in the apparent solubility values compared to 50 mM citrate). A summary of the % PEG_{midpt} and relative apparent solubility individual values of the VRC01-WT mAb under different formulation conditions is also presented in the supplemental data. (Supplemental Table 2.3)

2.3.4 Scaled down version of the micro-PEG assay

The experiments described above were performed in triplicate with VRC01-WT mAb samples across the protein vs. PEG concentration curves. This resulted in the need for ~1 mg of protein per condition. For initial screening purposes, if not even ~1 mg of protein is easily available, the amount of protein required in this micro-PEG assay can be reduced by either reducing the number of replicates or by lowering the number of test samples. As a proof of concept of further scaling down the micro-PEG assay, the arginine experiments were repeated with fewer concentrations and replicates of PEG-10,000 (% w/v) with the VRC01-WT mAb in citrate buffer, pH 6.0 with increasing concentrations of arginine. The PEG_{curves} (protein vs. PEG concentration) are shown in Figure 2.5E. It can be seen from these data that the trends are the same using both more and fewer sample points (compare Figure 2.4D to Figure 2.5E).

Since it may be more difficult to accurately determine % PEG_{midpt} and relative apparent solubility (thermodynamic activity) values with fewer data points (i.e., fewer test samples), an alternative approach was used: the % VRC01-WT mAb that was soluble at a set concentration of PEG was determined and compared. For example, at 8.3% (w/v) PEG increasing arginine concentration increased the % VRC01-WT mAb in solution as shown in Figure 2.5F. Increasing arginine concentration increased the % VRC01-WT soluble at 8.3% w/v PEG and statistically significant differences were observed for the % VRC01-WT mAb soluble at 8.3% w/v PEG

between control buffer (0 mM arginine) and each of the buffers with increasing concentrations of arginine tested (Figure 2.5F). This result can be obtained using only 0.1-0.2 mg of protein by initially using only ten different % PEG concentrations with n=1 replicate (requires 0.1 mg protein), and then determining the % mAb soluble at a fixed concentration of PEG vs. the control (no PEG) using five replicates each, requiring an additional 0.1 mg of protein. Thus, this additional scale down of the micro-PEG requires a total of 0.2 mg of protein.

2.4 Discussion

The solubility of therapeutic protein can be a critical quality attribute, especially if higher doses of the drug will be needed clinically or if large amounts will need to be manufactured. It is important to assess these types of considerations as early in development as possible including the molecule discovery phase as well as the early stages of formulation design and development[31]. For example, there are typically a plethora of mAb candidates against a target during the discovery stage of drug development, but usually only one or a few mAb(s) will progress into clinical development. Solubility screening can thus play an important role in selecting mAb drug candidates that offer the ability to formulate high concentration dosage forms as well as cost-effective manufacturability[5].

Direct quantitative protein solubility measurements using ultrafiltration or lyophilization are often experimentally difficult to perform due to problems such as gel formation/aggregation, or requirement of large amounts of protein for highly soluble proteins[2]. The lack of sufficient amounts of protein during discovery research, and even at early stages of development, often makes the ultrafiltration and lyophilization approaches impractical. An alternative approach to indirectly measure apparent protein solubility is using additives, such as ammonium sulfate or PEG, which reduce the solubility of a protein in a quantifiable manner. Both ammonium sulfate

and PEG have been used previously as tools for measuring relative apparent solubility (thermodynamic activity) of proteins including mAbs as well as for comparing different formulations of an IgG1 mAb[6,15,32-34].

Kramer et al. have demonstrated a good overall correlation between the apparent solubility measurements of different proteins using PEG and ammonium sulfate[6]. These results indicated that either of the precipitants can in principle be used to rank order the relative solubility of different proteins. Each precipitant, however, has its own advantages and disadvantages and the choice of selecting one precipitant over the other is largely based on empirical observations as well as different mechanisms that may lead to differences in relative solubility between different proteins. For example, the PEG precipitation method assumes inert behavior of PEG towards proteins which may not be true for some proteins under some solution conditions. It has been reported that PEG may induce subtle perturbations in protein structure and decrease the thermodynamic stability of some proteins[8,14,35,36]. In addition, protein-protein interactions can vary as a function of protein concentration and solution conditions which can also be affected by addition of PEG. These experimental limitations in turn can make the extrapolated apparent solubility values from the PEG precipitation assay a less accurate reflection of the true solubility of a protein. In contrast, other studies have shown that ammonium sulfate can stabilize the native protein conformation and thus can be used only for comparative solubility measurements while more representative solubility measurements can be obtained using PEG[6,33]. In addition, with low concentrations of ammonium sulfate, salting-in effects can be observed and the extrapolated solubility value obtained from the salting-out region may not be a true representation of protein solubility in the absence of salt. Further, ammonium sulfate may not be an effective precipitant for some highly charged proteins such as α-lactalbumin and may underestimate protein solubility

trends[6,37]. Nonetheless, both the methods remain useful tools for rank ordering of the relative apparent solubility of different proteins and/or solution conditions that effect protein solubility.

In recent years, Gibson et al.[15] and Yamniuk et al.[33] have reported an automated high throughput plate based solubility assay employing PEG and ammonium sulfate, respectively. Gibson et al. work using PEG required several mgs of protein for each experiment, which may not be attainable during discovery research and early stages of mAb development. In this work, we have demonstrated that the scale down version of the PEG assay (micro-PEG assay) requires much lower amounts of mAb (0.1 to 1 mg) for apparent solubility measurements, and thus is a more practical approach for developability assessments of different candidate mAbs. To this end, we used this new method to screen various different candidate bnAbs for HIV-1. In this early stage of candidate selection, hundreds of variants could be generated but there is a very limited amount of material of each individual protein. Thus, the micro-PEG assay can be extremely useful for screening a large number of candidate molecules.

We have shown in this work that the micro-PEG precipitation assay is straightforward, precise and provides an accelerated assessment of experimental parameters that have been previously demonstrated to be effective surrogates for assessing protein solubility[7,15]. The micro-PEG assay has potential utility to provide important information about relative protein solubility to not only better compare candidate protein molecules, but also during subsequent drug development of the selected candidate including formulation design and comparability assessments. For early candidate comparisons, the micro-PEG precipitation method was used in this work to rank order a series of broadly neutralizing anti-HIV1 mAb candidates based on both qualitative and quantitative experimental parameters such as the shape of the PEG_{curves}, $\%PEG_{midpt}$ values and relative apparent solubility (thermodynamic activity) values using ~1 mg

of protein. Moreover, an additional scaled down version of the micro-PEG assay requiring only about 0.1-0.2 mgs of protein was demonstrated to generate similar data for rank ordering purposes. Although providing more limited data sets, this version of the assay could be used as an initial solubility screening tool in cases where availability protein is severely limited.

In terms of formulation development applications, it is often a challenge for the formulation scientist to find conditions (pH, buffer system and excipient) that enable high concentration formulations of therapeutic mAbs (>100 mg/mL) for subcutaneous administration [3]. To better address this challenge in early development when limited amounts of protein are available, we applied the micro-PEG assay to screen different solution conditions with the VRC01-WT mAb including buffering agents (citrate, histidine and phosphate), solution pH (pH values from 5.0 to 8.0), and excipients (sodium chloride and arginine) to evaluate their relative effects on the same experimental parameters and to rank order relative solubility profiles of the VRC01-WT mAb. The results from these experiments, clearly demonstrate the potential of this method to screen for solution conditions that enhances solubility profiles. In addition, as a potential future application of this PEG assay, it is also very important to develop mAb formulations that minimize aggregation during long-term storage to reduce the risk of unwanted immunogenicity of a protein drug in patients. The inter-relationships between different excipients, protein solubility and protein aggregation are complex and highly dependent on the protein itself and the type of environmental stress encountered. We are currently using the PEG precipitation assay in our labs to assess excipient effects on both relative apparent solubility values as well as aggregation profiles over time using another IgG1 mAb (Kalonia et al., manuscript in preparation, 2016). Finally, the micro-PEG assay can be utilized in early comparability and/or biosimilarity evaluations which require an extensive physiochemical

analytical characterization toolset[38,39]. For example, the micro-PEG assay can be a quick way to initially compare the solubility profiles of pre- vs. post-change for bulk drug substance or final drug products, as well as for biosimilar vs. innovator protein drug at the early stages of development. Recently, we have successfully utilized the micro-PEG assay for biosimilarity assessment of four well-defined IgG1-Fc glycoforms with decreasing oligosaccharide content (High mannose-Fc> Man5-Fc>GlcNAc-Fc> N297Q aglycosylated form) as a model system[40]. Significant differences and similarities were found in % PEG_{midpt} values and relative apparent solubility (thermodynamic activity) values between these IgG1-Fc glycoforms. Thus, the micro-PEG assay can play an important role in screening and comparing therapeutic protein candidates and contribute towards their accelerated advancement through the different stages of biotherapeutic drug discovery and development.

Table 2.1. Precision of the Micro-PEG Assay for the Determination of %PEGmidpt and Relative Apparent Solubility (Thermodynamic Activity) Values Using VRC01-WT, a Broadly Neutralizing HIV-1 IgG1 Monoclonal Antibody.

Sample size (n=9)	**% PEG_{midpt} (% w/v)**	**Apparent solubility (mg/mL)**
Mean	8.2	19
Range	8.2-8.3	13-29
SD	0.1	6
% RSD	0.7	29

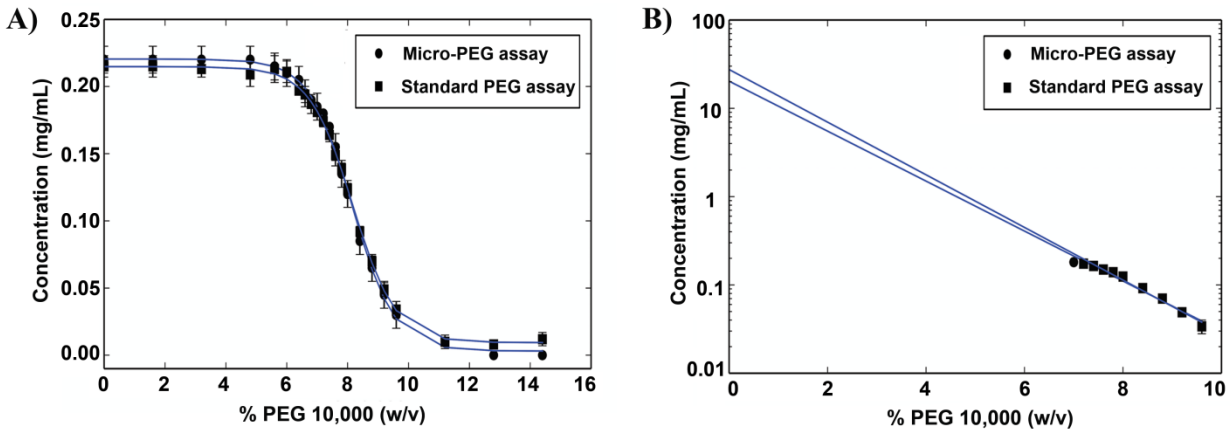

Figure 2.1. Comparison of the standard PEG protein precipitation assay and micro-PEG assay using the VRC01-WT mAb formulated in PBS buffer at pH 7.4. (a) Linear concentration scale over a PEG concentration range (0%-20% w/v PEG). (b) Logarithmic scale for extrapolation of the linear fit to determine the relative apparent solubility in the absence of PEG (y-intercept). The error bars denote standard deviation for n= 3 replicates for each %PEG concentration.

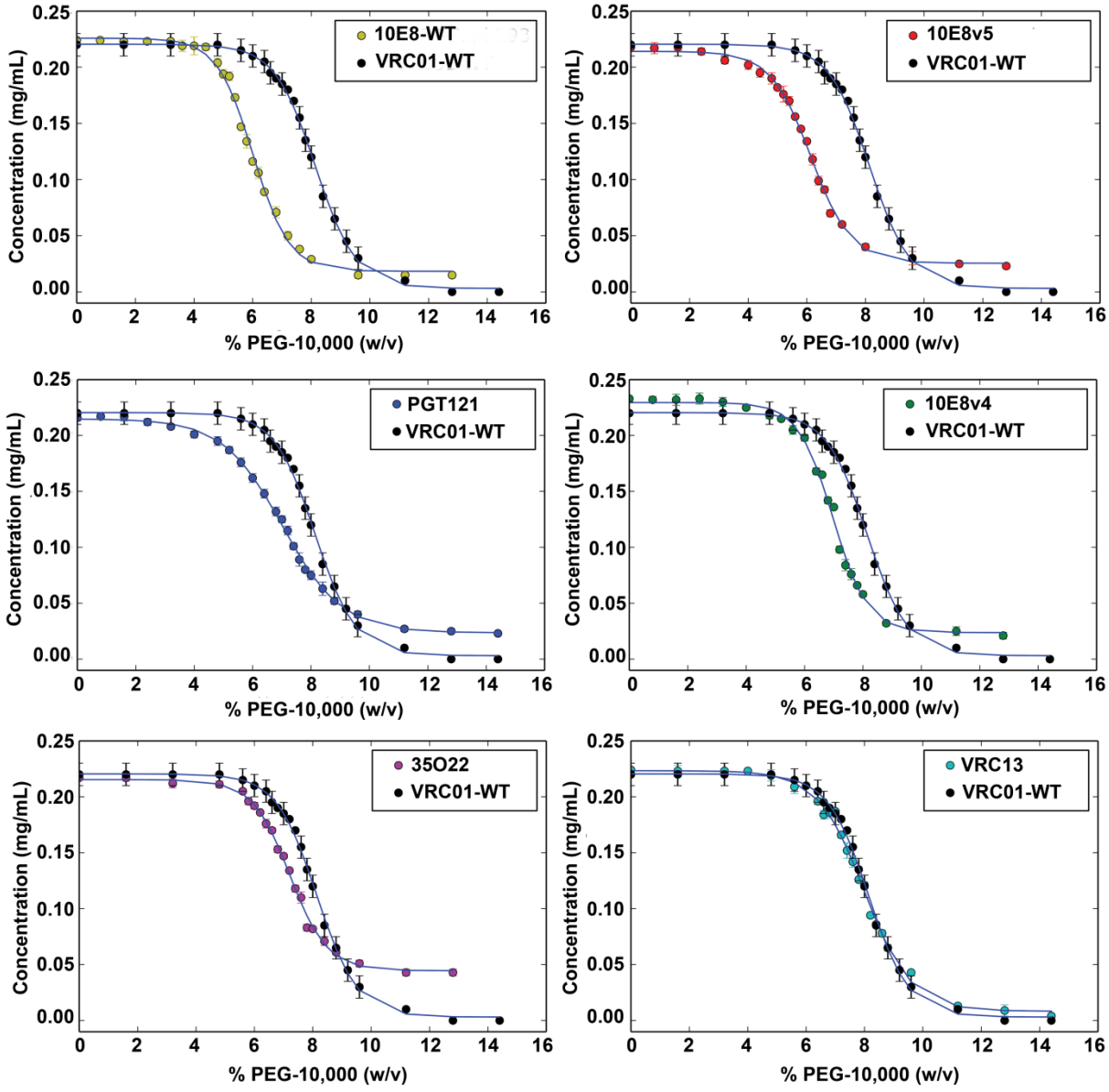

Figure 2.2. Comparison of the PEG_{curves} (protein vs. PEG concentration) of different broadly neutralizing HIV-1 mAbs versus VRC01-WT mAb. Samples are in PBS buffer at pH 7.4. The error bars denote standard deviation for n = 3 replicates for each %PEG concentration.

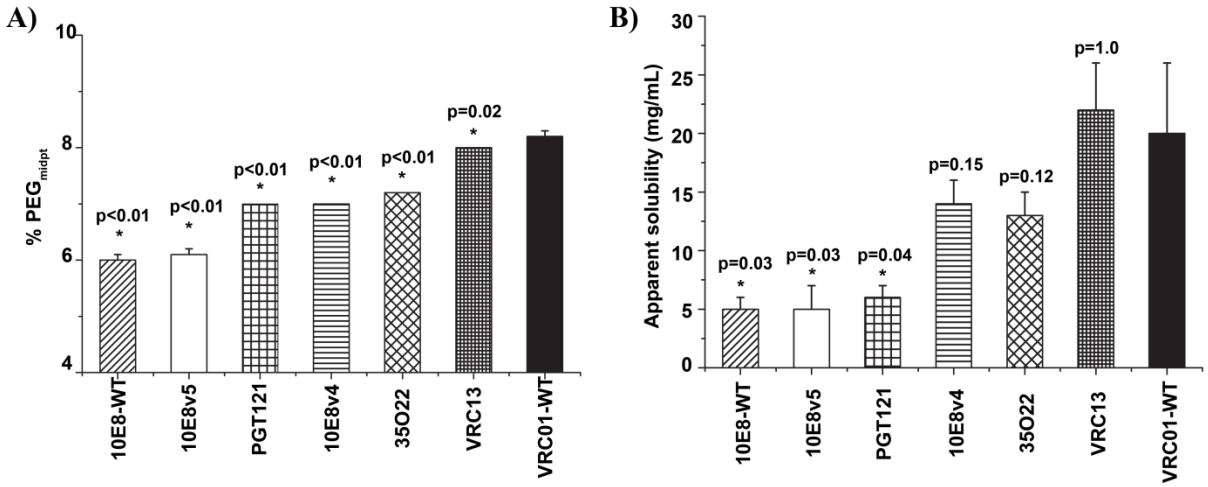

Figure 2.3. Comparison of different broadly neutralizing anti-HIV-1 mAbs versus VRC01-WT mAb by the micro-PEG assay**.** (a) % PEGmidpt values, (b) relative apparent solubility (thermodynamic activity) values. Error bars indicate the standard deviation of 3 replicates and statistical significance (*) compared to the VRC01-WT with a p value < 0.05 is indicated.

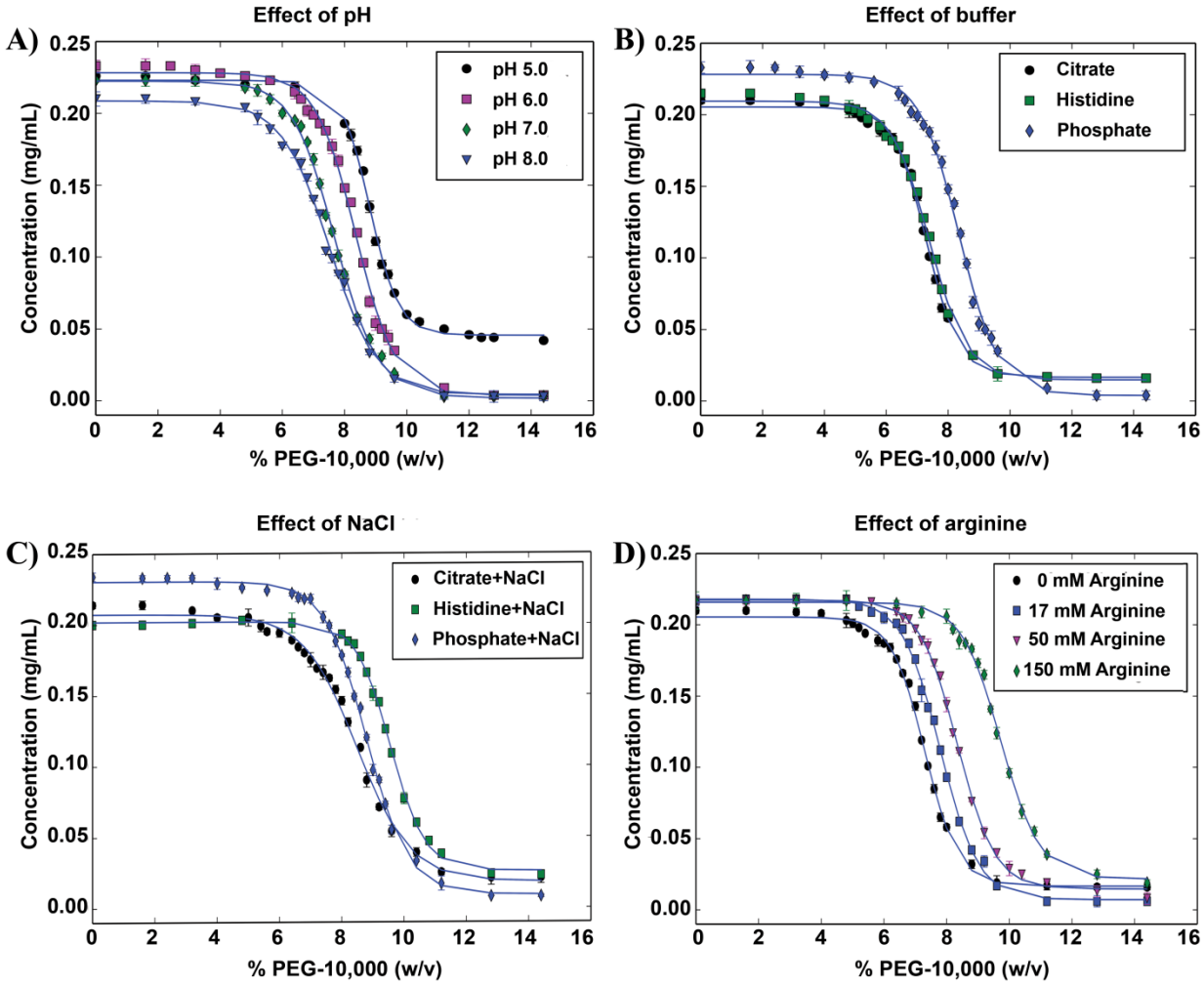

Figure 2.4. Effect of solution pH, buffers, NaCl, and arginine on the PEGcurves (protein vs. PEG concentration) for VRC01-WT mAb. (a) Effect of pH varying from 5.0 to 8.0, (b) effect of different buffering agents (citrate, phosphate, and histidine) without NaCl at pH 6.0, (c) effect of addition of 150 mM NaCl in the 3 different buffers (citrate, phosphate, and histidine) at pH 6.0, and (d) effect of arginine addition (17, 50, and 150 mM) in citrate buffer at pH 6.0. The error bars denote standard deviation for n = 3 replicates for each % PEG concentration.

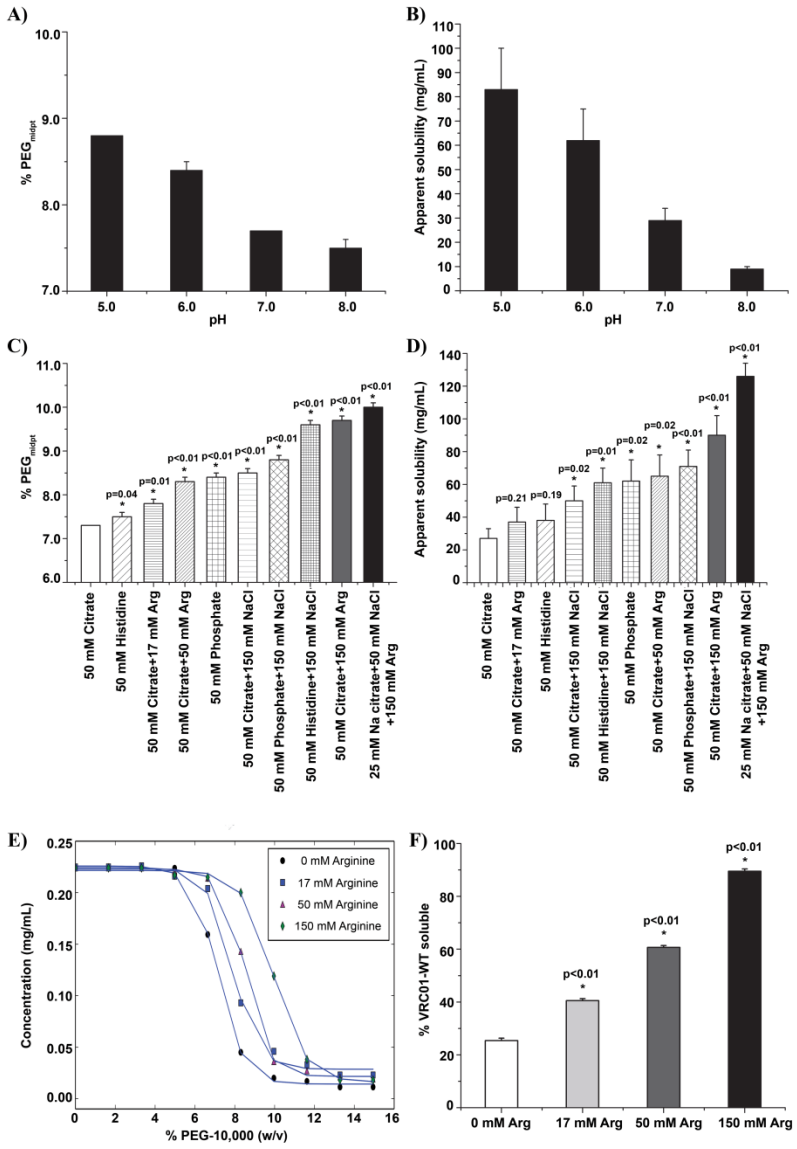

Figure 2.5. Effect of various formulation conditions on VRC01-WT mAb as measured by the micro-PEG assay. (a) $\%PEG_{midpt}$ values as a function of solution pH, (b) relative apparent solubility (thermodynamic activity) values as a function of pH, (c) % PEGmidpt values as a function of different buffers, with or without NaCl and arginine, (d) relative apparent solubility (thermodynamic activity) values as a function of different buffers, with or without NaCl and arginine. Error bars indicate the standard deviation of 3 replicates and statistical significance (*) compared to the control (50 mM citrate, p value < 0.05) is indicated. (e) The PEGcurves (protein vs. PEG concentrations) for VRC01-WT mAb with different concentrations of arginine in citrate buffer pH 6.0 using the additional scale-down version of the micro-PEG assay (mentioned in the text), and (f) %VRC01-WT mAb soluble at 8.3% w/v PEG-10,000 at different arginine concentrations. Error bars indicate the standard deviation of 5 replicates and statistical significance (*) compared to the control buffer without arginine (p value < 0.05) is indicated.

Supplemental Table 2.1. Summary of % PEG_{midpt} and relative apparent solubility (thermodynamic activity) values of seven different broadly neutralizing HIV-1 envelope IgG1 mAb candidates (n=3).

mAb	%PEG_{midpt} (% w/v)			Apparent Solubility (mg/mL)		
	Mean	SD	Range	Mean	SD	Range
10E8-WT	6.0	0.1	5.9-6.0	5	1	4-6
10E8v5	6.1	0.1	6.1-6.2	5	2	4-7
PGT121	7.0	0	7.0-7.0	6	1	5-7
10E8v4	7.0	0	7.0-7.0	14	2	13-16
35O22	7.2	0	7.2-7.2	13	2	11-14
VRC13	8.0	0	8.0-8.0	22	4	18-25
VRC01-WT	8.2	0.1	8.2-8.3	20	6	13-29

Supplemental Table 2.2. Summary of % PEG_{midpt} and relative apparent solubility (thermodynamic activity) values of VRC01-WT mAb, as a function of solution pH (5.0-8.0) when formulated in phosphate buffer as measured by the micro PEG assay (n=3).

Formulation	**pH**	**%PEG_{midpt} (% w/v)**			**Apparent Solubility (mg/mL)**		
		Mean	SD	Range	Mean	SD	Range
50 mM Phosphate	5.0	8.8	0.0	8.8-8.8	83	17	66-101
	6.0	8.4	0.1	8.3-8.4	62	13	53-78
	7.0	7.7	0.0	7.7-7.7	29	5	23-32
	8.0	7.5	0.1	7.5-7.6	9	1	8-10

Supplemental Table 2.3. Summary of % PEG_{midpt} and relative apparent solubility (thermodynamic activity) values of VRC01-WT mAb, formulated in different buffers (+/- NaCl), different concentrations of arginine, and in various combinations as determined by the micro-PEG assay (n=3).

Formulation	**%PEG_{midpt}(% w/v)**			**Apparent Solubility (mg/mL)**		
	Mean	SD	Range	Mean	SD	Range
50 mM Citrate pH 6.0	7.3	0.0	7.3-7.3	27	6	24-34
50 mM Histidine pH 6.0	7.5	0.1	7.4-7.5	38	10	32-49
50 mM Citrate +17 mM Arginine pH 6.0	7.8	0.1	7.7-7.8	37	9	28-45
50 mM Citrate +50 mM Arginine pH 6.0	8.3	0.1	8.3-8.4	65	13	54-80
50 mM Phosphate pH 6.0	8.4	0.1	8.3-8.4	62	13	53-78
50 mM Citrate + 150 mM NaCl pH 6.0	8.5	0.1	8.4-8.5	50	9	40-55
50 mM Phosphate + 150 mM NaCl pH 6.0	8.8	0.0	8.8-8.8	71	10	65-84
50 mM Histidine + 150 mM NaCl pH 6.0	9.6	0.1	9.5-9.6	61	9	54-70
50 mM Citrate +150mM Arginine pH 6.0	9.7	0.1	9.6-9.7	90	12	80-102
25 mM Na Citrate, 50 mM NaCl, 150 mM Arginine pH 5.8	10.0	0.0	10.0-10.0	126	8	118-133

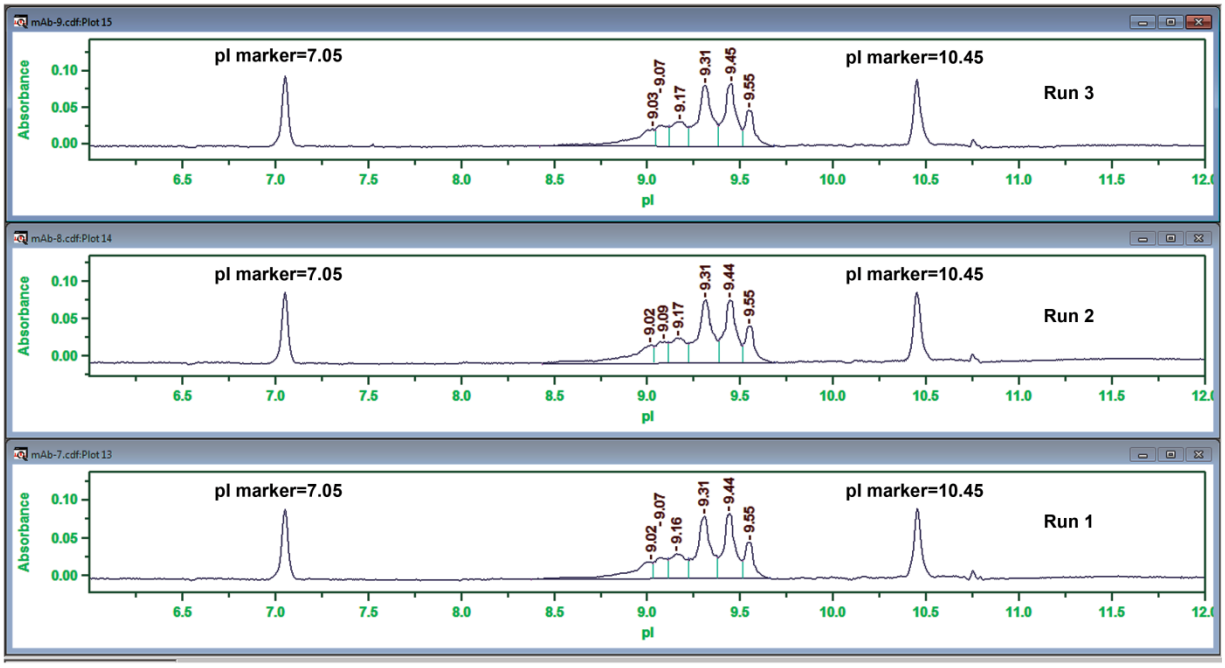

Supplemental Figure 2.1. cIEF electropherograms of VRC01-WT mAb showing a heterogeneous mixture of charged species with different isoelectric points from ~9.0 to 9.6. The pI markers are shown at pI values of 7.05 and 10.45. Triplicate runs of same VRC01-WT mAb sample are shown.

2.5 References

1. Ahern TJ, Manning MC. 1992. Stability of Protein Pharmaceuticals: Chemical and Physical Pathways of Protein Degradation. ed.: Plenum Press.

2. Trevino SR, Scholtz JM, Pace CN 2008. Measuring and increasing protein solubility. J Pharm Sci 97(10):4155-4166.

3. Shire SJ, Shahrokh Z, Liu J 2004. Challenges in the development of high protein concentration formulations. Journal of Pharmaceutical Sciences 93(6):1390-1402.

4. Ecker DM, Jones SD, Levine HL 2015. The therapeutic monoclonal antibody market. mAbs 7(1):9-14.

5. Wu S-J, Gilliland GL, Feng Y. 2014. Solubility and Early Assessment of Stability for Protein Therapeutics. Biophysical Methods for Biotherapeutics, ed.: John Wiley & Sons, Inc. p 65-91.

6. Kramer RM, Shende VR, Motl N, Pace CN, Scholtz JM 2012. Toward a molecular understanding of protein solubility: increased negative surface charge correlates with increased solubility. Biophys J 102(8):1907-1915.

7. Middaugh CR, Tisel WA, Haire RN, Rosenberg A 1979. Determination of the apparent thermodynamic activities of saturated protein solutions. Journal of Biological Chemistry 254(2):367-370.

8. Atha DH, Ingham KC 1981. Mechanism of precipitation of proteins by polyethylene glycols. Analysis in terms of excluded volume. Journal of Biological Chemistry 256(23):12108-12117.

9. Ingham KC. 1990. [23] Precipitation of proteins with polyethylene glycol. In Murray PD, editor Methods in Enzymology, ed.: Academic Press. p 301-306.

10. Middaugh CR, Lawson EQ, Litman GW, Tisel WA, Mood DA, Rosenberg A 1980. Thermodynamic basis for the abnormal solubility of monoclonal cryoimmunoglobulins. Journal of Biological Chemistry 255(14):6532-6534.

11. Tisel WA, Haire RN, White JG, Rosenberg A, Middaugh CR 1980. Polyphasic linkage between protein solubility and ligand binding in the hemoglobin-polyethylene glycol system. Journal of Biological Chemistry 255(19):8975-8978.

12. Annunziata O, Asherie N, Lomakin A, Pande J, Ogun O, Benedek GB 2002. Effect of Polyethylene Glycol on the Liquid-Liquid Phase Transition in Aqueous Protein Solutions. Proceedings of the National Academy of Sciences of the United States of America 99(22):14165-14170.

13. Stevenson CLC Estimation of recombinant bovine somatotropin solubility by excluded-volume interaction with polyethylene glycols. Pharmaceutical research 12(11):1671.

14. Sharma VK, Kalonia DS 2004. Polyethylene glycol-induced precipitation of interferon alpha-2a followed by vacuum drying: Development of a novel process for obtaining a dry, stable powder. AAPS PharmSci 6(1):31-44.

15. Gibson TJ, McCarty K, McFadyen IJ, Cash E, Dalmonte P, Hinds KD, Dinerman AA, Alvarez JC, Volkin DB 2011. Application of a high-throughput screening procedure with PEG-induced precipitation to compare relative protein solubility during formulation development with IgG1 monoclonal antibodies. J Pharm Sci 100(3):1009-1021.

16. Lynch RM, Boritz E, Coates EE, DeZure A, Madden P, Costner P, Enama ME, Plummer S, Holman L, Hendel CS, Gordon I, Casazza J, Conan-Cibotti M, Migueles SA, Tressler R, Bailer RT, McDermott A, Narpala S, O'Dell S, Wolf G, Lifson JD, Freemire BA, Gorelick RJ, Pandey JP, Mohan S, Chomont N, Fromentin R, Chun T-W, Fauci AS, Schwartz RM, Koup RA, Douek DC, Hu Z, Capparelli E, Graham BS, Mascola JR, Ledgerwood JE 2015. Virologic effects of broadly neutralizing antibody VRC01 administration during chronic HIV-1 infection. Science Translational Medicine 7(319):319ra206-319ra206.

17. Shingai M, Nishimura Y, Klein F, Mouquet H, Donau OK, Plishka R, Buckler-White A, Seaman M, Piatak M, Lifson JD, Dimitrov D, Nussenzweig MC, Martin MA 2013. Antibody-mediated immunotherapy of macaques chronically infected with SHIV suppresses viraemia. Nature 503(7475):277-280.

18. Klein F, Halper-Stromberg A, Horwitz JA, Gruell H, Scheid JF, Bournazos S, Mouquet H, Spatz LA, Diskin R, Abadir A, Zang T, Dorner M, Billerbeck E, Labitt RN, Gaebler C, Marcovecchio PM, Incesu R-B, Eisenreich TR, Bieniasz PD, Seaman MS, Bjorkman PJ, Ravetch JV, Ploss A, Nussenzweig MC 2012. HIV therapy by a combination of broadly neutralizing antibodies in humanized mice. Nature 492(7427):118-122.

19. Pegu A, Yang Z-y, Boyington JC, Wu L, Ko S-Y, Schmidt SD, McKee K, Kong W-P, Shi W, Chen X, Todd J-P, Letvin NL, Huang J, Nason MC, Hoxie JA, Kwong PD, Connors M, Rao SS, Mascola JR, Nabel GJ 2014. Neutralizing antibodies to HIV-1 envelope protect more effectively in vivo than those to the CD4 receptor. Science translational medicine 6(243):243ra288-243ra288.

20. Rudicell RS, Kwon YD, Ko S-Y, Pegu A, Louder MK, Georgiev IS, Wu X, Zhu J, Boyington JC, Chen X, Shi W, Yang Z-y, Doria-Rose NA, McKee K, O'Dell S, Schmidt SD, Chuang G-Y, Druz A, Soto C, Yang Y, Zhang B, Zhou T, Todd J-P, Lloyd KE, Eudailey J, Roberts KE, Donald BR, Bailer RT, Ledgerwood J, Program NCS, Mullikin JC, Shapiro L, Koup RA, Graham BS, Nason MC, Connors M, Haynes BF, Rao SS, Roederer M, Kwong PD, Mascola JR, Nabel GJ 2014. Enhanced Potency of a Broadly Neutralizing HIV-1 Antibody In Vitro Improves Protection against Lentiviral Infection In Vivo. Journal of Virology 88(21):12669-12682.

21. Barouch DH, Whitney JB, Moldt B, Klein F, Oliveira TY, Liu J, Stephenson KE, Chang H-W, Shekhar K, Gupta S, Nkolola JP, Seaman MS, Smith KM, Borducchi EN, Cabral C, Smith JY, Blackmore S, Sanisetty S, Perry JR, Beck M, Lewis MG, Rinaldi W, Chakraborty AK, Poignard P, Nussenzweig MC, Burton DR 2013. Therapeutic efficacy of potent neutralizing HIV-1-specific monoclonal antibodies in SHIV-infected rhesus monkeys. Nature 503(7475):224-228.

22. Kwong Peter D, Mascola John R 2012. Human Antibodies that Neutralize HIV-1: Identification, Structures, and B Cell Ontogenies. Immunity 37(3):412-425.

23. Mascola JR 2015. The modern era of HIV-1 vaccine development. Science 349(6244):139-140.

24. Kwong PD, Mascola JR, Nabel GJ 2013. Broadly neutralizing antibodies and the search for an HIV-1 vaccine: the end of the beginning. Nat Rev Immunol 13(9):693-701.

25. Kwon YD, Georgiev IS, Zhang B, McKee K, O'Dell S, Druz A, Shi W, Connors M, Mascola JR, Kwong PD 2014. Enhancing the Solubility of HIV-1-neutralizing Antibody 10E8. AIDS Research and Human Retroviruses 30(Suppl 1):A150-A150.

26. Chen J, Frey G, Peng H, Rits-Volloch S, Garrity J, Seaman MS, Chen B 2014. Mechanism of HIV-1 Neutralization by Antibodies Targeting a Membrane-Proximal Region of gp41. Journal of Virology 88(2):1249-1258.

27. Huang J, Kang BH, Pancera M, Lee JH, Tong T, Feng Y, Georgiev IS, Chuang G-Y, Druz A, Doria-Rose NA, Laub L, Sliepen K, van Gils MJ, de la Peña AT, Derking R, Klasse P-J, Migueles SA, Bailer RT, Alam M, Pugach P, Haynes BF, Wyatt RT, Sanders RW, Binley JM, Ward AB, Mascola JR, Kwong PD, Connors M 2014. Broad and potent HIV-1 neutralization by a human antibody that binds the gp41-120 interface. Nature 515(7525):138-142.

28. Zhou T, Georgiev I, Wu X, Yang Z-Y, Dai K, Finzi A, Kwon YD, Scheid J, Shi W, Xu L, Yang Y, Zhu J, Nussenzweig MC, Sodroski J, Shapiro L, Nabel GJ, Mascola JR, Kwong PD 2010. Structural Basis for Broad and Potent Neutralization of HIV-1 by Antibody VRC01. Science (New York, NY) 329(5993):811-817.

29. Walker LM, Huber M, Doores KJ, Falkowska E, Pejchal R, Julien J-P, Wang S-K, Ramos A, Chan-Hui P-Y, Moyle M, Mitcham JL, Hammond PW, Olsen OA, Phung P, Fling S, Wong C-H, Phogat S, Wrin T, Simek MD, Protocol GPI, Koff WC, Wilson IA, Burton DR, Poignard P 2011. Broad neutralization coverage of HIV by multiple highly potent antibodies. Nature 477(7365):466-470.

30. Matja Z. 2009. Purification and Characterization of Proteins. Introduction to Peptides and Proteins, ed.: CRC Press. p 147-158.

31. Siedler M, Kumar V, Chari R, Saluja S, Fraunhofer W. 2015. Development of Drug Product Formulations: Molecular Design and Early Candidates Screening. In Jameel F,

Hershenson S, Khan MA, Martin-Moe S, editors. Quality by Design for Biopharmaceutical Drug Product Development, ed.: Springer New York. p 61-85.

32. Li L, Kantor A, Warne N 2013. Application of a PEG precipitation method for solubility screening: A tool for developing high protein concentration formulations. Protein Science : A Publication of the Protein Society 22(8):1118-1123.

33. Yamniuk AP, Ditto N, Patel M, Dai J, Sejwal P, Stetsko P, Doyle ML 2013. Application of a Kosmotrope-Based Solubility Assay to Multiple Protein Therapeutic Classes Indicates Broad Use as a High-Throughput Screen for Protein Therapeutic Aggregation Propensity. Journal of Pharmaceutical Sciences 102(8):2424-2439.

34. Banks DD, Latypov RF, Ketchem RR, Woodard J, Scavezze JL, Siska CC, Razinkov VI 2012. Native-State Solubility and Transfer Free Energy as Predictive Tools for Selecting Excipients to Include in Protein Formulation Development Studies. Journal of Pharmaceutical Sciences 101(8):2720-2732.

35. Farruggia B, Garcia G, D'Angelo C, Picó G 1997. Destabilization of human serum albumin by polyethylene glycols studied by thermodynamical equilibrium and kinetic approaches. International Journal of Biological Macromolecules 20(1):43-51.

36. Farruggia B, Nerli B, Di Nuci H, Rigatusso R, Picó G 1999. Thermal features of the bovine serum albumin unfolding by polyethylene glycols. International Journal of Biological Macromolecules 26(1):23-33.

37. Trevino SR, Scholtz JM, Pace CN 2007. Amino acid contribution to protein solubility: Asp, Glu, and Ser contribute more favorably than the other hydrophilic amino acids in RNase Sa. Journal of molecular biology 366(2):449-460.

38. Lubiniecki A, Volkin DB, Federici M, Bond MD, Nedved ML, Hendricks L, Mehndiratta P, Bruner M, Burman S, DalMonte P, Kline J, Ni A, Panek ME, Pikounis B, Powers G, Vafa O, Siegel R 2011. Comparability assessments of process and product changes made during development of two different monoclonal antibodies. Biologicals 39(1):9-22.

39. Alsenaidy MA, Jain NK, Kim JH, Middaugh CR, Volkin DB 2014. Protein comparability assessments and potential applicability of high throughput biophysical methods and data visualization tools to compare physical stability profiles. Frontiers in Pharmacology 5:39.

40. More AS, Toprani VM, Okbazghi SZ, Kim JH, Joshi SB, Middaugh CR, Tolbert TJ, Volkin DB 2016. Correlating the Impact of Well-Defined Oligosaccharide Structures on Physical Stability Profiles of IgG1-Fc Glycoforms. Journal of Pharmaceutical Sciences 105(2):588-601.

Chapter 3 Structural Characterization, Physicochemical Stability Profile and Formulation Development of a Double Mutant Heat Labile Toxin (dmLT)-A Novel Protein Based Adjuvant Candidate

3.1 Introduction

There is a clinical need for new adjuvants to enhance and broaden mucosal immune responses for various vaccine candidates. Vaccines administered by the mucosal route have the potential to not only provide both mucosal as well as systemic immunity, but may also result in logistical and regulatory advantages over traditional vaccines given by injection [1-4]. One of the reasons for the current limited availability of vaccines that activate mucosal immunity is the lack of effective mucosal adjuvants. Bacterial enterotoxins such as cholera toxin (CT) and heat labile toxin (LT) are known to be potent mucosal adjuvants; however, their toxicity limits their use in humans[5-7]. *E.coli* LT exists as hetero-hexamer (AB_5) complex consisting of a single enzymatically active A-subunit (i.e., has adjuvant activity and mediates toxicity) which is non-covalently linked to a pentameric B-subunit that is responsible for binding to the host's intestinal epithelial cells [1,8]. The A-subunit is further divided into the enzymatically active A1 subunit and A2 peptide acting as a linker between the A1 and B subunit. Two mutations (R192G/L211A) were introduced into the A-subunit of LT (dmLT) that minimize the molecules toxicity while retaining its ability to stimulate immunogenicity [8, 9].

Multiple studies have shown that the co-administration of dmLT with different antigens such as tetanus toxoid, mycobacterial purified protein derivative, inactivated polio as well as whole cell vaccines against *Helicobacter pyroli*, and *Streptococcus pnuemoniae* enhance immune responses in various animal models [5,8-11]. Recent human studies have also demonstrated the adjuvant potential of dmLT to enhance and broaden mucosal immune responses for enterotoxigenic *E.coli* (ETEC) vaccine candidates such as ETVAX and ACE527 [12,13]. These Phase I/II human clinical studies have shown that addition of dmLT in these vaccine formulations was generally well-tolerated, and had the potential for improved mucosal immune

responses and protective efficacy as well as could potentially lower the antigen dose. A more recent study has shown that the dmLT protein possesses both antigen and adjuvant properties [13,14]. Phase I trials are underway to test the antigenic properties of dmLT as a potential stand-alone vaccine against ETEC caused diarrhea [15].

The inherent structural complexity and marginal stability of protein-based antigens and adjuvants requires extensive analytical characterization to monitor their structural integrity and conformational stability during process and product development. In fact, both analytical characterization and formulation stability studies are a key part of the overall clinical development of vaccine candidates in terms of CMC development and regulatory approval for use in patients[16,17]. For example, the therapeutic efficacy of a vaccine depends on the physicochemical stability of the antigen and adjuvant which in turn can affect the vaccine's potency during manufacturing, long-term storage, shipping and administration[18]. Therefore, there is ongoing need to better characterize and evaluate vaccine antigens and adjuvants to better understand the interrelationship of their physicochemical properties with critical biological attributes (e.g., ability to generate the appropriate immune response) of the vaccine[19]. Development of analytical characterization tools is especially important to facilitate monitoring the biomolecule's key structural and functional properties (critical quality attributes) as a function of process and product changes made during clinical development (i.e., clinical lots made in pilot plant) and/or during post approval manufacturing changes (e.g., regulatory comparability studies)[20].

Apart from analytical characterization, formulation development activities also play a key role in the overall pharmaceutical development of vaccines. However, systematic formulation development studies, which can be used to minimize instability and maintain/augment the

potency of adjuvants, is often poorly recognized in the field of vaccinology[21]. For example, *in vivo* animal studies are often used to monitor adjuvant structural integrity, while, sensitive biophysical and analytical assays can often help to better understand the structural characteristics and the instabilities of adjuvants and link them to the key critical quality attributes of a vaccine such as potency[19].

Since vaccine dosage forms are multicomponent and inherently complex in nature (e.g., biological antigens, adjuvants, excipients), it becomes essential as part of their development to study the factors that can affect their stability and potency. Recombinant or inactivated vaccine antigens, such as proteins, virus-like particles, and inactivated viruses, are often inherently marginally stable and are sensitive to external conditions such as changes in pH and temperature, surface interactions and agitation, light exposure, and even the presence of impurities from excipients[22]. For example, vaccines may be exposed to temperature fluctuations during manufacturing, storage, and transport from the manufacturer to the end user (e.g., clinic site) [23]. The fill finish process can induce mechanical stress on the protein antigen or adjuvant causing aggregation and structural alterations[24,25]. In addition, the lack of a robust cold chain in developing countries [16] can expose vaccines to elevated temperatures, as well as freeze thaw effects, causing degradation and loss of potency.

To design a stable and efficacious vaccine for clinical use, formulation development activities include preformulation characterization of the antigen including forced degradation studies to identify stability indicating assays, formulation design and excipient screening to define stabilizing solution conditions, and accelerated and real time stability studies as well as freeze-thaw studies [19,26] to ensure that the candidate formulations remain stable and maintain potency over a defined shelf life. Pharmaceutical excipients are added not only to stabilize the

vaccine antigen, but also to ensure appropriate interaction with the adjuvant (e.g., binding of antigen to aluminum adjuvant) as well as to maintain appropriate solubility, tonicity, and compatibility with containers and administration procedures [26-29].

In this work, we have characterized the structural and conformational stability profiles of a lyophilized preparation of an early clinical lot of dmLT (after reconstitution) from a pharmaceutical perspective including the aggregation propensity of dmLT due to agitation stress. Reconstituted dmLT samples were shown to be a heterogeneous mixture of intact holotoxin (AB_5) and free B_5 subunit which also contained low levels of glycated and aggregated protein. The physical stability profile of dmLT across different solution pH (5.5-8.0) and temperature conditions (10-90^{o}C) was also evaluated. Forced chemical degradation studies (e.g., elevated pH values, or addition of hydrogen peroxide) of the reconstituted dmLT sample were then used to identify specific "hot-spot" sites of Asn deamidation and Met oxidation. These results will not only enable characterization of improved manufacturing processes to produce future clinical lots of dmLT from an analytical comparability perspective, but will also facilitate monitoring lot-to-lot variability of dmLT made from the same process. In addition, we also seek to utilize the knowledge gained from the structural characterization and elucidation of physicochemical degradation pathways of dmLT to develop a more stable bulk formulation of dmLT that does not require lyophilization and permits maximal flexibility for use in the future in different vaccine dosage forms with different antigens.

3.2 Materials and Methods

3.2.1 Materials

Lyophilized vials of dmLT, produced and purified from *E.coli* as described elsewhere [8], were received from Walter Reed Army Institute of Research, MD, (Batch No: BPR-1037.00, 21 Nov

2011) and stored at -20 ^{o}C. Freeze-dried samples contained 0.7 mg protein in 42.7 mM Sodium phosphate, 10.7 mM Potassium phosphate, 82 mM NaCl, 5% Lactose, pH 7.4 (hereafter referred to as formulation buffer). Components of the formulation buffer prepared in the KU laboratory for dilution of samples and background correction of analytical methods, including monobasic potassium phosphate (N.F. grade), dibasic sodium phosphate (U.S.P grade), sodium chloride (U.S.P grade), and lactose monohydrate (N.F. grade), were purchased from Spectrum Chemical Mfg. Corp. (Gardena, CA). The lyophilized vials (0.7 mg dmLT/vial) were reconstituted in 0.7 mL of HPLC grade water (Fisher Scientific, PA) immediately prior to analysis and further diluted with formulation buffer as required (samples were not stored at lower concentrations/temperatures for analysis at a later time). For excipient screening, dialysis of dmLT protein was performed in Slide-A-Lyzer Mini Dialysis Devices (Product #88403, Thermo Scientific, Rockford, IL) with a 3,500 Da molecular weight cutoff. All reagents and excipients for preparing different formulations were purchased from Sigma-Aldrich (St. Louis, MO). Carbohydrates such as trehalose, sucrose and mannitol were purchased from Pfanstiehl Inc. (Waukegan, IL). All excipients were of high purity grade (>99 %).

3.2.2 Methods

3.2.2.1 Intact Protein Mass Spectrometry

ESI spectra of dmLT under both non-reducing and reducing conditions were acquired on a SYNAPT G2 hybrid quadrupole / ion mobility / Tof mass spectrometer (Waters Corp., Milford, MA). The instrument was operated in a sensitivity mode with all lenses optimized on the MH+ ion from the control Leucine Enkephalin. The sample cone voltage was 40eV. Argon was admitted to the trap cell that was operated at 4eV for maximum transmission. Spectra were acquired at 9091 Hz pusher frequency covering the mass range from 100 to 3000 u and

accumulating data for 2 seconds per cycle. Time to mass calibration was made with NaI cluster ions acquired under the same conditions. Mass spectra of [Glu^1]-Fibrinopeptide B were acquired in parallel scans and doubly charged ions at m/z 785.8426 were used as a lock mass reference. Samples were desalted on a reversed phase PRP-1 column, 1 cm, 1 mm I.D. (Hamilton, 10 µm particles packed by hand) using a NanoAcquity chromatographic system (Waters Corporation). The mobile phase solvents were A (99.9% H_2O, 0.1% formic acid) and B (99.9% acetonitrile, 0.1% formic acid). A short gradient was developed from 1 to 70% B in 4 min with a flow rate of 20 µL/min. MassLynx 4.1 software (Waters Corporation) was used to collect the data and to deconvolute the protein spectra for molecular weight determination.

3.2.2.2 Peptide Mapping

For proteolysis under reducing conditions, a sample of dmLT (50 µg) was incubated with 20 mM DTT and for 60 min at either 37 ºC or 80 ºC in both the presence and absence of 3M guanidine-HCl (GuHCl). The reduced Cys were then alkylated with 40 mM Iodoacetamide at 37ºC for 30 min. The samples were incubated at 37 ºC overnight with 2 µg of trypsin or chymotrypsin. Trifluoroacetic acid (0.05%) was added to quench the proteolysis and 12.5 µg of digested dmLT was subjected to LC-MS. For proteolysis under non-reducing conditions, a similar procedure was followed except DTT was omitted during the reduction step.

The peptides from the digested protein solution were separated by a liquid chromatography system (Thermo Scientific, Waltham, MA) prior to analysis. Peptides were injected onto a C_{18} column (1.7 µm, 2.1 x 150 mm, Waters) and an 85 min 0-30% B gradient (A: H_2O and 0.05% trifluoroacetic acid; B: ACN and 0.05% trifluoroacetic acid; 200 µl/min flow rate) for separation. MS was performed using a LTQ-XL ion trap (Thermo Scientific) and the Xcalibur *2.0* software (Thermo Scientific). The instrument was also tuned using a standard calibration peptide

(Angiotensin II, Sigma) for maximal sensitivity before running any experiments. The mass spectra were acquired in the LTQ over a mass range of m/z 300-2000. The ion selection threshold was 20,000 counts and the dynamic exclusion duration was 10 sec.

Raw experimental files were initially evaluated manually to determine if the ion counts and fragmentation of each peptide were sufficient for further analysis. The raw data files were then processed using *PepFinder 2.0* software (Thermo Scientific). The database used for this experiment consisted of dmLT-A and dmLT-B primary sequences [30] and the protease sequence. Potential Cys carbamidomethylation were included during the analysis. Peptide assignments of MS/MS spectra were validated using a confidence score of ≥95% and some manual validation.

3.2.2.3 SDS-PAGE

The dmLT samples were run under both non-reducing and reducing conditions by SDS-PAGE. The dmLT samples were mixed with 4X NuPAGE-LDS sample buffer (Life Technologies, Grand Island, NY) to a final concentration of 1X. For reduced samples, 50 mM dithiothreitol (DTT) (Life Technologies, Grand Island, NY) was added. The samples were incubated at 95 ^{o}C for 5 min. Ten µg of dmLT protein was analyzed by SDS-PAGE on a 4-12% Bis-Tris gradient gel (1.0 mm x 10 wells, #NP0321BOX) using 1X MES running buffer (Life Technologies, Grand Island, NY). Protein bands were visualized by staining with Coomassie blue R250 (Teknova, Hollister, CA) and destained with ultrapure water.

3.2.2.4 Far-UV Circular Dichroism Spectroscopy

Far-UV circular dichroism (CD) spectroscopy of dmLT was performed using a Chirascan-plus Circular Dichroism Spectrometer (Applied Photophysics Ltd, Leatherhead UK) equipped with a Peltier temperature controller and a 4-position cuvette holder. Quartz cuvettes (0.1 cm path length) sealed with a teflon stopper (Starna Cells Inc., Atascadero, CA) were used.

The spectra of dmLT were collected from 200-260 nm using 1 nm steps and 0.5 s sampling time. Thermal melts were performed over a temperature range of 10 to 90 °C. The spectra were collected at 2.5 ºC intervals with a 2 min equilibration time at each temperature. The final protein concentration of the dmLT sample was 0.2 mg/mL and the measurements were conducted in triplicate.

3.2.2.5 Fourier Transform Infrared Spectroscopy (FTIR)

FTIR spectra of dmLT were collected with a Bruker Tensor 27 spectrometer (Bruker Optics, Billerica, MA) equipped with a temperature controlled BioATR cell and MCT detector with constant purging with N_2. Spectra were recorded from 4000 to 600 cm^{-1} at 22 °C. A resolution of 4 cm^{-1} was used and 256 consecutive scans were collected for dmLT sample at ~0.9 mg/mL. Buffer spectra were also recorded under each experimental condition and subtracted from the sample spectra using a straight baseline between 1770 and 2050 cm^{-1} as the criterion for correct subtraction. The resulting blank-subtracted spectra were smoothed with a Savitsky-Golay function and second-derivative analysis was used to identify band components in the amide-I region. Curve fitting was then performed using a mixed Gaussian–Lorentzian function between 1700 and 1600 cm^{-1}. Subtraction, smoothing and second-derivative analysis were performed using OPUS V6.5 software (Bruker Optics).

3.2.2.6 Intrinsic Tryptophan Fluorescence Spectroscopy

The intrinsic tryptophan fluorescence of dmLT was measured in triplicate using a Photon Technology International (PTI) spectrofluorometer (Lawrenceville, NJ) equipped with a turreted four-position Peltier-controlled cell holder and a xenon lamp. Fluorescence emission spectra of dmLT at 0.2 mg/mL using 1 cm path length quartz cuvettes were recorded as a function of temperature (10-90 ºC). An excitation wavelength of 295 nm was used (>95% Trp emission)

with the slit width set at 4 nm. Emission spectra were collected from 305-405 nm with a step size of 1 nm and an integration time of 1 s. The spectra were collected at 2.5 ºC intervals with a 2 min equilibration time at each temperature. The initial signal was kept at ~800,000 counts per second for fluorescence spectra and an emission maximum of ~20,000 counts per second for light scattering spectra. The data analysis was performed using the in-house software (Middaugh Suite). The corresponding buffer spectrum was subtracted from each protein spectrum prior to data analysis. The emission peak position was determined using a mean spectral center of mass method (MSM) executed in the Middaugh Suite. Although this calculation method increases the signal to noise ratio for more accurate determination of lambda max values, it shifts the apparent peak position by 5-10 nm from their actual values. The T_{onset} values were determined by identifying the point at which the baseline deviated from linearity using Origin software.

A second photomultiplier located 180° to the fluorescence detector was used to study aggregation behavior of dmLT. The static light scattering intensity values were collected simultaneously during the intrinsic fluorescence experiments using a 0.25 nm slit width. The scattering intensities at 295 nm were obtained as a function of temperature (10-90ºC). Scattering from the buffer alone was subtracted from each protein sample value before data analysis.

3.2.2.7 Extrinsic Fluorescence Spectroscopy

8-Anilino-1-naphthalene sulfonate (ANS) was used as an extrinsic fluorescence probe in the presence of dmLT with the same instrument as described above. A dye to protein molar ratio of 25:1 was used for sample preparation. ANS was excited at 372 nm, and emission spectra of ANS was collected from 400-600 nm every 2 nm as a function of temperature from 10 to 90^{o}C. The corresponding buffer spectrum was subtracted from protein spectrum prior to data analysis. The emission peak intensity was determined using a mean spectral center of mass method

(MSM) executed in the Middaugh Suite. The T_{onset} values were determined by identifying the point at which the baseline deviated from linearity using Origin 8.0 software.

3.2.2.8 Differential Scanning Calorimetry

Differential Scanning Calorimetry (DSC) thermograms for dmLT were collected with a Microcal VP-DSC capillary cell microcalorimeter (GE Health Sciences, Pittsburgh, PA). Thermograms were recorded from 10 to 100 °C at a scan rate of 1 °C/min. A protein concentration of 0.4 mg/mL was employed and the measurements were performed in triplicate. A buffer baseline was subtracted from each protein thermogram and the data were normalized to molar heat capacity using Microcal DSC software in Origin 7.0 (OriginLab, Northampton, MA). The peaks were fitted using a mathematical model in Origin 7.0 to quantify T_{onset} and T_m values.

3.2.2.9 Sedimentation Velocity Analytical Ultracentrifugation

Sedimentation velocity analytical ultracentrifugation (SV-AUC) experiments were performed with an Optima XL-I (Beckman Coulter, Fullerton, CA) analytical ultracentrifuge equipped with a scanning UV-Visible optical system. All experiments were conducted at 20 °C after 1h of equilibration after the AUC reached temperature, at a rotor speed of 50,000 RPM with detection at 280 nm. Samples and reference were loaded into Beckman charcoal-epon two sector cells with a 12 mm centerpiece and either sapphire or quartz windows.

The data were analyzed using Sedfit (courtesy of Peter Schuck, NIH). A partial specific volume of 0.73 mL/g was calculated for dmLT using Sednterp (courtesy of Professor Thomas Laue, University of New Hampshire) based on amino acid sequence, and used in the analysis. The buffer density and viscosity used in the analysis were also calculated using Sednterp software based on buffer composition. A continuous c(s) distribution was used with 200 scans. A range of 0 to 15 svedbergs was used, after verifying that there was no signal sedimenting outside

of this range, with a resolution of 300 points per distribution and a confidence level of 0.95. Baseline, radial independent noise, and time independent noise were fit, while the meniscus and bottom positions were set manually. Integrations were performed in Origin (OriginLab Corporation, Northampton, MA) after importing the distributions.

3.2.2.10 Hydrophobic Interaction Chromatography (HIC)

A Shimadzu Prominence UFLC HPLC system equipped with a diode array detector was used. 20 μg of protein was injected onto a TSKgel Butyl-NPR column (4.6 x 100mm, 2.5μm TOSOH Biosciences P/N 42168) for each run, and the experiment was performed in triplicate. The mobile phases consisted of (A) 2M ammonium sulfate, 20 mM sodium phosphate, pH 6.8; (B) 20 mM sodium phosphate, pH 6.8. The columns were operated at 25ºC and equilibrated with mobile phase A (20 mM sodium phosphate, 2 M ammonium sulfate, pH 6.8) prior to sample injection. A flow rate of 0.7 mL/minute was used with a 60 min run time. Chromatographic separation was then conducted in a step wise gradient of 0-5 min (0% B), 5-35 min (0→60% B), 35-40 min (60→100% B), 40-45 min (100% B), and 45-60 min (0% B). Protein peaks were monitored using the absorbance signal at 214 nm. LC solutions software (Shimadzu) was used for data analysis.

3.2.2.11 Reversed-Phase Ultra High Performance Liquid Chromatography (RP-UHPLC)

A Thermo Ultimate 3000 UHPLC system (Thermo Scientific) equipped with a diode array detector was used. 20 μg was injected onto a Waters Acquity C18 column (2.1 x 150 mm, 1.7 μm Waters Corporation) for each run, and the experiment was performed in triplicate. The columns were operated at 60 ºC and equilibrated with 99% mobile phase A (0.1% TFA, water) and 1% mobile phase B (0.1% TFA, acetonitrile) prior to sample injection. A flow rate of 0.2 mL/min was used with a 35 min run time. The mobile phase gradient consisted of 1% B (5 min),

1-60% B (10 min), 75% B (12 min), 75%B (15 min), 75-1% B (22 min), 99% B (28 min) and 1% B (35 min). Chromeleon software (Thermo Scientific) was used for data analysis.

3.2.2.12 Construction of Three Index Empirical Phase Diagram (EPD) and Radar Plots

For the physical stability studies, dmLT was dialyzed into the formulation buffer (pH 5.5-8.0, at 0.5 pH unit increments). Dialysis was performed at 4^{o}C using Slide A Lyser dialysis devices (ThermoScientic, Rockford, IL) with 3.5-kDa molecular weight cutoff with four buffer exchanges. Samples were then diluted to 0.2 mg/mL for intrinsic tryptophan fluorescence and static light scattering measurements while a higher concentration of 0.4 mg/mL was used for DSC. Data from intrinsic tryptophan fluorescence peak position, the static light scattering signal at 295 nm, and DSC were used in the construction of the three-index EPD and radar chart using in-house software *(Middaugh Suite)*.

A detailed description of the construction of three-index EPD and radar chart can be found elsewhere [31,32]. Briefly, the three index EPD and radar chart use a specific color (red (R), green (G), blue (B)) and shape (an equiangular polygon) respectively to reflect the characteristics of the underlying biophysical data, that define protein structural states as a function of solution variables like temperature and pH. For three-index EPD from this work, data from static light scattering, differential scanning calorimetry and MSM peak position were mapped to red, green and blue color respectively. Data sets obtained from each of above biophysical techniques were assigned to a color gradation from black to the full color of their technique, with minimum value in the dataset assigned a black color and maximum value to the full color intensity. However, for DSC the color assignment was reversed where the maximum value was mapped to black and the least value to maximum color intensity (i.e. green for DSC) for better visualization. Thus, a color produced by the summation of these RGB components produced a single color at each point in

pH and temperature space, which was mapped to a specific structural state of dmLT. For example, in the native state of dmLT, the light scattering, MSM peak position and DSC will have their least signals (black color) but this combination showed a green color, because the DSC color assignment was reversed and shows the maximum color for the lowest values. The individual RGB components were also displayed in a separate panel alongside the 3-index EPDs (Figure 4D) because it is difficult to determine the amount of an RGB component with a given color. The explicit display of its RGB components helps to better understand the interpretation of a color and more distinctly detect changes in the structure of the protein. A k-means clustering algorithm using in-house software (*Middaugh Suite*) was applied to the datasets to better probe regions of structural similarities and differences.

Radar plots use a polar coordinate system incorporating n axes, in which each axis represents a value of one technique. The changes in signal for each technique was integrated and normalized from 0 to 1 to construct structure indexes, which are mapped to points in the polar coordinates which are connected to form a polygon. Zero and 1 represent the most native-like structure and the most altered state, respectively. Small polygons represent more native-like structure, while larger polygons represent more altered structures. A K-means clustering algorithm was employed to define boundaries of different apparent phases. In this study, intrinsic tryptophan fluorescence peak position, static light scattering signal at 295 nm, and differential scanning calorimetry thermograms were used for construction of the radar charts. These techniques monitor different structural aspects of dmLT: Trp fluorescence (peak position) monitors tertiary structure, light scattering aggregation behavior and DSC measures the overall thermal stability of the protein.

3.2.2.13 Aggregation study of dmLT

For colloidal stability studies during agitation stress, lyophilized vials of dmLT (BPR # 1037.00) were reconstituted in 0.7 mL of HPLC grade water prior to analysis resulting in a dmLT solution in 42.7 mM Sodium phosphate, 10.7 mM Potassium phosphate, 82 mM NaCl, 5% Lactose, pH 7.4 (formulation buffer) at 0.9 mg/mL. The protein solution was further diluted to 0.2 mg/mL using the formulation buffer. Three mL Fiolax clear, Schott (Lebanon, PA) glass vials were then filled with 1.1 mL of 0.2 mg/mL dmLT in formulation buffer and stoppered (Cat#10122128, West Pharmaceutical, PA). The vials were then shaken sideways at 300 RPM for 2h at room-temperature. Control vials were filled with 1.1 mL of the formulation buffer alone and shaken under similar conditions. All techniques were performed in triplicate.

3.2.2.14 Turbidity

The reconstituted dmLT samples were visually assessed for visible particles with an Adelphi Apollo II liquid viewer (Adelphi Co., UK). Turbidity was measured for all samples in triplicate using a Hach 2100 AN Laboratory Turbidimeter, at a concentration of 0.2 mg/mL. Prior to analysis, the instrument was calibrated using standards in the range of <0.1 NTU to 2,000 NTU. The turbidity of the empty tube and buffer were subtracted from all readings prior to reporting.

3.2.2.15 UV-Visible Absorption Spectroscopy

The UV-Visible absorption spectra of dmLT were recorded with an Agilent 8453 UV-Visible spectrophotometer (Palo Alto, CA) equipped with a Peltier temperature controller. Spectra were collected from 190-1100 nm at an experimental resolution of 1 nm in 1 cm path length quartz cuvette. The concentration was calculated based on the reported extinction coefficient of cholera toxin (0.1% solution) 1.14 mg/ml^{-1} cm^{-1} [1]. Samples were measured before

and after centrifugation (5000 rpm for 15 min, Thermo Scientific, Sorvall Centrifuge, MA). The instrument was first blanked using the formulation buffer prior to measuring solutions containing dmLT. All UV-Visible absorbance spectra were corrected for light scattering using a technique included in the manufacturers data analysis software (Chemstation UV-Vis analysis software, Agilent Technologies): first, the spectra data where the optical density values are only due to light scattering (350-400 nm) are fitted to an equation, and then this curve is extrapolated across the entire protein spectrum and then subtracted from the spectrum, to produce the light-scatter corrected absorbance spectra. The optical density value at 350 nm (OD_{350}) was also recorded from the uncorrected spectra. A similar procedure was followed for measuring protein concentration after dialysis, both before and after centrifugation. The percentage loss in protein compared to protein stock was also calculated.

3.2.2.16 Micro-Flow Imaging

The total number and distribution of sub-visible particles in the range of 2 µm to 100 µm were examined using a MFI DPA-4200 (Protein Simple, Santa Clara, CA) system with a 100 µm silane coated flow cell. Measurements were made in triplicate at ambient temperature for all samples. Illumination was optimized using particle free water prior to all measurements.

3.2.2.17 Resonant Mass Measurement (RMM)

The total number and distribution of sub-micron particles in the range of 200 nm to 1 µm were examined using an Archimedes particle metrology system (Malvern Instruments Inc., Westborough, MA) equipped with Hi-Q microsensor. Prior to analysis, the flow cell was flushed with particle free water to achieve a clean baseline. All measurements were performed in triplicate at ambient temperature. A limit of detection of 0.03 Hz was used, and the length of

each measurement was set to 200 particles. A particle density of 1.37 g/mL was used in the analysis.

3.2.2.18 Nanosight Tracking Analysis (NTA)

The total number and distribution of sub-micron particles in the range of 50 nm to 1 µm were examined using A NanoSight LM-14 (Malvern Instruments Inc., Westborough, MA) equipped with CCD camera and 635 nm laser. Measurements were made in triplicate at ambient temperature for all samples. Three sixty second measurements were taken from different areas of the flow cell per triplicate for a total of nine measurements per experimental condition. NanoSight NTA version 2.2 software was used for data analysis, with a camera gain of 5 and a detection threshold of 25.

3.2.2.19 Size Exclusion Chromatography (SEC)

A Shimadzu Prominence UFLC HPLC system equipped with a diode array detector was used. dmLT samples (+/- shaking, in triplicate) were centrifuged for 5 min at 13,000 rpm, and 20 µg was injected onto a TSK-Gel BioAssist G3SWxl column (7.8 x 300 mm, TOSOH Biosciences, King of Prussia, PA) and the corresponding guard column (TOSOH Biosciences). The columns were operated at 30 ºC and equilibrated with at least 10 column volumes of mobile phase (0.2 M sodium phosphate, pH 6.8) prior to sample injection. A flow rate of 0.7 mL/min was used with a 30 min run time. A gel filtration standard (Bio-Rad, Hercules, CA) was subjected to SEC before and after three runs of dmLT to ensure column and HPLC system integrity.LC solutions software (Shimadzu, Kyoto, Japan) was used for data analysis.

3.2.2.20 Forced Deamidation Method

Forced deamidation studies were carried out with dmLT formulated under three different solution pH conditions:

a) 42.7 mM Sodium Phosphate, 10.7 mM Potassium Phosphate, 82 mM NaCl, 5% Lactose, pH 7.4 (formulation buffer)
b) 42.7 mM Sodium Phosphate, 10.7 mM Potassium Phosphate, 82 mM NaCl, 5% Lactose, pH 8.0
c) 250 mM Ammonium Bicarbonate, 21.4 mM Sodium Phosphate, 5.4 mM Potassium Phosphate, 82 mM NaCl, 5% Lactose, pH 9.0

The dmLT samples in the three different formulations (at 0.4 mg/mL) were incubated in triplicate at 4^{o}C for 7 days. On days 0 and 7, the samples were subjected to intact mass analysis and peptide mapping.

3.2.2.21 Forced Oxidation Method

For forced oxidation studies, dmLT samples at 0.4 mg/mL in formulation buffer were oxidized in triplicate for one hour at ambient temperature at each of the following H_2O_2 concentrations: 0.025 %, 0.05 %, 0.1 %, 0.25 %, 0.5 % and 1% v/v. Reactions were quenched with D-Met and all samples were subjected to intact mass analysis, RP-UHPLC and peptide mapping.

3.2.2.22 Thermal and agitation stress studies of dmLT

For excipient screening studies as a function of both a thermal stress and shake-stress, lyophilized dmLT samples (BPR # 1037.00) were reconstituted in HPLC grade water at room temperature. Reconstitution time was less than 1 min. Multiple vials of reconstituted dmLT were then pooled and the protein concentration was determined (~1 mg/mL). The samples were centrifuged for 15 min at 5,000 rpm and the protein concentration was determined (~0.9 mg/ml). The dmLT protein was dialyzed in Slide-A-Lyzer Mini Dialysis Devices (Product #88403, Thermo Scientific, Rockford, IL) with a 3,500 Da molecular weight cutoff and a 2 mL capacity

against various base buffers, (10 mM Sodium Phosphate, containing 50 or 150 mM NaCl, pH 6.0) or (50 mM sodium phosphate, 50 mM NaCl, pH 7.4) overnight at 4°C with three buffer changes at three hr. intervals, and incubation overnight before dialysate recovery. The protein concentration in the dialysate was determined both pre and post centrifugation (13,000 rpm for 5 min). Excipients were prepared as concentrated solutions in the indicated base buffers. Each of the excipients, dmLT, and additional base buffer were then combined to achieve the concentrations of excipients indicated in the text and a final concentration of 0.15 mg/mL dmLT. For shake stress studies, 2 mL Fiolax clear, Schott (Lebanon, PA) glass vials were filled with 0.6 mL of 0.15 mg/mL dmLT and stoppered (Cat#10122128, West Pharmaceutical, PA). The vials were then shaken sideways at 300 RPM for 4 hr. at room-temperature. Additionally, control vials were filled with 0.6 mL of each buffer without dmLT and shaken under similar conditions. All analytical techniques mentioned below were performed in triplicate on control/non-shake samples and the 4 hr. shaking stress samples.

3.2.2.23 Freeze-thaw studies of dmLT

The dmLT vials were reconstituted with water and dialyzed against the indicated base buffers (see above) in Slide-A-Lyzer Mini Dialysis Devices (Product #88403, Thermo Scientific, Rockford, IL) with a 3,500 Da molecular weight cutoff overnight at 4°C with three buffer changes at three hr. intervals, and incubation overnight before dialysate recovery. Excipients were prepared as concentrated solutions in indicated base buffer. Each of the excipients, dmLT, and additional base buffer were combined to achieve the final formulations as indicated in text. Then, 1.1 mL of dmLT at 0.4 mg/mL was filled in 3 mL Fiolax clear, Schott (Lebanon, PA) glass vials and then frozen at -80^{o}C for 24 hrs. The vials were thawed at room temperature for ~20 min for complete thawing. Samples were then frozen again at -80^{o}C and the freeze-thaw

(F/T) cycles were repeated five times. Samples were analyzed at 0, 1 and 5 F/T cycles using UV-Visible absorption spectroscopy, hydrophobic interaction chromatography described above.

3.2.2.24 OD_{350} measurements

Thermal stress measurements were performed using a Cary 100 UV-Visible spectrophotometer (Varian medical Systems, Inc., Palo Alto, California) equipped with a 12 cell holder with a Peltier type temperature controller. Samples contained 0.15 mg/ml protein with a total volume of 225 µl in 1 cm path length quartz cells. Optical density at 350 nm (OD_{350}) was monitored as the temperature was raised in increments of 1.25˚C from 10 to 90˚C with a heating rate of 60˚C/h. Protein samples were run in triplicate and corresponding buffer blanks were run and subtracted from each sample. The OD_{350} value was plotted against temperature, and the temperature at which the OD_{350} value reached an optical density value of 0.1 was determined.

3.2.2.25 Chemical Stability Studies with dmLT in Candidate vs Current Formulation (Oxidation and Glycation)

Forced glycation studies were carried out with dmLT in the two formulations namely:

a) 42.7 mM Sodium Phosphate, 10.7 mM Potassium Phosphate, 82 mM NaCl, 5% Lactose, pH 7.4 (Current formulation)
b) 50 mM Sodium phosphate, 50 mM NaCl, 10% sucrose, 5 mM methionine, 0.1% PS-80, pH 7.4 (Candidate Formulation)

The dmLT samples in the two different formulations (at 0.4 mg/mL) were incubated in triplicate at 40^{o}C for 7 days. On days 0 and 7, the samples were subjected to intact mass analysis

For forced oxidation studies, dmLT samples at 0.4 mg/mL in the current and candidate formulation was oxidized in triplicate for four hours at 37^{o}C with each of the following H_2O_2

concentrations: 0, 1, 2.5 and 5 mM. Reactions were quenched with 70 mM of D-Met and all samples were subjected to intact mass analysis.

3.3 Results

3.3.1 Primary Structure and Post-translational Modification Analysis

Figure 3.1A shows the intact mass spectrometry data of dmLT under non-reducing conditions. This shows three peaks that corresponded to the dmLT A chain (27,645.5 $\pm$ 0.2 Da), B chain (11,719.1 $\pm$ 0.1 Da) and modified B chain (12,043.0 $\pm$ 0.4 Da). The modified B chain with a molecular weight increase of 323.5 Da could potentially be a glycated species since lactose, a known reducing sugar, is present in the lyophilized formulation (see below). Based on the relative abundance of the native and glycated B-chain (Figure 3.1A), there was only partial (~20%) glycation of the B-chain.

The dmLT protein was then subjected to peptide mapping analysis to confirm the primary amino acid sequence of the protein. Two different proteases (chymotrypsin and trypsin) were required for digesting the A-chain and B-chain of dmLT, respectively, with high sequence coverage. Figure 3.1B and 3.1C shows the $UV_{214\ nm}$ chromatogram of the A-chain and B-chain, respectively. The A chain of dmLT was completely digested at 37^{o}C with chymotrypsin in the presence of 3M GuHCl, but complete digestion of the dmLT-B chain was only accomplished by reduction at a higher temperature (80ºC) in 3M GuHCl and then treating the sample with trypsin overnight at 37 ºC. Using these optimized conditions, sequence coverage of $\geq$ 95% was attained for both the A and B-chain of dmLT (Supplemental Figure 3.1). The requirement of two different experimental conditions to achieve proteolysis suggested not only higher proteolysis resistance, but increased thermodynamic stability, of the B chain compared to the A-chain (see below).

Post translational modifications such as Met oxidation or Asn deamidation were not detected in either A-chain or B-chain by peptide mapping analysis (data not shown). However, a glycated peptide was identified within the dmLT B-chain following trypsin proteolysis. A mass difference of 324 Da (seen by intact mass spectrometry as described above) was observed between two peptides peaks, eluting at 44.4 min (monoisotopic mass of 2,814.6 Da) and 45.1 min (monoisotopic mass of 2,517.6 Da) indicated by arrows in Figure 1C. Following automated identification and manual verification, the 45.1 min peptide was identified as Ile^{82}-Asn^{103} (containing a carbamidomethylation modification at Cys^{86}). Given the labile nature of a lactose moiety in mass spectrometry, the 44.5 min species was identified manually using the MS/MS spectra of the 948.2 m/z precursor ion (Figure 3.1D). Multiple b- and y-ions corresponded to Ile^{82}-Asn^{103} with Lys^{84} containing a +324 Da modification. Additional analysis of overlapping peptides supported Lys^{84} as the site of glycation (data not shown). Interestingly, no glycation was observed at Lys^{91}, which was within the same Ile^{82}-Asn^{103} peptide.

3.3.2 Protein Size and Purity

A combination of SDS-PAGE, sedimentation velocity analytical ultracentrifugation (SV-AUC), hydrophobic interaction chromatography (HIC) and reversed phase ultrahigh pressure chromatography (RP-UHPLC) were used to evaluate the protein size and purity. Reconstituted dmLT was composed of two protein bands as observed under denaturing conditions by both non-reducing and reducing SDS-PAGE (Figure 3.2A). The apparent molecular weights of these two bands (~28 and ~12 kDa) corresponded to the A chain (theoretical MW: 27.6 kDa) and B chain (theoretical MW: 11.7 kDa) of dmLT. Protein purity was estimated to be >99 % and no other protein impurities were visually observed by SDS-PAGE.

The size and purity of dmLT were then assessed under non-denaturing solution conditions by sedimentation velocity analytical ultracentrifugation (SV-AUC). SV-AUC showed two main species at 3.5 $\pm$ 0.1 s and 4.3 $\pm$ 0.1 s (Figure 2B), which accounted for 26 $\pm$ 3 % and 72 $\pm$ 4 % of the total peak area, respectively for triplicate measurements. The deconvoluted molecular weights of these two species corresponded to ~59 kDa (3.5s) and ~86 kDa (4.5s) species. The 59 kDa species is consistent with a putative B_5 species and the 86 kDa population probably corresponds to an intact AB_5 dmLT complex. A small amount (~1 $\pm$ 1 %) of larger species (~6-8s) was also observed in the reconstituted sample that represents larger oligomeric or aggregated species (inset, Figure 3.2B).

To further assess the heterogeneity of free B_5 versus intact dmLT (AB_5), HIC and RP-UHPLC methods were developed (Figure 3.2C and 3.2D). The HIC results also showed that this particular dmLT sample contained a heterogeneous mixture of the intact holotoxin (AB_5), and free B_5 subunit that accounted for 73 ± 1 % and 27 ± 1% of the total peak area, respectively for triplicate measurements (consistent with SV-AUC results). By RP-UHPLC analysis, the relative % of AB_5 was 31 $\pm$ 1 % and free B_5 was 69 $\pm$ 1 % for triplicate measurements. Interestingly, the relative % peak area of free B-chain versus AB_5 complex was seen as comparatively more by RP-UHPLC than by HIC, likely due to the presence of trifluoroacetic acid in the RP-UHPLC mobile phase which exposed dmLT to low pH conditions (unlike the HIC mobile phase in which dmLT remained under neutral pH conditions). Low pH conditions have been shown to cause the dissociation of the A-subunit from the B-subunit as demonstrated by Lonnroth et al. and Van Heyningen et al. for the related cholera toxin[33,34]. As a result, the free B chain peak area increased while a reduction in peak area of AB_5 complex was observed. To further confirm the nature of the two species that were observed, the two peaks were collected during HIC and RP-

UHPLC and subjected to intact mass spectrometry (Supplemental Figure 3.2) which showed their molecular weights to be consistent with the presence of free B chain (MW ~11,719 Da) and AB_5 (A-chain MW ~27,645 Da and B-chain MW ~11,719 Da). The glycated B-chain (MW ~12,043 Da) was present in both the free B-chain and AB_5 components.

3.3.3 Higher Order Structure (HOS) and Overall Conformational Stability

Circular dichroism (CD) and Fourier transform infrared spectroscopy (FTIR) were used to monitor the overall secondary structure of dmLT. At 10^{o}C, CD in the far UV region (200-260 nm) showed a broad minimum between 215-220 nm suggesting beta-sheet structure as the predominant secondary structure (Figure 3.3A). The second derivative spectrum in the Amide 1 region (1700-1600 cm^{-1}) of dmLT by FTIR spectroscopy showed multiple peaks suggesting the presence of several secondary structural components within the protein (see Figure 3.3 B and Supplemental Table 3.1 for peak assignments). The majority of these peaks (1631, 1676 and 1690 cm^{-1}) corresponded to beta structure in the protein supporting the CD results. The overall secondary structure content within the dmLT sample was further quantified using deconvolution of the Amide I peak. The relative percentage of alpha helix, beta sheet and beta turns/unassigned were 26 $\pm$ 3 %, 58 $\pm$ 8%, and 16 $\pm$ 9 %, respectively for triplicate measurements.

Intrinsic Trp fluorescence spectroscopy was performed to evaluate the overall tertiary structure of dmLT (at 10^{o}C) and to monitor the conformational stability of the protein as a function of temperature (10 to 90^{o}C). The fluorescence spectrum of dmLT (see Figure 3.3C inset) showed the wavelength of maximum intensity (λ_{max}) at 332 nm at 10^{o}C indicating a relatively hydrophobic environment for the average Trp residue. After heating up to 90^{o}C, λ_{max} red shifted to 348 nm indicating the average Trp residues to be in relatively more hydrophilic environment demonstrating extensive structural alterations in the protein's tertiary structure upon

heating. The plot of peak position as a function of temperature (Figure 3C) showed two thermal transitions in the dmLT molecule above 45^{o}C indicated by arrows.

The aggregation behavior of dmLT was studied by simultaneous monitoring of light scattering (at 295 nm) during intrinsic fluorescence spectroscopy. Light scattered from the dmLT solution as a function of temperature (10 to 90°C) was monitored (Figure 3.3D) which resulted in significant scattering beginning at ~46°C (T_{onset}) presumably due to aggregation of the A chain in dmLT. Further increase in temperature increased the scattering intensity before dropping twice above 55 and 80°C, a result probably due to precipitation of the A chain and B chain, respectively (see Figure 3.3D).

Extrinsic ANS (8-Anilinonaphthalene-1-sulfonic acid) fluorescence spectroscopy was also used, as a complementary technique to intrinsic Trp fluorescence, to monitor changes in the overall tertiary structure of dmLT by detecting increased fluorescence intensity of ANS, due to exposure to increased apolar environments presumably as a result of structural changes and/or aggregate formation in the protein. A blue shift in the emission maximum from 490 nm (at 10°C) to 480 nm (at 90°C) (Figure 3.3E, inset) indicated increased accessibility of the ANS dye to protein's apolar interior/surfaces suggesting tertiary structure alterations in dmLT (and/or aggregation) with the increase in temperature. An increase in fluorescence peak intensity (T_{onset} of 45°C) was observed as the sample was heated from 10 to 90°C (Figure 3.3E) implying protein unfolding and concomitant protein aggregation at higher temperatures, an observation consistent with intrinsic Trp fluorescence and static light scattering results. Similar to intrinsic Trp fluorescence results, two thermal structural transition events were also observed by ANS fluorescence peak intensity as depicted by arrows in Figure 3.3E.

The overall conformational stability of dmLT was further assessed by differential scanning calorimetry (DSC) as the sample was heated from 10 to 100°C. As shown in Figure 3.3F, two major endothermic peaks were observed at approximately 52°C and 80°C, with onset temperatures of ~45°C and 70°C, respectively. These two major peaks were further fitted to four transitions (T_m1, T_m2, T_m3, T_m4) by the best mathematical fit shown in red in Figure 3.3F. The resulting thermal unfolding temperature values for dmLT are shown in Supplemental Table 3.2. From the DSC data, it is apparent that the thermal unfolding and stability of dmLT primarily reflects the behavior of the two individual protein subunits (A and B chain). To summarize, all the above biophysical techniques revealed two thermal events in dmLT molecule, one for A-subunit and other for the B-subunit. Based on the properties of the independent B-chain of cholera toxin (a close relative of LT and ~80% homologous to LT in terms of nucleotide sequences) and its comparison to the intact toxin[35], the lower temperature transition in dmLT can be attributed to structural alterations in the A-subunit while the higher temperature transition corresponds to the B-subunit.

3.3.4 Elucidation of Physicochemical Degradation Pathways of dmLT

3.3.4.1 Physical stability profile of dmLT as a function of pH and temperature

The physical stability profile of the reconstituted dmLT was evaluated in the formulation buffer under a wider range of pH conditions (pH 5.5 to 8.0) vs. temperature (10 to 90^{o}C) with respect to tertiary structural integrity, aggregation and overall conformational stability using intrinsic tryptophan fluorescence, static light scattering, and differential scanning calorimetry, respectively (Figures 3.4 A, B and C). An increase in Trp fluorescence peak position (Figure 3.4A) of dmLT was observed with increases in temperature for each of the pH conditions evaluated with two thermal transitions again observed in each sample. A red shift in peak

position was observed for dmLT at each of the pH conditions evaluated vs. an increase in temperature indicating structural alterations in the protein. Also, an increase in scattered light with increases in temperature was observed for dmLT at each of the pH conditions with two transition events again seen (see Figure 3.4B), of which the T_{onset} values were calculated as shown in Supplemental Table 3.3. For lower pH conditions (pH 5.5-6.0), the thermal transition temperature values (T_m) were lower (~43ºC) than values seen at the higher pH conditions (pH 6.5-8.0), which were ~45ºC. These results indicated that the aggregation propensity of dmLT as a function of temperature was slightly lower at pH 6.5-8.0 than at pH 5.5-6.0. Finally, DSC thermograms showed increased overall conformational stability of dmLT from pH 5.5 to pH 8.0, with the protein being thermally more stable between pH 6.5-7.5 in comparison to pH 5.5, 6.0 and 8.0 (Figure 3.4C), consistent with the results from static light scattering.

Using the large biophysical datasets from the above three techniques, two data visualization tools were utilized, a three index EPD (left panel) and a radar chart (right panel) to better assess the overall physical stability profile of dmLT as a function of pH and temperature (Figure 3.4D). The three index EPD displayed changes in the structural characteristics of dmLT, as measured by the three different biophysical techniques (intrinsic tryptophan fluorescence, static light scattering, and differential scanning calorimetry), as a function of temperature and pH (see supplemental methods for construction and interpretation of three index EPDs). The datasets from the three techniques were mapped to red (static light scattering), green (differential scanning calorimetry) and blue (MSM peak position from intrinsic Trp fluorescence) colors, respectively (an RGB system), as shown in a separate panel alongside the 3-index EPD. The display of individual RGB components helps to better understand the interpretation of the final colors and thus reflect changes in the structure of the protein as measured by the three

biophysical techniques. The different colors highlighted regions with similar structural characteristics, designated as Regions I-VI. The changes in color represented structural alterations in dmLT as a function of pH and temperature as reflected in the biophysical stability data sets from the individual biophysical measurements. The EPD shows 6 regions that represented 6 structural states of dmLT; the native conformation (Region I, green), altered A-chain (Region II, light magenta), partially altered dmLT structure (Region III, light green), altered B-chain (Region IV, dark magenta), extensively altered dmLT structure (Region V, light blue), and an aggregated state of dmLT (Region VI, light yellow) observed only at pH 5.5. Radar plots were also constructed to visualize the same physical stability data sets using a different method (see supplemental methods section). Overall, the construction of three index EPD and radar plots both gave similar results and indicate that dmLT in formulation buffer displays six different conformational states (Regions I-VI) as a function of pH and temperature, with the protein's structural integrity and conformational stability most favored between solution pH 6.5-7.5 and at temperatures below 50 ^{o}C.

3.3.4.2 Aggregation of dmLT as a function of agitation

To assess the aggregation propensity of dmLT, agitation stress was used in which reconstituted dmLT vials were shaken sideways at 300 RPM for 2h at room temperature (see supplemental methods section). The aggregates formed were characterized using various analytical methods based on their different sizes ranging from ~5nm to over 100µm as outlined in Table 3.1. The shake-stressed samples after 2h of dmLT had a lower optical density values at 280 nm (~20% loss in protein), higher turbidity and an overall higher concentration of sub-micron and sub-visible sized particles compared to the control samples. A small increase in soluble aggregates was also observed by SV-AUC with a concomitant loss of AB_5 and increase

in the B_5 components of dmLT. Additionally, the monomer peak decreased in the shake stressed dmLT samples compared to the control samples as assessed by SEC and SV-AUC. The total area of the SEC monomer peak was substantially lower in the shake stressed samples compared to the control samples, indicating formation of larger, insoluble aggregates/particles (also confirmed by SV-AUC). Overall, these results highlight the propensity of dmLT to aggregate upon agitation and exposure to air-liquid interfaces, which may be encountered during manufacturing and transport of dmLT formulation.

3.3.4.3 Effect of elevated pH and the presence of oxidants on the chemical stability of dmLT

Forced chemical degradation studies using elevated pH and temperature or the addition of hydrogen peroxide of the reconstituted dmLT sample were used to determine specific sites prone to Asn deamidation and Met oxidation.Protein glycation was also monitored. Intact mass spectrometry analysis of dmLT (Figure 3.5A) incubated at 4^{o}C for 7 days at pH 7.4, 8.0 and 9.0 showed that dmLT incubated at pH 9.0 had one Da increase in the mass of the A-chain, while no mass change observed under pH 7.4 and 8.0. This can be attributed to the Asn deamidation reaction which results in the formation of a mixture of isoaspartate and aspartate above pH 6.0 [36]. Preliminary peptide mapping analysis suggested that the N-terminal Asn^{1}-(Gly^{2}) residue in the A-chain of dmLT was most susceptible to deamidation under basic conditions. However, additional optimization of the LC-MS peptide map is ongoing to more fully quantify the extent of deamidation and the amounts of deamidation byproducts.

Results of intact mass spectrometry analysis of dmLT samples exposed to two concentrations of hydrogen peroxide (0% and 1% v/v), produced three peaks corresponding to the dmLT A chain (27645.5 Da), B chain (11719.5 Da) and modified B chain (12043.0 Da)

(Figure 3.6A). In addition to the above main peaks, several oxidized species were observed with increasing hydrogen peroxide concentration. RP-UHPLC results of hydrogen peroxide treated dmLT (Figures 3.6B and 3.6C) showed an oxidation peak (~10.80-10.85 min) with the main free B_5 peak compared to the control (0% H_2O_2). The areas of oxidized peaks increased, while the area of the main free B_5 peak at ~10.9 min concurently decreased with increasing H_2O_2. A small AB_5-oxidized peak was observed at high concentration of hydrogen peroxide (i.e., >0.5% H_2O_2) but its peak area did not contribute substantially to the overall decrease in total peak area of AB_5. Peptide mapping was used to confirm and identify the Met residues of dmLT (3 Met residues in A-chain and 4 Met residues in B-chain) that are generally susceptible to oxidation[36]. Utilizing two different proteolysis methods, 100% of the A and B chain sequence of dmLT was identified. Therefore, the relative amount of Met oxidation was quantified for each Met residue within the protein; however oxidation of Met_{101} in the dmLT B chain could not be quantified due to low abundant peptides in the presence of H_2O_2. The relative percentages of each Met residue oxidized in the A and B-chains are shown in Figures 3.6D and E, respectively. In the absence of H_2O_2, no measurable oxidation of the Met residues in dmLT was observed. In the presence of H_2O_2, most of the Met residues were not substantially oxidized at lower concentrations H_2O_2 (<0.25%) except Met_{37} of the A chain, which was markedly oxidized at 0.25% H_2O_2. These results suggest that Met_{37} in the dmLT A chain is more susceptible to oxidation than the other Met residues in the dmLT protein.

Finally, the presumptive glycation reaction in dmLT, incubated under pH 7.4 at 40^{o}C for 7 days was monitored by intact mass analysis (Figure 3.5B). The relative abundance of the glycated B chain increased and additional modified B-chain peaks (+381 Da and +648 Da mass increases) were seen possibly indicating increased glycation during stress. Future work will

involve quantification and identification of the additional modified glycated B-chain peaks by further peptide map analysis.

3.3.5 Screening of pharmaceutical excipients to improve physical stability of dmLT

Since thermal and agitation induced aggregation was identified as a major physical degradation pathway for dmLT (see above), assays used to monitor dmLT aggregation were used to identify stabilizing conditions and additives as a first step to design an optimized formulation. To permit effective screening of excipients that minimize thermal (heat) and agitation induced aggregation, high throughput stability-indicating assays such as increases in optical density at 350 nm (during heating) and micro-flow imaging particle counting (after agitation) were implemented. By starting the excipient screening with the goal of minimizing aggregation, we subsequently identified conditions/excipients that would also minimize the chemical degradation pathways such as Asn deamidation, Lys glycation and Met oxidation. A base buffer of 10 mM sodium phosphate, 150 mM NaCl, pH 6.0 was chosen for these initial excipient screening studies since this solution pH resulted in suboptimal dmLT physical stability (based on biophysical studies described above), allowing for efficient screening of excipient's ability to improve dmLT stability. Ten different categories of pharmaceutical excipients were evaluated including carbohydrates, polyols, amino acids, carboxylic acids, salts, metal ions/chelators, detergents, cyclodextrins, polymers/proteins, and polyions/osmolytes (see Supplemental Table 3.4 for complete list of excipients examined in this work).

Figure 3.7 shows the effect of excipients on the aggregation propensity of dmLT during thermal stress. The average delta temperature value to reach 0.1 OD_{350} unit in the dmLT control formulation plus excipient *vs.* dmLT control formulation alone (10 mM sodium phosphate, 150 mM NaCl, pH 6.0) were sorted from highest to lowest values, indicating highest to lowest

stability of dmLT in terms of aggregation behavior. Carbohydrates and polyols including glycerol, sucrose, mannitol, trehalose, sorbitol and lactose showed a larger stabilizing effect towards minimizing dmLT aggregation compared to other excipients such as amino acids and detergents, which ranged from moderate to low/no increase in dmLT stability against aggregation. The effect of these additives on the aggregation propensity of dmLT during agitation (shaking of vials containing dmLT in different solutions) as measured by MFI is shown in Figure 3.8, where the excipients added to the control formulation were sorted from highest to lowest values of total sub-visible particle concentration. With the exception of trehalose, the sub-visible particle concentration of the dmLT solutions after shaking was lower with each of the tested excipient conditions compared to the control formulation alone. Excipients such as hydrolyzed gelatin, human albumin and sodium acetate were found to be the most stabilizing against shaking induced aggregation. However, since albumin and gelatin are proteins, their effect on dmLT aggregation in OD_{350} assay could not be evaluated since the additives themselves may aggregate. Sodium acetate was not further investigated due to its minimal effect on thermally induced aggregation as compared to carbohydrates. A tabular summary of the results from OD_{350} measurements (thermal stress, Figure 3.7) and total sub-visible particle concentration from MFI measurements (agitation stress, Figure 3.8) for the dmLT samples in the presence of various excipients are also summarized in Supplemental Table 3.4.

Different concentrations of top performing aggregation inhibitors from four different excipient categories (sugars, amino acids, metal chelators and detergents) were then selected and further evaluated to explore the concentration dependence of their stabilizing effect on dmLT using both thermal and agitation stresses (Table 3.2). Higher concentrations of polyols and sugars resulted in a higher dmLT thermal stability as seen by increased delta temperature values

from the OD_{350} assay. Several different amino acids exhibited a slight positive concentration effect by increasing the thermal stability of dmLT while chelators/detergents did not have a detectable effect. For agitation induced aggregation of dmLT monitored by MFI, all of the tested concentrations of stabilizers had a protective effect against shaking induced destabilization of dmLT measured by the total number of sub-visible particles. Amino acids and polysorbate 20/80 appeared to be the most promising excipients in limiting sub-visible particle formation during agitation stress.

Based on these results, only a selected number of the most promising excipients were chosen for further combination screening based on their demonstrated stabilizing effect on dmLT (Table 3.2) as well as practical considerations from a formulation development perspective such as their effect on solution osmolality. For example, for the selection of sucrose, even though many of polyols/sugars (such as glycerol, sorbitol, mannitol and lactose) inhibited thermally induced aggregation of dmLT to a greater extent than sucrose, these additives were not selected for further optimization. Glycerol and mannitol solutions of equal w/v ratio have higher osmolality values compared to sucrose solutions. When sucrose and glycerol are compared at equivalent osmolality (10 % sucrose vs 5% glycerol), sucrose is equally effective at inhibiting heat-induced aggregation of dmLT, and in addition, resulted in a lower number of sub-visible particles formed during agitation. Similarly, sorbitol and lactose solutions also showed higher number of sub-visible particle formation than sucrose solutions during agitation. Moreover, sorbitol and mannitol may manifest a lesser ability to protect during freezing and thawing compared to disaccharides at equivalent solution osmolality values[37-40], a consideration of importance for dmLT as described below. Finally, lactose is a reducing sugar which can glycate Lys residues in proteins (as was observed with dmLT, Toprani et al., 2017), a reaction that can

potentially lead to protein instability as well as formation of advanced glycation products [41,42]. As shown below, addition of sucrose in the formulation does inhibit glycation of dmLT, compared to lactose, under forced degradation conditions of elevated temperature. Based on these considerations, 10 % sucrose was selected as a sugar-based stabilizer to improve overall stability of dmLT against aggregation without the concern of causing protein glycation.

In addition, polysorbate-80 and methionine were the other two stabilizers selected for further work to develop a stabilizing formulation of dmLT (Table 3.2). Polysorbate-80 greatly minimized agitation induced aggregation of dmLT (despite its mild destabilizing effect on thermally induced aggregation). Methionine showed some stabilization against agitation induced aggregation (and no destabilization against thermally induced aggregation) of dmLT (Table 3.2), yet was primarily selected for its ability to mitigate the potential of oxidative stress (oxidation was identified as major chemical degradant pathway of dmLT as shown during forced oxidation studies above. As shown below, addition of Met in the formulation does inhibit hydrogen peroxide induced oxidation of Met residues in dmLT.

3.3.6 Salt optimization for dmLT stability

Sodium chloride was observed to be essential to maintain the solubility of dmLT in solution during dialysis. Higher sodium chloride concentrations in combination with other excipients, however, can lead to high solution osmolality which may be undesirable for clinical administration. Therefore, to balance sufficient dmLT solubility with total solution osmolality values, different concentrations of sodium chloride (50, 100, and 150 mM) in 10 mM sodium phosphate buffer pH 6.0 (+/-10% w/v sucrose) were tested to identify the salt concentration-dependence of the stabilizing effect on dmLT. As shown in Figure 3.9A, in the absence of sucrose, increasing NaCl concentration had no major effect on the thermal stability of dmLT as

measured by the OD_{350} thermal stress assay. In the presence of sucrose, however, dmLT formulated with 50 and 100 mM NaCl showed higher thermal stability in comparison to 150 mM NaCl. In terms of agitation stress as shown in Figure 3.9B, MFI results showed that the 50 mM sodium chloride containing solutions of dmLT produced a lower number of sub-visible particles compared to 100 and 150 mM sodium chloride. These results demonstrated that, in general, dmLT samples formulated with sucrose were thermally more stable toward aggregation compared to samples without sucrose, and a combination of sucrose (10% w/v) and 50 mM NaCl limited aggregation and particle formation caused by agitation stress. Finally, dmLT formulated in the presence of 10% w/v sucrose and 50 mM sodium chloride at pH 6.0 had lower solution osmolality than formulations containing higher sodium chloride concentrations (~450 mOsm for 50 mM NaCl vs ~650 mOsm for 150 mM NaCl). Based on these results, 10 mM sodium phosphate, 50 mM NaCl, 10% w/v sucrose, pH 6.0 was selected as the base buffer for further optimization of dmLT physical stability in combination with other promising excipients such as methionine and polysorbate-80.

3.3.7 Identifying optimal combinations of lead stabilizers

Combinations of the lead stabilizers were tested to determine any potential additive or synergistic effects on dmLT stability and to check for incompatibility between excipients. Based on the considerations outlined above, a candidate formulation including sodium phosphate buffer, sodium chloride, sucrose, methionine and PS-80 was identified which showed protection against aggregation induced by thermal and agitation stresses, and potentially could help prevent oxidation in dmLT.

The effect of both solution pH and phosphate concentration on the physical stability of dmLT in the candidate formulation was first evaluated. Briefly, 10, 20, 35 and 50 mM phosphate

at both pH 6.0 and 7.4 were evaluated (in combination with 50 mM NaCl, 10% sucrose, 5 mM methionine and 0.01 % v/v PS-80). The phosphate concentration did not appear to affect the thermal stability of dmLT at pH 6.0 (Figure 3.10A) as measured by the OD_{350} assay. Interestingly at pH 7.4, however, an increase in phosphate concentration increased the thermal stability of dmLT as measured by the same OD_{350} assay. To further understand these results, differential scanning calorimetry was employed to assess the effect of the higher phosphate concentration on the overall conformational stability of dmLT at the two different pH values. Figure 3.10B shows the thermal melting temperature (Tm) values for dmLT formulated in both 10 and 50 mM phosphate at both pH 6.0 and 7.4 (in combination with 50 mM NaCl, 10% sucrose, 5 mM methionine and 0.01 % v/v PS-80). No major differences were observed in the Tm values of dmLT formulated in 10 vs. 50 mM phosphate at pH 6.0. However, dmLT formulated in 50 mM phosphate at pH 7.4 had slightly higher Tm values compared to 10 mM phosphate pH 7.4 (a ~2^{o}C increase in Tm1, corresponding to unfolding of the A-chain of dmLT). These studies showed two different pathways of excipient stabilization of dmLT at the two different pH conditions, pH 6.0 and 7.4 (see discussion section below). At pH 6.0, the presence of sucrose had a major stabilizing effect on dmLT, while phosphate concentration did not affect thermal stability. Conversely at pH 7.4, a higher phosphate concentration showed higher dmLT thermal stability. Based on these results, two candidate dmLT formulations were identified for additional evaluations (1) 10 mM sodium phosphate (pH 6.0), 50 mM NaCl, 10% w/v sucrose, 5 mM methionine, 0.01 % v/v PS-80, and (2) 50 mM sodium phosphate (pH 7.4), 50 mM NaCl, 10% w/v sucrose, 5 mM methionine, 0.01 % v/v PS-80.

The effect of multiple freeze-thaw (F/T) cycles (0, 1 and 5 cycles) on dmLT in these two candidate liquid formulations, along with a comparison to the current dmLT formulation used to

prepare the lyophilized dosage form, was evaluated using UV-Visible spectroscopy to monitor protein concentration (and aggregation) as well as MFI to measure subvisible particle formation. The current lyophilized dmLT formulation showed a higher protein loss (~17 %) as compared to the two candidate formulations (~6%) after five F/T cycles (Supplemental Figure 3.4A). The current formulation also showed a greater number of sub-visible particles/aggregates in comparison to both the candidate formulations after five F/T cycles. Between the two candidate formulations, the pH 6.0 formulation showed higher numbers of particles than the pH 7.4 formulation after five F/T cycles (Supplemental Figure 3.4B).

Based upon these results, the candidate formulation at pH 7.4 was further optimized to limit protein loss during multiple F/T cycles. The loss of protein during F/T in the candidate formulation at pH 7.4 was minimized by increasing the PS-80 concentration from 0.01 % v/v PS-80 to 0.05 and 0.1 % v/v PS-80 as shown in Figure 3.11. The effect of increasing PS-80 concentration in the candidate formulation on the freeze-thaw stability of dmLT was monitored by a combination UV-Vis spectroscopy (protein loss), hydrophobic interaction chromatography (HIC, to measure relative percent AB_5) and MFI (particle formation). Increasing the PS-80 concentration in the candidate formulation mitigated protein loss following freeze-thaw as measured by A280 using UV-Vis spectroscopy compared to the current formulation (Figure 3.11A). No protein loss was observed in the candidate formulation with 0.1% PS-80, pH 7.4 formulation after 5 FT cycles. The HIC analysis showed no loss of native dmLT (AB_5) for the candidate formulation with 0.1% v/v PS-80 while a substantial loss of native dmLT (~19 %) was observed in the current formulation after five F/T cycles (Figure 3.11B). The size distribution and total number of sub-visible particles/aggregates formed during F/T in all the formulations was analyzed by MFI and is shown as a radar plot in Figure 3.11C. The number of sub-visible

particles increased slightly in the candidate formulation with 0.01% PS-80 but no change in the number of sub-visible particles was observed in the candidate formulation with 0.05% or 0.1% PS-80 after five FT cycles. The majority of sub-visible particles in all samples were 2-5 µm. In summary, increasing the PS-80 concentration from 0.01 to 0.1 % v/v helped to minimize the protein loss and loss of the AB_5 species, without causing any major change in the total number or distribution of sub-visible particles after 5 F/T cycles.

3.3.8 Summary of physicochemical stabilization of dmLT in candidate bulk formulations

The optimized candidate formulation for bulk dmLT which displayed increased thermal stability, reduced propensity to aggregate, robust freeze-thaw stability as well possession of acceptable solution tonicity was 50 mM sodium phosphate, 50 mM NaCl, 10 % w/v sucrose, 5 mM methionine, 0.1 % v/v PS-80, pH 7.4.

The new candidate formulation provided improved physical stability of dmLT, compared to the current formulation (used for lyophilization), upon agitation and F/T stresses as observed by the lower number of sub-visible particle formed and the lack of loss of protein concentration after five F/T cycles, respectively (Table 3.3). Although the aggregation propensity of dmLT upon thermal stress in the new candidate bulk formulation was slightly higher than in the current formulation (~2^{o}C difference in OD_{350} values), given such high thermal stability values in either formulation (>70^{o}C), it is unlikely that the two formulation will differ in thermal stability when exposed to more moderate temperatures during accelerated and real time stability studies. Furthermore, no major differences were observed between dmLT in the two formulations in terms of relative AB_5 ratio as measured by HIC and overall conformational stability (Tm values) as measured by DSC.

The new candidate bulk formulation also improved the chemical stability profile of dmLT, in terms of Lys glycation and Met oxidation, in comparison to dmLT in the current formulation (used for lyophilization). After incubation of dmLT at 40^{o}C for 7 days in the candidate formulation, no increase in relative abundance of the glycated B-chain, nor the formation of additional modified B-chain peaks (+381 Da and +648 Da mass increases), was observed by intact mass spectrometry (see Supplemental Figure 3.5 and Supplemental Table 3.5). In contrast, dmLT in the current formulation under the same stress conditions showed increases in these chemically modified (glycated) species (see Supplemental Figure 3.5 and Supplemental Table 3.5). Results of intact mass spectrometry analysis of dmLT in the two formulations exposed to different concentrations of hydrogen peroxide (0, 1, 2.5 and 5 mM) showed oxidized dmLT species (+16 Da) in the current formulation at 1, 2.5 and 5 mM H_2O_2 (see Supplemental Figure 3.6 and Supplemental Table 3.6). However, no dmLT oxidation was detected in the candidate bulk formulation up to 2.5 mM H_2O_2, and thus, the new formulation appeared to be overall better than the current formulation in terms of protecting dmLT against oxidation stress (see Supplemental Figure 3.6).

A comparative summary of the physicochemical properties of dmLT in the current (lyophilized and reconstituted) and new candidate formulation (bulk stored frozen) in terms of aggregation propensity due to thermal, agitation and F/T stresses, conformational stability as measured by DSC, chemical stability under forced oxidation and glycation conditions, AB5 ratio as measured by HIC, and solution osmolality are summarized in Table 3.4.

3.4 Discussion

The development and eventual successful commercial manufacturing of a well-defined, stable, scalable production process of a clinically efficacious protein vaccine adjuvant (dmLT)

will depend in part of a detailed mechanistic understanding of the protein's physicochemical properties, integrity and stability as well as the interrelationships between these structural properties and functional attributes. Extensive analytical characterization is often necessary to study the complex nature of protein based vaccines to ensure their purity, potency and stability during production, storage and administration [18,19]. In this work, we utilize a series of biophysical and biochemical analytical technologies to better characterize the primary structure, post translational modifications, size and higher order structure of dmLT as well as to identify the potential physicochemical degradation pathways of this adjuvant. By developing a set of stability indicating methods to monitor the key structural attributes of dmLT, it will now be possible to rapidly evaluate the effect of process and formulation changes implemented for production of future clinical lots on the structural integrity of the dmLT molecule without relying solely on extensive biological testing such as animal potency assays.

Based on the HIC and SV-AUC analysis, this particular lot of dmLT is a heterogeneous mixture of the intact holotoxin (AB_5, ~75%) and free B_5 subunit (~25%) in solution, although it is possible the AB_5:B_5 ratio could vary between lots or with different preparations depending on the purification protocols used. One possible reason for the presence of free B5 subunit might be the differing efficiencies of the A- and B subunit Shine-Delgarno sequences on the polycistronic mRNA that codes for both subunits. Alternatively, the inherent instability of the A-chain (observed by a variety of biophysical measurements) may cause a relatively larger loss during expression and purification. Joffré et al.[43] have reported the presence of free B subunit and intact holotoxin AB_5 in several LT preparations produced from different ETEC strains using an ELISA. In our work, each of the biophysical techniques (DSC, fluorescence spectroscopy, static light scattering) reveal two thermal events in dmLT molecule, one corresponding to the A-subunit and

the other for the B-subunit. Our findings are consistent with the work of Goins et al.[35] concerning the CT protein which also shows two thermal unfolding events centered at ~51^{o}C (A-subunit) and 74^{o}C (B-subunit). Since LT is ~80% homologous to CT in terms of nucleotide sequences and overall structurally similar to CT[35,44], the dmLT results in this work are well correlated with the previous studies of CT. The work presented here clearly demonstrates that the A-subunit, which possesses the adjuvant activity, is thermally less stable than the B-subunit as observed by a variety of complementary biophysical techniques.

Vaccines often encounter a wide variety of environmental stresses during manufacturing, storage, transport and administration to patients. Stresses such as pH changes, temperature fluctuations, agitation or light exposure can affect the stability and potency of vaccines[45,46]. Forced physical and chemical degradation studies are employed during the development of vaccines to elucidate potential causes and molecular mechanisms of degradation, develop stability indicating methods[45], and design stable formulations including pharmaceutical excipients[26] to minimize degradation. The major physical instability pathways of a vaccine constitute structural/ conformational changes and aggregation of either the antigen or adjuvant. Structural alterations in the protein antigen could result in the loss of key epitopes or exposure of additional epitopes, previously buried within the protein structure, potentially leading to the formation of non-neutralizing antibody responses against the vaccine antigen that may compete with formation of neutralizing antibodies[46,47]. In this study, the forced physical degradation studies as a function of pH and temperature identified structural/conformational changes in dmLT by multiple biophysical techniques. Optimal stability conditions of dmLT between pH 6.5-7.5 and temperatures below 50^{o}C were established from the biophysical stability data sets using data visualization tools such as three-index EPDs and radar plots. Based on these analyses,

high throughput assays for screening stabilizers can be developed and used as a key part of formulation development experiments of dmLT (Toprani et al.[48]*)*. This approach has been extensively used for biophysical characterization and stabilization for a number of vaccine candidates[49].

Protein aggregation is known to affect potency as well as reduce yields of a number of vaccine antigens[50-53], making it critical to characterize protein aggregates and control their formation during vaccine development. Adjuvants can undergo colloidal instability leading to potency loss. For example, lyophilization or freeze-thaw induced aggregation of aluminum salt adjuvants in vaccines is well reported[54]. A major challenge with studying aggregates during protein/vaccine formulation is the multiple size ranges within which aggregates can be grouped and the need for several orthogonal techniques to probe the different size aggregates[55]. Our results find that dmLT is highly prone to aggregation during agitation stress with different sized aggregates formed ranging from 1 nm to >100 µm with a concomitant loss of protein content. While these observations were derived from an early clinical lot of material, the data indicate aggregation as a major physical degradation pathway of dmLT which may present challenges during manufacturing or lead to loss of potency during long term storage. Future work needs to minimize the agitation-induced aggregation as part of formulation development of this adjuvant as well to study the activity of these aggregates in comparison to native dmLT in terms of adjuvant activity.

Chemical instabilities involving modifications of covalent bonds in proteins such as deamidation, oxidation, glycation, etc. represents a major degradation pathway for protein vaccines [36]. Investigation of these chemical instabilities is very relevant in formulation development of protein drugs since these modified molecules can potentially affect protein

conformation, stability, bioactivity, efficacy and immunogenicity[42,56,57]. For vaccines, Asn deamidation in critical epitopes of the recombinant protective antigen leads to a change in the conformation of epitopes that causes reduction in potency and immunogenicity of a recombinant anthrax vaccine[58,59]. As a part of chemical stability studies, we have identified a glycated B-chain species in this lyophilized dmLT formulation by intact mass spectrometry. The presence of reducing sugars is known to cause glycation in therapeutic proteins by a condensation type reaction with Lys residues known as the Maillard reaction[60-62]. A lactose glycan on the B chain would increase the protein's molecular weight by 324 Da, which was consistent with the observed molecular weight of the modified B chain. Although the involvement of Lys91 in binding of lactose to B-chain of LT within the sugar binding site is well established[63], we observed an adjacent lysine residue, Lys84, as the site of glycation. We suspect the surface exposed nature of Lys84 make it more susceptible to glycation during the lyophilization process given that lactose is present in the lyophilization buffer. As part of forced degradation studies, increased amounts of glycated B-chain (and additionally modified peaks) were observed under temperature stress, which is consistent with observed protein glycation[42].

Preliminary forced deamidation studies indicate the N-terminal asparagine which is followed by Gly in the A-chain of dmLT to be the most susceptible to Asn deamidation. It is well known that Asn-Gly and Asn-Ser residues are more prone to deamidation than any other Asn residue sequences[36,64]. In the presence of H_2O_2, we report the high susceptibility of the Met_{37} residue in the dmLT A chain towards oxidation compared to the other Met residues in dmLT. Additionally, we show that RP-UHPLC and LC-MS can be used as orthogonal techniques to identify the oxidation degradants. The forced chemical degradation studies of this

work not only reveal the major degradation pathways of dmLT but also will help in future to generate stable and robust formulations of dmLT.

During the clinical development and post approval lifecycle management of a vaccine product, changes to the composition, manufacturing process, equipment or facilities can occur [65,66]. For example, changes in manufacturing facilities (e.g., scale-up to larger facility) or changes in the final vaccine dosage form (e.g., lyophilized to liquid formulation) may occur to meet market demands. These types of process and product changes can potentially affect the identity, strength, purity, quality and potency of the antigen/adjuvant or the final vaccine product. Comparability assessments requiring an extensive combination of analytical and biological tests [20,67,68] are performed to evaluate the impact of such changes with regard to the safety and efficacy of the vaccine product. As the dmLT adjuvant advances in clinical development, it is likely to undergo manufacturing or process changes that could potentially cause physicochemical changes in the protein. The analytical and stability indicating methods developed in this work could be very useful not only to demonstrate analytical comparability and quality consistency between pre- and post-change dmLT, but also monitor lot-to-lot variability of dmLT made from the same process. For example, an LC-MS peptide map can be used to identify any post-translational modifications in the protein primary structure by comparing the peptide map profiles for the pre and post-change dmLT while HIC and SV-AUC can be potential QC or characterization assays to assess purity in different batches of the dmLT adjuvant. Furthermore, the stability profile of vaccines is a key component to comparability assessments, since stability is often a very sensitive indicator of subtle alterations in higher order structure. Data visualization tools such as three index EPDs and radar plots of large biophysical stability data

sets cannot only be used in formulation development, but as part of comparability studies as has been demonstrated with a wide variety of protein based drug and vaccine candidates [32,49,69].

Preformulation characterization and formulation development activities of vaccine candidates (both antigens and adjuvants) are critical activities for their clinical development and regulatory approval. A proper vaccine formulation should not only be stable (including the antigen and adjuvant are physically compatible), but the vaccine also must remain potent and the adjuvant must enhance the immunogenicity of the vaccine antigen. It is therefore imperative to assess and identify the structural integrity as well as physicochemical degradation pathways of antigen and adjuvant as part of formulation development. A rational design of stable formulation conditions is possible based on understanding the causes and mechanisms of vaccine antigen and adjuvant stability (and interactions), to maintain vaccine potency throughout the shelf life at the defined storage temperature(s). In this work, we have developed an improved bulk formulation of the dmLT adjuvant with the goal of providing long term frozen storage as well as flexibility for potential use with different vaccine antigens administered by various routes (e.g., injection, oral, nasal, etc.). The systematic formulation strategy described in this paper provides an overview of the physicochemical stability of dmLT in the presence of different excipients and not only helps to elucidate degradation pathways, but provides strategies for dmLT stabilization within a pharmaceutical dosage form.

The major physicochemical instabilities identified with the current formulation of dmLT were glycation and oxidation of specific Lys and Met residues, respectively, as well as protein aggregation induced by agitation and thermal stress. Physical instability due to either heat and/or freeze stress of antigens or adjuvants can be a major cause of potency loss in various vaccines during manufacturing, storage and administration even within the vaccine cold chain [23,70]. The

lack of integrity of the vaccine cold-chain exposes vaccines to temperature fluctuations (either accidental heat exposure or freezing) during shipping, handling, distribution and administration to patients [16,23,70]. This puts an additional requirement on vaccine manufacturers to develop more thermostable vaccines or vaccine formulations to make their products more widely available in global markets.

With the aim to develop a more stable bulk dmLT formulation that does not require lyophilization, this work involved identifying pharmaceutical excipients that enhanced dmLT stability (i.e., minimized aggregation during thermal and agitation stresses). Sucrose and phosphate were identified as stabilizers that increased dmLT thermal stability against aggregation and limited its aggregation. Sucrose is a widely used pharmaceutical excipient that stabilizes biomolecules, including antibodies, protein drugs and vaccines[71-73] by offering protection against elevated temperatures as well as freezing stress via preferential exclusion mechanisms[74,75]. Additionally, its non-reducing nature doesn't cause glycation in proteins unless exposed to very low pH or high temperatures [42]. In fact, our results demonstrated that dmLT in the candidate formulation (containing sucrose) showed essentially no Lys glycation formation during elevated temperature studies compared to dmLT in the current formulation (containing lactose) under the same conditions which displayed increased formation of glycated protein.

The investigation of the effect of phosphate on the thermal stability of dmLT at two pH conditions revealed that relatively higher concentrations (50 mM) of phosphate at pH 7.4 showed an increased thermal stability of dmLT compared to pH 6.0. At pH 7.4, a potential reason for the increased thermal stability (in terms of aggregation propensity) of dmLT under higher phosphate concentrations can probably be attributed to phosphate binding or intermolecular electrostatic effects. Proteins are net negatively charged above their isoelectric point (pI) and net positively

charged below its pI[76]. The theoretical pI of the A-subunit of dmLT based on its amino acid sequence is ~6.48. In the pH 7.4 formulation, above the A-subunit's pI, the A-subunit is expected to have a net negative charge with a smaller proportion of positive charges. Addition of increased amounts of phosphate anions can effectively shield positive charges on the protein surfaces. This would cause an increase in intermolecular charge-charge repulsions between dmLT molecules making it less favorable for the two molecules to interact (aggregate) with an increase in stability as was observed in this work by OD_{350} thermal melt results. In contrast, at pH 6.0 (closer to the theoretical A chain pI=6.48), the A-subunit of dmLT has anisotropic charge distribution which may give rise to dipoles which in turn could make attractive forces between dmLT molecules to dominate, making aggregation more favorable. Multiple studies on different proteins have also demonstrated the role of increasing repulsive charge-charge interactions in stabilizing protein solutions (i.e., colloidal stability) and thereby reducing/preventing protein aggregation[77-79].

Agitation is a common physical stress experienced during manufacturing, shipping and handling of protein based drugs and vaccines[80]. It can cause protein structural alterations at the air-liquid interface leading to formation of nucleating aggregated species in the bulk solution causing more extensive aggregation in the bulk formulation[80,81]. To protect dmLT against aggregation caused by agitation stress, polysorbate-80 was identified as a stabilizing excipient. PS-80 mitigated aggregate/particle formation in dmLT during agitation by presumably outcompeting proteins for the air-water interface and thus inhibiting surface adsorption and structural alterations of proteins due to the hydrophobic nature of air water interfaces. PS-80 is a non-ionic surfactant widely used with protein drugs and some vaccines to prevent aggregation against a number of interfacial stresses including agitation and freeze thaw[82,83]. PS-80 is also known to protect freezing induced perturbations in protein conformation leading to protein

aggregation and reduce the unfolding of proteins at ice-water interfaces[84]. These effects are presumably responsible for the stabilization of dmLT (no loss of protein) observed in this work during multiple freeze-thaw cycles.

Protein oxidation is a major chemical degradation pathway for protein drugs[57]. Oxidation can be induced during manufacturing by trace metal ions leached from equipment or exposure of proteins to light and oxygen from the surrounding air. Certain excipients such as non-ionic surfactants can also form peroxides which are a major catalyst of protein oxidation [57]. Oxidation can affect pharmaceutical properties of proteins, including solubility, conformation, biological activity and shelf-life[57]. There are many potential ways to protect against oxidation such as site-directed mutagenesis to remove labile amino acid residues, development of solid state vs liquid formulations, or addition of excipients with anti-oxidant properties such as methionine in the formulation. To protect dmLT against oxidation, the amino acid methionine was added in the formulation since Met can act as an oxidation scavenger. Lam et.al [85] have reported that addition of methionine to a formulation of rhuMAb HER2 protected it against temperature and light induced oxidation. The authors concluded that exogenous methionine can act as an antioxidant by either inhibiting the free radical chain reactions during oxidation or by competing with the endogenous methionine residues in the protein for reactions with hydroxyl radicals. In fact, our results demonstrated that dmLT in the candidate formulation containing methionine showed reduced levels of oxidation of Met residues in the dmLT protein compared to dmLT in the current formulation under the same forced oxidation conditions.

One important aspect of vaccine formulation development is to permit stable, long term frozen storage of the bulk vaccine antigen (or in this case, dmLT adjuvant). Freezing protein bulk offers several potential advantages such as increased protein storage stability and shelf life,

a decreased risk of microbial growth, elimination of agitation during transport and flexibility in subsequent fill-finish manufacturing [86]. For example, if the bulk protein vaccine antigen (or in this case, dmLT adjuvant) can withstand freeze-thaw cycle, it may be frozen at the bulk manufacturing site until transport to the fill finish site, and the subsequent drug product could potentially be stored and shipped frozen to a clinical site. However, freeze-thaw stress can negatively impact the structural integrity and potency of protein drugs and vaccine[84,87,88], including the freeze-thaw induced aggregation of aluminum salt adjuvants used in recombinant protein vaccines [89,90] leading to loss of biologic activity [91]. Freeze-thaw studies provide data on the impact of freezing on structure and conformation of protein adjuvants and antigens. Currently, majority of vaccines in preclinical or clinical development are based on recombinant proteins which require an adjuvant to increase their potency[92,93]. Hence, if the vaccine requires freezing for storage with dmLT as an adjuvant, then both the antigen and dmLT adjuvant should be able to withstand freeze-thaw effects. The freeze-thaw study here showed that dmLT in the newly developed formulation was freeze-thaw stable for up to five FT cycles. Neither aggregation nor loss of protein was observed after five freeze thaw cycles.

A combination of the key excipients such as phosphate ion, sucrose, methionine and polysorbate 80 showed protection of dmLT against thermal, agitation, and freeze-thaw stresses. This was due to inhibition of aggregation as well as minimization of chemical alterations including Lys glycation and Met oxidation. The potential benefits of this candidate formulation can not only be in protecting and stabilizing the dmLT protein adjuvant against different stresses, but also offering flexibility in terms of combining dmLT with different antigens. Furthermore, an additional benefit of the candidate bulk formulation of dmLT offers is its pH (pH 7.4) since formulations at physiological pH may minimize aggregation or precipitation caused by

transitioning from formulation pH to physiological pH conditions[94]. Finally, the replacement of lactose with sucrose in the new candidate formulation should eliminate Lys glycation of dmLT with a simultaneous increase in thermal and freeze-thaw stability of dmLT.

In conclusion, this work not only demonstrates the use of an extensive analytical toolset to characterize the higher order structure and physicochemical stability profile of an early clinical lot of dmLT, but also establishes the utility of these analytical tools for use as a part of future analytical comparability assessments to evaluate the effect of the inevitable process and formulation changes that occur during clinical development. Furthermore, this study provides the initial development of a new candidate bulk formulation of dmLT adjuvant by better understanding the protein's key structural features, identifying its physicochemical degradant pathways, and identifying stabilizing excipients to minimize protein instability by the use of appropriate stability indicating analytical assays. The dmLT protein adjuvant has shown potential to function as a mucosal adjuvant with a wide variety of antigens in both animal and human studies by a variety of administration routes [13]. For further pharmaceutical development of dmLT in the new candidate bulk formulation, long term bulk storage stability studies, and compatibility testing with different vaccine antigens in a final drug product will be necessary. In addition, immunogenicity studies in animal models of dmLT in candidate formulations along with a co-administered antigen are also suggested. For example, the adjuvanticity and antigenicity of dmLT with a tetanus toxoid antigen has been evaluated in mice by measuring serum anti-antigen IgG and serum anti-LT IgG levels, respectively[8].

Table 3.1. Aggregation Propensity of Reconstituted dmLT in Formulation Buffer in Stoppered Glass Vials After Agitation for 2 h as Measured by Various Analytical Methods. Data represent the average and SD for n = 3 replicates. NTU, nephelometric turbidity unit.

Size Range	**Analytical Methods**	**Time zero**	**T=2hr**
>100 µm	Visual assessment	Absence of visible particles	Visible particles present
1 nm-100 µm	UV-Visible Absorption Spectroscopy	A280 = 0.24± 0.0 OD_{350} = 0.0 ±0.0	A280 = 0.19 ± 0.02 OD_{350} = 0.62 ± 0.01
	Turbidimetry	0.5± 0.0 NTU	20.8 ± 0.2 NTU
2-100 µm	Micro-Flow Imaging	Total particles/mL = 6.4 ± 0.06 x 10^3	Total particles/mL = 2.1± 0.13 x10^6
0.1-1 µm	Resonant Mass Measurement	Total particles/mL = 0.2 ± 0.05 x 10^6	Total particles/mL = 3.5 ± 0.75 x10^6
	Nanosight Tracking Analysis	Total particles/mL = 49.3 ± 12.5 x 10^6	Total particles/mL = 86.4 ± 29.5 x10^6
~1-100 nm	Sedimentation Velocity-Analytical Ultracentrifugation	B_5 = 34 ±1 % AB_5 =66 ±1 % Aggregates =0 ± <1 %	B_5 = 82 ±4 % AB_5 =17 ±4 % Aggregates =1 ± 1 %
	Size-Exclusion Chromatography	Monomer = 100 ± <1 % Soluble+Insoluble Aggregates = 0 ± <1	Monomer = 65±1% Soluble+Insoluble Aggregates = 36±1

Table 3.2. Concentration optimization of lead stabilizing excipients for their stabilizing effect on dmLT (0.15 mg/mL) aggregation due to thermal stress as measured by OD_{350} thermal melt and agitation stress as monitored by MFI. All excipients were formulated in 10 mM sodium phosphate, 150 mM NaCl, pH 6.0. Data represents mean and standard deviation of three replicates. NA indicates not applicable.

Excipient	**Concentration**	**Thermal Stress** Δ**Temperature@**OD_{350}**= 0.1 unit (**^{o} **C)**		**Agitation Stress MFI** (Δ**Total particles**$_{4hr-0hr}$ **> 2µm,number/mL)**	
		Mean	SD	Mean	SD
Glycerol	5 % w/v	3.8	0.2	96360	475
	7.5 % w/v	20.0	0.2	41429	9753
	10 % w/v	23.0	0.5	3956	2063
	15 % w/v	NA	NA	16228	1311
Sorbitol	5 % w/v	3.5	0.2	49199	11559
	7.5 % w/v	16.1	0.1	92553	602
	10 % w/v	18.0	0.2	83439	7221
	15 % w/v	20.8	0.1	23767	2478
Mannitol	5 % w/v	2.8	0.2	1105	1055
	7.5 % w/v	14.4	0.8	433	791
	10 % w/v	15.8	0.2	5375	2743
	15 % w/v	20.9	0.5	-702	2198
Sucrose	5 % w/v	2.0	0.2	-2419	127
	7.5 % w/v	3.1	0.5	-336	538
	10 % w/v	3.6	0.4	4322	533
	15 % w/v	19.9	0.3	33934	8183
Lactose	5 % w/v	3.3	0.3	717	117
	7.5 % w/v	13.4	0.2	15616	4412
	10 % w/v	15.5	0.2	36470	14092
	15 % w/v	18.1	0.2	14196	7817
Aspartic acid	25 mM	0.1	0.2	9017	3617
	75 mM	1.2	0.1	7718	4069
	150 mM	3.9	0.1	7927	11322
Methionine	25 mM	-0.2	0.1	4494	3747
	75 mM	0.1	0.1	6255	6446
	150 mM	2.2	0.2	-2224	4911
Arginine	25 mM	0.5	0.2	-1794	602
	75 mM	-0.1	0.2	-3523	1861
	150 mM	-0.2	0.2	2672	4301
Histidine	25 mM	0.6	0.2	22812	3262
	75 mM	0.7	0.2	994	258
	150 mM	0.7	0.2	1657	2920
EDTA	0.05 mM	-0.3	0.6	-4672	1168
	0.1 mM	-0.5	0.5	8195	691
	1 mM	0.4	0.1	39368	10677
Polysorbate 80	0.01 % v/v	-0.3	0.4	-9167	2773
	0.025 % v/v	-0.7	0.0	-10018	495
	0.05 % v/v	-0.4	0.3	7241	7172
Polysorbate 20	0.01 % v/v	-0.5	0.1	15616	1794
	0.025 % v/v	-0.8	0.2	-12947	5294
	0.05 % v/v	-0.6	0.1	3881	6758

Table 3.3. Comparison of final candidate formulation vs current dmLT formulation in terms of relative percent AB_5 as measured by HIC, solution osmolality as well as physicochemical stability (thermal, agitation, freeze-thaw, chemical and conformational stability) properties as measured by OD_{350} assay, MFI, UV visible spectroscopy, Intact MS and DSC, respectively.

Formulation	**HIC** *Relative % (AB_5)*	**Osmolality (mOSm)**	**Agitation Stability** *MFI (ΔTotal particles$_{4hr-0hr}$ > 2µm,number/mL)*	**Thermal Stability (against aggregation)** *Temperature@OD_{350}=0.1 unit (^{o} C)*	**F/T Stability** *% Protein loss after 5FT*	**Chemical Stability Glycation** *(Stressed at 40^{o}C for 7 days)*	**Chemical Stability Oxidation** *(Addition of 0,1,2.5 and 5 mM H_2O_2)*	**Conformational Stability** *Tm values (DSC)*
50 mM sodium phosphate, 50 mM NaCl, 10% w/v sucrose, 5mM methionine, 0.1 %v/v PS-80 pH 7.4 ***(Candidate formulation)***	66±1	500±7	8.9 ± 2.9 x 10^2	72.5 ± 0.2	0.0 ± 0.1	No change in relative abundance of the glycated B-chain nor formation of additional glycated peaks	No oxidation detected at 1 and 2.5 mM H_2O_2	T_m1= 50.9 ± 0.2 T_m2= 52.8 ± 0.1 T_m3= 79.3 ± 0.1 T_m4= 82.0 ± 0.1
42.7 mM Sodium phosphate, 10.7mM potassium phosphate, 82 mM NaCl, 5% Lactose pH 7.4 ***(Current formulation)***	66±1	408±3	275.2 ± 11.8 x 10^2	74.4 ± 0.2	15.2 ± 0.3	Increased glycation and formation of additional glycated peaks	Oxidation detected at 1, 2.5 and 5 mM H_2O_2	T_m1= 51.3 ± 0.2 T_m2= 52.8 ± 0.1 T_m3= 79.5 ± 0.1 T_m4= 81.9 ± 0.1

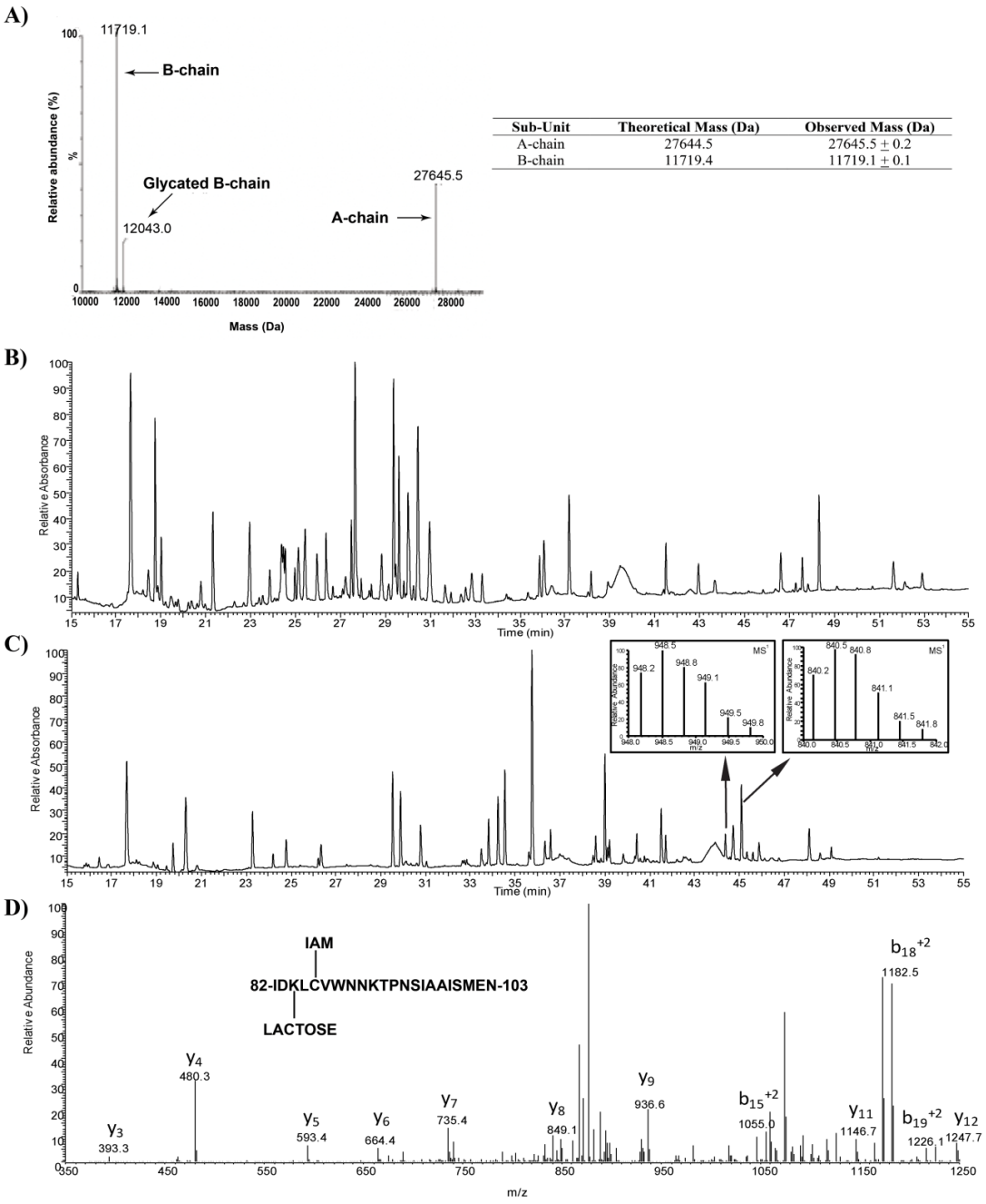

Sub-Unit	Theoretical Mass (Da)	Observed Mass (Da)
A-chain	27644.5	27645.5 ± 0.2
B-chain	11719.4	11719.1 ± 0.1

Figure 3.1. Primary structure analysis of dmLT. (a) Representative deconvoluted MS spectrum of intact mass protein spectrometry analysis of dmLT sample under nonreduced conditions and MW values from n = 3 measurements, (b) representative UV214 nm chromatograms from peptide map analysis of chymotrypsin-digested dmLT, (c) representative UV214 nm chromatograms from peptide map analysis of trypsin-digested dmLT with an inset showing the MS1 spectrum of the 2 peptide peaks which eluted at 44.4 min (948.2 m/z precursor ion) and 45.1 min (840.2 m/z precursor ion), (d) MS2 spectrum of the 948.2 m/z precursor ion corresponding to Ile82-Asn103 with Lys84 containing a lactose (+324 Da) modification.

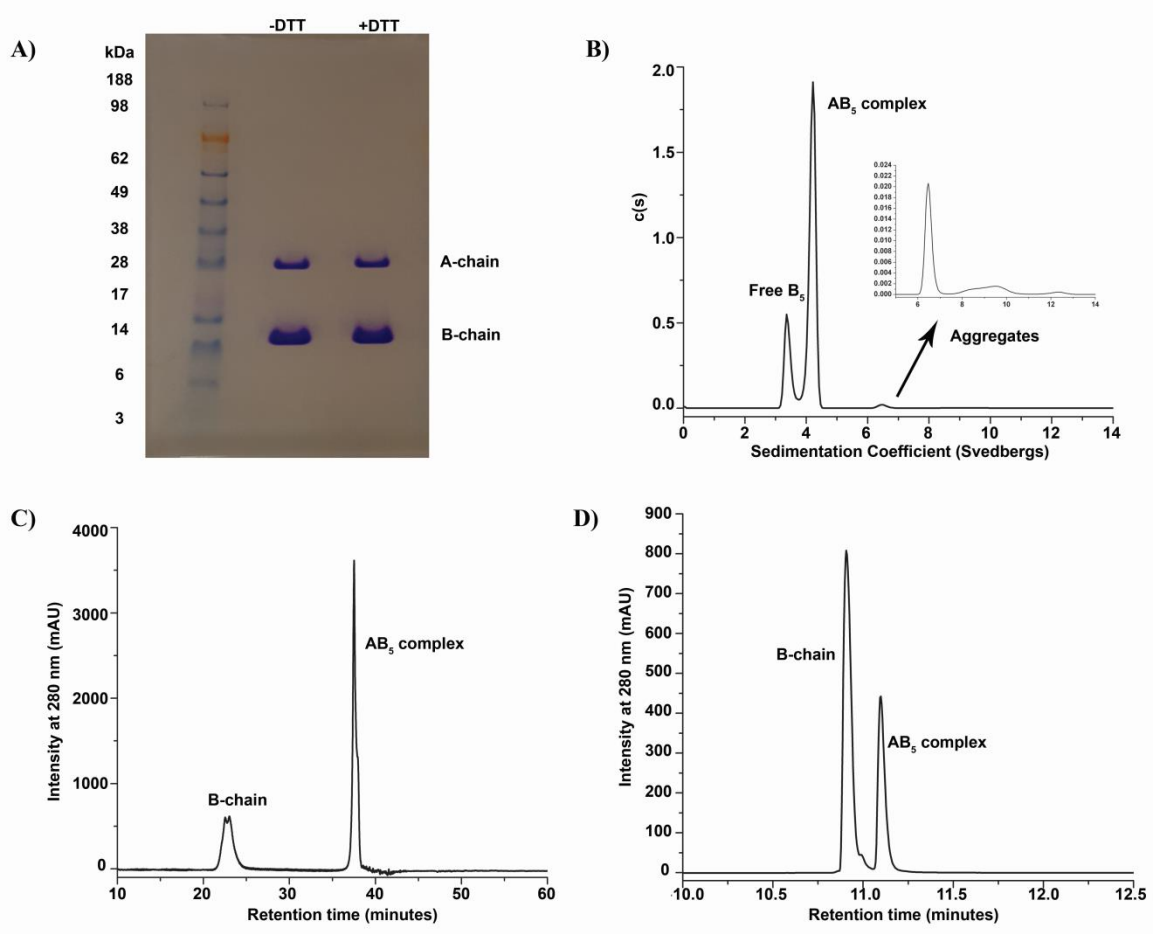

Figure 3.2. Protein size and heterogeneity analysis of dmLT. (a) SDS-PAGE analysis of dmLT under nonreducing (-DTT) and reducing conditions (+DTT), (b) SV-AUC studies of dmLT.Sedimentation coefficient distribution are shown from 0 to 14 svedbergs. The inset shows the distributions from 6 to 14 svedbergs to better visualize the aggregate peaks, (c) representative HIC chromatogram of dmLT sample, and (d) representative RP-UHPLC chromatogram of dmLT sample. DTT, dithiothreitol.

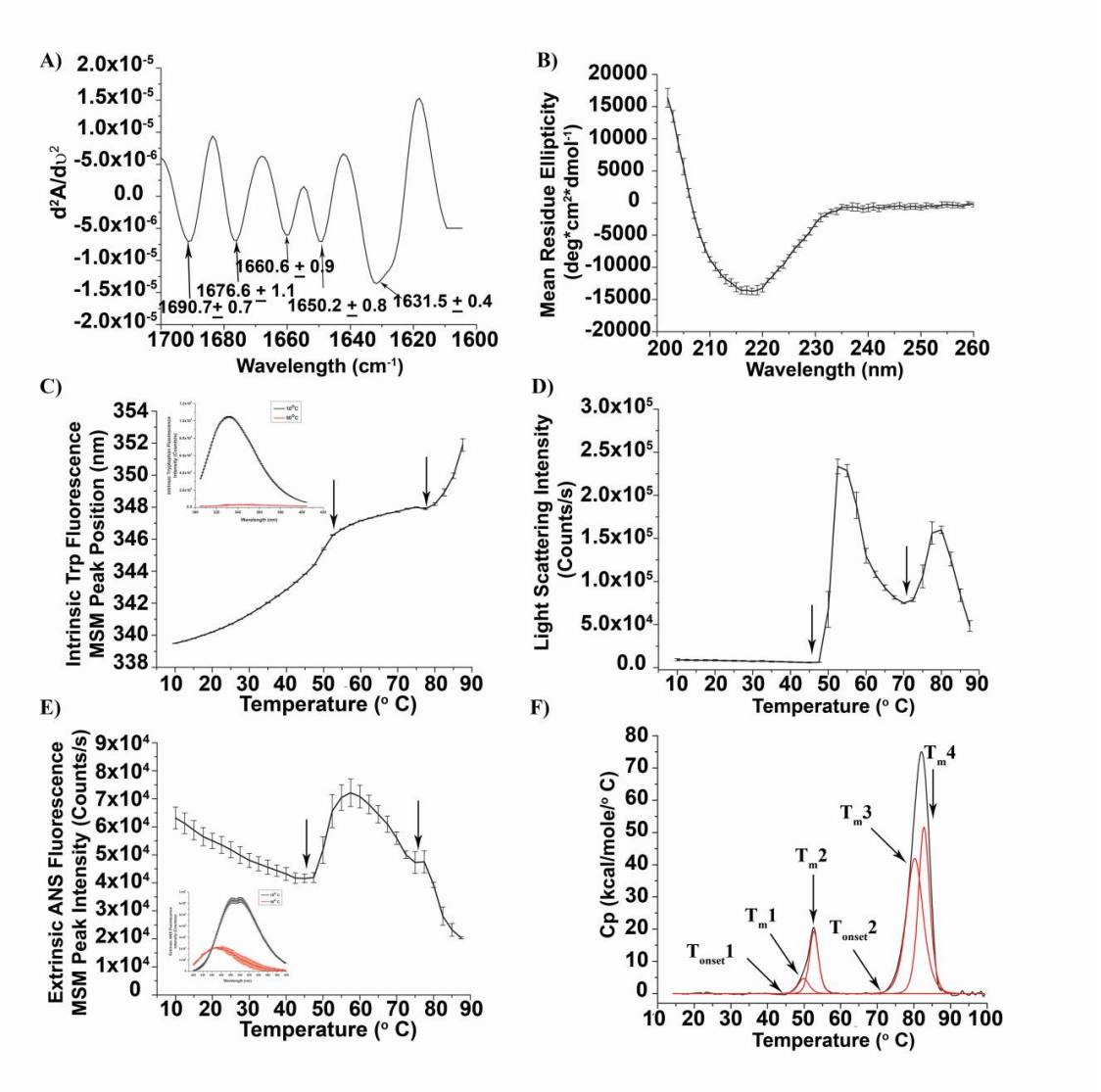

Figure 3.3. Higher order structure and overall conformational stability of dmLT in formulation buffer (see materials section) at pH 7.4. (A) representative second derivative FTIR spectrum of dmLT in the Amide I region (see supplemental Table 3.1 for individual peak assignments), (B) far-UV CD spectrum at 10 °C, (C) thermal melt for intrinsic Trp fluorescence peak position (10 to 90 ^{o}C); the inset shows intrinsic tryptophan fluorescence spectra's at 10 °C and 90 ^{o}C, (D) static light scattering at 295 nm (10 to 90 ^{o}C), (E) extrinsic ANS fluorescence peak intensity (10 to 90 ^{o}C); the inset shows the extrinsic ANS fluorescence spectra at 10 and 90 ^{o}C. Two major transitions as indicated by arrows, one for A-chain (~50^{o}C) and the second for B-chain (~70^{o}C) are observed using variety of biophysical measurements. (F) Representative DSC thermogram of dmLT. The black line represents raw thermogram and the red line represents the curve fitted data to four peaks. The Tm1, Tm2 values indicate the thermal melting transitions for the A-chain and Tm3, Tm4 values indicate the thermal melting transitions for the B-chain of dmLT. Error bars are standard deviation from triplicate experiments.

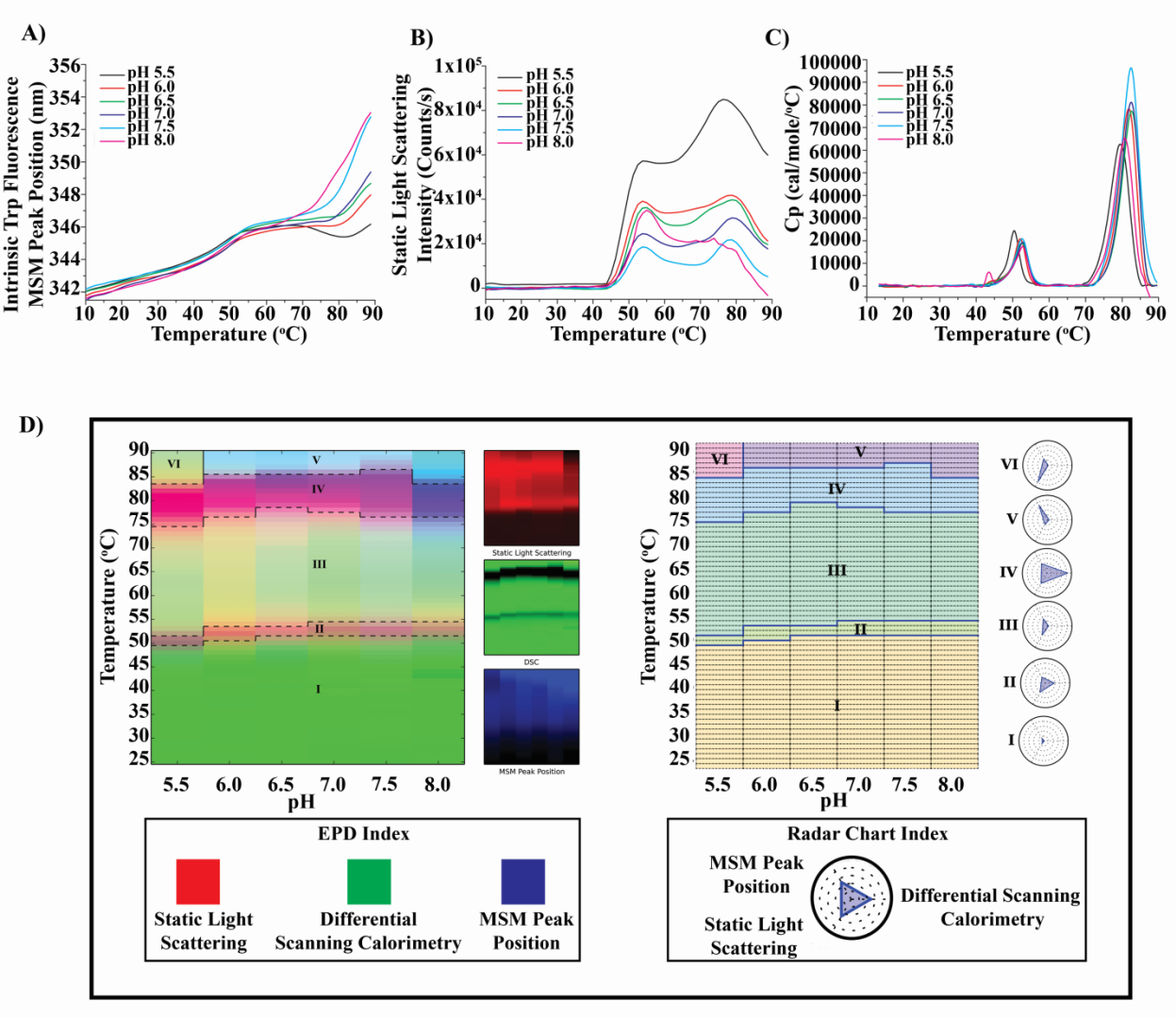

Figure 3.4. Biophysical characterization and 3-index EPD and radar chart analysis of dmLT versus temperature across the pH range of 5.5-8.0 in formulation buffer. Biophysical measurements including (a) intrinsic Trp fluorescence, (b) static light scattering at 295 nm, and (c) DSC, and (d) 3-index EPDs (left panel) and radar chart (right panel) for dmLT were generated using the data sets obtained from intrinsic Trp fluorescence peak position, static light scattering at 295 nm, and DSC. The error bars have been removed from the data sets for better visualization of data. See Supplemental Figure 3.3 for data sets with error bars.

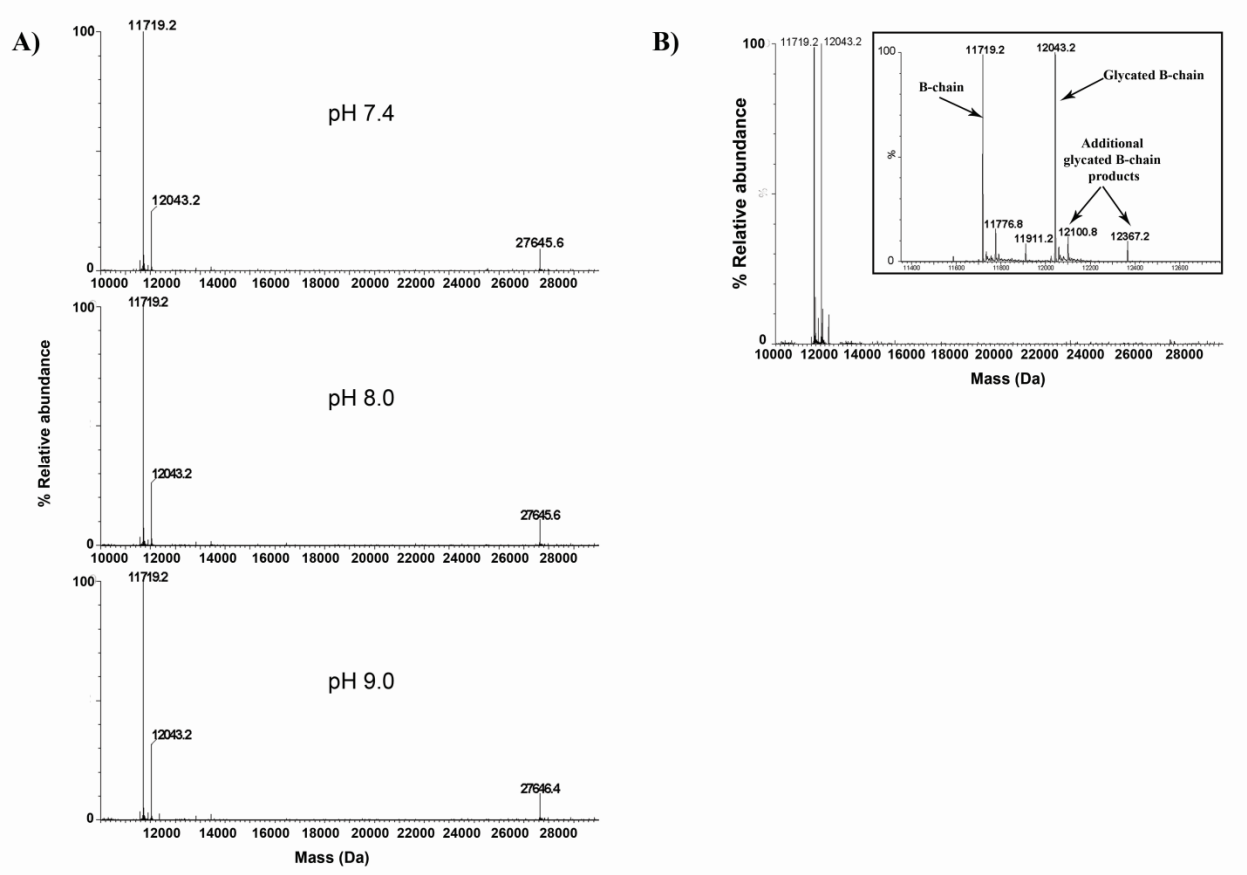

Figure 3.5. Forced deamidation and glycation studies of dmLT as a function of pH and temperature, respectively. (a) Intact protein MS analysis of dmLT sample after 1 week of incubation at 4^{o}C under 3 different pH conditions (7.4, 8.0, and 9.0), (b) intact protein MS of dmLT at pH 7.4 after 1 week of incubation at 40^{o}C, showing an increase in glycation of the B chain as well as formation of additional glycated B chain products.

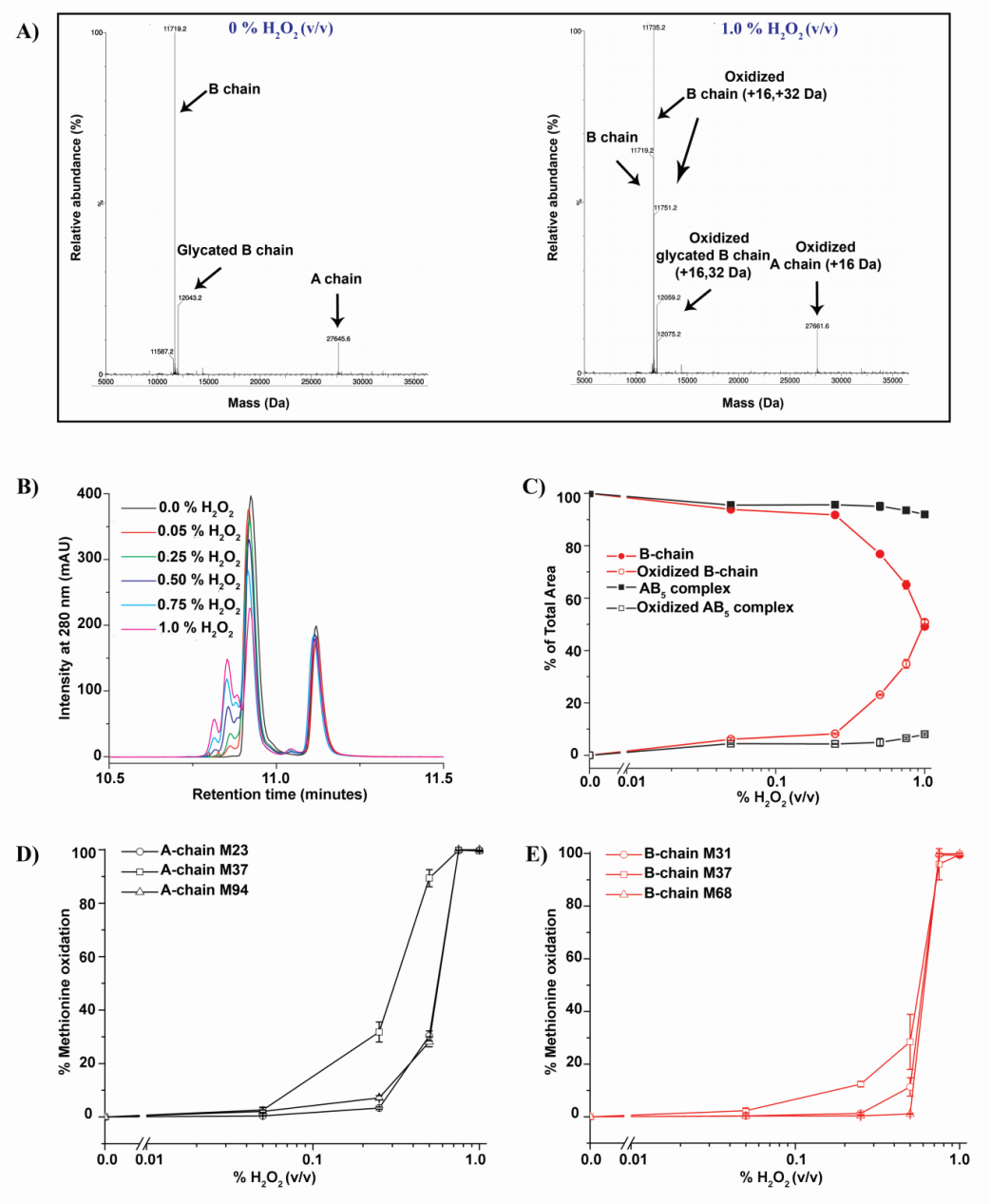

Figure 3.6. Forced oxidation studies of dmLT as a function of hydrogen peroxide concentration. (a) Representative intact protein MS analysis of dmLT samples after incubation with different concentrations of H_2O_2, 0% and 1% v/v, respectively. (b) Representative RP-UHPLC chromatograms as a function of H_2O_2 concentration, (c) % of total area of the free B chain and AB5 complex peaks as a function of H_2O_2 concentration, (d) hydrogen peroxide effect on the relative oxidation percentage of 3 methionine residues in dmLT A chain, and (e) hydrogen peroxide effect on the relative oxidation percentage of 3 out of 4 methionine residues in dmLT B chain. Note that oxidation of Met101 in the dmLT B chain could not be quantified due to low abundant peptides in the presence of H_2O_2. Error bars represent the SD from triplicate experiments

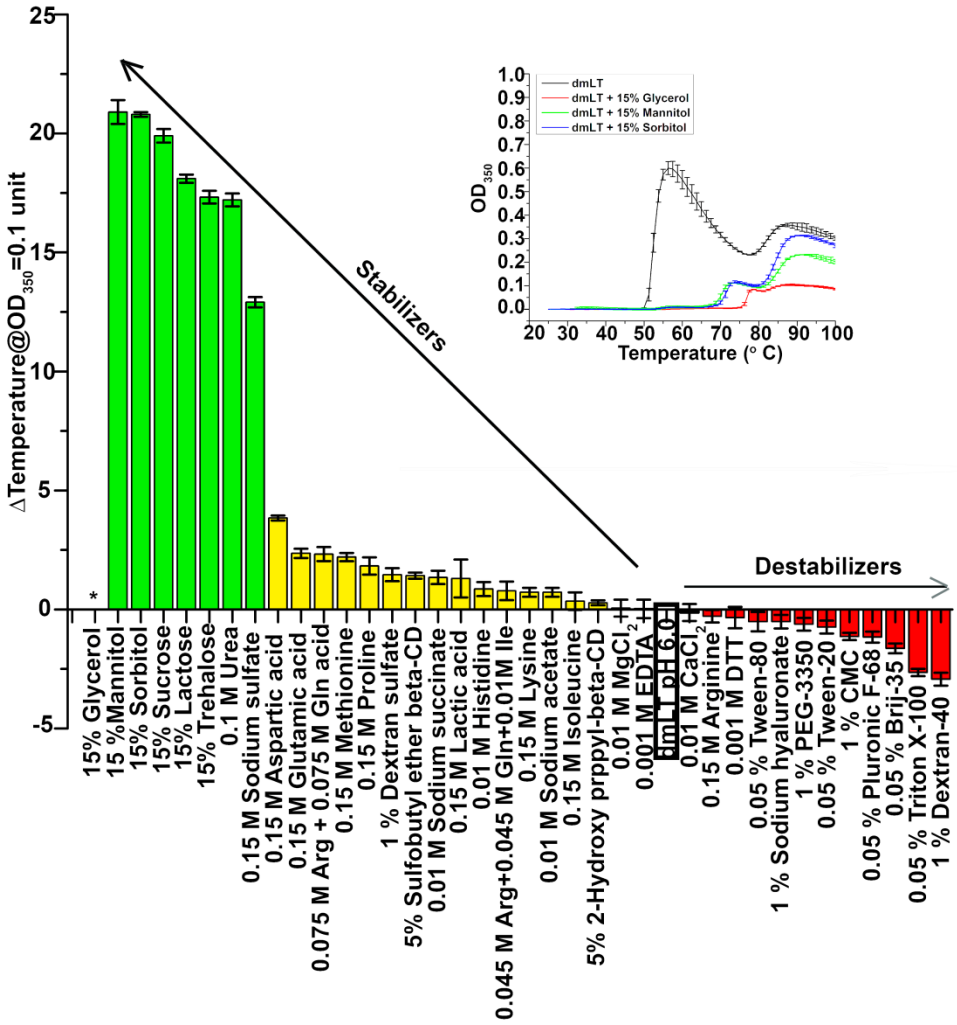

Figure 3.7. OD_{350} studies of aggregation propensity (delta temperature values) of dmLT containing solutions after thermal stress in presence of different excipients. Average delta temperature value at which the OD_{350} value reaches 0.1 absorbance unit for dmLT (0.15 mg/mL) in control buffer plus excipient vs. dmLT in control buffer alone (10 mM sodium phosphate, 150 mM NaCl, pH 6.0 with no additional excipient; highlighted box). The dmLT samples are shown in order of highest to lowest OD_{350} (indicating highest to lowest stability in terms of aggregation behavior). Error bars represent the standard deviation from triplicate experiments. The inset shows the representative OD_{350} thermal melt experiment of dmLT formulated in control buffer alone and control buffer in the presence of glycerol, mannitol and sorbitol. Excipients in green, yellow and red showed a large increase, moderate increase and low/no increase in stability, respectively. *For 15% glycerol, OD_{350} value did not reached 0.1 absorbance unit and hence delta temperature could not be calculated.

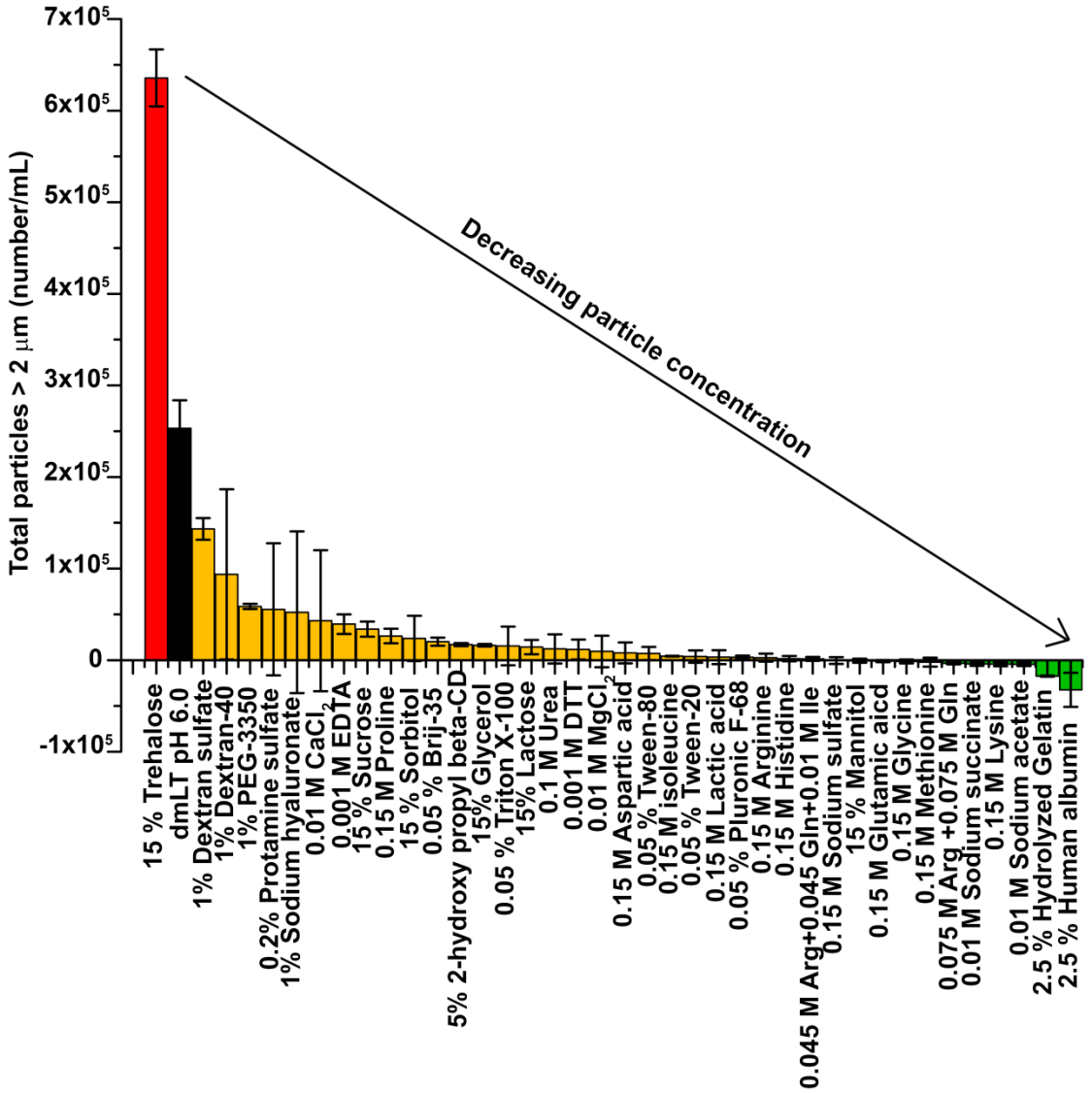

Figure 3.8. MFI studies of subvisible particle formation in dmLT containing solutions after agitation stress as a function of excipient addition. Total increase in the sub-visible particle concentration (after 4 h of agitation minus time zero results from the same solution) is shown for each of the dmLT samples in order of decreasing particle concentration. The control (dmLT (0.15 mg/mL) in 10 mM sodium phosphate, 150 mM NaCl, pH 6.0 with no additional excipient) is indicated by black bar and is included for reference. Error bars represent the standard deviation from triplicate experiments. Excipients added to dmLT in control buffer in green, yellow and red showed a large increase, moderate increase and low/no increase in number of sub-visible particles, respectively.

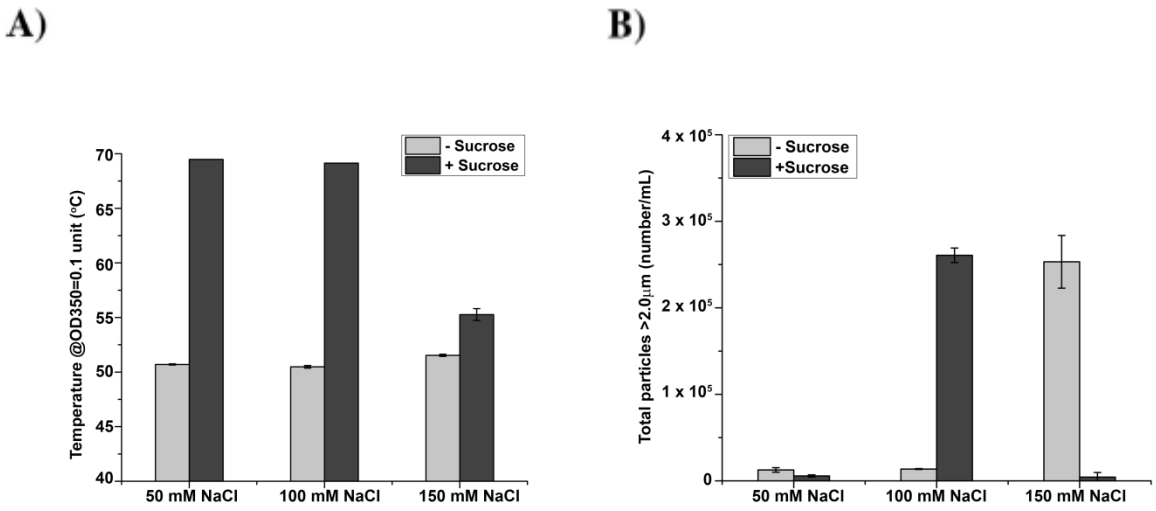

Figure 3.9. Effect of sodium chloride concentration on dmLT physical stability profile at 0.15 mg/mL in a base buffer containing 10 mM phosphate buffer, ±10% w/v sucrose, pH 6.0. (A) Thermal stress as monitored by OD_{350} temperature values of dmLT as a function of salt concentration. Average temperature value at which the OD_{350} value reaches 0.1 of different concentrations of salts is shown, and (B) agitation stress as measured by MFI in terms of total increase in sub-visible particle concentration (agitation for 4 h minus time zero for same solution) is shown for each of the dmLT samples. Error bars represent the standard deviation from triplicate experiments.

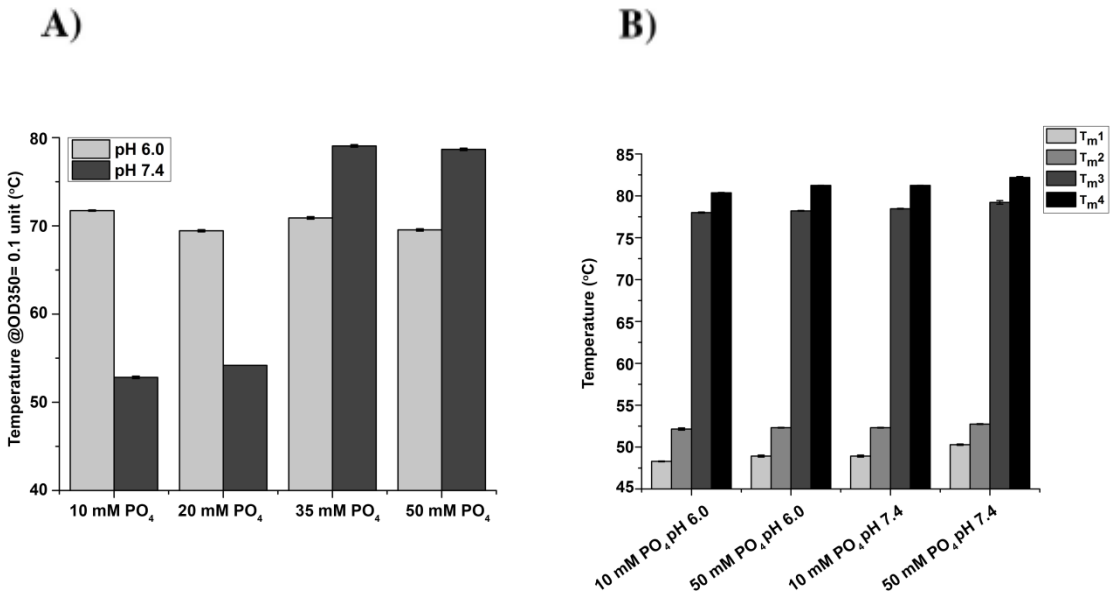

Figure 3.10. Effect of phosphate buffer concentration and pH on the thermal stability of dmLT at pH 6.0 and pH 7.4 in two different candidate formulations (see text for formulation conditions). (A) Temperature to reach 0.1 absorbance unit as measured by OD_{350} thermal melts assay with dmLT in different solutions, and (B) Tm values for dmLT in two different candidate formulations (pH 6.0 and pH 7.4) containing an additional 10 and 50 mM phosphate ion as measured by DSC. Error bars represent the standard deviation from triplicate experiments.

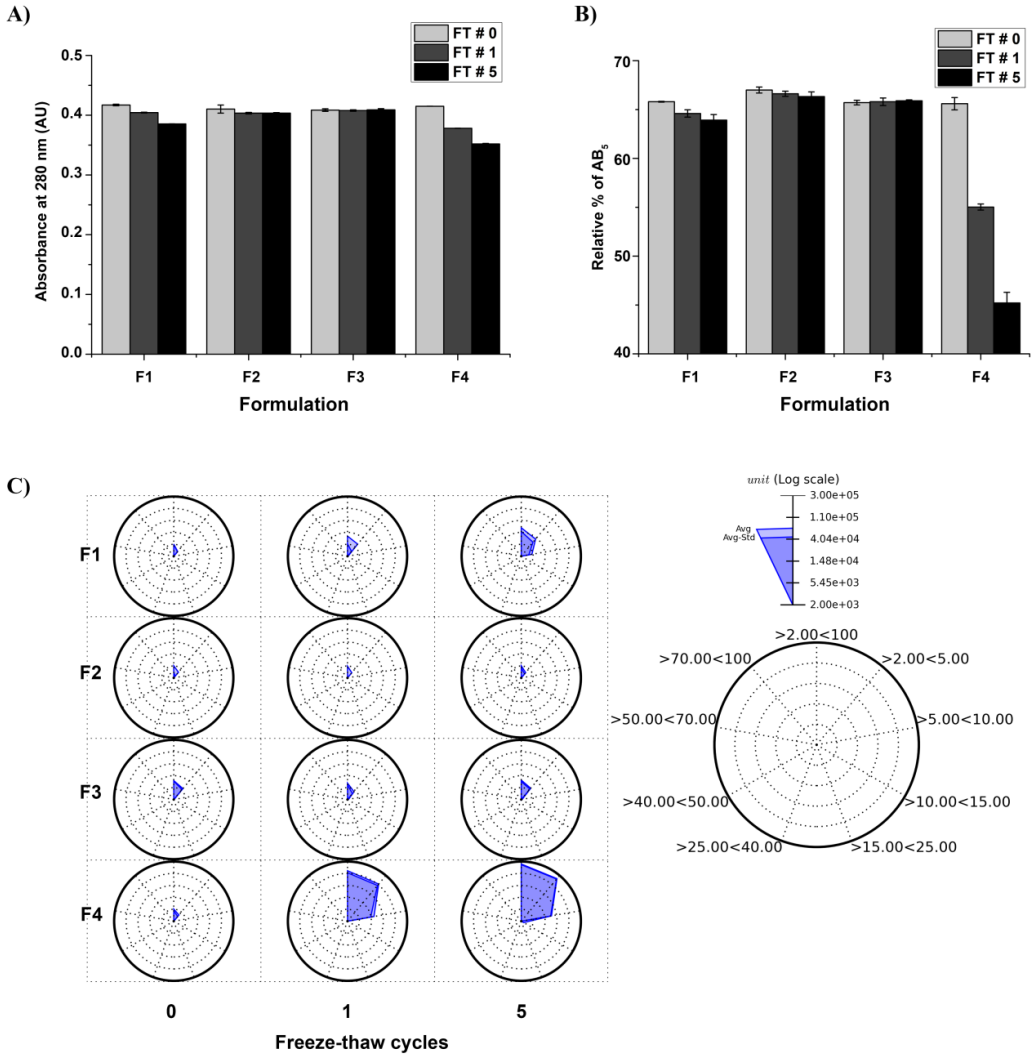

Figure 3.11. Effect of PS-80 concentration (0.01, 0.05 and 0.1% w/v) on freeze-thaw (0, 1 and 5 freeze-thaw cycles) stability of dmLT compared to dmLT in the current formulation.(A) Absorbance at 280 nm showing protein loss with increasing freeze thaw cycles, (B) % of native dmLT (AB5 complex) as a function of freeze-thaw cycles as measured by HIC, and (C) radar plot analysis of the number and size distribution of sub-visible particles formed upon freeze-thaw as measured by MFI. The dmLT protein concentration was 0.4 mg/mL in the four formulations namely F1: 50 mM sodium phosphate, 50 mM NaCl, 10% w/v sucrose, 5 mM methionine, 0.01% v/v PS-80 pH 7.4; F2: 50 mM sodium phosphate, 50 mM NaCl, 10% w/v sucrose, 5 mM methionine, 0.05% v/v PS-80 pH 7.4; F3: 50 mM sodium phosphate, 50 mM NaCl, 10% w/v sucrose, 5 mM methionine, 0.1% v/v PS-80 pH 7.4 and F4: 42.7 mM sodium phosphate, 10.7 mM potassium phosphate, 82 mM NaCl, 5% lactose, pH7.4 (current formulation buffer). Error bars indicate standard deviation of triplicate samples.

Supplemental Table 3.1. Assignment of secondary structure of dmLT based on the second derivative of the Amide I region (1700-1600 cm-1) as measured by FTIR. Data represent the average and standard deviation for n=3 replicates.

Wavenumber (cm^{-1})	Type of secondary structure
1690.7 ± 0.7	Beta turns
1676.6 ± 1.1	Beta sheet
1660.6 ± 0.9	Alpha helix/random coil
1650.2 ± 0.8	Alpha helix/loops/disordered
1631.5 ± 0.4	Beta sheet

Supplemental Table 3.2. Summary of thermal onset temperature values (Tonset1, Tonset2) and thermal melting Temperature values (Tm1, Tm2, Tm3, and Tm4) for the dmLT protein as measured by DSC. The dmLT is at 0.4 mg/mL in formulation buffer at pH 7.4. Values represent mean and standard deviation of n=3 replicates.

	$T_{onset}1$ (°C)	**$T_{onset}2$ (°C)**	**T_m1 (°C)**	**T_m2 (°C)**	**T_m3 (°C)**	**T_m4 (°C)**
dmLT pH 7.4	46.3 $\pm$ 0.4	73.1 $\pm$ 0.2	51.0 $\pm$ 0.1	52.7 $\pm$ 0.1	80.8 $\pm$ 0.2	83.0 $\pm$ 0.2

Supplemental Table 3.3. Summary of thermal onset temperature values (Tonset) and thermal melting temperature values (Tm) for the dmLT protein (0.2 mg/mL) in the formulation buffer under different pH conditions (pH 5.5, 6.0, 6.5, 7.0, 7.5 and 8.0) measured by static light scattering (SLS) and differential scanning calorimetry (DSC). The values represent the average and standard deviation of n=3 replicates.

Technique	**pH**	**$T_{onset}1$ (°C)**	**$T_{onset}2$ (°C)**	**T_m1 (°C)**	**T_m2 (°C)**	**T_m3 (°C)**	**T_m4 (°C)**
SLS	5.5	43.1 ± 0.1	NA	NA	NA	NA	NA
	6.0	44.9 ± 0.1					
	6.5	45.3 ± 0.0					
	7.0	45.5 ± 0.1					
	7.5	46.0 ± 0.0					
	8.0	45.1 ± 0.0					
DSC	5.5	45.2 ± 0.0	67.6 ± 0.1	47.1 ± 0.3	50.7 ± 0.0	77.6 ± 0.3	80.3 ± 0.5
	6.0	45.5 ± 0.0	72.1 ± 0.0	49.4 ± 0.1	52.2 ± 0.0	79.9 ± 0.1	82.3 ± 0.1
	6.5	45.8 ± 0.1	72.5 ± 0.1	50.5 ± 0.4	52.7 ± 0.1	80.6 ± 0.1	83.1 ± 0.1
	7.0	45.9 ± 0.1	72.5 ± 0.1	50.2 ± 0.1	52.9± 0.1	80.5 ± 0.2	83.0 ± 0.2
	7.5	46.7 ± 0.1	73.2 ± 0.1	50.8 ± 0.2	52.8 ± 0.1	81.1 ± 0.1	83.3 ± 0.1
	8.0	42.5 ± 0.1	47.8 ± 0.1 *70.5 ± 0.1 *($T_{onset}3$)	43.9 ± 0.0	52.5 ± 0.0	81.6 ± 0.1	79.0 ± 0.1

Supplemental Table 3.4. List of pharmaceutical excipients selected for further optimization for formulation design of dmLT. Excipients with a (+) sign indicate the excipient added to base buffer (10 mM sodium phosphate, 150 mM NaCl, pH 6.0) that showed a potential stabilizing effect on inhibiting dmLT aggregation as measured by OD_{350} assay for thermal stability and as measured by MFI for agitation stability. The excipients highlighted in yellow in Supplemental Table 3.4 were chosen for further optimization based on their most effective overall stabilizing effect with dmLT.

Excipient Category	Excipient	Thermal Stress	Agitation stress
Salts/Buffers	Sodium acetate	+	+
	Sodium sulfate (salt)	+	+
	Sodium succinate	+	
Proteins	Human Albumin		+
	Hydrolysed Gelatin		+
	Protamine sulfate		+
Amino acids and Miscellaneous	Arginine		+
	Aspartic acid	+	+
	Glutamic acid	+	+
	Glycine		+
	Histidine		+
	Isoleucine		+
	Lactic acid		+
	Lysine		+
	Methionine	+	+
	Proline	+	+
	Urea		+
	Arginine + Glutamic acid		+
	Arginine + Glutamic acid + Isoleucine		
Metal ions/Chelators/Reducing agents	Calcium chloride		+
	DTT		+
	EDTA		+
	Magnesium chloride		+
Detergents	Brij 35		+
	Poloxamer 188 (Pluronic F-68)		+
	Polysorbate 20		+
	Polysorbate 80		+
	Triton X-100		
Carbohydrates	Lactose	+	+
	Sucrose	+	+
	Trehalose	+	
Polyols	Glycerol	+	+
	Mannitol	+	+
	Sorbitol	+	+
Cyclodextrins	2-OH propyl b-CD		+
Polymers/Osmolyte/Polyions	Carboxymethyl cellulose		+
	Dextran sulfate		+
	Dextran 40		+
	PEG-3350		+
	Sodium Hyaluronate		+

Supplemental Table 3.5. A summary of the intact protein mass spectrometry analysis of dmLT in the candidate vs current formulation after forced glycation studies. Data represent the average and standard deviation for n=3 replicates.

Time	Candidate Formulation MW(Da)	Current Formulation MW(Da)
Day = 0	A chain = 27645.6 ± 0.4 B-chain =11718.8 ± 0.1 Glycated B-chain = 12043.3 ± 0.3	A chain = 27645.5 ± 0.2 B-chain =11718.9 ± 0.2 Glycated B-chain = 12043.5 ± 0.1
Day = 7	A chain = 27646.1 ± 0.4 B-chain =11719.2 ± 0.1 Glycated B-chain = 12044.0 ± 0.0	A chain =27646.1 ± 0.2 B-chain =11719.6 ± 0.1 Glycated B-chain = 12043.8 ± 0.1 12101.2 ± 0.2 12367.9 ± 0.1

Supplemental Table 3.6. A summary of the intact protein mass spectrometry analysis of dmLT in the candidate vs current formulation after forced oxidation studies. Data represent the average and standard deviation for n=3 replicates. NA is not applicable.

H_2O_2 (mM)	Subunit of dmLT	Candidate Formulation MW (Da)	Current Formulation MW (Da)
0	A-chain	27645.6 ± 0.4	27645.3 ± 0.3
	B-chain	11719.2 ± 0.2	11719.0 ± 0.2
	Glycated B-chain	12043.9 ± 0.3	12043.5 ± 0.1
	Oxidized A-chain (+16 Da)	NA	NA
	Oxidized B-chain (+16 Da)	NA	NA
	Oxidized glycated B-chain (+16 Da)	NA	NA
1	A-chain	27645.3 ± 0.2	27646.0 ± 0.2
	B-chain	11719.0 ± 0.1	11719.1 ± 0.1
	Glycated B-chain	12044.0 ± 0.0	12044.0 ± 0.1
	Oxidized A-chain (+16 Da)	NA	27662.1± 0.2
	Oxidized B-chain (+16 Da)	NA	NA
	Oxidized glycated B-chain (+16 Da)	NA	NA
2.5	A-chain	27645.2 ± 0.3	27646.0 ± 0.3
	B-chain	11719.2 ± 0.2	11719.1 ± 0.1
	Glycated B-chain	12043.8 ± 0.1	12044.0 ± 0.1
	Oxidized A-chain (+16 Da)	NA	27662.1± 0.1
	Oxidized B-chain (+16 Da)	NA	NA
	Oxidized glycated B-chain (+16 Da)	NA	NA
5	A-chain	27645.6 ± 0.3	NA
	B-chain	11718.9 ± 0.2	11718.7± 0.2
	Glycated B-chain	12043.8 ± 0.1	12043.5 ± 0.1
	Oxidized A-chain (+16 Da)	27662.0 ± 0.3	27662.1 ± 0.2
	Oxidized B-chain (+16 Da)	NA	11735.0± 0.4
	Oxidized glycated B-chain (+16 Da)	NA	12059.7 ± 0.2

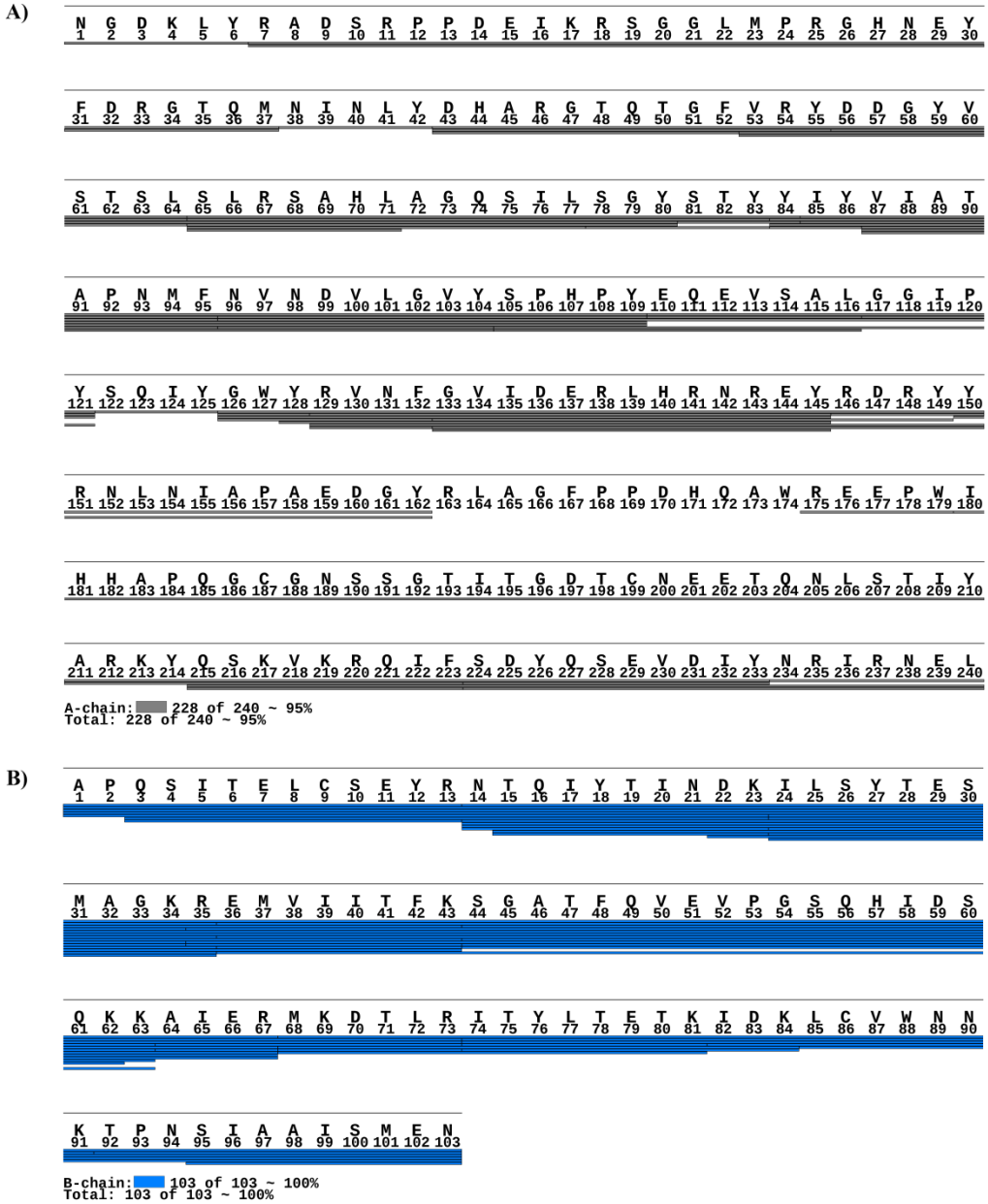

Supplemental Figure 3.1. Sequence coverage from peptide map analysis of dmLT with either trypsin or chymotrypsin-digestion. (A) sequence coverage of dmLT A-chain, (B) sequence coverage of dmLT B-chain. The sequence coverages for both A and B-chain were $\geq$ 95%.

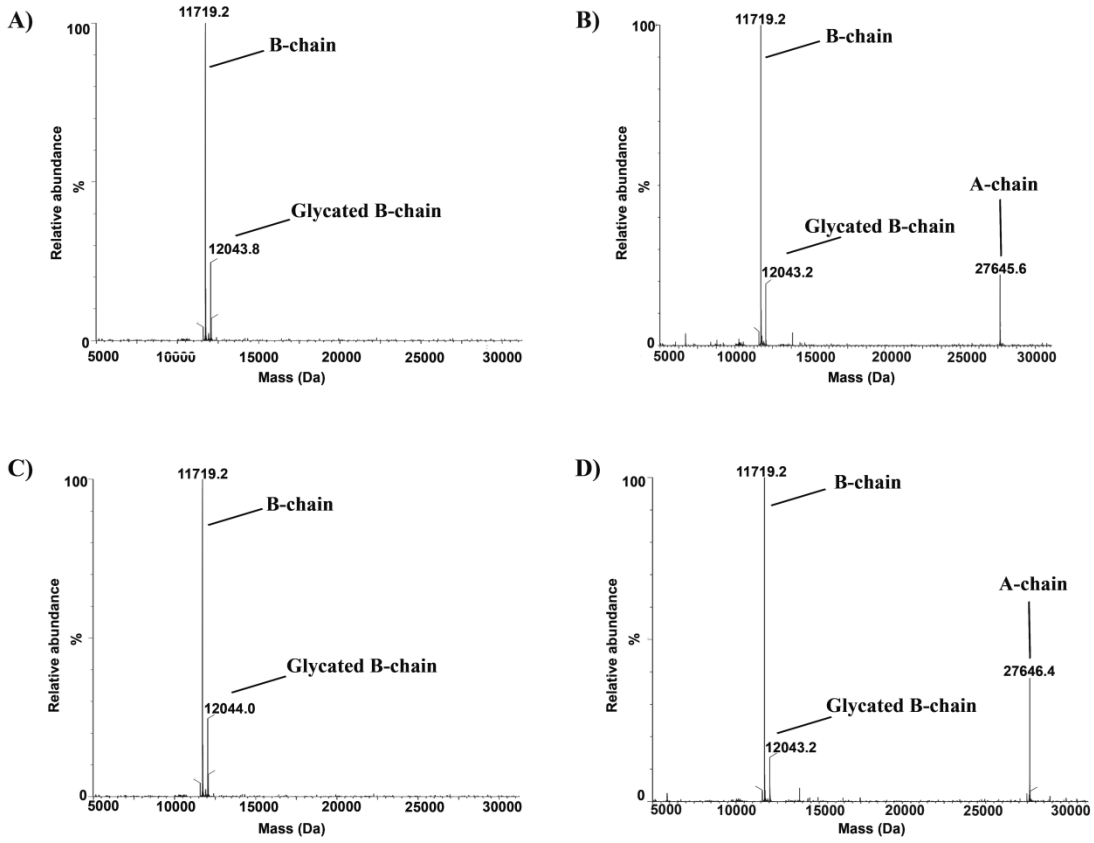

Supplemental Figure 3.2. Intact mass analysis of peaks collected during HIC and RP-UHPLC of dmLT. (Panels A, C) Peak 1 collected from HIC and RP- UHPLC showing B-chain, (Panels B, D) Peak 2 collected from HIC and RP-UHPLC, showing a mixture of A and B-chain (AB_5).

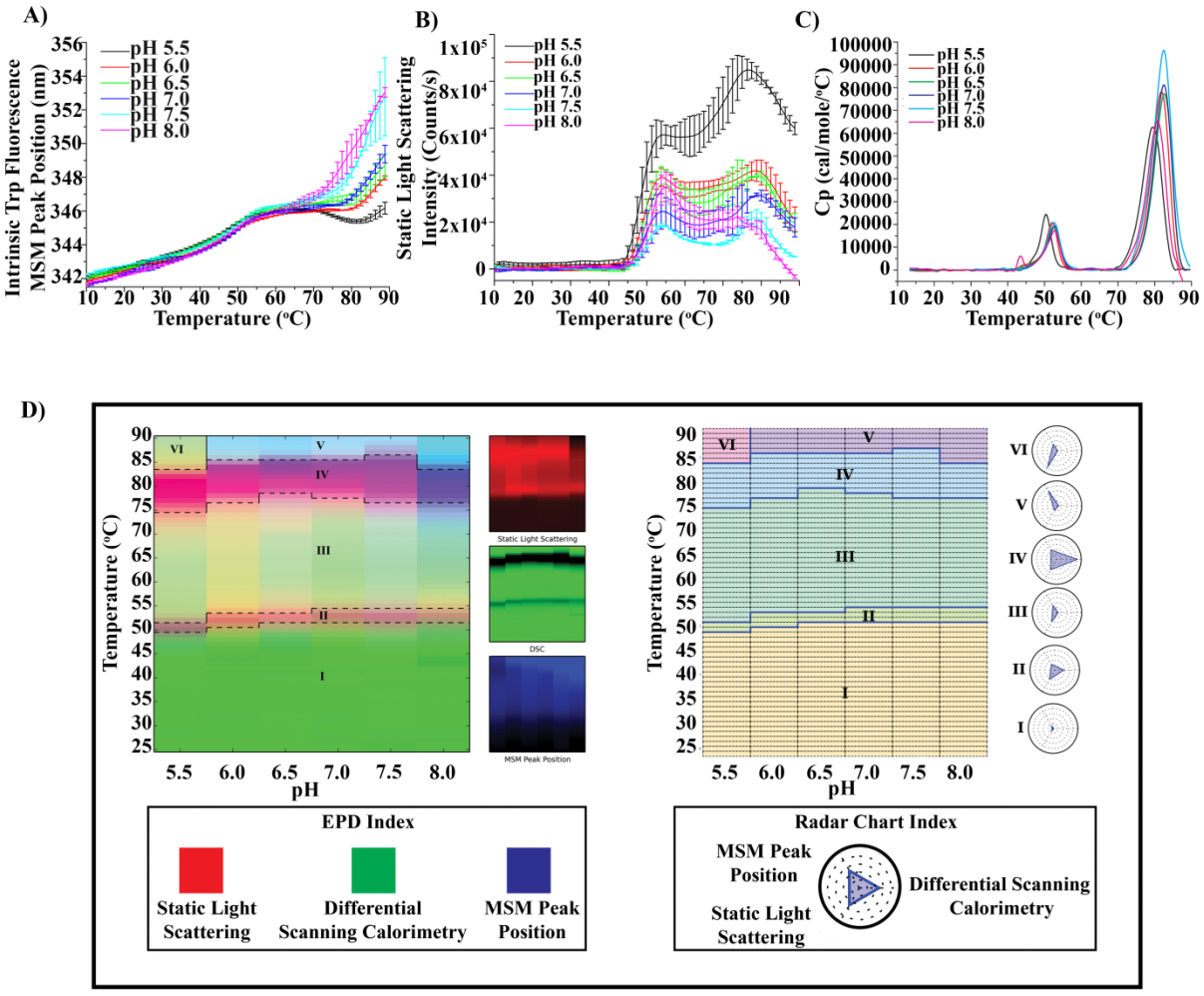

Supplemental Figure 3.3. Biophysical characterization and three-index EPD and radar chart analysis of dmLT versus temperature across the pH range of 5.5-8.0 in formulation buffer. Biophysical measurements include (A) intrinsic Trp fluorescence, (B) static light scattering at 295 nm, (C) differential scanning calorimetry, (D) three index empirical phase diagrams (left panel) and radar chart (right panel) for dmLT were generated using the datasets obtained from intrinsic Trp fluorescence peak position, static light scattering at 295 nm and differential scanning calorimetry. The error bars represent standard deviation from triplicate samples.

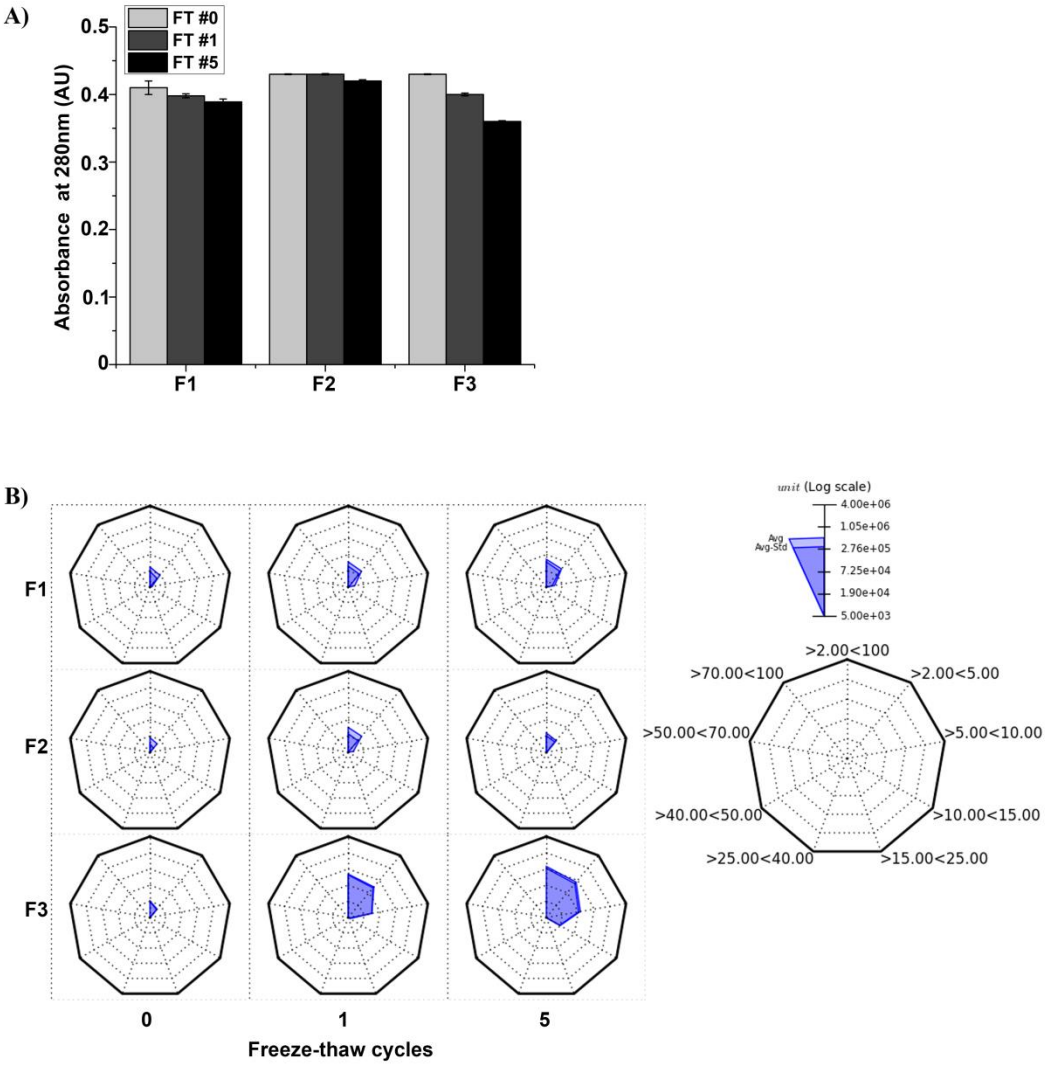

Supplemental Figure 3.4. Effect of freeze-thaw (0, 1 and 5 freeze-thaw cycles) on stability of dmLT in two candidate formulations vs current formulation. (A) Absorbance at 280 nm showing protein loss with increasing freeze thaw cycles, (B) radar plot analysis of the number and size distribution of sub-visible particles formed upon freeze-thaw as measured by MFI. The dmLT protein concentration was 0.4 mg/mL in the three formulations namely candidate formulation F1- (10 mM phosphate, 50 mM NaCl, 10% w/v sucrose, 5 mM methionine, 0.01% v/v PS-80 pH 6.0), candidate Formulation F2- (50 mM phosphate, 50 mM NaCl, 10% w/v sucrose, 5 mM methionine, 0.01% v/v PS-80, pH 7.4) and Formulation F3- Current dmLT formulation, (42.7 mM sodium phosphate, 10.7 mM potassium phosphate, 82 mM NaCl, 5% lactose , pH 7.4). Error bars indicate standard deviation of triplicate samples.

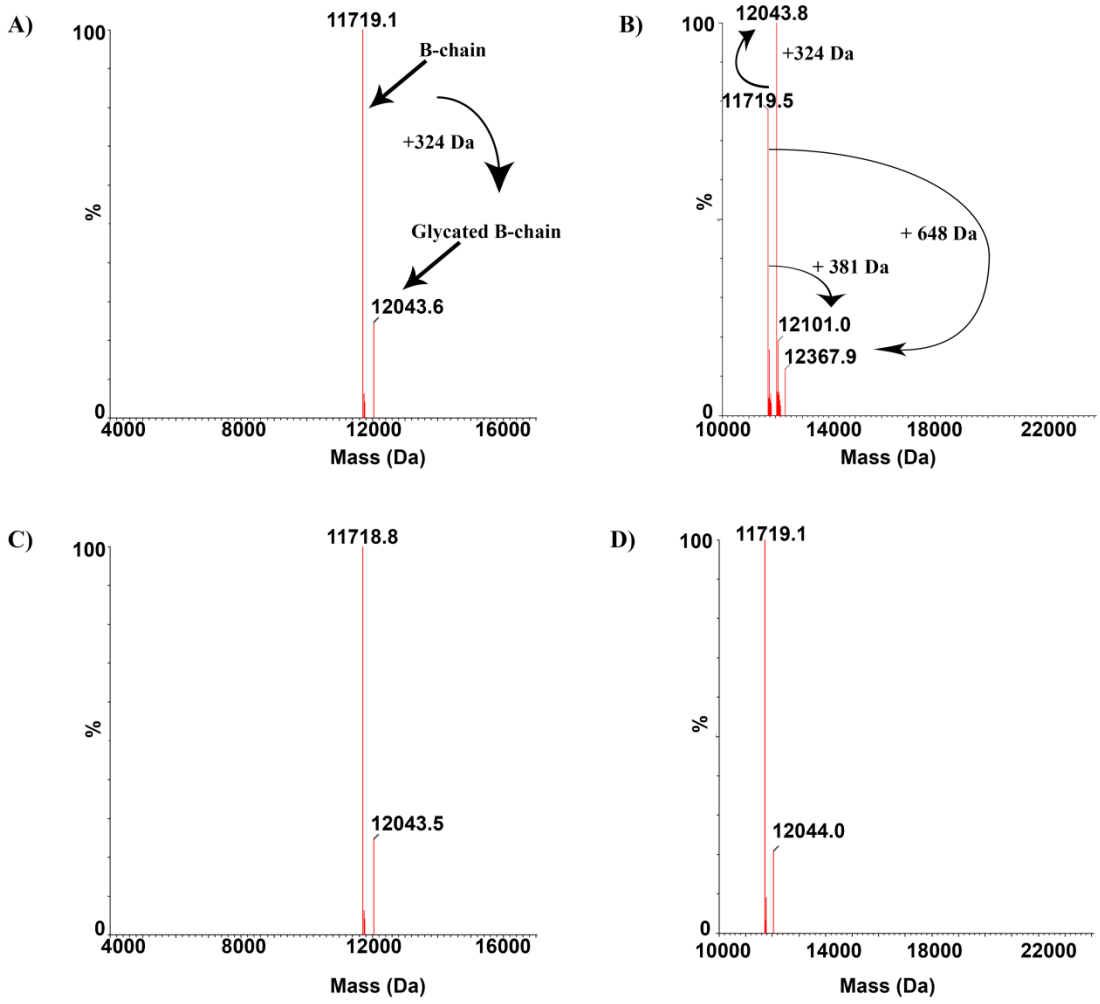

Supplemental Figure 3.5. Forced glycation studies of dmLT formulated in candidate vs current formulations. (A and B). Representative intact protein mass spectrometry analysis of B-chain of dmLT in current formulation sample at time zero and after incubation at 40 ^{o}C for 7 days, respectively, showing an increase in glycation of the B-chain as well as formation of additional glycated B-chain products (+381 and +648 Da), and (C and D) representative intact protein mass spectrometry analysis of B-chain of dmLT in new candidate formulation at time zero and after incubation at 40 oC for 7 days, respectively.

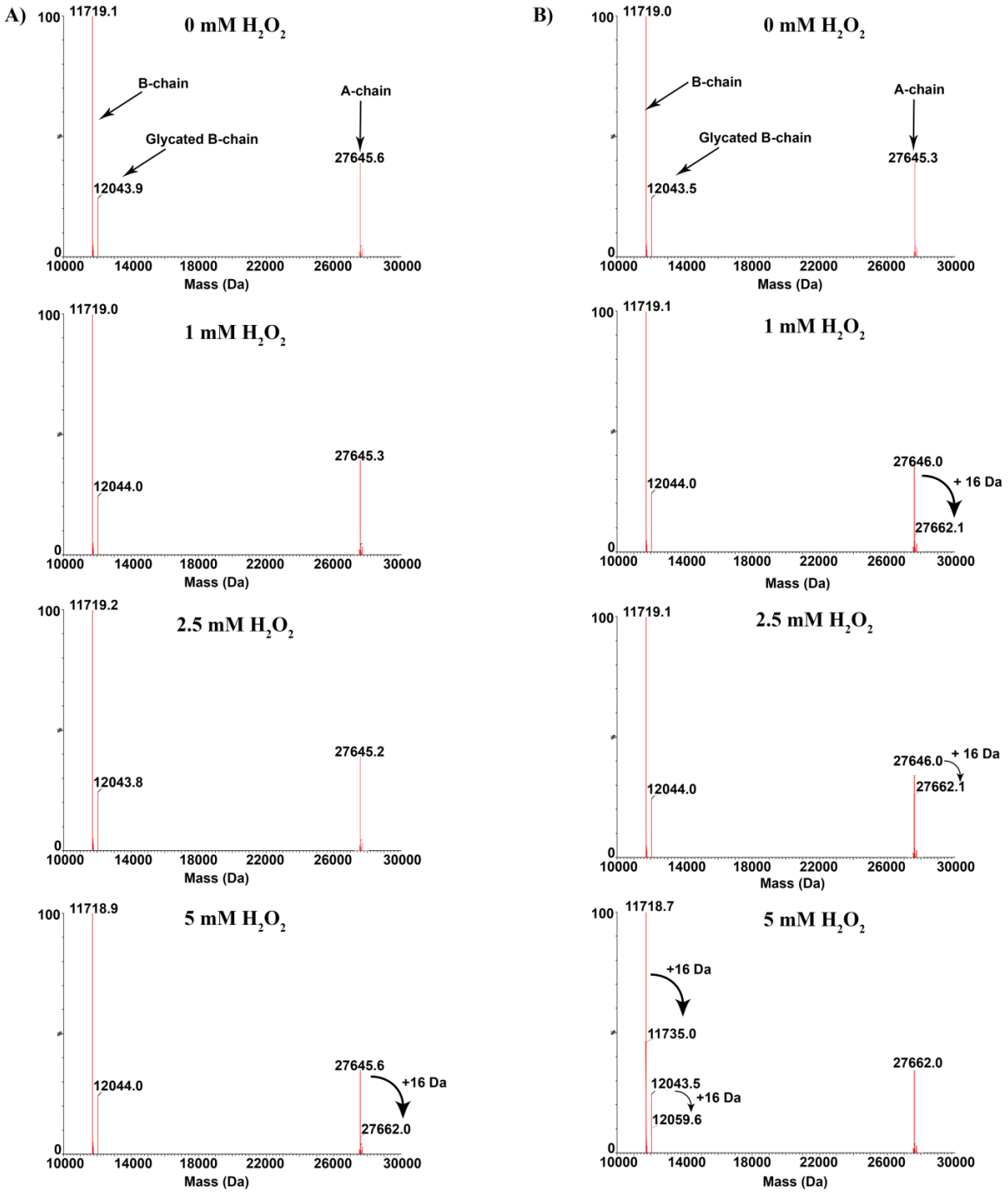

Supplemental Figure 3.6. Forced oxidation studies of dmLT in candidate vs current formulation. A) Representative intact protein mass spectrometry analysis of dmLT in candidate formulation incubated for four hours at 37°C with 0, 1, 2.5 and 5 mM hydrogen peroxide, and B) representative intact mass spectrometry analysis of dmLT in the current formulation incubated under the same stress conditions.

3.5 References

1. Freytag LC, Clements JD 2005. Mucosal adjuvants. Vaccine 23(15):1804-1813.

2. Levine MM 2010. Immunogenicity and efficacy of oral vaccines in developing countries: lessons from a live cholera vaccine. BMC Biology 8(1):1-10.

3. Lycke N 2012. Recent progress in mucosal vaccine development: potential and limitations. Nat Rev Immunol 12(8):592-605.

4. Holmgren J, Czerkinsky C, Eriksson K, Mharandi A 2003. Mucosal immunisation and adjuvants: a brief overview of recent advances and challenges. Vaccine 21, Supplement 2:S89-S95.

5. Leach S, Clements JD, Kaim J, Lundgren A 2012. The Adjuvant Double Mutant Escherichia coli Heat Labile Toxin Enhances IL-17A Production in Human T Cells Specific for Bacterial Vaccine Antigens. PLoS ONE 7(12):e51718.

6. Rappuoli R, Pizza M, Douce G, Dougan G 1999. Structure and mucosal adjuvanticity of cholera and Escherichia coli heat-labile enterotoxins. Immunology Today 20(11):493-500.

7. Pizza M, Giuliani MM, Fontana MR, Monaci E, Douce G, Dougan G, Mills KHG, Rappuoli R, Del Giudice G 2001. Mucosal vaccines: non toxic derivatives of LT and CT as mucosal adjuvants. Vaccine 19(17–19):2534-2541.

8. Norton EB, Lawson LB, Freytag LC, Clements JD 2011. Characterization of a Mutant Escherichia coli Heat-Labile Toxin, LT(R192G/L211A), as a Safe and Effective Oral Adjuvant. Clinical and Vaccine Immunology : CVI 18(4):546-551.

9. Norton EB, Bauer DL, Weldon WC, Oberste MS, Lawson LB, Clements JD 2015. The novel adjuvant dmLT promotes dose sparing, mucosal immunity and longevity of antibody responses to the inactivated polio vaccine in a murine model. Vaccine 33(16):1909-1915.

10. Summerton NA, Welch RW, Bondoc L, Yang H-H, Pleune B, Ramachandran N, Harris AM, Bland D, Jackson WJ, Park S, Clements JD, Nabors GS 2010. Toward the development of a stable, freeze-dried formulation of Helicobacter pylori killed whole cell vaccine adjuvanted with a novel mutant of Escherichia coli heat-labile toxin. Vaccine 28(5):1404-1411.

11. Lu Y-J, Yadav P, Clements JD, Forte S, Srivastava A, Thompson CM, Seid R, Look J, Alderson M, Tate A, Maisonneuve J-F, Robertson G, Anderson PW, Malley R 2010. Options for Inactivation, Adjuvant, and Route of Topical Administration of a Killed, Unencapsulated Pneumococcal Whole-Cell Vaccine. Clinical and Vaccine Immunology : CVI 17(6):1005-1012.

12. Lundgren A, Bourgeois L, Carlin N, Clements J, Gustafsson B, Hartford M, Holmgren J, Petzold M, Walker R, Svennerholm A-M 2014. Safety and immunogenicity of an improved oral inactivated multivalent enterotoxigenic Escherichia coli (ETEC) vaccine administered alone and

together with dmLT adjuvant in a double-blind, randomized, placebo-controlled Phase I study. Vaccine 32(52):7077-7084.

13. Bourgeois AL, Wierzba TF, Walker RI 2016. Status of vaccine research and development for enterotoxigenic Escherichia coli. Vaccine 34(26):2880-2886.

14. World Health Organization. Status of Vaccine Research and Development for Enterotoxigenic Escherichia coli. http://who.int/immunization/research/meetings_workshops/ETEC_vaccineRD_Sept2014.pdf;2014 [accessed 29.06.16]

15. Health. USNIo. 2016. Phase 1 Study of dmLT ID Vaccination in Healthy Adults, https://clinicaltrials.gov/ct2/show/NCT02531685;2016 [accessed 29.06.16]

16. Kumru OS, Joshi SB, Smith DE, Middaugh CR, Prusik T, Volkin DB 2014. Vaccine instability in the cold chain: Mechanisms, analysis and formulation strategies. Biologicals 42(5):237-259.

17. Hickey JM, Sahni N, Toth Iv RT, Kumru OS, Joshi SB, Middaugh CR, Volkin DB 2016. Challenges and opportunities of using liquid chromatography and mass spectrometry methods to develop complex vaccine antigens as pharmaceutical dosage forms. Journal of Chromatography B 1032:23-38.

18. O'Hagan DT, Fox CB 2015. New generation adjuvants – From empiricism to rational design. Vaccine 33:B14-B20.

19. Dey AK, Malyala P, Singh M 2014. Physicochemical and functional characterization of vaccine antigens and adjuvants. Expert Review of Vaccines 13(5):671-685.

20. Alsenaidy MA, Jain NK, Kim JH, Middaugh CR, Volkin DB 2014. Protein comparability assessments and potential applicability of high throughput biophysical methods and data visualization tools to compare physical stability profiles. Frontiers in Pharmacology 5:39.

21. Brito LA, Malyala P, O'Hagan DT 2013. Vaccine adjuvant formulations: A pharmaceutical perspective. Seminars in Immunology 25(2):130-145.

22. Frokjaer S, Otzen DE 2005. Protein drug stability: a formulation challenge. Nat Rev Drug Discov 4(4):298-306.

23. Kartoglu U, Milstien J 2014. Tools and approaches to ensure quality of vaccines throughout the cold chain. Expert Review of Vaccines 13(7):843-854.

24. Vázquez-Rey M, Lang DA 2011. Aggregates in monoclonal antibody manufacturing processes. Biotechnology and Bioengineering 108(7):1494-1508.

25. Wang W, & Roberts, Christopher John. 2010. Aggregation of therapeutic proteins. ed., Hoboken, N.J.: Hoboken, N.J. : Wiley.

26. Kamerzell TJ, Esfandiary R, Joshi SB, Middaugh CR, Volkin DB 2011. Protein–excipient interactions: Mechanisms and biophysical characterization applied to protein formulation development. Advanced Drug Delivery Reviews 63(13):1118-1159.

27. Parkins DA, Lashmar UT 2000. The formulation of biopharmaceutical products. Pharmaceutical Science & Technology Today 3(4):129-137.

28. Ohtake S, Kita Y, Arakawa T 2011. Interactions of formulation excipients with proteins in solution and in the dried state. Advanced Drug Delivery Reviews 63(13):1053-1073.

29. Capelle MAH, Gurny R, Arvinte T 2007. High throughput screening of protein formulation stability: Practical considerations. European Journal of Pharmaceutics and Biopharmaceutics 65(2):131-148.

30. Clements JD. 1999. Double mutant enterotoxin for use as an adjuvant. ed.: Google Patents.

31. Kim JH, Iyer V, Joshi SB, Volkin DB, Middaugh CR 2012. Improved data visualization techniques for analyzing macromolecule structural changes. Protein Science 21(10):1540-1553.

32. Maddux NR, Joshi SB, Volkin DB, Ralston JP, Middaugh CR 2011. Multidimensional methods for the formulation of biopharmaceuticals and vaccines. Journal of Pharmaceutical Sciences 100(10):4171-4197.

33. LÖNNROTH I, HOLMGREN J 1973. Subunit Structure of Cholera Toxin. Microbiology 76(2):417-427.

34. van Heyningen S 1976. The Subunits of Cholera Toxin: Structure, Stoichiometry, and Function. The Journal of Infectious Diseases 133:S5-S13.

35. Goins BB Thermal stability and intersubunit interactions of cholera toxin in solution and in association with its cell-surface receptor ganglioside GM1. Biochemistry (Easton) 27(6):2046-2052.

36. Manning MC, Chou DK, Murphy BM, Payne RW, Katayama DS 2010. Stability of Protein Pharmaceuticals: An Update. Pharmaceutical Research 27(4):544-575.

37. Piedmonte DM, Summers C, McAuley A, Karamujic L, Ratnaswamy G 2007. Sorbitol Crystallization Can Lead to Protein Aggregation in Frozen Protein Formulations. Pharmaceutical Research 24(1):136-146.

38. Piedmonte DM, Hair A, Baker P, Brych L, Nagapudi K, Lin H, Cao W, Hershenson S, Ratnaswamy G 2015. Sorbitol Crystallization-Induced Aggregation in Frozen mAb Formulations. Journal of Pharmaceutical Sciences 104(2):686-697.

39. Meyer JD, Nayar R, Manning MC 2009. Impact of bulking agents on the stability of a lyophilized monoclonal antibody. European Journal of Pharmaceutical Sciences 38(1):29-38.

40. Han Y, Jin B-S, Lee S-B, Sohn Y, Joung J-W, Lee J-H 2007. Effects of sugar additives on protein stability of recombinant human serum albumin during lyophilization and storage. Archives of Pharmacal Research 30(9):1124-1131.

41. Morgan F, Léonil J, Mollé D, Bouhallab S 1999. Modification of Bovine β-Lactoglobulin by Glycation in a Powdered State or in an Aqueous Solution: Effect on Association Behavior and Protein Conformation. Journal of Agricultural and Food Chemistry 47(1):83-91.

42. Fischer S, Hoernschemeyer J, Mahler H-C 2008. Glycation during storage and administration of monoclonal antibody formulations. European Journal of Pharmaceutics and Biopharmaceutics 70(1):42-50.

43. Joffré E, von Mentzer A, Abd El Ghany M, Oezguen N, Savidge T, Dougan G, Svennerholm A-M, Sjöling Å 2015. Allele Variants of Enterotoxigenic Escherichia coli Heat-Labile Toxin Are Globally Transmitted and Associated with Colonization Factors. Journal of Bacteriology 197(2):392-403.

44. Spangler BD 1992. Structure and function of cholera toxin and the related Escherichia coli heat-labile enterotoxin. Microbiological Reviews 56(4):622-647.

45. World Health O 2009. Guidelines on stability evaluation of vaccines. Biologicals 37(6):424-434.

46. Brandau DT, Jones LS, Wiethoff CM, Rexroad J, Middaugh CR 2003. Thermal stability of vaccines. Journal of Pharmaceutical Sciences 92(2):218-231.

47. Rudolph MJ, Vance DJ, Cassidy MS, Rong Y, Shoemaker CB, Mantis NJ 2016. Structural analysis of nested neutralizing and non-neutralizing B cell epitopes on ricin toxin's enzymatic subunit. Proteins: Structure, Function, and Bioinformatics 84(8):1162-1172.

48. Toprani VM, Hickey JM, Sahni N, Robertson GA, Middaugh CR, Joshi SB, Volkin DB 2017. Development of a candidate stabilizing formulation for bulk storage of a double mutant heat labile toxin (dmLT) protein based adjuvant. Vaccine:1-10.

49. Cheng Y, Thomas JC, Joshi SB, Volkin DB, Middaugh CR. 2015. The Physical Analysis of Vaccines. In Foged C, Rades T, Perrie Y, Hook S, editors. Subunit Vaccine Delivery, ed., New York, NY: Springer New York. p 385-412.

50. Diminsky D, Moav N, Gorecki M, Barenholz Y 1999. Physical, chemical and immunological stability of CHO-derived hepatitis B surface antigen (HBsAg) particles. Vaccine 18(1–2):3-17.

51. Volkin DB, Burke CJ, Marfia KE, Oswald CB, Wolanski B, Middaugh CR 1997. Size and Conformational Stability of the Hepatitis a Virus used to Prepare VAQTA⊥, a Highly Purified Inactivated Vaccine. Journal of Pharmaceutical Sciences 86(6):666-673.

52. Amador-Molina JC, Valerdi-Madrigal ED, Domínguez-Castillo RI, Sirota LA, Arciniega JL 2016. Temperature-mediated recombinant anthrax protective antigen aggregate development: Implications for toxin formation and immunogenicity. Vaccine 34(35):4188-4195.

53. Chen Y, Zhang Y, Quan C, Luo J, Yang Y, Yu M, Kong Y, Ma G, Su Z 2015. Aggregation and antigenicity of virus like particle in salt solution—A case study with hepatitis B surface antigen. Vaccine 33(35):4300-4306.

54. Braun LJ, Tyagi A, Perkins S, Carpenter J, Sylvester D, Guy M, Kristensen D, Chen D 2009. Development of a freeze-stable formulation for vaccines containing aluminum salt adjuvants. Vaccine 27(1):72-79.

55. Wang T, Joshi SB, Kumru OS, Telikepalli S, Middaugh CR, Volkin DB. 2013. Case Studies Applying Biophysical Techniques to Better Characterize Protein Aggregates and Particulates of Varying Size. In Narhi OL, editor Biophysics for Therapeutic Protein Development, ed., New York, NY: Springer New York. p 205-243.

56. Virella G, Thorpe SR, Alderson NL, Stephan EM, Atchley D, Wagner F, Lopes-Virella MF, Group atDER 2003. Autoimmune response to advanced glycosylation end-products of human LDL. Journal of Lipid Research 44(3):487-493.

57. Li S, Schöneich C, Borchardt RT 1995. Chemical instability of protein pharmaceuticals: Mechanisms of oxidation and strategies for stabilization. Biotechnology and Bioengineering 48(5):490-500.

58. Verma A, Ngundi MM, Burns DL 2016. Mechanistic Analysis of the Effect of Deamidation on the Immunogenicity of Anthrax Protective Antigen. Clinical and Vaccine Immunology 23(5):396-402.

59. D'Souza AJM, Mar KD, Huang J, Majumdar S, Ford BM, Dyas B, Ulrich RG, Sullivan VJ 2013. Rapid Deamidation of Recombinant Protective Antigen when Adsorbed on Aluminum Hydroxide Gel Correlates with Reduced Potency of Vaccine. Journal of Pharmaceutical Sciences 102(2):454-461.

60. Ledesma-Osuna AI, Ramos-Clamont G, Vázquez-Moreno L 2008. Characterization of bovine serum albumin glycated with glucose, galactose and lactose. Acta Biochim Pol 55(3):491-497.

61. Quan CP, Wu S, Dasovich N, Hsu C, Patapoff T, Canova-Davis E 1999. Susceptibility of rhDNase I to Glycation in the Dry-Powder State. Analytical Chemistry 71(20):4445-4454.

62. Watkins NG, Thorpe SR, Baynes JW 1985. Glycation of amino groups in protein. Studies on the specificity of modification of RNase by glucose. Journal of Biological Chemistry 260(19):10629-10636.

63. Sixma TK, Pronk SE, Kalk KH, van Zanten BAM, Berghuis AM, Hol WGJ 1992. Lactose binding to heat-labile enterotoxin revealed by X-ray crystallography. Nature 355(6360):561-564.

64. Robinson NE, Robinson ZW, Robinson BR, Robinson AL, Robinson JA, Robinson ML, Robinson AB 2004. Structure-dependent nonenzymatic deamidation of glutaminyl and asparaginyl pentapeptides. The Journal of Peptide Research 63(5):426-436.

65. Kirkitadze M, Arunachalam A, Carpick B 2013. Comparability of biotherapeutics: characterization of protein vaccine antigens. Pharmaceutical Bioprocessing 1(4):373-380.

66. Organization WH. 2015. Guidelines on procedures and data requirements for changes to approved vaccines. TRS 993 Annex 4, http://www.who.int/biologicals/vaccines/Annex4_Guidelines_changes_to_approved_vaccines_eng.pdf?ua=1 [accessed 31.08.16]. ed.

67. Federici M, Lubiniecki A, Manikwar P, Volkin DB 2013. Analytical lessons learned from selected therapeutic protein drug comparability studies. Biologicals 41(3):131-147.

68. Abraham D. 2015. WCBP 2015.Establishing Comparability with Process and Manufacturing Changes for Recombinant Vaccine: A case study of HPV Vaccine, http://c.ymcdn.com/sites/casss.siteym.com/resource/resmgr/WCBP_Speaker_Slides/2015_WCBP_AbrahamDicky.pdf [accessed 31.08.16]. WCBP, ed., Washington DC.

69. More AS, Toprani VM, Okbazghi SZ, Kim JH, Joshi SB, Middaugh CR, Tolbert TJ, Volkin DB 2016. Correlating the Impact of Well-Defined Oligosaccharide Structures on Physical Stability Profiles of IgG1-Fc Glycoforms. Journal of Pharmaceutical Sciences 105(2):588-601.

70. Chen DD Opportunities and challenges of developing thermostable vaccines. Expert review of vaccines 8(5):547-557.

71. Prevention CfDCa. Vaccine Excipient & Media Summary Excipients Included in U.S. Vaccines, by Vaccine http://www.cdc.gov/vaccines/pubs/pinkbook/downloads/appendices/B/excipient-table-2.pdf [accessed 23.07.16]. ed.

72. Kendrick BS, Chang BS, Arakawa T, Peterson B, Randolph TW, Manning MC, Carpenter JF 1997. Preferential exclusion of sucrose from recombinant interleukin-1 receptor antagonist: Role in restricted conformational mobility and compaction of native state.

Proceedings of the National Academy of Sciences of the United States of America 94(22):11917-11922.

73. Carpenter JF, Pikal MJ, Chang BS, Randolph TW 1997. Rational Design of Stable Lyophilized Protein Formulations: Some Practical Advice. Pharmaceutical Research 14(8):969-975.

74. Lee JC, Timasheff SN 1981. The stabilization of proteins by sucrose. Journal of Biological Chemistry 256(14):7193-7201.

75. Kim Y-S, Jones LS, Dong A, Kendrick BS, Chang BS, Manning MC, Randolph TW, Carpenter JF 2003. Effects of sucrose on conformational equilibria and fluctuations within the native-state ensemble of proteins. Protein Science : A Publication of the Protein Society 12(6):1252-1261.

76. Dill KA 1990. Dominant forces in protein folding. Biochemistry 29(31):7133-7155.

77. Chi EYEY Roles of conformational stability and colloidal stability in the aggregation of recombinant human granulocyte colony-stimulating factor. Protein science 12(5):903-913.

78. Chi EY, Krishnan S, Randolph TW, Carpenter JF 2003. Physical Stability of Proteins in Aqueous Solution: Mechanism and Driving Forces in Nonnative Protein Aggregation. Pharmaceutical Research 20(9):1325-1336.

79. Tsai AMA II. Electrostatic effect in the aggregation of heat-denatured RNase A and implications for protein additive design. Biotechnology and bioengineering 59(3):281-285.

80. Krielgaard L, Jones LS, Randolph TW, Frokjaer S, Flink JM, Manning MC, Carpenter JF 1998. Effect of tween 20 on freeze-thawing- and agitation-induced aggregation of recombinant human factor XIII. Journal of Pharmaceutical Sciences 87(12):1597-1603.

81. Mahler H-C, Fischer S, Randolph TW, Carpenter JF. 2010. Protein Aggregation and Particle Formation: Effects of Formulation, Interfaces, and Drug Product Manufacturing Operations. Aggregation of Therapeutic Proteins, ed.: John Wiley & Sons, Inc. p 301-331.

82. Lee HJ, McAuley A, Schilke KF, McGuire J 2011. Molecular origins of surfactant-mediated stabilization of protein drugs. Advanced Drug Delivery Reviews 63(13):1160-1171.

83. Kerwin BA 2008. Polysorbates 20 and 80 Used in the Formulation of Protein Biotherapeutics: Structure and Degradation Pathways. Journal of Pharmaceutical Sciences 97(8):2924-2935.

84. Chang BS, Kendrick BS, Carpenter JF 1996. Surface-Induced Denaturation of Proteins during Freezing and its Inhibition by Surfactants. Journal of Pharmaceutical Sciences 85(12):1325-1330.

85. Lam XM, Yang JY, Cleland JL 1997. Antioxidants for Prevention of Methionine Oxidation in Recombinant Monoclonal Antibody HER2. Journal of Pharmaceutical Sciences 86(11):1250-1255.

86. Singh SK, Kolhe P, Mehta AP, Chico SC, Lary AL, Huang M 2011. Frozen State Storage Instability of a Monoclonal Antibody: Aggregation as a Consequence of Trehalose Crystallization and Protein Unfolding. Pharmaceutical Research 28(4):873-885.

87. 1990. Cold Denaturation of Protein. Critical Reviews in Biochemistry and Molecular Biology 25(5):281-306.

88. Jaenicke R, Heber U, Franks F, Chapman D, Griffin MCA, Hvidt A, Cowan DA 1990. Protein Structure and Function at Low Temperatures [and Discussion]. Philosophical Transactions of the Royal Society B: Biological Sciences 326(1237):535-553.

89. Clausi AL, Morin A, Carpenter JF, Randolph TW 2009. Influence of Protein Conformation and Adjuvant Aggregation on the Effectiveness of Aluminum Hydroxide Adjuvant in a Model Alkaline Phosphatase Vaccine. Journal of pharmaceutical sciences 98(1):114-121.

90. Salnikova MS, Davis H, Mensch C, Celano L, Thiriot DS 2012. Influence of Formulation pH and Suspension State on Freezing-Induced Agglomeration of Aluminum Adjuvants. Journal of Pharmaceutical Sciences 101(3):1050-1062.

91. Bhatnagar BS Protein Stability During Freezing: Separation of Stresses and Mechanisms of Protein Stabilization. Pharmaceutical development and technology 12(5):505-523.

92. Nascimento IP, Leite LCC 2012. Recombinant vaccines and the development of new vaccine strategies. Brazilian Journal of Medical and Biological Research 45(12):1102-1111.

93. Perrie Y, Mohammed AR, Kirby DJ, McNeil SE, Bramwell VW 2008. Vaccine adjuvant systems: Enhancing the efficacy of sub-unit protein antigens. International Journal of Pharmaceutics 364(2):272-280.

94. Kolhe P, Shah M, Rathore N. 2013. Molecule and manufacturability assessment leading to robust commercial formulation for therapeutic proteins, Sterile Product Development. ed.: Springer New York. p 33-45.

Chapter 4 Structural Characterization and Formulation Development of a Trivalent Equine Encephalitis Virus-like Particle Vaccine Candidate

4.1 Introduction

Equine encephalitis viruses (EEV), including Eastern (EEEV), Western (WEEV) and Venezuelan (VEEV), are mosquito-borne enveloped single-stranded RNA viruses in the Alphavirus genus of the *Togaviridae* family[1,2]. These viruses measure 60 to 70 nm in diameter. EEV infections can cause debilitating diseases with moderate morbidity and potentially severe mortality in equids and humans [3]. EEV infections usually begin with non-specific illness, such as fever, chills, myalgia and abdominal pain, followed by, in severe cases, neurological signs indicative of encephalitis, such as confusion, seizures, coma and paralysis[4-6]. Children and the elderly have a higher risk for developing severe disease after EEV infection. EEEV, WEEV and VEEV have different geographic distributions and epidemiologic profiles. For example, EEEV primarily occurs in eastern Canada and United States[7,8], with a fatality rate of approximately 30-70%[9]. WEEV infections are mainly reported in western Canada and states west of the Mississippi river in the United States with an overall mortality rate of approximately 3-7%[1]. VEEV outbreaks have occurred in Central and South America[2] with a mortality rate of 1-3 %.

Due to the severity of the disease that can be caused by EEV infections and their potential use for bioterrorism, EEEV, WEEV and VEEV have been identified as category B priority pathogens by the National Institute of Allergy and Infectious Diseases[10,11]. Currently, there are neither known antiviral treatments nor any commercially licensed human vaccines against EEV infections. There is a live attenuated vaccine (TC-83) against VEEV for use in US military personnel, however, the low efficacy and potential side effects of the vaccine hinder its widespread use in the general population[12,13]. The Vaccine Production Program at the Vaccine Research Center at NIAID/NIH has initiated a program to develop an effective virus-like particle (VLP) based vaccine against EEV based on the positive safety and efficacy profile of VLPs and

prior Phase I clinical experience with a related Chikungunya virus VLP[14] and early non-clinical EEV studies. Three strains of EEV, Eastern, Western and Venezuelan, are under investigation as components of a multivalent recombinant VLP vaccine product candidate.

In this work, we characterized the structural integrity and physical stability of purified recombinant VLPs of three strains of EEV using a variety of physicochemical techniques. A comparison of the similarities and differences between the VLPs, both intrinsic physical properties and degradation profiles versus thermal and pH stress, are presented. Furthermore, a series of pharmaceutical excipients were evaluated for their stabilizing effect on the thermal stability of these VLPs to identify stabilizers for a new bulk formulation. An optimally stable new bulk formulation was developed based on the results from excipient screening studies as well as subsequent stability assessments (storage and freeze-thaw stability). The adsorption of the three VLPs to aluminum salt adjuvants and the stability profile of the aluminum adjuvanted VLPs was also evaluated. In addition, the time dependence of the ability to desorb these VLPs from the adjuvant's surface after storage was also examined. The implications of these findings for future development of a stable parenteral multivalent VLP vaccine formulation, both with and without aluminum adjuvants, are also discussed.

4.2 Materials and Methods

4.2.1 Materials

Venezuelan equine encephalitis virus-like particles (VEE VLPs), eastern equine encephalitis virus-like particles (EEE VLPs) and western equine encephalitis virus-like particles (WEE VLPs) were expressed by transient transfection of HEK293 cells (VRC293) with plasmids encoding the viral capsid protein (C) and two envelope glycoproteins (E1 and E2) of the native virus. These enveloped VLPs were then purified to homogeneity using a purification scheme

which includes a combination of tangential flow filtration and tandem flow-through column chromatography. Each of the three VLPs was supplied by National Institute of Allergy and Infectious Diseases, (National Institutes of Health), in a 25 mM Tris buffer containing 100 mM sodium citrate, pH 8.5. The VLP solutions were shipped to KU on dry ice and stored frozen at -80^{o}C upon receipt. The initial characterization of the VLPs was performed in the Tris/Citrate buffer described above. For the remaining studies, the VLP samples were thawed and buffer exchanged three times into target buffers, depending on the experiments, by overnight dialysis at 4^{o}C using Slide-A-Lyzer® dialysis cassettes (3.5 kDa MWCO, Thermo Scientific, Rockford, IL). All reagents and excipients for preparing different formulations were purchased from Sigma-Aldrich (St. Louis, MO). Carbohydrates such as trehalose and sucrose were purchased from Pfanstiehl Inc. (Waukegan, IL). All excipients were of high purity grade (>99%).

4.2.2 Methods

4.2.2.1 Transmission electron microscopy (TEM)

Ten μL of the three VLP samples were applied to a carbon grid (Ted Pella, Redding, CA) and left to air dry. Each preparation was fixed by adding 1 % v/v Glutaraldehyde solution (Sigma-Aldrich, St. Louis, MO) for two min by immersing the carbon coated side of the grid onto a drop of glutaraldehyde solution suspended on parafilm, which was immediately blotted dry using blotting paper. The grids were washed twice with ultrapure water. The VLP samples were then negatively stained by adding 2% uranyl acetate (Sigma-Aldrich, St. Louis, MO) for 2 min. The morphology of the VLPs were studied using an FEI Tecnai F20 XT Transmission Electron Microscope equipped with a CCD camera (ThermoFisher, Waltham, MA). The particle size was calculated by averaging the diameters of 50 particles using ImageJ (https://imagej.nih.gov/ij/).

4.2.2.2 Dynamic light scattering (DLS)

DLS was performed using the dynamic light scattering mode of a ZetaPALS zetasizer (Brookhaven Instruments Corporation, Holtsville, NY) using quartz cuvettes that were cleaned to remove dust and air-dried. Four hundred microliter of each VLP sample at 0.2 mg/mL was analyzed. For each sample, ten measurements were recorded three times using an acquisition time of 30 sec. The z-average diameter was then calculated using the instrument software. All measurements were performed at ambient temperature.

4.2.2.3 SDS-PAGE

The VLP samples were run under both non-reducing and reducing conditions by SDS-PAGE. The VLP samples were mixed with 4X NuPAGE-LDS sample buffer (Life Technologies, Grand Island, NY) to a final concentration of 1X. For reduced samples, 50 mM dithiothreitol (DTT) (Life Technologies, Grand Island, NY) was added. The samples were incubated at 70 $^{\circ}$C for 5 min. Ten μg of VLP protein was analyzed by SDS-PAGE on a 4-12% Bis-Tris gradient gel (1.0 mm x 10 wells, #NP0321BOX) using 1X MES running buffer (Life Technologies, Grand Island, NY). Protein bands were visualized by staining with Coomassie blue R250 (Teknova, Hollister, CA) and destained with ultrapure water.

4.2.2.4 UV-Absorbance Spectroscopy

UV absorbance spectra were obtained using an Agilent 8453 UV-visible absorbance spectrophotometer (Agilent Technologies, Santa Clara, CA). Absorbance spectra were recorded over the wavelength range of 190-400 nm with a step size of 1 nm. All measurements were conducted in triplicate at room temperature using 1 cm path length cuvettes. All UV-Visible absorbance spectra were corrected for light scattering using a technique included in the

manufacturers data analysis software (Chemstation UV-Vis analysis software, Agilent Technologies).

4.2.2.5 Far-UV Circular Dichroism Spectroscopy

Far-UV circular dichroism (CD) spectroscopy of VLPs was performed using a Chirascan-plus Circular Dichroism Spectrometer (Applied Photophysics Ltd, Leatherhead UK) equipped with a peltier temperature controller and a 6-position cuvette holder. Quartz cuvettes (0.1 cm path length) sealed with a teflon stopper (Starna Cells Inc., Atascadero, CA) were used. The spectra of each VLP were collected from 200-260 nm using 1 nm steps and 0.5 s sampling time at 10 °C. The final protein concentration of the VLP sample was 0.2 mg/mL and the measurements were conducted in triplicate. For, thermal melts a temperature range of 10-87.5 °C at 2.5 °C intervals and an equilibration time of 2 min at each temperature was used. All thermal measurements were performed in duplicate. Data analysis was performed using in-house *Middaugh Suite* software. The CD signal at 214 nm was extracted to detect change in secondary structure with increasing temperature. Baseline measurement of the buffer was performed and subtracted prior to data analysis.

4.2.2.6 Intrinsic Tryptophan Fluorescence Spectroscopy

The intrinsic tryptophan fluorescence of VLPs was measured using a Photon Technology International (PTI) spectrofluorometer (Lawrenceville, NJ) equipped with a turreted four-position peltier-controlled cell holder and a xenon lamp. An excitation wavelength of 295 nm was used (>95% tryptophan emission), and emission spectra at 10^{o}C were collected from 305 to 405 nm by a photomultiplier with a step size of 1 nm and an integration time of 1 s. Thermal melts were performed over a temperature range of 10-87.5 °C at 2.5 °C intervals and an equilibration time of 2 min at each temperature. All thermal measurements were conducted in

duplicate with 1 cm path length quartz cuvettes. . The data analysis was performed using the in-house software (*Middaugh Suite*). The corresponding buffer spectrum was subtracted from each protein spectrum prior to data analysis. The emission peak position was determined using a mean spectral center of mass method (MSM) executed in the *Middaugh Suite*. Although this calculation method increases the signal to noise ratio for more accurate determination of lambda max values, it shifts the apparent peak position by 5-10 nm from their actual values.

4.2.2.7 Turbidity (OD_{350} measurements)

Thermal stress measurements were performed using a Cary 100 UV-Visible spectrophotometer (Varian medical Systems, Inc., Palo Alto, California) equipped with a 12 cell holder with a peltier type temperature controller. Samples contained 0.15 mg/ml protein with a total volume of 225 µl in 1 cm path length quartz cells. Optical density at 350 nm (OD_{350}) was monitored as the temperature was raised in increments of 1.25˚C from 10 to 90˚C with a heating rate of 60˚C/h. VLP samples were run in duplicate and corresponding buffer blanks were run and subtracted from each sample.

4.2.2.8 Differential Scanning Calorimetry (DSC)

DSC thermograms for the three VLPs were collected with a Microcal VP-DSC capillary cell microcalorimeter (MicroCal/GE Health Sciences, Pittsburgh, PA). Thermograms were recorded from 10 to 100 °C at a scan rate of 1 °C/min. The concentration of VLP was 0.15 mg/mL and the experiment was performed in triplicate. A buffer baseline was subtracted from each protein thermogram and the data were normalized to molar heat capacity using Microcal DSC software in Origin 7.0. The peaks were fitted using mathematical model fit in Origin 7.0 to calculate the values of T_{onset} and T_m.

4.2.2.9 Construction of Three Index Empirical Phase Diagram (EPD)

For the physical stability studies, the three VLPs were dialyzed into the 20 mM phosphate, 150 mM NaCl buffer (pH 6.5-8.5, at 0.5 pH unit increments). Dialysis was performed at 4^{o}C using Slide A Lyser dialysis devices (ThermoScientic, Rockford, IL) with 3.5-kDa molecular weight cutoff with four buffer exchanges. Samples were then diluted to 0.15 mg/mL for circular dichroism, intrinsic tryptophan fluorescence and turbidity measurements. Data from these three techniques were used in the construction of the three-index EPD and radar chart using in-house software *(Middaugh Suite).*

A detailed description of the construction of three-index EPD can be found elsewhere[15,16]. Briefly, the three index EPD use a specific color (red (R), green (G), blue (B)) scheme to reflect the characteristics of the underlying biophysical data, that define protein structural states as a function of solution variables like temperature and pH. For three-index EPD from this work, data from circular dichroism, MSM peak position and turbidity measurements were mapped to red, green and blue color respectively. Data sets obtained from each of above biophysical techniques were assigned to a color gradation from black to the full color of their technique, with minimum value in the dataset assigned a black color and maximum value to the full color intensity. However, for circular dichroism and MSM peak position color assignments were reversed where the maximum value was mapped to black and the least value to maximum color intensity (i.e. green for MSM peak position) for better visualization. Thus, a color produced by the summation of these RGB components produced a single color at each point in pH and temperature space, which was mapped to a specific structural state of the VLPs. The individual RGB components were also displayed in a separate panel alongside the 3-index EPDs (Figure 3) because it is difficult to determine the amount of an RGB component with a given color. The explicit display

of its RGB components helps to better understand the interpretation of a color and more distinctly detect changes in the structure of the protein. A k-means clustering algorithm using in-house software (*Middaugh Suite*) was applied to the datasets to draw the dotted lines.

4.2.2.10 Excipient Screening

Intrinsic Trp fluorescence spectroscopy based thermal melt analysis was employed to screen for pharmaceutical excipients for their ability to enhance the conformational stability of each of the three VLPs. Fluorescence experiments were performed as mentioned in the supplemental methods section in the temperature range of 10 to 90^{o}C (in 2.5^{o}C increments) in a buffer containing 10 mM sodium phosphate and 100 mM NaCl, pH 7.5. The VLP concentration used in this study was 0.1 mg/ml. Twenty-six (26) excipients (listed in Figure 4) were examined for their ability to shift the unfolding onset temperature (T_{onset}) and the midpoint of the unfolding transition temperature (T_m) of VEEV VLPs to higher temperatures. Seven different categories of excipients were screened including carbohydrates, polyols, amino acids/carboxylic acids, metal chelators, non-ionic surfactants, cyclodextrins and polymers/polyions. To determine T_m values, the first derivative spectra of Trp peak position versus temperature plots were calculated and the peak temperature of this derivative spectrum was considered to be the T_m.

4.2.2.11 Freeze-thaw studies

The VLPs were dialyzed against 10 mM sodium phosphate, 50 mM NaCl, pH 7.5 in Slide-A-Lyzer Dialysis Cassettes (Product #66110, Thermo Scientific, Rockford, IL) with a 3,500 Da molecular weight cutoff overnight at 4°C with three buffer exchanges at 3h intervals, and an overnight incubation before dialysate recovery. Excipients were prepared as concentrated stock solutions in indicated base buffer (10 mM $NaPO_4$, 50 mM NaCl, pH 7.5). Each of the excipients, VLP, and additional base buffer were combined to achieve the final formulations

indicated in text. Then, 1.1 mL of VLP at 0.15 mg/mL was filled in 3 mL Fiolax clear, Schott (Lebanon, PA) glass vials and frozen at -20^{o}C and -80^{o}C for 24 h. The vials were thawed at room temperature for ~20 min for complete thawing. Samples were then frozen again at -20 and -80^{o}C and the freeze-thaw (F/T) cycles were repeated 5X. Samples were analyzed at 0, 1 and 5 F/T cycles using UV absorption spectroscopy, dynamic light scattering and differential scanning calorimetry (DSC) as described in supplemental methods section.

4.2.2.12 Accelerated and Real-Time Stability

All three VLPs were prepared in a similar manner as described above in the freeze-thaw method and the six formulations (as indicated in text) were incubated at 4, 25, 40, -20 and -80^{o}C for 28 days. On days 0, 14 and 28, the samples were analyzed by dynamic light scattering and the z-average diameter was determined. All measurements were performed in triplicate.

4.2.2.13 Adsorption studies of EEV VLPs with aluminum salt adjuvants

The three VLPs were first tested separately to determine whether they adsorb preferentially to aluminum hydroxide (Alhydrogel®) or aluminum phosphate (Adjuphos®). Fifty micrograms of EEEV, WEEV or VEEV was incubated with 500 µg Alhydrogel® / Adjuphos® in the original sample buffer (25 mM Tris, 100 mM sodium citrate, pH 8.5) for 30 min at 4 ^{o}C and then centrifuged @ 2,100 rcf for 10 min. The amount of unadsorbed protein was determined by measuring the amount of free protein in the supernatant using UV absorbance spectroscopy after centrifugation. An adsorption isotherm for each of the three VLPs and their 1:1:1 mixture in both the base buffer (10 mM $NaPO_4$, 50 mM NaCl, pH 7.8) and the formulation buffer (10 mM $NaPO_4$, 50 mM NaCl, 5% sucrose, 5% sorbitol, 0.05% Pluronic F-68, pH 7.8) was constructed by mixing varying amounts of VLPs (0-240 µg) with 50 µg Alhydrogel® and the total volume was adjusted to 0.5 mL. Samples were incubated at 4^{o}C for 1 h on an inverting/tumbling shaker

before being centrifuged (Thermo scientific- Sorvall legend micro 17R centrifuge) at 2,100 rcf for 10 min at 4^{o}C. Supernatant (300 µl) was then removed and examined by UV spectroscopy. The absorbance at 280 nm (light scattering corrected) was used to determine the amount of unbound VLPs in the supernatant. A graph (binding isotherm) of the amount of VLPs bound (y-axis) against the total amount of VLPs added (x-axis) was plotted.

4.2.2.14 Desorption studies of EEV VLPs from aluminum adjuvant

To prepare Alhydrogel®-adsorbed VLPs, 40 µL of stock Alhydrogel® (10 mg/ml) was incubated with VLP samples (760 µl, in the formulation buffer) at 4^{o}C for 1 h on an inverting/tumbling shaker, in a total volume of 800 µL. The final concentration of the VLPs and Alhydrogel® in the mixture was 120 and 500 µg/mL, respectively. The mixture was then centrifuged at 2,100 rcf for 10 min at 4^{o}C to separate unbound VLPs from Alhydrogel®-adsorbed VLPs. After removing the supernatant (720 µl) of each sample, the pellets (Alhydrogel®-adsorbed VLPs) were then resuspended in 500 µl desorption media and incubated at 4^{o}C or room temperature for different time points (0, 0.5, 1, 2, 3, 4, 5, 6, and 24 h) on an inverting/tumbling shaker. Samples were then centrifuged (Thermo scientific- Sorvall legend micro 17R centrifuge) at 2,100 rcf for 10 min to separate Alhydrogel® from the solution. After centrifugation, the A_{280} value (light scattering corrected absorption at 280 nm) of the supernatant was determined by UV spectroscopy to calculate the amount of VLPs desorbed from Alhydrogel®.

The time dependence of susceptibility to desorption was also examined since the reversibility of this process often decreases with time[17,18]. Three desorption time durations (0.5, 4, and 24 h) were further selected to determine the effect of longer storage times on the VLP-adjuvant desorption process and strength of binding. The EEE VLPs were adsorbed on the surface of Alhydrogel® and stored for a period of 8 weeks at 4^{o}C. Adjuvanted VLPs were

removed from incubation/storage at various time points (0 day, 1 day, 3 days, 1, 2 , 4 , 6 , and 8 wk) to study desorption by 500 mM sodium phosphate, pH 7.8 (selected as the desorption medium). The amount of desorbed VLP was measured using UV spectroscopy (A_{280}) with light scattering correction applied. The amount of desorbed VLPs was compared to control samples to calculate the percent removed from the surface of the adjuvant after a set duration (0.5, 4, and 24 h) of desorption.

4.3 Results

4.3.1 Size Analysis of EEE, WEE and VEE virus-like particles

As part of initial characterization, the size and morphology of the three VLPs (EEE, WEE and VEE) were studied using TEM analysis. As seen in Figures 4.1A, 4.1B and 4.1C, each of the three VLPs are enveloped, mostly spherical in shape with diameters ranging from 64-74 nm. These results are in good agreement with the hydrodynamic diameter values obtained by dynamic light scattering, DLS (D_h, 67-72 nm) as well as with the previously reported sizes[2,19,20] of the three equine encephalitis viruses (Figure 4.1D). In addition, the polydispersity values of each of the three VLP samples as measured by DLS varied between 3-7 % indicating that these VLP preparations were relatively homogenous.

4.3.2 Protein purity and overall higher order structure (HOS) of EEE, WEE and VEE virus-like particles

A combination of SDS-PAGE, UV-Visible absorption, circular dichroism and intrinsic tryptophan fluorescence spectroscopy were used to evaluate the purity and overall higher order structure of the proteins contained in the VLPs (formulated in a Tris-citrate, pH 8.0 buffer; see Materials). The three VLPs showed two or three protein bands as observed using SDS-PAGE under both non-reducing and reducing conditions (Figure 4.2A). The protein bands between 28-

49 kDa markers correspond to the E1 and E2 envelope proteins (theoretical MW: 47 kDa) while the protein band at ~29 kDa corresponds to the capsid protein (theoretical MW: 29 kDa). A separation of the E1 and E2 protein bands were apparent for EEE VLP, while for WEE and VEE VLPs, one band was primarily observed for the two envelope proteins, probably due to a similarity in MW between the E1 and E2 proteins. Overall protein purity levels (bands corresponding to VLP proteins) was estimated to be >99 % by SDS-PAGE.

UV absorbance spectra were utilized to provide an indication of the nucleic acid and protein content of these VLP solutions. Each of the three VLPs showed a peak maximum of 265 nm (after light scattering correction) as shown in Figure 4.2B. Since the UV absorbance spectra of pure protein species have a peak at 280 nm, while those of pure nucleic acids are present at 260 nm[21], the observed peak maximum indicates the presence of both proteins and nucleic acids in these VLP samples. Viruses with internalized nucleic acids have been shown by Zlotnick *et al* [22] to have similar UV absorbance spectra. In addition, since a pure protein (~100 %) displays a A_{260}/A_{280} ratio of 0.57 while a mixture of 90% protein and 10 % nucleic acid has an A_{260}/A_{280} ratio of 1.32[23,24], the observed $A_{260}/_{280}$ ratios of 1.25-1.40 (Figure 4.2) indicate each of the three VLP samples contain ~10 % nucleic acids (see Discussion).

Circular dichroism (CD) was used to monitor the overall secondary structure of the proteins contained in each of the three VLPs. At 10^{o}C, CD spectra in the far UV region (200-260 nm) showed a broad minimum between 209-220 nm suggesting a mixture of alpha and beta-sheet secondary structures (Figure 4.2C). Intrinsic Trp fluorescence spectroscopy was performed to evaluate the overall tertiary structure of the proteins within the VLPs (at 10^{o}C). The fluorescence emission spectra (Figure 4.2D) showed the wavelength of maximum intensity (λ_{max}) at 332 nm at 10^{o}C for EEE and WEE VLPs while that of VEE was blue shifted to 322 nm. The lower λ_{max} of

VEE VLP indicated that the average Trp amino acid residues in proteins in this VLP were in a relatively more hydrophobic environment compared to the Trp residues within the proteins contained in the EEE and WEE VLPs.

4.3.3 Physical stability profile of EEE, WEE and VEE VLPs as a function of pH and temperature

The physical stability profile of the three VLPs with respect to secondary and tertiary structural integrity as well as aggregation propensity was evaluated using circular dichroism, intrinsic tryptophan fluorescence, and turbidity (OD_{350} as a function of temperature) analysis, respectively in 20 mM sodium phosphate, 150 mM NaCl buffer under a wide range of pH conditions (pH 6.5 to 8.5) and temperature (10 to 87.5 ^{o}C) (Supplemental Figure 4.1 A, B and C). The pH and temperature stability profile of the overall secondary structure of the proteins of the three VLPs were monitored using CD signals at 214 nm plotted as a function of temperature in the pH range of 6.5-8.5 (Supplemental Figure 4.1 A) and the corresponding T_{onset} values of the thermal transitions are summarized in Supplemental Table 4.1. The pH and temperature stability profile of the overall tertiary structure of the proteins of the three VLPs were monitored using intrinsic Trp fluorescence peak position, (Supplemental Figure 4.1B) versus temperature for each of the pH conditions evaluated and the corresponding T_{onset} values of the thermal transitions are summarized in Supplemental Table S1.

To assess the effect of solution pH on the stability of the overall secondary structure of the proteins contained in each of the three VLPs, the CD signal intensity at 214 nm as a function of solution pH (6.5-8.5) and temperature (10 to 87.5 ^{o}C) was evaluated (Supplemental Figure 4.1A). For EEE VLPs, the CD signal intensity remained consistent up to ~50 ^{o}C at pH 6.5, after which a increase in intensity was observed. This notable alteration in CD signals indicates structural

alterations in the secondary structure of EEE VLPs. As shown in Supplemental Table S1, the onset temperatures (T_{onset}) of the transitions in CD signals were largely pH dependent with values steadily increasing with pH from 6.5 to 7.5, remaining consistent through 8.5. For the WEE VLPs, the T_{onset} values of the main transition occurred around 52 ^{o}C at pH 6.5, with values of ~55 ^{o}C at the other pH conditions. Overall, the secondary structure of WEE VLPs appeared to be more stable at higher pH values (≥ 7.0) and less stable at lower pH value (pH 6.5). For VEE VLP, under all tested pH conditions, the CD signal at 214 nm did not change substantially as temperature was increased, indicating no major change in secondary structure with increases in temperature. The lack of a distinct thermal transition prevented accurate calculation of T_{onset} values.

To assess the effect of solution pH on the stability of the overall tertiary structure of the proteins contained in each of the three VLPs, the fluorescence wavelength maximum values as a function of solution (pH 6.5 to 8.5) and temperature (10 to 87.5 ^{o}C) was evaluated (Supplemental Figure 4.1B). An increase in Trp fluorescence peak position, (i.e. a red shift was observed with increasing temperature for each of the pH conditions) was seen for all VLP samples, probably reflecting changes in the tertiary structure of the VLPs. For EEE VLPs, peak positions remained largely unchanged up to ~40 ºC, with a dramatic alteration occurring at ~40 ºC to 49 ºC, with onset temperature values increasing as the pH increased from 6.5 to 8.5. The maximum peak position values of WEE VLPs showed apparent transitions at ~30 ^{o}C, with the main transition at 45 ^{o}C (pH 6.5), 47 ^{o}C (pH 7.0 through 8.0), and 48 ^{o}C (pH 8.5). For VEE VLPs at each of pH conditions examined, peak positions slowly red shifted as the temperature increased from 10 to 40 ºC and a more dramatic alteration in peak position is observed at ~40 ºC (T_{onset}), indicating

major perturbation in tertiary structure. Thus, the overall tertiary structure of the proteins in the three VLPs appeared to be less stable at pH 6.5 and more stable between pH values 7.0-8.5.

Finally, the aggregation propensity of these VLPs was examined by measuring changes in turbidity (O.D. at 350 nm) as a function of temperature and pH (Supplemental Figure 4.1C) and the corresponding T_{onset} values of the thermal transitions are summarized in Supplemental Table S1. EEE VLPs showed a dramatic increase in turbidity ranging from ~45^{o}C to ~53^{o}C, with lower pH values resulting in lower T_{onset} values. The WEE VLPs showed similar trends at pH 6.5 showing turbidity at ~48 ^{o}C, pH 7.0 around 50 ^{o}C, and the higher pH conditions around ~53^{o}C. The VEE VLPs showed minimal aggregation from pH 7.5-8.5. Interestingly, pH 6.5 condition showed the highest change in O.D. with a T_{onset} of ~53^{o}C, while at pH 7.0, VEE VLPs had a slightly higher T_{onset} at ~54^{o}C, but displayed markedly lower overall change in the O.D. signal indicating less turbidity. Hence, all three VLPs appeared to be colloidally most stable between pH values 7.0-8.5 and less stable at low pH.

The biophysical stability results were summarized using a three index empirical phase diagram data visualization tool described previously[25,26]. For EEE, WEE and VEE VLPs, (as seen in Figure 4.3A, 4.3B and 4.3C, respectively), the three-index EPDs revealed three distinct regions. The first region (I) or the native region represented by the yellowish-green colors demonstrated most stable regions for the VLPs with characteristics similar to native like structures as seen by the presence of red and green colors in CD and fluorescence panels respectively, and absence of color (black) in turbidity panels. For EEE and WEE VLPs (Figure 4.3 A and B, respectively), this region covers the range of pH 6.5 to 8.5 and temperatures from 10 to ~50 ^{o}C. Similarly, for VEE VLPs (Figure 4.3 C), the first region covers the range of pH 6.5 to 8.5 and temperatures from 10 to ~48^{o}C. Thus, the VEE VLP has slightly lower thermal

conformational stability than EEE and WEE VLPs across all the pH conditions (especially at higher pH). The second region (II) is denoted by the orange-red colors and represents conformationally altered states of the VLPs as observed by black regions in the fluorescence panels. However, the secondary structure is observed to remain unchanged in this region as seen by the presence of red color in the CD panels. For EEE and WEE (Figure 4.3 A and B, respectively) this region lies from ~50 ^{o}C to ~60 ^{o}C, but for VEE (Figure 4.3 C) it is more wide spread. For all of the VLPs, this region II suggests the presence of molten globule like states indicating loss of tertiary structure but intact secondary structure. Finally, the bluish-pink regions, which represents conformationally altered and aggregated states of the VLPs, defines the third region (III). The VLPs in this region manifest changes in intrinsic Trp fluorescence and CD ellipticity (seen by presence of black regions in their individual panels) along with a significant contribution from turbidity data (blue colored regions). This third region is representative of aggregated states occupying the pH ranges above 60^{o}C. At these elevated temperatures, EEE and WEE (Figure 4.3 A and B, respectively) were prone to aggregation over all tested pH conditions, as indicated by the presence of bluish colors from turbidity measurements. However, VEE appeared to be prone to aggregation only at pH 6.5 (Figure 4.3 C). Hence, overall, the EPDs indicated that although VEE showed lesser propensity to aggregate in the conformationally altered states, it had lower thermal conformational stability compared to EEE and WEE VLPs. We emphasize, however, that these EPDs do not reflect thermodynamic behavior. Furthermore, they are a result of effects of multiple proteins and as such are only useful in an empirical sense.

4.3.4 Screening of pharmaceutical excipients to improve physical stability of VLPs in solution

To screen excipients for their ability to enhance the thermal stability of the three VLPs, intrinsic tryptophan fluorescence spectroscopy vs temperature melt analysis was employed. Initial evaluation of this method was conducted using the least thermally stable VLP (VEE VLPs; see above). A base buffer containing 10 mM sodium phosphate and 100 mM NaCl, pH 7.5, was chosen for the excipient screening studies since this solution pH resulted in optimal VLP physical stability (see above). Seven categories of pharmaceutical excipients including carbohydrates, polyols, amino acids/carboxylic acids, metal chelators, non-ionic surfactants, cyclodextrins and polymers/polyions were examined for their effect on the transition onset temperature (T_{onset}) and the midpoint of the unfolding transition temperature (T_m) of VEE VLPs.

Figure 4.4 shows the average ΔT_{onset} and ΔT_m values of VEE VLPs in presence of different excipients. The delta values represent the difference between VEE VLPs formulated in 10 mM sodium phosphate, 100 mM NaCl, pH 7.5 with added excipient minus the VEE VLPs formulated in same buffer without additive (control), and values are sorted from highest to lowest, indicating highest to lowest stability of VEE VLPs (Figure 4.4). The inset graph shows a representative plot of the effect of a selected stabilizer (sorbitol) and a destabilizer (alpha-cyclodextrin) on the thermal stability of the VEE VLP. It can be seen that 18 out of the 26 tested excipients shifted T_{onset} values to higher temperature, with the increase ranging from 1.5 °C to 14 °C. Six of these 18 excipients were not further evaluated as stabilizers due to a minimal influence on T_m values given experimental error. The top performing stabilizers identified in this initial screen included sorbitol, trehalose, mannitol, sucrose, pluronic F-68, glycine and 2-(hydroxypropyl)-γ-cyclodextrin. These additives increased T_{onset} values by as much as 14 ^{o}C, as

well as increasing T_m values up to ~4°C. Similar stabilizing effects with these lead stabilizers were also observed for both EEE and WEE VLPs as summarized in Supplemental Table 4.2.

Based on the above results, different concentrations of the top performing stabilizers (from four different excipient categories including sugars, amino acids, cyclodextrins and detergents) were then evaluated to explore the concentration dependence of their stabilizing effect on VEE VLPs using thermal stress (Table 4.1). Higher concentrations of sugars (sorbitol, trehalose and sucrose) and detergent (pluronic F-68) resulted in an improved VEE VLP thermal stability profile as seen by increased ΔT_{onset} values from the intrinsic Trp fluorescence thermal melt results. Glycine and 2-(hydroxypropyl)-γ-cyclodextrin showed a slight increase in delta T_{onset} values compared to sugars and pluronic F-68. The shift in T_m values due to concentration effects of these excipients was less apparent, increasing the values by ~1 to 4 ^oC for most of the stabilizing excipients. Similarly, higher concentrations of sugars and pluronic F-68 increased the ΔT_{onset} values of WEE and EEE VLPs as summarized in Supplemental Table 4.3.

As a final set of experiments, different concentrations of sodium chloride (25, 50, 75 and 100 mM) were tested to explore the salt concentration-dependence of its stabilizing effect on VEE VLP. No major differences were observed across the different sodium chloride concentrations on the thermal stability of VEE VLP (data not shown), permitting the use of lower sodium chloride concentrations to achieve lower solution tonicity in the presence of other excipients. However, sodium chloride was observed to be essential to maintain the solubility of VEE VLPs in solution during dialysis into various solutions (data not shown). Therefore, for subsequent formulation development experiments described below, a balance between sufficient VEE VLP solubility and total solution osmolality values was required (because high solution osmolality values are undesirable for parenteral administration). Thus, the salt concentration was

lowered from 100 to 50 mM resulting in selection of a base buffer (10 mM sodium phosphate, 50 mM NaCl, pH 7.5) for further optimization of VEE VLP physical stability in combination with other promising excipients such as sorbitol, sucrose and pluronic F-68 as described below.

4.3.5 Optimization of lead stabilizers to design candidate bulk formulations

Various concentrations and combinations of three best performing excipients (sorbitol, sucrose, pluronic F-68) in the presence of 10 mM sodium phosphate and 50 mM NaCl, pH 7.5, were tested to identify any additive or synergistic effects on VEE VLP stability as well as on total solution osmolality values. As shown in Table 4.2, tested excipients as well as their combinations resulted in an increase in thermal stability of VEE VLP. There was no major difference in the extent of stabilization (T_{onset} and T_m values) between 5 and 10 % of sugars/sugar alcohols. Lower concentrations of sucrose and sorbitol, however, resulted in solutions with low osmolality values. Similarly, all of the tested excipients and their combinations had a stabilizing effect on the thermal stability of EEE and WEE VLPs (see Supplemental Table 4.4). Based on the osmolality consideration, lower concentrations of sugars and their combinations with pluronic F-68 were further evaluated for their stabilizing effect on freeze-thaw and accelerated stability studies.

4.3.6 Freeze-thaw and accelerated stability studies of three VLPs in candidate bulk formulations

Based on the results described above, six candidate bulk formulations were selected for the three VLPs, and their effect on freeze-thaw and accelerated storage stability conditions were evaluated (since the bulk may be stored frozen long term and then thawed for use in the drug product). The candidate formulations included: (F1) 10 mM sodium phosphate, 50 mM NaCl, pH 7.5 (control buffer); (F2) control buffer + 5.0 % sorbitol; (F3) control buffer + 7.5 % sorbitol;

(F4) control buffer + 7.5 % sorbitol, 0.05% pluronic F-68; (F5) control buffer + 5% sorbitol, 5% sucrose; and (F6) control buffer + 5% sorbitol, 5% sucrose, 0.05 % Pluronic F-68. Each of the three VLPs were formulated in the six-candidate bulk formulations, and were first evaluated for freeze-thaw stability.

The effect of multiple freeze-thaw (F/T) cycles (0, 1 and 5 cycles) on the physical stability of the three VLPs in these six candidate liquid formulations at -20 and -80^{o}C was evaluated using UV-Visible spectroscopy to monitor VLP (protein) concentration, dynamic light scattering to monitor particle size and differential scanning calorimetry to assess the overall conformational stability of the VLPs. As shown in Figure 5 for the VEE VLPs, there was a substantial loss of protein concentration (Figure 4.5A) after 5 FT cycles at -20^{o}C as well as an increase in the size of VEE VLP as measured by DLS (Figure 4.5B) across all the candidate bulk formulations. In addition, DSC data also showed that VEE VLPs were conformationally destabilized upon freeze thaw stress at -20^{o}C in all of the candidate formulations (Figure 4.5C). Similar results were observed for EEE and WEE VLPs during freeze thaw stress at -20^{o}C (see Supplemental Figures S2 and S4).

The freeze-thaw physical stability of the VEE VLPs was also evaluated at -80^{o}C. As seen in Figure 4.6A, VEE VLP formulated in the F6 formulation did not show detectable protein loss following five freeze-thaw cycles as measured by A_{280} using UV-Vis spectroscopy compared to other candidate formulations F1-F5. The DLS analysis (Figure 4.6B) showed no major changes in the hydrodynamic diameter of VEE VLP in formulations F5 and F6 compared to formulations F1-F4. Lastly, DSC analysis also did not detect any major conformational changes in VEE VLPs formulated in F5 and F6 compared to formulations F1-F4. Overall, F6 was the most stable formulation for VEE VLPs to protect against freeze-thaw stress at -80^{o}C. Similarly, EEE and

WEE VLPs formulated in F6 had the best overall freeze-thaw stability profile at -80^{o}C compared to formulations F1 to F5 (Supplemental Figure 4.3 and 4.5).

We employed accelerated stability studies to compare the different candidate bulk formulations. Each of the three VLPs, each of the three VLPs was formulated in the six candidate bulk formulations and stored at 4, 25, 40, -20 and -80^{o}C for 28 days, and the particle size (hydrodynamic diameter) of the VLPs was monitored by DLS. As shown in Figure 4.6 for VEE VLPs, the F6 formulation did not show any increase in VLP particle size while the other formulations showed an increase in size of VEE VLP to varying extents at 4, 25, 40 and -80^{o} C after 28 days. VEE VLPs in all of the formulations (including F6) stored at -20^{o}C were unstable and showed a substantial increase in the particle size of VEE VLP. Both EEE and WEE VLPs showed similar trends of increases in the size of particles across all formulations at -20^{o}C. The F6 formulation appeared to be the most stable for all three of the VLPs across the 4, 25, 40 and -80^{o}C storage conditions (see Supplemental Figures 4.6 and 4.7).

4.3.7 Drug product formulation development-Aluminum adjuvant interaction and stability studies with the three VLPs

In preliminary experiments, the individual binding of EEE, WEE and VEE VLPs to two different aluminum salt adjuvants, Alhydrogel® and AdjuPhos®, were first studied in the original formulation buffer (25 mM Tris, 100 mM sodium citrate, pH 8.5 used prior to initiation of this work) to select between the two adjuvants (see Methods). As seen in Figure 4.8A, all three VLPs were found to nearly completely bind to Alhydrogel® (98-100 %). EEE bound to both Alhydrogel® and AdjuPhos® equally well while only 24% WEE and 37 % VEE were bound to AdjuPhos®. Based on these results, Alhydrogel® was selected for subsequent adjuvant antigen interaction studies.

The final drug product vaccine is targeted to contain the three EEV VLPs, aluminum adjuvant, and a stable formulation buffer. The adsorptive capacity (maximum amount of VLP that can be adsorbed to a given amount of adjuvant matrix) of EEV VLPs to Alhydrogel® was determined by constructing binding isotherms of the three EEV VLPs (0-240 µg) with 50 µg of Alhydrogel® adjuvant in total volume of 0.5 mL each of base buffer (10 mM sodium phosphate, 50 mM NaCl, pH 7.8) and the lead candidate formulation buffer F6 (10 mM sodium phosphate, 50 mM NaCl, 5% sucrose, 5% sorbitol, 0.05% Pluronic F-68, pH 7.8; the pH of this buffer was adjusted from pH 7.5 to pH 7.8 based on results from a separate short term stability study, data not shown). As shown in Figures 4.8B and 4.8C, the adsorptive capacity of the EEE and WEE VLPs to 50 µg Alhydrogel® in the base buffer was similar (~140 µg), while the VEE VLPs had lower adsorptive capacity (~100 µg). Interestingly, in the new formulation buffer, EEE VLPs had the highest levels of maximum adsorption (~130 µg) to 50 µg Alhydrogel®, followed by WEE VLPs (~110 µg) and VEE VLPs (~ 95 µg). Next, with a goal to develop a trivalent adjuvanted vaccine containing all three VLPs, a 1:1:1 mixture of varying amounts of EEE, WEE and VEE (0-240 µg) with 50 µg of Alhydrogel® was incubated in total volume of 0.5 mL with both base buffer and the new formulation to generate a binding isotherm. The adsorptive capacity of the trivalent mixture was very similar in both the base and lead candidate formulation buffers (~100 µg bound to 50 µg of Alhydrogel®; data not shown).

The conformational stability of Alhydrogel®-adsorbed VLPs in either the base buffer or the lead candidate formulation buffer was evaluated using intrinsic tryptophan fluorescence spectroscopy as a function of temperature. The fluorescence thermal melts (peak position versus temperature graphs) are shown in Supplemental Figure 4.8, and the corresponding T_{onset} and T_m values of each individual VLP and a mixture of the three VLPs are plotted in Figure 8E and

Figure 4.8F, respectively. At lower temperatures, the peak positions (lambda max) for the VLP samples with adjuvant were observed to be slightly red shifted (~2 nm) compared to the corresponding VLP samples with no adjuvant. This slight increase in the MSM peak position presumably signifies a subtle structural alteration in the VLP proteins when adsorbed on the surface of the adjuvant. The thermal onset (T_{onset}) and melting (T_m) temperatures for the VLPs were then determined from the thermal melting curves. Adsorption of the VLPs to the aluminum adjuvant reduced their thermal stability (T_{onset}, ~2-3^oC and T_m, ~1-3^oC) in both the base buffer and candidate formulation buffer. The formulation buffer, however, increased the thermal stability (T_{onset}) of the non-adjuvanted individual VLPs and their 1:1:1 mixture compared to the VLPs in the base buffer. This effect was not observed, however, when comparing the Tm values (see Figures 4.8E and 4.8F).

The ability to desorb each of the aluminum adjuvant adsorbed VLPs was examined in the presence of various additives listed in Supplemental Figure 4.9A. Additionally, the effect of increased incubation time and temperature on desorption process of the 1:1:1 mixture of the VLPs was examined under various conditions (Supplemental Figure 4.9B). The most effective solution for desorbing the VLPs was 0.5 M sodium phosphate (pH 7.8), with ~90 and 100% desorption being observed after 3 h and 16 h incubation at room temperature (RT), respectively. For conditions that were tested at both 4°C and RT, no major differences in VLP desorption from the adjuvant were observed between these two temperatures. Next, desorption of each individual VLP, and a 1:1:1 mixture of the three VLPs in 0.5 M sodium phosphate (pH 7.8) was evaluated (Supplemental Figure 4.9C), and nearly 100% desorption of the VLP samples was observed demonstrating that 0.5 M sodium phosphate pH 7.8 was effective at removing the adsorbed WEE, VEE and EEE VLPs from Alhydrogel®.

The concentration dependence of sodium phosphate mediated desorption of VLPs from Alhydrogel® was investigated for each individual VLP and the mixture of the three VLPs to examine the strength of interaction between the antigens and adjuvant. No VLP desorption was observed when the concentration of sodium phosphate was below 20 mM as shown in Figure 4.9A. However, WEE, VEE and EEE VLPs displayed significant desorption starting at 50, 100 and 200 mM sodium phosphate, respectively, indicating the weakest, intermediate and highest strength of adsorption to Alhydrogel®, respectively. Additionally, the time dependence (kinetics) of VLP desorption from adjuvant in the presence of 0.5 M sodium phosphate showed desorption values of ~70% at 0 h, which followed an increase to 90% at ~1 h, followed by a leveling off at ~98-99% after 24 h (Figure 4.9B).

Finally, three time durations (0.5, 4, and 24 h) for desorption in 0.5 M sodium phosphate were selected to examine the effect of storing the VLP-adjuvant samples for over 8 weeks at 4^{o}C to evaluate if there is a storage time dependence of susceptibility towards desorption of VLPs from the aluminum adjuvant. As shown in Figure 4.9 C, D, E and F, in general, the percentage desorption of EEE, WEE and VEE VLPs and the trivalent mixture, respectively, decreased over 8 weeks. For example, for the mixture of three VLPs, about 95% and 56% desorption was observed at zero day and 0.5 h storage time, respectively. However, there appeared to be a general trend of continuing decreasing VLP desorption from the aluminum adjuvant with an increase in the storage time (up to 8 weeks) for the VLP-adjuvant samples.

4.4 Discussion

Virus-like particle (VLP) based vaccines consist of highly ordered repetitive structures that form spontaneously upon recombinant expression of one or more structural viral proteins[27]. These particulate protein assemblies are structurally similar to viruses but do not contain native

viral genetic information potentially yielding safer vaccine candidates[28,29]. During pharmaceutical development of VLP based vaccine candidates, an extensive analytical characterization toolset is used to study the complex nature of these vaccines to ensure that the native conformation of the protein epitopes is maintained during manufacturing, storage and administration. Additionally, stability indicating analytical methods are also required to elucidate molecular mechanisms of vaccine degradation, to monitor the accelerated and long term stability, and to design new formulations by screening different conditions and additives. Furthermore, analytics serve as the foundation for comparability assessments to monitor critical quality attributes (CQA's) of vaccines during both product and process related changes such as changes in cell lines, scale-up of the bulk process or changing a lyophilized to a liquid dosage form[30-32].

The particle size range of the VLPs was relatively homogeneous and closely resembled the native viruses as measured by TEM and DLS. The morphology and composition of the three VLPs were spherical (~70 nm in diameter), comprised of capsid, E1 and E2 proteins as determined by TEM and SDS-PAGE analysis. The VLPs also contained some residual nucleic acid (presumably host-cell DNA and/or RNA) impurity, as suggested by the high A_{260}/A_{280} ratio measured by UV-Visible spectroscopy and confirmed by nucleic acid quantitation (data not shown). In comparison, there are currently two licensed recombinant VLP based vaccines, one against human papillomavirus (HPV) and another against hepatitis B virus (HBV). Each contains only a single viral surface protein (L1 and HBsAg, respectively) and are expressed in yeast. HPV VLPs are predominantly spherical or ellipsoidal in shape, lack a lipid envelope and are ~50-60 nm in diameter[33-35] while HBV VLPs are also spherical, contain a lipid envelope derived from yeast lipids, and are smaller in diameter (~22 nm)[36,37].

It is critical to monitor both the higher order structure (HOS) and concomitant stability of vaccine antigens to ensure that the vaccine can be reproducibly manufactured, retains critical quality attributes during any process changes (comparability) and remains stable during storage. Understanding the changes in the structural integrity of the antigen as a function of stress (pH, temperature, ionic strength) helps in outlining the physical stability parameters along with development of a stable formulation. In this work, the physical stability profiles of the three VLPs were evaluated using different spectroscopic techniques to monitor their secondary structure, tertiary structure and aggregation propensity. Although the nucleic acid dominates the UV absorption spectra of the VLPs, the lack of fluorescence of DNA permits isolated analysis of the protein components by fluorescence spectroscopy. The DNA is most-likely encapsulated within the particles; therefore aggregation events are expected to be primarily driven by the external protein shell. Therefore, we discuss the VLPs behavior in terms of protein although we cannot exclude contributions by the nucleic acids. Additionally, these biophysical techniques coupled with three index empirical phase diagrams were used to evaluate the higher order structure (HOS) and stability of each of the VLPs over a wide range of pH and temperature. The utility of such data visualization approaches for a better understanding of the physical stability profiles of variety of proteins and vaccines (for formulation development and comparability assessments) has been widely demonstrated in previous work[38-42]. Here, the comparison of stability profiles of the three VLPs using the 3-index EPD approach helped in detecting differences in the HOS and physical stability of the VLPs under stress conditions. Overall, the EPD (see Figure 3) showed that all of the VLPs were more stable at basic pH 7.5-8.5 compared to pH 6.5 and 7.0 as function of temperature. Subtle physical stability differences were detected

between the secondary and tertiary structures and aggregation propensities of the three variants which suggested the VEE VLP may be the least physically stable of the three VLPs.

In addition to identifying an solution pH for optimal VLP stability, this work examined various classes of pharmaceutical excipients for their ability to enhance the thermal and freeze-thaw stability of the three EEV VLPs. Sucrose, sorbitol and pluronic F-68 were identified as candidate stabilizers and their combination increased the thermal and freeze-thaw stability of each of the VLP. Sugars such as sucrose and sorbitol are known to act via preferential exclusion mechanism and stabilize proteins and vaccines against thermal and freezing stress.[43-46] Pluronic® copolymers, a class of non-ionic detergents is known to prevent agitation and freezing induced aggregation for a number of proteins by outcompeting protein molecules at air-water interfaces and preventing freezing induced structural perturbations leading to aggregation.[47,48] A total of six candidate formulations comprising of a base formulation (F1, no excipients) and combinations of the above three excipients (Formulations F2-F6) were short listed for accelerated and freeze-thaw stability studies.

Freezing of protein solutions is known to potentially negatively impact protein structure and can cause aggregation and/or conformational destabilization (which may in turn affect the potency of protein antigen vaccines)[49-51]. Upon freezing and thawing at -20^{o}C vs. -80^{o}C, the EEV VLPs showed higher losses of protein amount, increased hydrodynamic diameters and a higher degree of T_{onset} / T_m shifts to lower temperatures in DSC thermograms (indicating conformational destabilization) at -20^{o}C (vs -80^{o}C). These results for VLPs in Formulation 1 (lacking additives) may possibly be attributed to flexibility differences or supercooling phenomena. For example, the observed lower stability at -20^{o}C could reflect the comparatively higher flexibility of VLP polypeptide chains and increased interactions with ice crystals than at -80^{o}C. At -80^{o}C mobility

reduces due to increased viscosity of the frozen matrix minimizing aggregation during freeze thaw. The phenomenon of supercooling causes more uniform nucleation, rapid formation of ice crystals and subsequent interaction with the glass surface of the vials, potentially destabilizing the VLPs at -20^{o}C. In contrast, at -80^{o}C there is heterogeneous nucleation from the vial surface to the center of the solution, minimizing protein-surface interactions and aggregation as demonstrated by Kerwin et al.[52]

For VLPs in formulations F2-F6, an increase in freeze-thaw stability was observed compared to F1 formulation across all VLPs at both -20 and -80 ^{o}C. However, the extent of stabilization was lower at -20^{o}C than -80^{o}C, which may primarily be attributed to their Tg' values (e.g., sorbitol has Tg' ~-45^{o}C, sucrose is ~-32^{o}C)[53]. Multiple studies have shown that proteins formulated with sugars when frozen above their Tg' value, result in destabilization of protein structure and increased aggregation. This is due to crystallization of freeze-concentrated sugars and the higher mobility of protein molecules in a less viscous frozen matrix[53-56]. Similarly, in our work we observed increased aggregation in the form of increases in hydrodynamic diameters and losses in protein amount for all the VLPs when frozen above the Tg' values (at -20^{o}C) vs when frozen below the Tg values (at -80^{o}C). Finally, DSC is a powerful tool to assess the conformational changes in a protein in the form of a T_m shift or changes in the shape of the endothermic peaks[57,58]. DSC proved here to be a sensitive tool to detect VLP destabilization during freeze thaw at -20^{o} vs -80^{o}C in different formulations. Overall, the freeze-thaw stability data demonstrated that Formulation F6 imparted the maximal relative stability to the VLPs under freeze-thaw stress.

VLP based vaccines generally induce stronger immune responses than other protein subunit based vaccines due to the repetitive display of antigenic epitopes[59,60]. However, many studies

have found that these immune responses can be further augmented by the use of aluminum containing adjuvants[61,62]. Both the HPV and HBV licensed VLP vaccines are formulated with aluminum adjuvants. The most commonly used aluminum adjuvants are aluminum hydroxide (Alhydrogel®) and aluminum phosphate (Adju-Phos®). The adsorption of antigens to these adjuvants depends on several factors such as charges on the antigen and adjuvant, as well as solution pH, ionic strength and buffer components[63,64]. All of the three VLPs demonstrated nearly complete binding to Alhydrogel®. The VLPs are probably adsorbed to Alhydrogel® primarily through electrostatic interactions, since at pH 8.5 of the adsorption buffer, the positively charged Alhydrogel® (pI of ~11) interacts with negatively charged clusters on the surface of the VLPs. In the case of Adju-Phos® binding, an opposite trend is expected since the negatively charged Adju-Phos® (pI of ~5) might not bind to all of the VLPs due to electrostatic repulsion. We observed minimal binding of WEE and VEE VLPs to Adju-Phos®. However, it is was surprising to find that EEE VLP showed complete binding to Adju-Phos® indicating additional binding mechanisms other than electrostatics. Previous work by multiple research groups (Al-Shakhshir *et.al*[65], Peek et.al[66] and Jones et.al[17]) have also found that certain proteins get adsorbed to both aluminum salt adjuvants through mechanisms other than electrostatics such as ligand exchange, hydrogen bonding, van der Waals forces and attractive hydrophobic interactions.

To probe if the adsorption of the VLPs to Alhydrogel® affects the structural integrity and stability of adsorbed VLPs, fluorescence spectroscopy was used to measure the thermal stability both in the presence and absence of the adjuvant in base buffer and lead candidate formulation buffer F6. Overall, adjuvanted and non-adjuvanted VLPs in the candidate formulation buffer had increased conformational stability compared to VLPs in the base buffer (except the adjuvanted

VLP mixture which showed similar stability in both buffers). In general, the aluminum adjuvated EEV VLPs showed decreased thermal stability in formulation buffer compared to the non-adjuvanted VLPs. Our findings are in agreement with the work of multiple research groups, where adsorption of antigen to Alhydrogel® caused structural alterations in the antigen and/or detrimentally affected the physical stability profile of vaccine antigen.[17,66-68]

Desorption of the antigen from the adjuvant is desirable to better characterize the final vaccine drug product for total antigen content, amount of antigen adsorbed, conformational integrity and bioactivity by *in vivo* animal models.[69]. Common desorption methods using surfactants employing sodium dodecyl sulfate (SDS) or cetylpyridinium chloride (CPC) can be quite effective in eluting the antigen from aluminum adjuvant[70]. These surfactants, however, may denature the antigens or alter their functional epitopes. In this study, phosphate buffer was found to the most efficient desorption media for all three VLPs and their mixture with varying degree of desorption observed for the three VLPs. A number of previous studies have shown that phosphate ions can affect desorption of antigens from Alhydrogel® primarily through replacement of the hydroxyl ions of Alhydrogel® with phosphate ions and subsequent decrease of the adjuvant pI from ~11 to ~4 (depending on phosphate concentration) [71-73]. This disrupts the electrostatic interactions between the bound antigen and aluminum adjuvant. We also observed that the strength of interaction between the aluminum adjuvant and the VLPs differed since different amounts of phosphate could elute the VLP from the surface. EEE, WEE and VEE VLPs required the highest, intermediate and lowest amounts of phosphate, respectively indicating the highest, intermediate and weakest strength of adsorption to Alhydrogel®. We also noted a decreased ability to elute the VLPs over time using this approach, indicating additional

interactions between the antigen and aluminum adjuvant are occurring during long term storage[67,74].

This work provides a set of analytical characterization tools to monitor the structural and conformational integrity of three different EEV VLPs. Stability indicating methods were developed and used to identify stabilizing excipients for a stable candidate formulation for bulk storage of the three VLP vaccine candidates. The set of analytical methods developed in this study will be very useful for comparability assessments to monitor the effect of both process and product related changes to the physical quality of these VLPs as they further advance into clinical development. It also lays the groundwork for future pharmaceutical development of monovalent and trivalent aluminum adsorbed drug product equine encephalitis VLP vaccine candidates using common buffer and excipient conditions. In further work, we are correlating the physicochemical data from this work with immunogenicity assays (*in vitro* binding and animal potency assays) to monitor key protective epitopes.

Table 4.1. Concentration optimization of lead stabilizing excipients for their stabilizing effect on the overall tertiary structure of VEE VLPs (0.1 mg/mL) as measured by intrinsic tryptophan fluorescence spectroscopy as a function of temperature. Excipients were formulated at indicated excipient concentration in 10 mM sodium phosphate, 100 mM NaCl, pH 7.5. Delta T_{onset} and delta T_m values are shown for different excipients where delta values represent the difference between VEE VLP formulated in 10 mM sodium phosphate, 100 mM NaCl, pH 7.5 with added excipient and VEE VLP formulated in same buffer without additive (control) Data represent mean and range of duplicate replicates. The results for EEE and WEE VLPs are shown in Supplemental Table 4.2.

Excipient	**Concentration**	**Intrinsic Trp Fluorescence**			
		ΔT_{onset} (^oC)		**ΔT_m (^oC)**	
		Mean	Range	Mean	Range
Sorbitol	5 % w/v	9.2	9.0, 9.4	2.3	2.1, 2.5
	10 % w/v	9.6	9.4, 9.8	1.8	1.5, 2.1
	15 % w/v	9.7	9.6, 9.8	2.9	2.6, 3.2
	20 % w/v	13.8	13.5, 14.1	3.5	3.5, 3.6
Trehalose	5 % w/v	7.3	7.2, 7.4	1.3	1.2, 1.4
	10 % w/v	7.8	7.6, 8.0	1.3	1.1, 1.5
	15 % w/v	10.0	9.8, 10.1	1.8	1.5, 2.1
	20 % w/v	10.5	10.3, 10.6	2.2	2.1, 2.4
Sucrose	5 % w/v	8.4	7.8, 9.0	1.9	1.7, 2.1
	10 % w/v	9.8	9.6, 10.0	0.7	0.6, 0.8
	15 % w/v	9.9	9.5, 10.3	1.6	1.5, 1.8
	20 % w/v	10.8	10.6, 10.9	2.4	2.3, 2.5
Pluronic F-68	0.025 % w/v	8.0	7.6, 8.4	1.9	1.7, 2.1
	0.05 % w/v	8.5	8.5, 8.5	1.2	0.9, 1.6
	0.1 % w/v	10.4	10.0, 10.8	-1.5	-1.4, 1.6
Glycine	0.05 M	0.7	0.5, 0.9	1.2	0.5, 1.8
	0.1 M	2.0	1.0, 2.9	1.6	1.1, 2.2
	0.15 M	2.9	2.5, 3.3	0.8	0.5, 1.2
	0.3 M	0.2	0.0, 0.4	-3.6	-2.5, 4.7
2-(Hydroxypropyl)-γ-Cyclodextrin	2.5 % w/v	2.1	1.5, 2.7	2.3	2.1, 2.5
	5 % w/v	2.8	2.5, 3.1	2.0	1.1, 2.9
	7.5 % w/v	4.3	3.8, 4.8	2.4	2.2, 2.6
	10 % w/v	8.5	6.4, 10.6	0.8	0.7, 0.9

Table 4.2. Effect of lead excipient combinations on the overall tertiary structure stability of VEEV (0.1 mg/mL) as measured by intrinsic tryptophan fluorescence as a function of temperature and the corresponding osmolality values of the formulations. Excipients were formulated at indicated levels in 10 mM sodium phosphate, 50 mM NaCl, pH 7.5. Delta T_{onset} and delta T_m values are shown for different excipients where delta values represent the difference between VEE VLP formulated in 10 mM sodium phosphate, 100 mM NaCl, pH 7.5 with added excipient and VEE VLP formulated in same buffer without additive (control) Data represent mean and range of duplicate replicates for thermal melt analysis. Data from osmolality measurements represent the mean and standard deviation for triplicate measurements. The results for EEE and WEE VLPs are shown in Supplemental Table 4.3.

Excipient Combination (% w/v)	**Intrinsic Trp Fluorescence**				**Osmolality mOsm/kg**	
	ΔT_{onset} (^oC)		**ΔT_m (^oC)**			
	Mean	Range	Mean	Range	Mean	SD
5 % Sorbitol	9.2	9.0, 9.3	2.4	2.4, 2.4	358	6
7.5 % Sorbitol	10.2	10.0,10.3	3.5	3.5, 3.5	483	7
10 % Sorbitol	10.6	10.3,10.8	4.7	4.7, 4.7	677	5
10 % Sucrose	8.0	7.9, 8.1	0.7	0.2, 1.0	394	1
15 % Sucrose	9.1	8.9, 9.2	2.1	2.1, 2.1	601	7
5 % Sorbitol + 5 % Sucrose	9.6	9.5, 9.6	1.9	1.9, 1.9	501	4
5 % Sorbitol + 0.05 % Pluronic F-68	8.7	8.7, 8.7	2.4	2.3, 2.5	364	5
7.5 % Sorbitol + 0.05 % Pluronic F-68	9.5	9.5, 9.5	2.5	2.5, 2.5	486	3
10 % Sorbitol + 0.05 % Pluronic F-68	9.7	9.7, 9.7	3.2	3.0, 3.3	668	11
10 % Sucrose + 0.05 % Pluronic F-68	7.8	7.7, 7.8	2.2	2.1, 2.2	405	2
15 % Sucrose + 0.05 % Pluronic F-68	9.1	9.0, 9.2	2.7	2.6, 2.7	620	3
5 % Sorbitol + 5 % Sucrose + 0.05 % Pluronic F-68	9.3	9.2, 9.3	2.5	2.4, 2.5	502	7

A) EEE B) VEE C) WEE

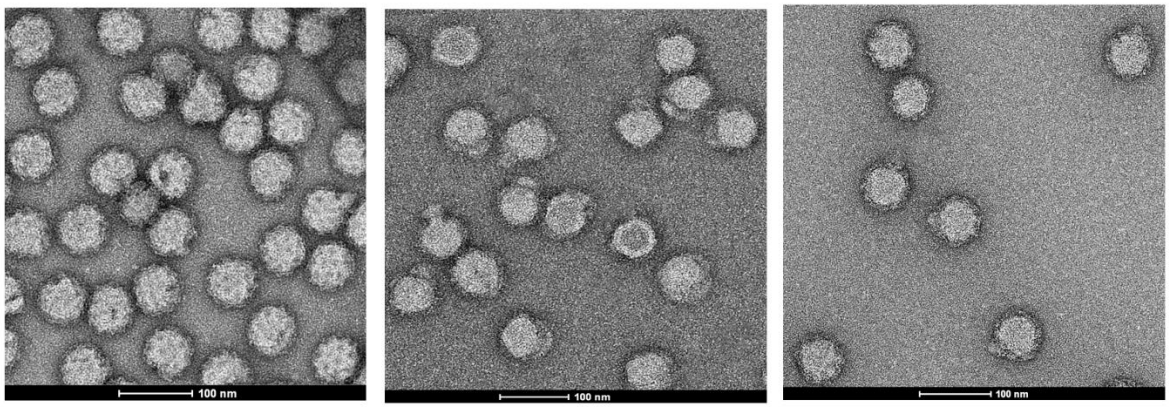

D)

VLP	Hydrodynamic diameter (nm)			Polydispersity (%)
	Literature value	Transmission electron microscopy (TEM)	Dynamic Light Scattering (DLS)	
EEE	60-65	66 ± 2	67.7 ± 0.4	4± 1
VEE	70	70 ± 2	71.4 ± 0.7	6 ± 1
WEE	70	72± 2	72.0 ± 0.6	4 ± 1

Figure 4.1. Size analysis of three equine encephalitis virus-like particles (EEE, VEE and WEE VLP). (A, B, C) Representative transmission electron microscopy (TEM) images of each VLP with size bar of 100 nm displayed below the images, and (D) Comparison of hydrodynamic diameter values as reported previously[2,19,20] and as measured by dynamic light scattering (DLS) and TEM. The polydispersity values from DLS measurements are also shown. The values represent mean ± 1 SD for n=50 particles for TEM analysis and n=3 measurements by DLS.

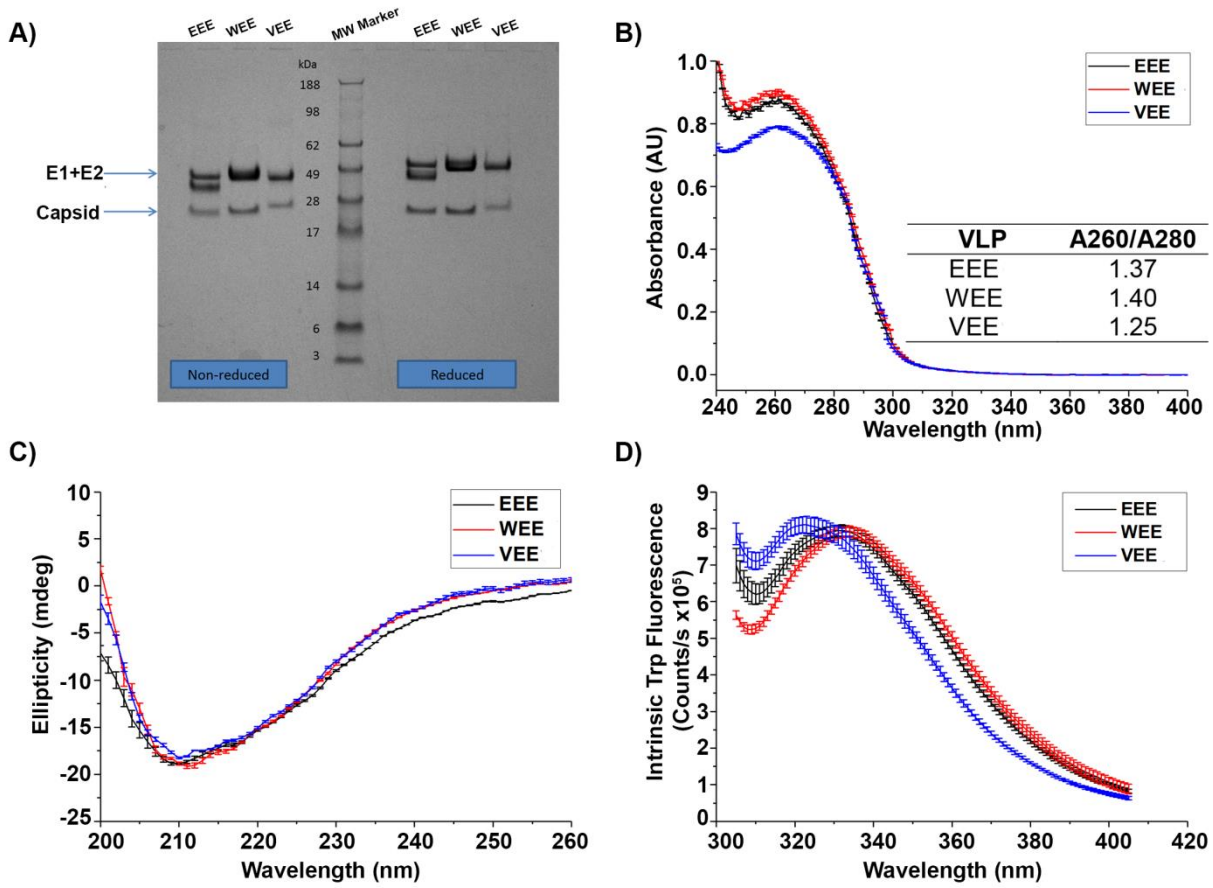

Figure 4.2. Structural characterization of three equine encephalitis virus-like particles (EEE, VEE and WEE VLPs). (A) Representative SDS-PAGE analysis of VLPs under non-reducing and reducing conditions (in presence of DTT), (B) UV-Visible absorption spectroscopy of VLPs. The inset shows the A260/280 ratios for each of the VLP, indicating presence of ~10 % nucleic acid, (C) Far-UV circular dichroism spectra at 10 °C, and (D) Intrinsic tryptophan fluorescence spectra at 10 °C. Data in panels B, C and D represent average and standard deviation from triplicate measurements.

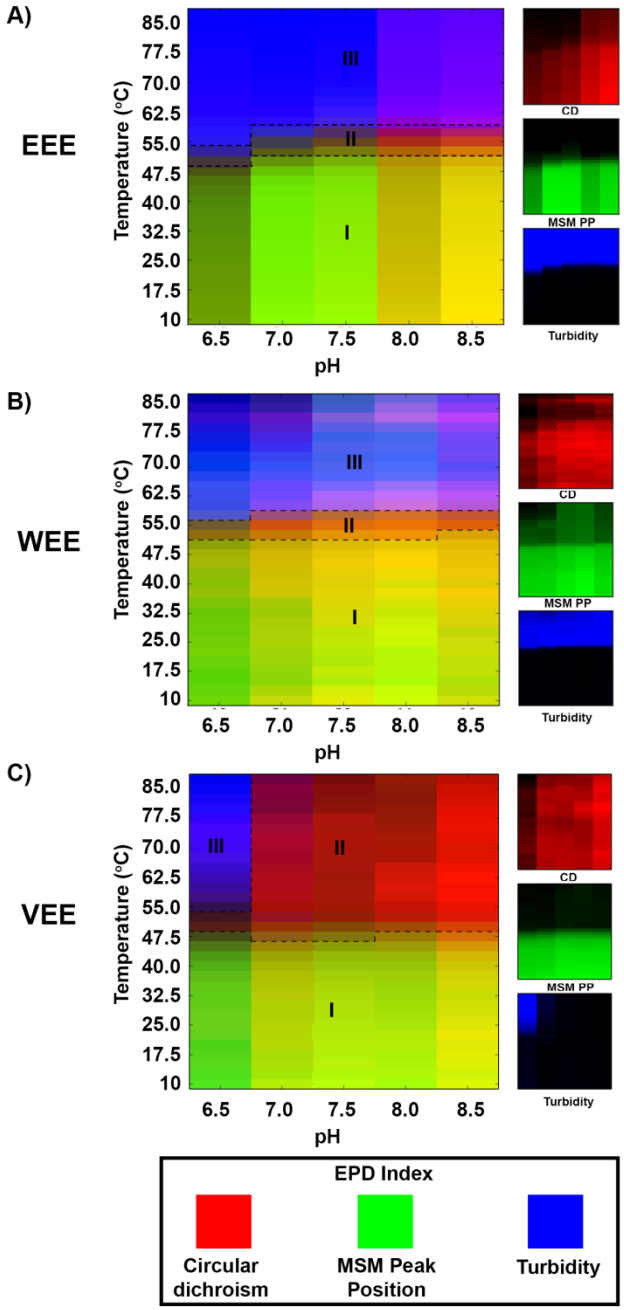

Figure 4.3. Three-index empirical phase diagrams of biophysical stability profile (vs. temperature and pH) of three equine encephalitis virus-like particles in 20 mM phosphate, 100 mM NaCl buffer. (A) EEE, (B) WEE, and (C) VEE VLP. EPDs were generated using the biophysical datasets obtained from circular dichroism, intrinsic Trp fluorescence peak position, and turbidity analyses. Refer to Supplemental Figure 4.1 for biophysical data sets from circular dichroism, intrinsic Trp fluorescence peak position, and turbidity measurements, and the methods section for experimental details of data visualization tool.

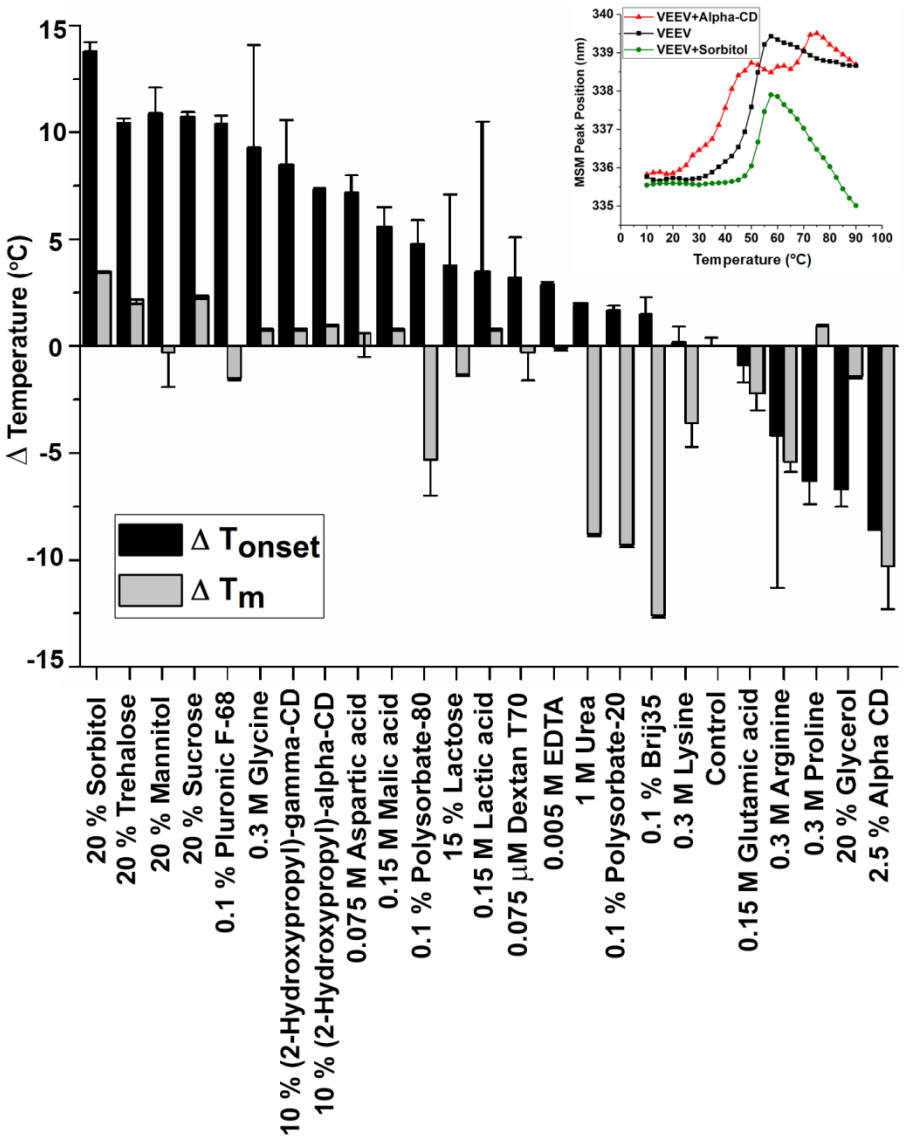

Figure 4.4. Effect of excipients on the thermal stability of VEE VLP as measured by intrinsic tryptophan fluorescence spectroscopy. Delta T_{onset} and delta T_m values are shown for different excipients where delta values represent the difference between VEE VLP formulated in 10 mM sodium phosphate, 100 mM NaCl, pH 7.5 with added excipient and VEE VLP formulated in same buffer without additive (control). Samples were formulated at 0.1 mg/mL and the data represents the mean values and error bars of range values from duplicate experiments. The results for EEE and WEE VLPs are shown in Supplemental Table 4.1.

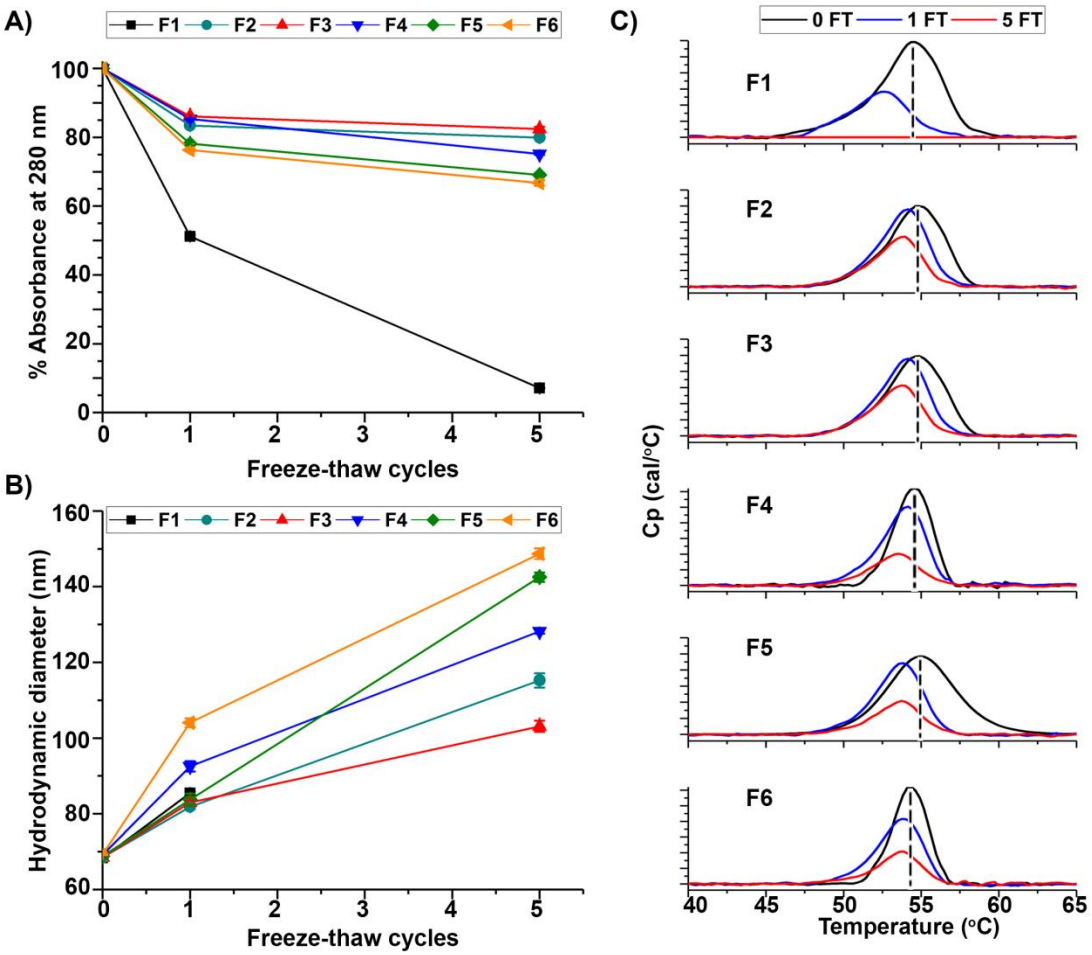

Figure 4.5. Effect of different candidate formulations on freeze-thaw stability (0, 1 and 5 freeze-thaw cycles) of VEE VLPs at -20^{o}C. (A) % Absorbance at 280 nm showing protein loss with increasing freeze thaw cycles, (B) hydrodynamic diameter as a function of freeze-thaw cycles as measured by DLS, and (C) conformational stability of VEE VLP as measured by DSC. The VEE VLP protein concentration was 0.15 mg/mL in all six formulations: (F1) 10 mM sodium phosphate, 50 mM NaCl, pH 7.5; (F2) F1 buffer + 5 % sorbitol; (F3) F1 buffer + 7.5 % sorbitol; (F4) F1 buffer + 7.5 % sorbitol, 0.05 % pluronic F-68; (F5) F1 buffer + 5% sorbitol, 5% sucrose and (F6) F1 buffer + 5% sorbitol, 5% sucrose, 0.05 % Pluronic F-68. Data represent average and standard deviation from triplicate measurements. *VEE VLP formulated in F1 aggregated after 5 FT cycles and hence there is no DLS data point for 5 FT cycles. The dotted line represents the average Tm values at prior to FT (0 FT) for better visualization of the deviation in Tm values after five FT cycles.

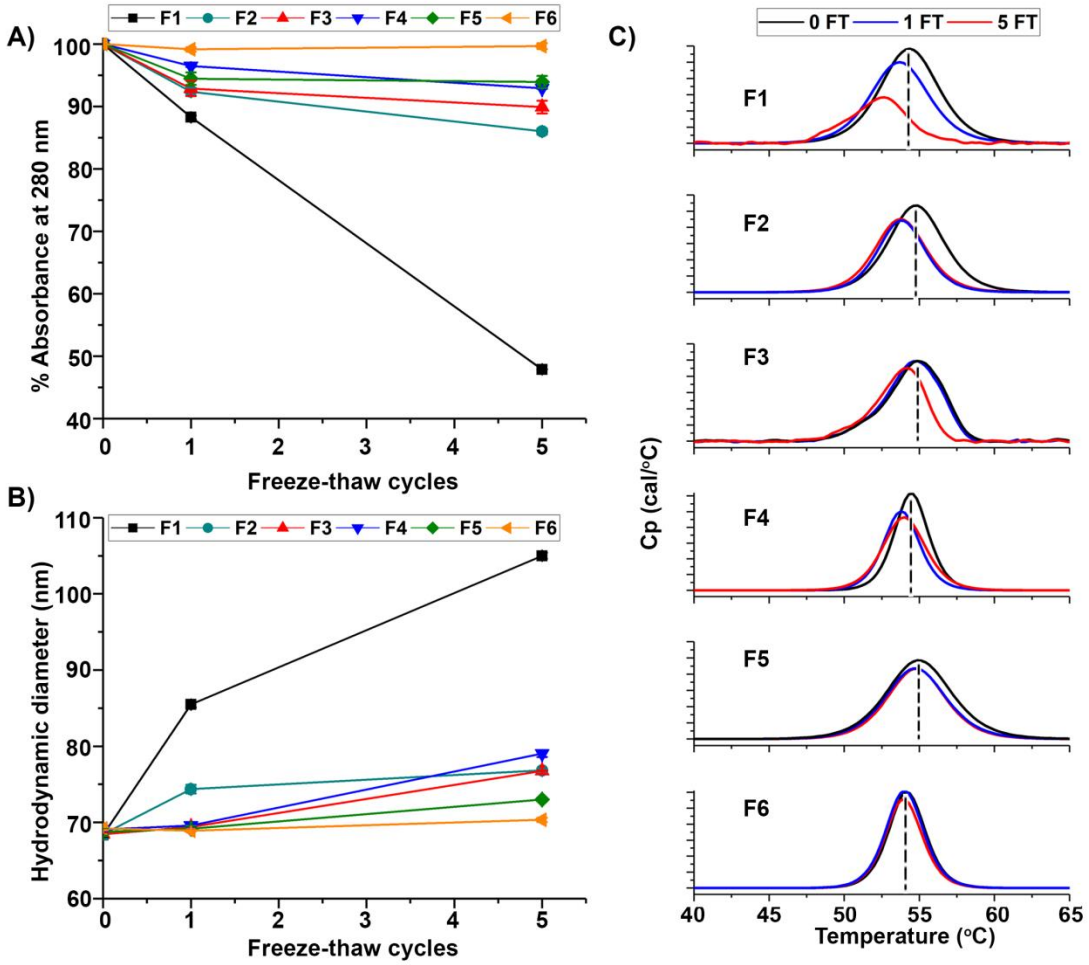

Figure 4.6. Effect of different candidate formulations on freeze-thaw stability (0, 1 and 5 freeze-thaw cycles) of VEE VLPs at -80°C. (A) % Absorbance at 280 nm showing protein loss with increasing freeze thaw cycles, (B) hydrodynamic diameter as a function of freeze-thaw cycles as measured by DLS, and (C) conformational stability of VEE VLP as measured by DSC. The VEE VLP protein concentration was 0.15 mg/mL in all six formulations: (F1) 10 mM sodium phosphate, 50 mM NaCl, pH 7.5; (F2) F1 buffer + 5 % sorbitol; (F3) F1 buffer + 7.5 % sorbitol; (F4) F1 buffer + 7.5 % sorbitol, 0.05 % pluronic F-68; (F5) F1 buffer + 5% sorbitol, 5% sucrose and (F6) F1 buffer + 5% sorbitol, 5% sucrose, 0.05 % Pluronic F-68. Data represent average and standard deviation from triplicate measurements. The dotted line represents the average Tm values at prior to FT (0 FT) for better visualization of the deviation in Tm values after five FT cycles.

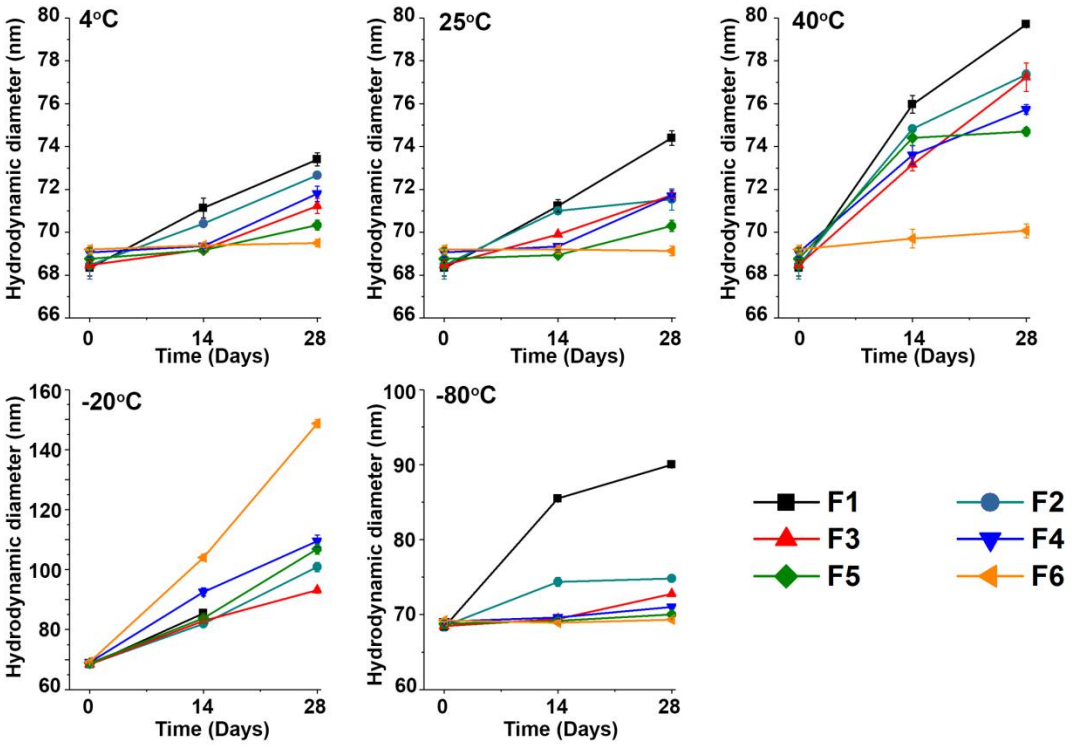

Figure 4.7. Accelerated stability studies of particle size of VEE VLPs in six different candidate formulations when stored at different temperatures (4, 25, 40, -20 and -80^{o}C) for 28 days as measured by DLS. The VEE VLP protein concentration was 0.15 mg/mL in the six formulations: (F1) 10 mM sodium phosphate, 50 mM NaCl, pH 7.5; (F2) F1 buffer + 5 % sorbitol; (F3) F1 buffer + 7.5 % sorbitol; (F4) F1 buffer + 7.5 % sorbitol, 0.05 % pluronic F-68; (F5) F1 buffer + 5% sorbitol, 5% sucrose and (F6) F1 buffer + 5% sorbitol, 5% sucrose, 0.05 % Pluronic F-68. Data represent mean and standard deviation from triplicate measurements.

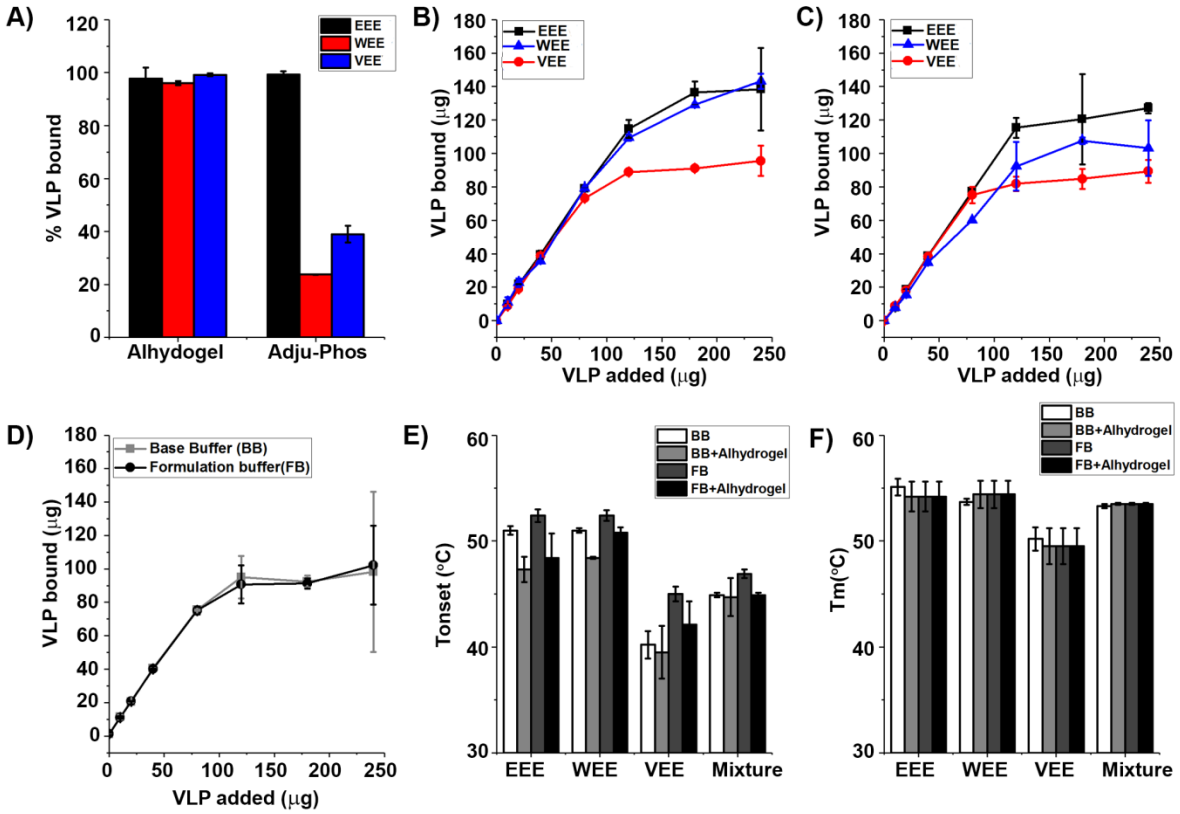

Figure 4.8. Adsorption studies of three equine encephalitis virus-like particles (EEE, VEE and WEE VLPs) onto aluminum adjuvant. (A) Percent adsorption of the three virus-like particles on two different aluminum salt adjuvants, Alhydrogel® and Adjuphos®. Fifty micrograms of protein was adsorbed onto 200 µg of adjuvant in a 25 mM Tris, 100 mM sodium citrate, pH 8.5, (B, C) Binding isotherms of the three VLPs with 50 µg Alhydrogel® in the base buffer (B) or the formulation buffer (C), (D) Binding isotherms of a mixture of different concentrations of mixed EEE, WEE and VEE VLPs (1:1:1 ratio) with 50 µg Alhydrogel® in the base buffer (BB) or the formulation buffer (FB), and (E,F) Thermal onset temperature (T_{onset}) and thermal melting temperatures (Tm) of individual VLPs +/- Alhydrogel and the 1:1:1 trivalent mixture +/- Alhydrogel in base buffer (BB) and formulation buffer (BB) as measured by intrinsic Trp fluorescence spectroscopy. The non-adjuvanted samples contained 0.12 mg/ml VLPs, and the adjuvanted samples contained 0.12 mg/ml VLPs and 0.5 mg/ml Alhydrogel. Base buffer (BB) was 10 mM NaPO4, 50 mM NaCl, pH 7.8 and the formulation buffer (FB) was 10 mM NaPO4, 50 mM NaCl, 5% sucrose, 5% sorbitol, 0.05% Pluronic F-68, pH 7.8. Data represents mean and standard deviation from triplicate measurements.

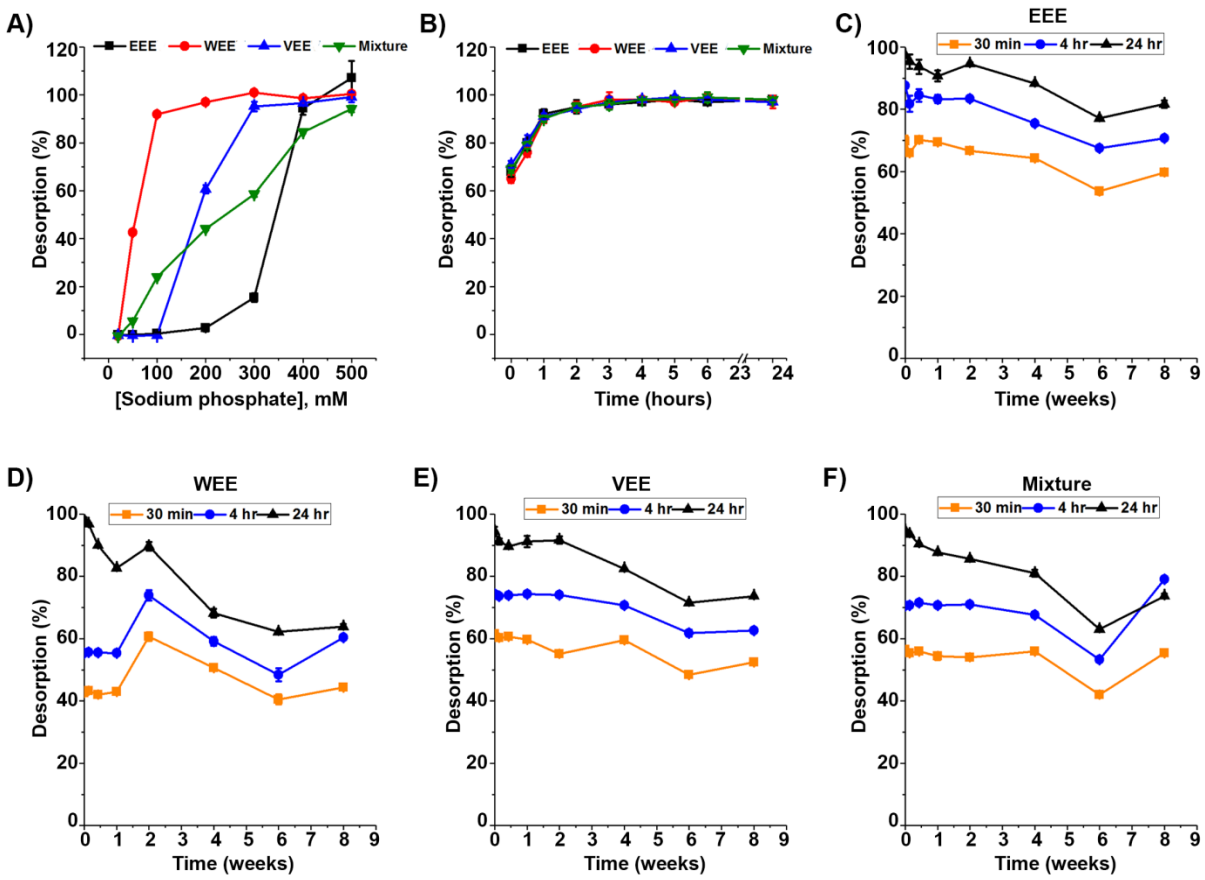

Figure 4.9. Desorption studies of three equine encephalitis virus-like particles (EEE, VEE and WEE) from Alhydrogel® adjuvant. (A) Desorption of individual VLPs and a mixture of the three VLPs from Alhydrogel® in the presence of increasing concentrations of sodium phosphate (pH 7.8), (B) Time course profiles for the desorption of individual EEV VLPs and a mixture of the three VLPs from Alhydrogel® in the presence of 0.5 M sodium phosphate (pH 7.8), (C, D, E, F) Changes in the extent of VLP desorption from Alhydrogel® measured over eight weeks of storage time in formulation buffer at 4°C (10 mM NaPO4, 50 mM NaCl, 5% sucrose, 5% sorbitol, 0.05% Pluronic F-68, pH 7.8). The orange, blue and black traces are for 30 minutes, 4 hours, and 24 hours of sample incubation with the 0.5 M sodium phosphate desorption buffer (pH 7.8), respectively. Data represents mean and standard deviation from triplicate measurements.

Supplemental Table 4.1. Summary of thermal onset temperature values (T_{onset}) for the EEE, WEE and VEE VLPs at 0.15 mg/mL in 20 mM citrate-phosphate, 100 mM NaCl under different pH conditions (pH 6.5, 7.0, 7.5, 8.0 and 8.5) measured by circular dichroism at 214 nm, intrinsic fluorescence MSM peak position and turbidity (OD_{350} nm) analysis. Data represent mean duplicate replicates. ND indicates that no transition was detected and as a result T_{onset} values could not be determined.

pH	Circular dichroism			MSM Peak Position			Turbidity (OD_{350})		
	EEE	WEE	VEE	EEE	WEE	VEE	EEE	WEE	VEE
6.5	50.2	52.6	ND	40.2	45.2	39.5	45.2	47.8	46.7
7.0	52.6	54.9	ND	43.8	47.3	40.5	47.8	50.6	49.2
7.5	55.4	55.1	ND	46.8	47.3	40.8	51.2	52.3	56.7
8.0	56.3	55.3	ND	49.3	47.4	40.8	52.0	52.5	ND
8.5	56.3	55.0	ND	49.0	48.2	40.8	52.5	52.5	ND

Supplemental Table 4.2. Effect of excipients on the thermal stability of EEE and WEE VLPs as measured by intrinsic tryptophan fluorescence spectroscopy vs temperature measurements. Delta T_{onset} and delta T_m values of VLPs are shown for in presence of different excipients where delta values represent the difference between EEE/WEE VLPs formulated in 10 mM sodium phosphate, 100 mM NaCl, pH 7.5 with added excipient and EEE/WEE VLPs formulated in only 10 mM sodium phosphate, 100 mM NaCl, pH 7.5. All samples were formulated at 0.1 mg/mL and the data represent mean and range of duplicate replicates.

Excipient	**EEE**				**WEE**			
	ΔTonset (^{o}C)		**ΔTm (^{o}C)**		**ΔTonset (^{o}C)**		**ΔTm (^{o}C)**	
	Mean	Range	Mean	Range	Mean	Range	Mean	Range
20 % Sorbitol	14.4	14.3,14.5	2.9	2.9,2.9	5.0	4.8,5.1	3.1	3.0,3.1
20 % Trehalose	15.7	13.3,18.0	4.1	2.6,5.5	2.5	2.4,2.5	2.5	2.3,2.6
10 % Mannitol	11.5	11.4.11.5	1.1	0.7,1.4	3.8	3.4,4.2	3.0	2.9,3.0
20% Sucrose	12.8	12.2,13.3	2.6	2.6,2.6	2.2	2.2,2.2	0.4	0.4,0.5
0.1 % Pluronic F-68	3.3	-0.2,6.8	0.8	0.2,1.4	2.3	2.1,2.3	1.0	1.0,1.0
0.3 M Glycine	4.7	4.1,5.2	1.0	0.2,1.7	2.4	2.4,2.4	2.1	2.0,2.1
10 % 2-OH propyl γ-CD	11.1	9.0,13.1	3.0	2.9,3.1	-2.9	-2.9,-3.1	-1.3	-1.3,-1.3
10 % 2-OH propylα-CD	10.3	9.7,10.9	3.4	2.6,4.1	-2.3	-2.3,-2.4	-0.1	-0.1,-0.2
10 % 2-OH propylβ-CD	3.7	3.6,3.8	0.8	0.2,1.4	-5.5	-5.1,-5.5	-4.6	-4.3,-4.8
0.075 M Aspartic Acid	-5.5	-4.2,-6.7	0.7	0.2,1.2	1.5	1.3,1.5	0.3	0.2,0.3
0.15 M Malic Acid	-0.5	-0.4,-0.6	2.6	2.6,2.6	0.7	0.5,0.7	0.1	0.0,0.1
15 % Lactose	3.3	3.2,3.3	2.9	2.9,2.9	2.5	2.3,2.5	2.1	2.0,2.1
0.15 M Lactic Acid	3.6	3.3,3.9	0.8	0.2,1.4	2.2	1.9,2.2	0.3	0.3,0.3
7.5 uM Dextran T70	-4.2	-1.7,-6.7	0.2	0.2,0.2	1.0	0.3,1.0	0.2	0.1,0.3

Supplemental Table 4.3. Concentration optimization of lead stabilizing excipients for their stabilizing effect on the overall tertiary structure of EEE and WEE VLPs (0.1 mg/mL) as measured by intrinsic tryptophan fluorescence spectroscopy vs. temperature. Delta T_{onset} and delta T_m values of VLPs are shown for in presence of different excipients where delta values represent the difference between EEE/WEE VLPs formulated in 10 mM sodium phosphate, 100 mM NaCl, pH 7.5 with added excipient and EEE/WEE VLPs formulated in only 10 mM sodium phosphate, 100 mM NaCl, pH 7.5. Data represent mean and range of duplicate replicates.

Excipient	**Concentration**	**EEE**				**WEE**			
		ΔTonset (^{o}C)		**ΔTm (^{o}C)**		**ΔTonset (^{o}C)**		**ΔTm (^{o}C)**	
		Mean	Range	Mean	Range	Mean	Range	Mean	Range
	2.5 % w/v	1.8	1.5,2.0	0.1	0.0,0.2	0.5	0.4,0.6	0.6	0.4,0.8
	5 % w/v	1.5	1.3,1.6	-0.3	-0.2,-0.4	2.7	2.6,2.8	0.2	0.0,0.4
	7.5 % w/v	3.7	3.4,4.0	0.1	-0.1,0.3	2.8	2.6,3.0	1.5	0.4,2.5
Sorbitol	10 % w/v	3.3	3.2,3.3	-0.2	-0.1,-0.3	2.7	2.6,2.7	0.1	0.0,0.2
	2.5 % w/v	1.8	1.5,2.0	0.2	0.0,0.4	1.3	1.1,1.5	0.1	0.0,0.2
	5 % w/v	1.4	1.2,1.5	0.0	0.0,0.0	1.3	1.2,1.4	0.2	0.2,0.2
	7.5 % w/v	2.5	2.4,2.6	0.0	-0.2,0.3	2.0	1.9,2.1	1.3	1.2,1.3
Trehalose	10 % w/v	1.1	0.3,1.9	-0.2	-0.1,-0.3	2.2	2.0,2.3	0.1	0.0,0.2
	2.5 % w/v	0.4	0.2,0.6	-1.2	-0.4,-2.0	0.3	0.2,0.4	0.2	0.2,0.2
	5 % w/v	1.2	0.3,2.0	0.0	-0.1,0.1	0.9	0.8,1.0	1.3	0.4,2.1
	7.5 % w/v	2.0	1.8,2.1	-0.6	-0.4,-0.8	0.9	0.9,1.0	0.1	0.0,0.2
Sucrose	10 % w/v	2.5	2.0,3.0	-0.1	0.0,-0.3	2.4	2.3,2.5	1.3	1.0,1.5
	0.01 % w/v	1.9	1.8,2.0	0.1	-0.1,0.4	0.1	0.0,0.2	0.0	0.0,0.0
	0.05 % w/v	0.4	0.0,0.9	-0.9	-0.3,-1.5	1.6	1.4,1.7	0.1	0.0,0.2
Pluronic F-68	0.1 % w/v	2.0	1.7,2.3	-0.1	-0.2,0.1	1.9	1.7,2.1	0.0	0.0,0.0

Supplemental Table 4.4. Effect of lead excipient combinations on the overall tertiary structure stability of EEE and WEE VLPs (0.1 mg/mL) as measured by intrinsic tryptophan fluorescence vs. temperature. Delta T_{onset} and delta T_m values of VLPs are shown for in presence of different excipients where delta values represent the difference between EEE/WEE VLPs formulated in 10 mM sodium phosphate, 100 mM NaCl, pH 7.5 with added excipient and EEE/WEE VLPs formulated in only 10 mM sodium phosphate, 100 mM NaCl, pH 7.5. Data represent mean and range of duplicate replicates.

Excipient Combination (% w/v)	**EEE**				**WEE**			
	ΔTonset (°C)		**ΔTm (°C)**		**ΔTonset (°C)**		**ΔTm (°C)**	
	Mean	Range	Mean	Range	Mean	Range	Mean	Range
7.5% Sorbitol	3.2	3.1,3.3	0.5	0.4,0.6	3.9	3.7,4.1	1.5	1.3,1.7
7.5% Sorbitol 0.05% Pluronic -F68	3.2	3.1,3.3	0.4	0.4,0.5	3.9	3.8,4.0	1.4	1.1,1.7
10% Sucrose	1.3	1.2,1.4	0.1	0.0,0.2	4.0	3.6,4.4	2.0	1.3,2.7
10% Sucrose 0.05% Pluronic -F68	1.6	1.4,1.8	0.1	0.0,0.1	3.9	3.8,3.9	2.0	1.5,2.5
5% Sucrose 5% Sorbitol	3.1	3.1,3.1	0.4	0.2,0.5	4.5	4.2,4.8	2.3	1.9,2.7
5% Sucrose 5% Sorbitol 0.05% Pluronic -F68	3.2	3.1,3.2	1.4	1.3,1.4	3.9	3.6,4.2	1.2	0.9,1.5
7.5% Sucrose 5% Sorbitol 0.05% Pluronic -F68	3.1	2.9,3.3	1.2	1.0,1.3	3.9	3.4,4.4	2.5	1.7,3.3
2.5% Sucrose 7.5% Sorbitol 0.05% Pluronic -F68	3.3	3.2,3.3	1.6	1.4,1.7	3.4	3.0,3.8	1.2	0.9,1.5
5% Sucrose 7.5% Sorbitol 0.05% Pluronic -F68	3.3	3.3,3.3	1.1	1.0,1.1	3.7	3.6,3.7	3.0	2.7,3.3
10% Trehalose	1.3	1.1,1.5	0.5	0.3,0.7	2.5	2.4,2.5	0.1	0.1,0.1
10% Trehalose 0.05% Pluronic -F68	1.8	1.8,1.8	0.4	0.2,0.5	4.1	4.0,4.2	0.1	0.1,0.1
5% Trehalose 5% Sorbitol	2.8	2.7,2.9	1.1	0.8,1.4	4.0	3.8,4.2	1.3	1.2,1.3
5% Trehalose 5% Sorbitol 0.05% Pluronic -F68	2.5	2.4,2.5	0.9	0.7,1.0	3.9	3.6,4.2	1.8	1.1,2.5
7.5% Trehalose 5% Sorbitol 0.05% Pluronic -F68	3.0	2.9,3.1	1.3	1.1,1.4	3.0	2.6,3.4	1.9	1.1,2.7
2.5% Trehalose 7.5% Sorbitol 0.05% Pluronic -F68	2.6	2.5,2.7	0.9	0.8,1.0	4.0	3.8,4.2	1.9	1.2,2.5
5% Trehalose 7.5% Sorbitol 0.05% Pluronic -F68	3.2	3.1,3.3	1.5	1.4,1.5	3.2	3.0,3.4	0.7	0.3,1.1

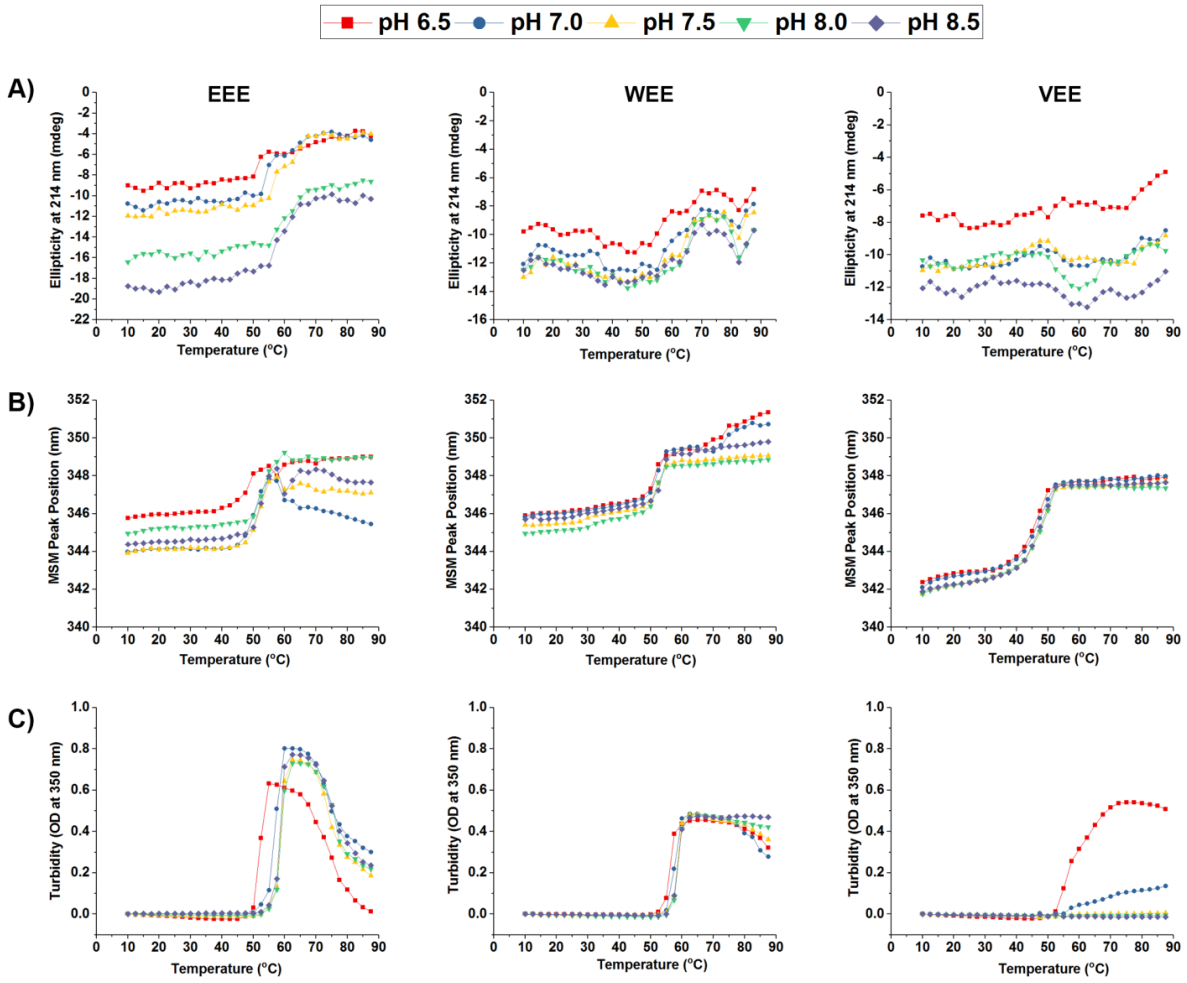

Supplemental Figure 4.1. Biophysical characterization of three equine encephalitis virus-like particles (0.15 mg/mL) as a function of temperature across the pH range 6.5-8.5 in 20 mM sodium phosphate, 150 mM NaCl buffer. Biophysical measurements include (A) circular dichroism at 214 nm, (B) intrinsic fluorescence MSM peak position, (C) turbidity (OD_{350} nm). Data represent the mean of duplicate experiments.

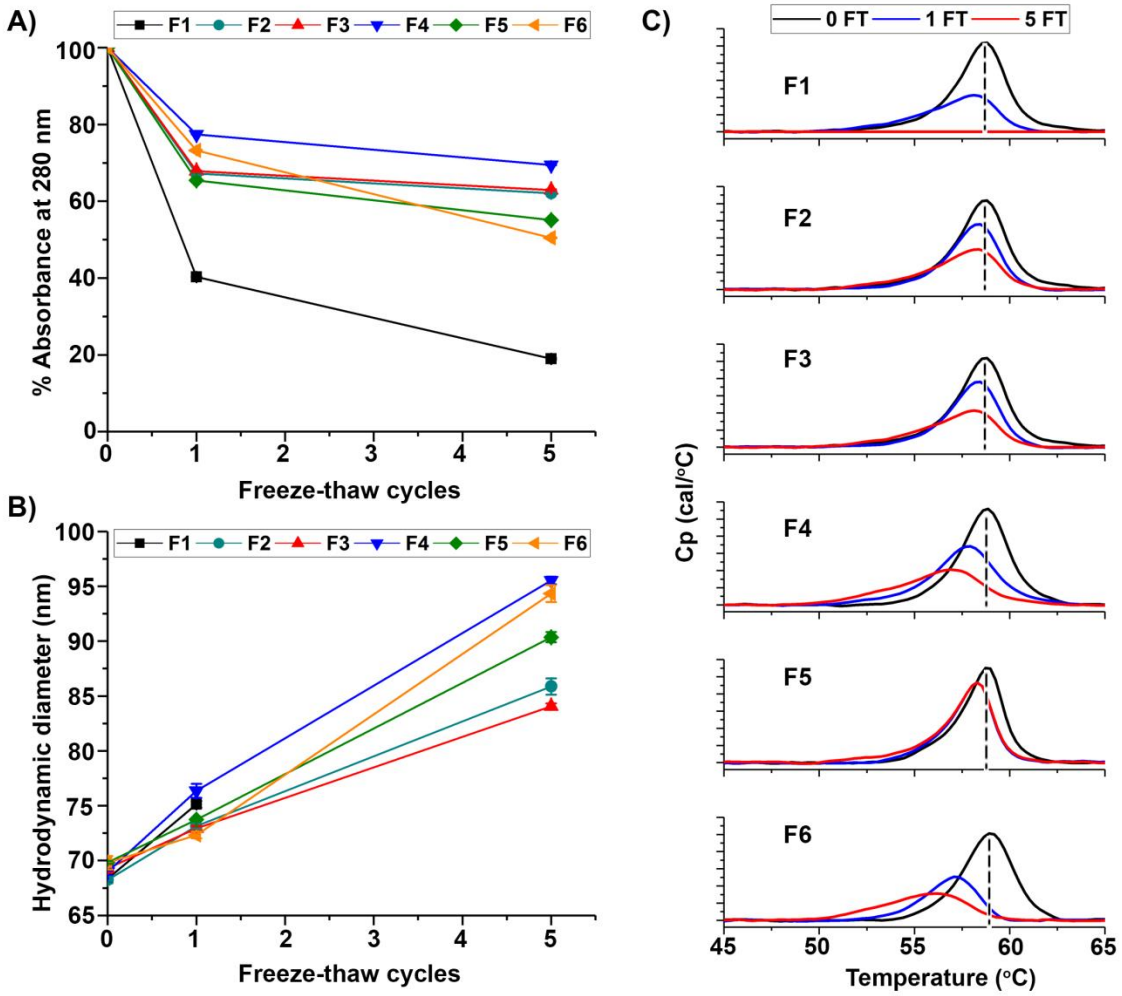

Supplemental Figure 4.2. Effect of different candidate formulations on freeze-thaw stability (0, 1 and 5 freeze-thaw cycles) of EEE VLPs at -20°C. (A) % Absorbance at 280 nm showing protein loss with increasing freeze thaw cycles, (B) hydrodynamic diameter as a function of freeze-thaw cycles as measured by DLS, and (C) conformational stability of EEE VLPs as measured by DSC. The EEE protein concentration was 0.15 mg/mL in all six formulations namely: (F1) 10 mM sodium phosphate, 50 mM NaCl, pH 7.5; (F2) F1 buffer + 5 % sorbitol; (F3) F1 buffer + 7.5 % sorbitol; (F4) F1 buffer + 7.5 % sorbitol, 0.05 % pluronic F-68; (F5) F1 buffer + 5% sorbitol, 5% sucrose and (F6) F1 buffer + 5% sorbitol, 5% sucrose, 0.05 % Pluronic F-68. Data represent average and standard deviation from triplicate measurements.*EEE formulated in F1 aggregated after 5 FT cycles and hence there is no DLS data point for 5 FT cycles. The dotted line represents the average Tm at 0 FT for better visualization of the deviation in Tm after five FT cycles.

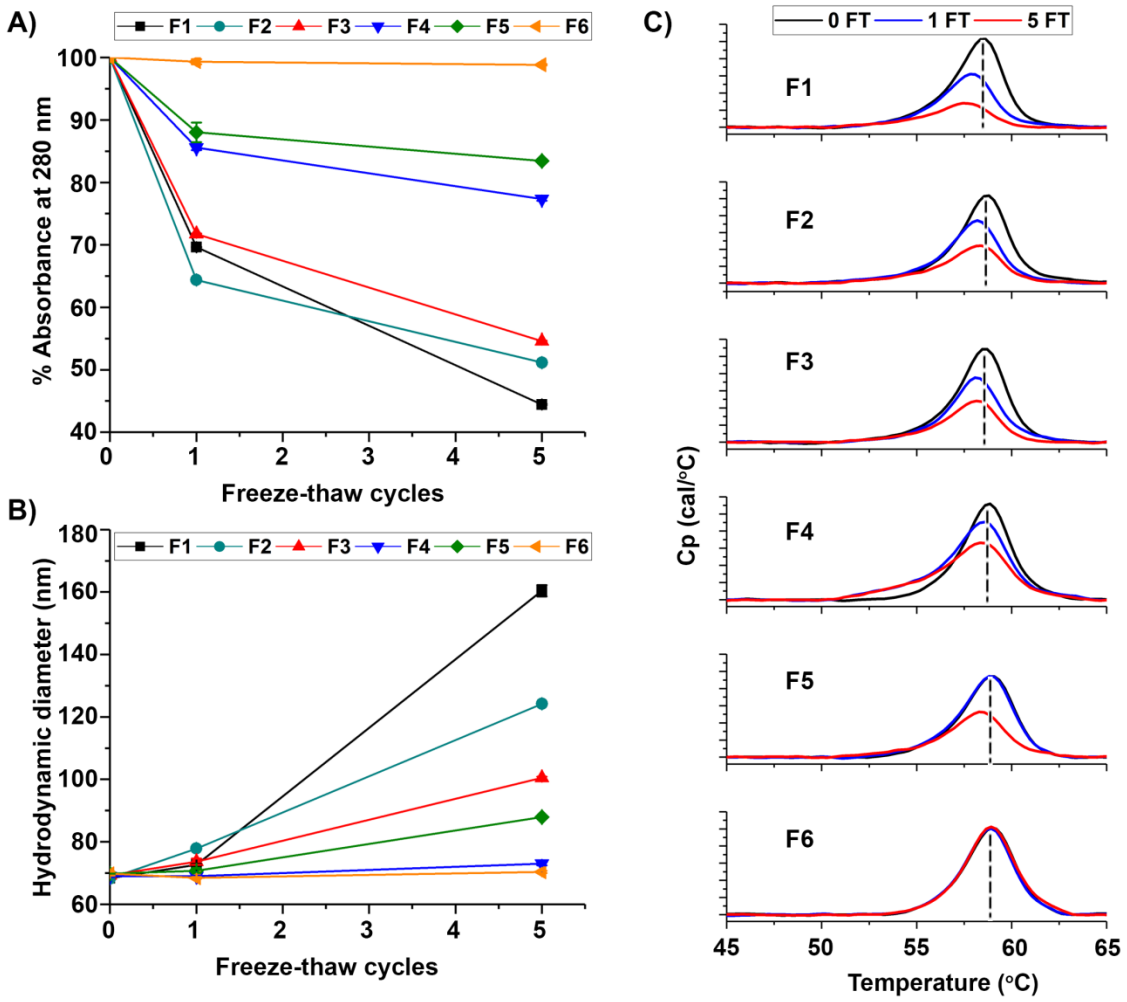

Supplemental Figure 4.3. Effect of different candidate formulations on freeze-thaw stability (0, 1 and 5 freeze-thaw cycles) of EEE VLPs at -80°C. (A) % Absorbance at 280 nm showing protein loss with increasing freeze thaw cycles, (B) hydrodynamic diameter as a function of freeze-thaw cycles as measured by DLS, and (C) conformational stability of EEE VLPs as measured by DSC. The EEE protein concentration was 0.15 mg/mL in all six formulations: (F1) 10 mM sodium phosphate, 50 mM NaCl, pH 7.5; (F2) F1 buffer + 5 % sorbitol; (F3) F1 buffer + 7.5 % sorbitol; (F4) F1 buffer + 7.5 % sorbitol, 0.05 % pluronic F-68; (F5) F1 buffer + 5% sorbitol, 5% sucrose and (F6) F1 buffer + 5% sorbitol, 5% sucrose, 0.05 % Pluronic F-68. Data represent average and standard deviation from triplicate measurements. The dotted line represents the average Tm value at 0 FT for better visualization of the deviation in Tm after five FT cycles.

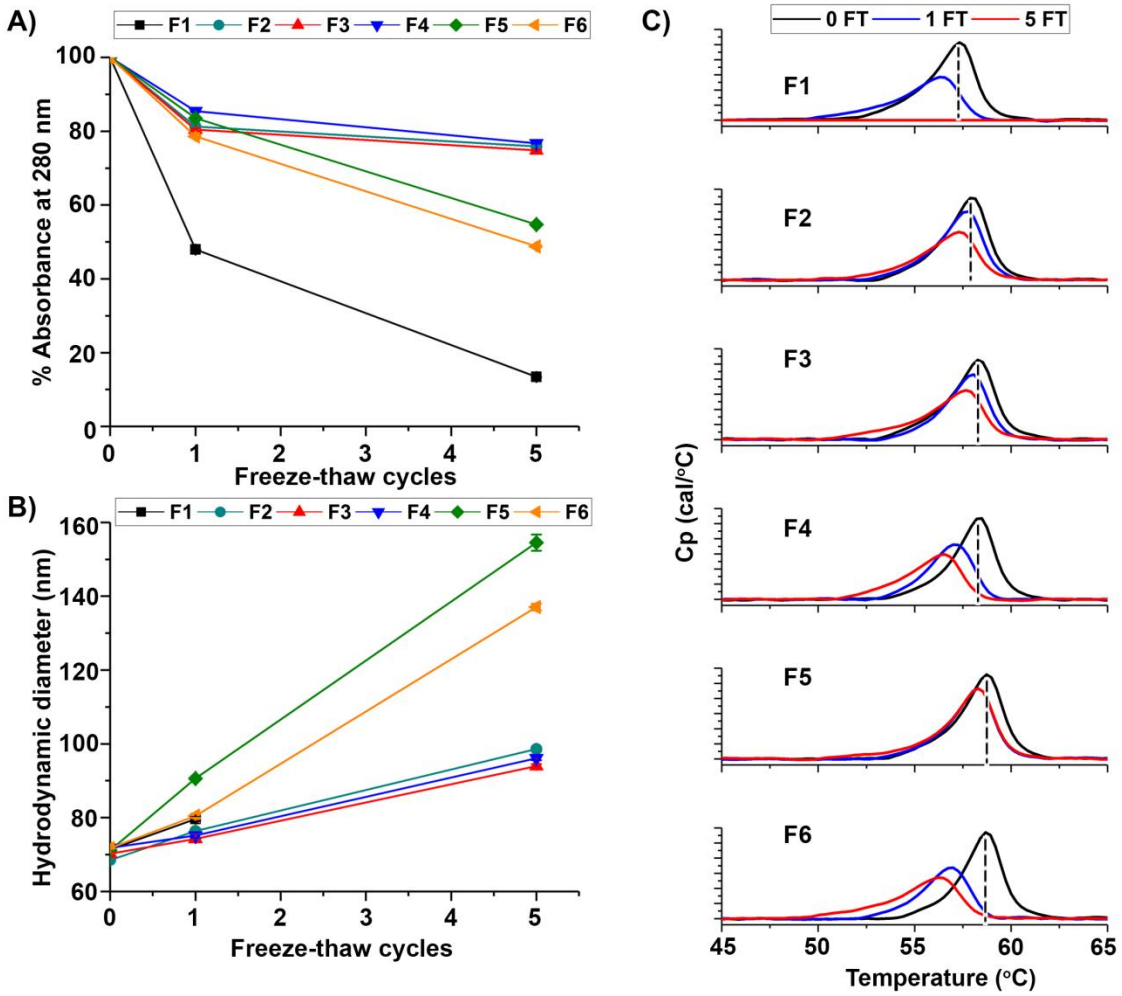

Supplemental Figure 4.4. Effect of different candidate formulations on freeze-thaw stability (0, 1 and 5 freeze-thaw cycles) of WEE VLPs at -20°C. (A) % Absorbance at 280 nm showing protein loss with increasing freeze thaw cycles, (B) hydrodynamic diameter as a function of freeze-thaw cycles as measured by DLS, and (C) conformational stability of WEE VLPs as measured by DSC. The WEE protein concentration was 0.15 mg/mL in all six formulations: (F1) 10 mM sodium phosphate, 50 mM NaCl, pH 7.5; (F2) F1 buffer + 5 % sorbitol; (F3) F1 buffer + 7.5 % sorbitol; (F4) F1 buffer + 7.5 % sorbitol, 0.05 % pluronic F-68; (F5) F1 buffer + 5% sorbitol, 5% sucrose and (F6) F1 buffer + 5% sorbitol, 5% sucrose, 0.05 % Pluronic F-68. Data represent average and standard deviation from triplicate measurements. *WEEV formulated in F1 aggregated after 5 FT cycles and hence there is no DLS data point for 5 FT cycles. The dotted line represents the average Tm value at 0 FT for better visualization of the deviation in Tm after five FT cycles.

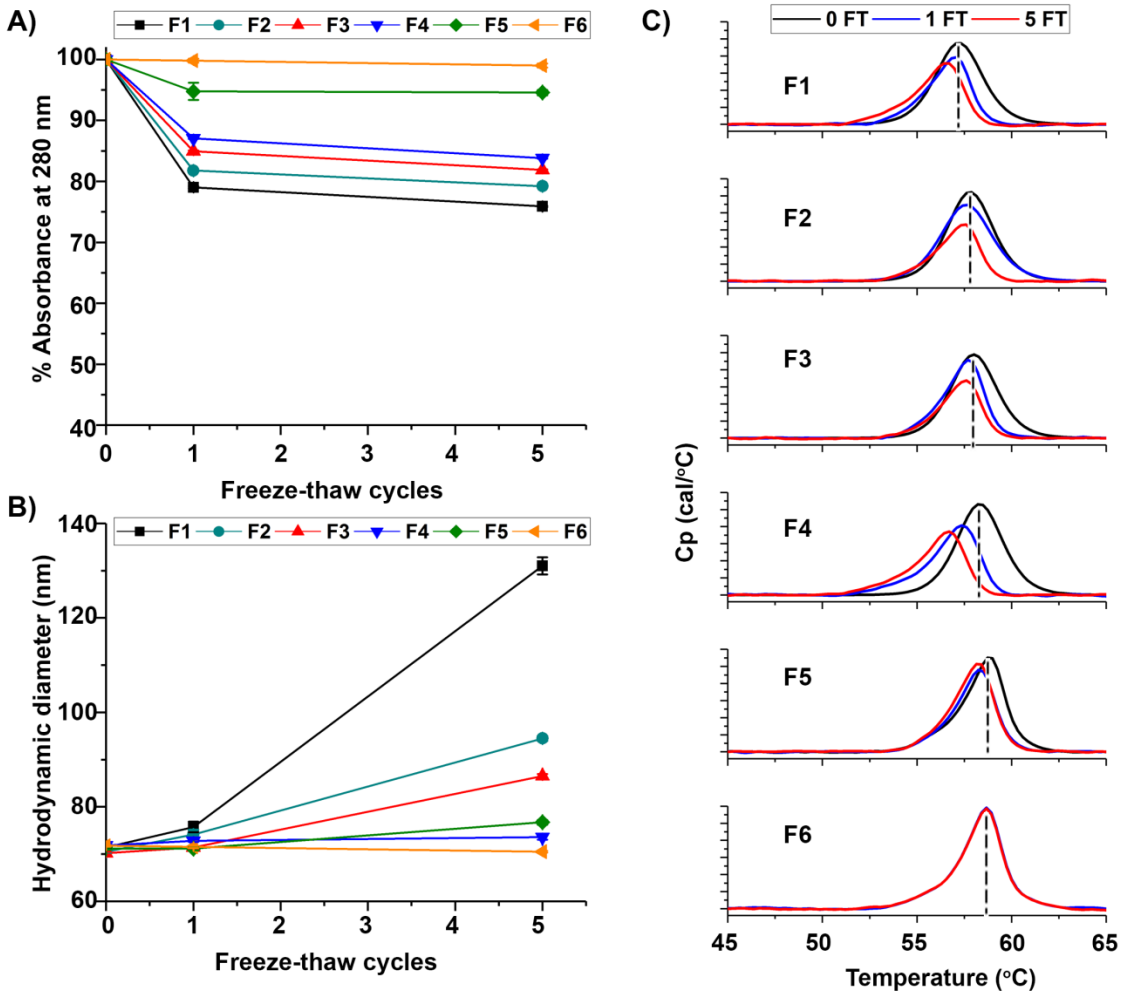

Supplemental Figure 4.5. Effect of different candidate formulations on freeze-thaw stability (0, 1 and 5 freeze-thaw cycles) of WEE VLPs at -80°C. (A) % Absorbance at 280 nm showing protein loss with increasing freeze thaw cycles, (B) hydrodynamic diameter as a function of freeze-thaw cycles as measured by DLS, and (C) conformational stability of WEE VLPs as measured by DSC. The WEE protein concentration was 0.15 mg/mL in all six formulations: (F1) 10 mM sodium phosphate, 50 mM NaCl, pH 7.5; (F2) F1 buffer + 5 % sorbitol; (F3) F1 buffer + 7.5 % sorbitol; (F4) F1 buffer + 7.5 % sorbitol, 0.05 % pluronic F-68; (F5) F1 buffer + 5% sorbitol, 5% sucrose and (F6) F1 buffer + 5% sorbitol, 5% sucrose, 0.05 % Pluronic F-68. Data represent average and standard deviation from triplicate measurements. The dotted line represents the average Tm at 0 FT for better visualization of the deviation in Tm after five FT cycles.

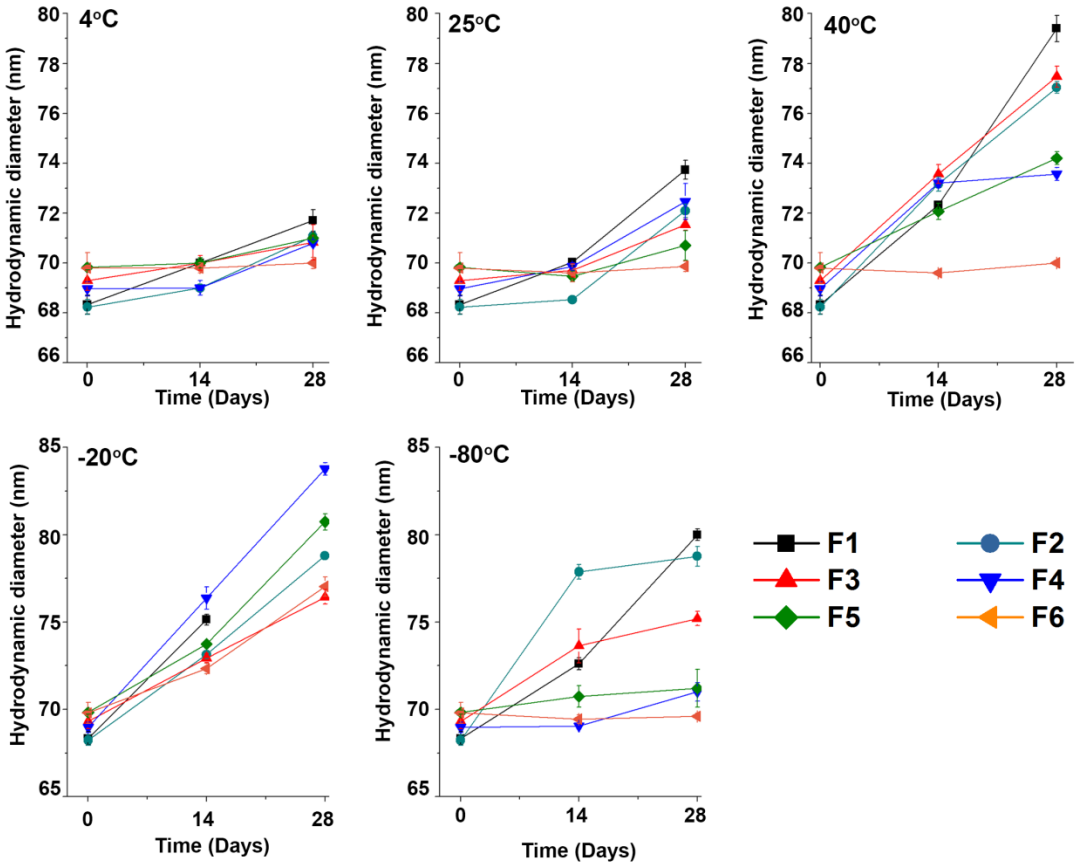

Supplemental Figure 4.6. Accelerated stability studies of size of EEE VLPs in different candidate formulations at different temperatures (4, 25, 40, -20 and -80°C) for 28 days as measured by DLS. The EEE protein concentration was 0.15 mg/mL in the six formulations: (F1) 10 mM sodium phosphate, 50 mM NaCl, pH 7.5; (F2) F1 buffer + 5 % sorbitol; (F3) F1 buffer + 7.5 % sorbitol; (F4) F1 buffer + 7.5 % sorbitol, 0.05 % pluronic F-68; (F5) F1 buffer + 5% sorbitol, 5% sucrose and (F6) F1 buffer + 5% sorbitol, 5% sucrose, 0.05 % Pluronic F-68. Data represents mean and standard deviation from triplicate measurements.

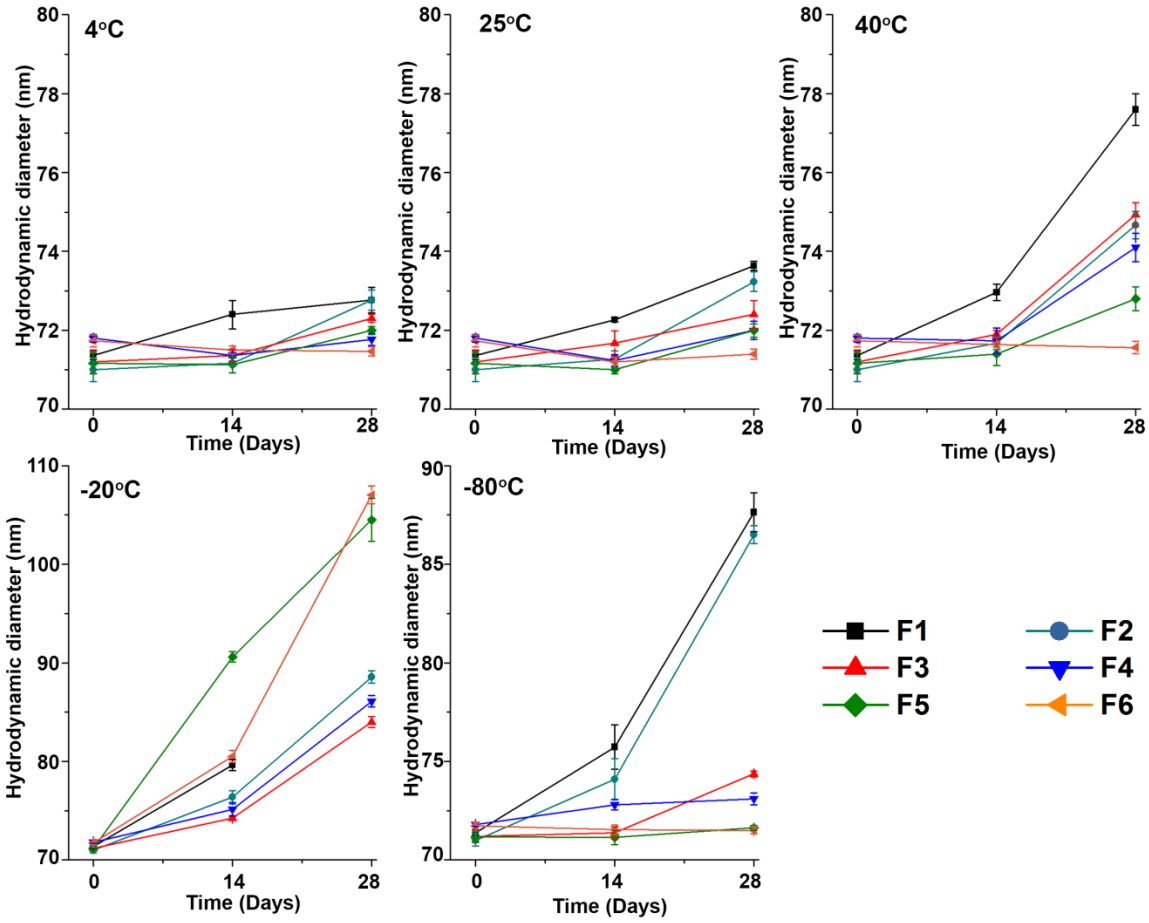

Supplemental Figure 4.7. Accelerated stability studies of size of WEE VLPs in different candidate formulations at different temperatures (4, 25, 40, -20 and -80°C) for 28 days as measured by DLS. The WEE protein concentration was 0.15 mg/mL in the six formulations: (F1) 10 mM sodium phosphate, 50 mM NaCl, pH 7.5; (F2) F1 buffer + 5 % sorbitol; (F3) F1 buffer + 7.5 % sorbitol; (F4) F1 buffer + 7.5 % sorbitol, 0.05 % pluronic F-68; (F5) F1 buffer + 5% sorbitol, 5% sucrose and (F6) F1 buffer + 5% sorbitol, 5% sucrose, 0.05 % Pluronic F-68. Data represent mean and standard deviation from triplicate measurements.

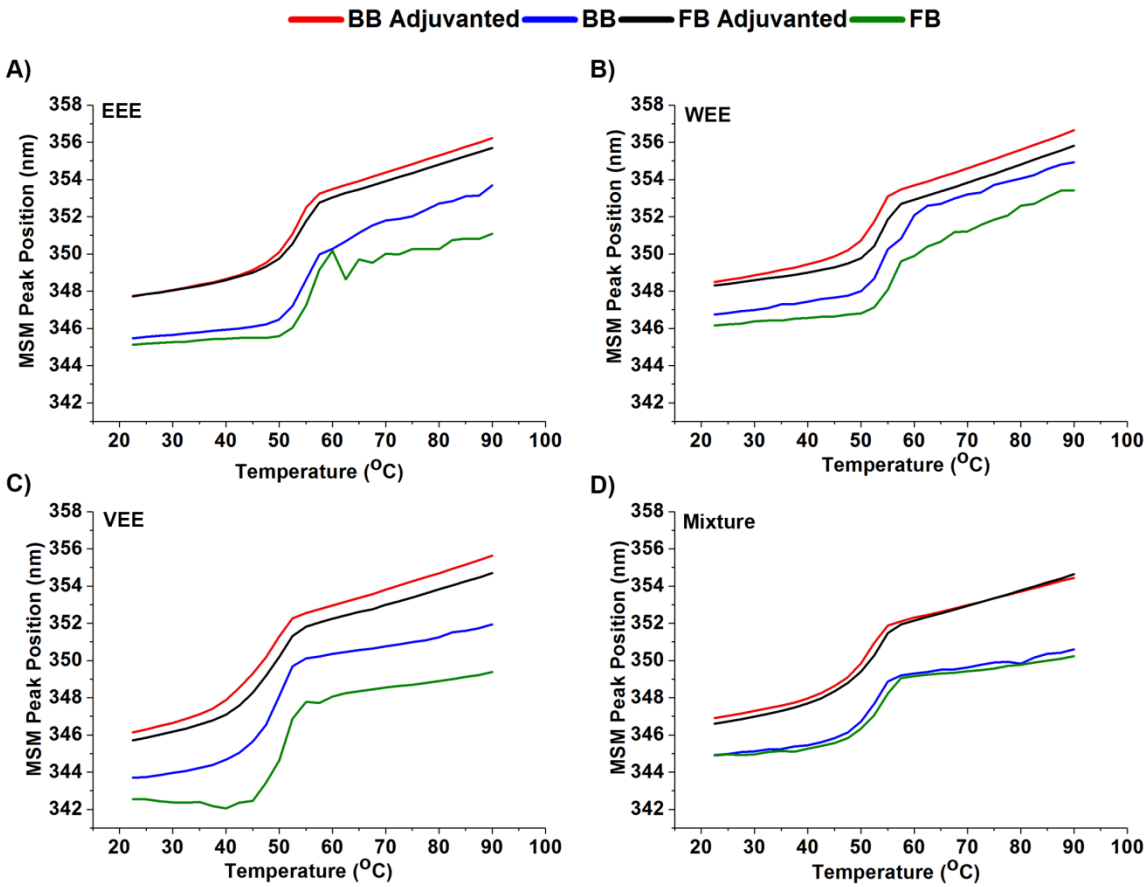

Supplemental Figure 4.8. Conformational stability of three equine encephalitis virus-like particles VLPs (and a trivalent mixture) with and without adsorption to Alhydrogel® as measured by intrinsic Trp fluorescence spectroscopy vs. temperature. Peak position (mean spectral mass method) versus temperature graphs of the three VLPs and adjuvanted mixtures, in base buffer (with and without adjuvant) and formulation buffer (with and without adjuvant). Base buffer (BB) was 10 mM NaPO4, 50 mM NaCl, pH 7.8 and the formulation buffer (FB) was 10 mM NaPO4, 50 mM NaCl, 5% sucrose, 5% sorbitol, 0.05% Pluronic F-68, pH 7.8. The graphs show an average for three runs and error bars have been removed for clarity.

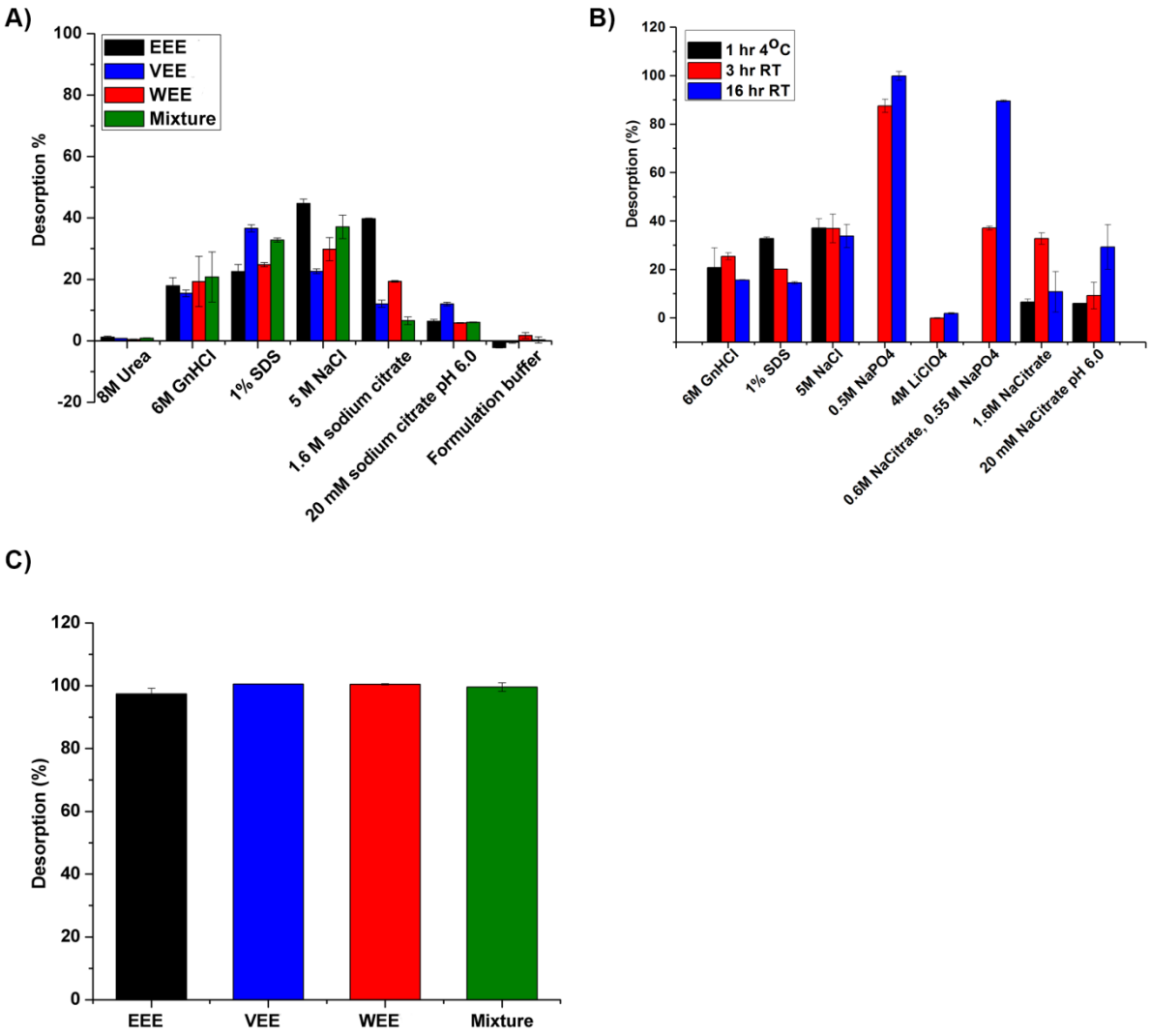

Supplemental Figure 4.9. Desorption studies of three equine encephalitis virus-like particles (EEE, VEE and WEE) and their mixture from Alhydrogel® adjuvant. (A) Desorption of EEV VLPs from Alhydrogel® in various desorption media. All the desorption media shown above, except 20 mM sodium citrate (pH 6.0), contained 20 mM sodium phosphate and had a pH value of 7.8. The formulation buffer (10 mM $NaPO_4$, 50 mM NaCl, 5% sucrose, 5% sorbitol, 0.05% Pluronic F-68, pH 7.8) was included here as a negative control Desorption was measured after incubating VLP-Alhydrogel® mixtures with desorption media for 1 hr at 4°C, (B) Desorption of EEV VLPs as a function of both time and temperature with various desorption media for 1 hr at 4°C, or for either 3 hr and 16 hr at room temperature (RT), and (C) Desorption of individual EEV VLPs and a "mixture" of the three VLPs from Alhydrogel® in the presence of 500 mM sodium phosphate (pH 7.8) after incubating the samples with sodium phosphate for 3 hr at room temperature. Data represent mean and standard deviation from triplicate measurements.

4.5 References

1. Zacks MA, Paessler S 2010. Encephalitic alphaviruses. Veterinary Microbiology 140(3):281-286.

2. Long MT 2014. West Nile Virus and Equine Encephalitis Viruses. Veterinary Clinics of North America: Equine Practice 30(3):523-542.

3. Weaver SC, Powers AM. 2014. Alphaviruses: equine encephalitis and others. Viral Infections of Humans, ed.: Springer. p 123-145.

4. Acha P, Szyfres B. 2003. Zoonoses and communicable diseases common to man and animals. Volume 2.Chlamydioses, rickettsioses, and viroses. 3rd ed.Washington DC: PAHO; 2003. Scientific and Technical Publication No. 580. Eastern equine encephalitis; p. 110-115. ed.

5. Acha P, Szyfres B. 2003. Zoonoses and communicable diseases common to man and animals. Volume 2.Chlamydioses, rickettsioses, and viroses. 3rd ed.Washington DC: PAHO; 2003. Scientific and Technical Publication No. 580. Venezuelan equine encephalitis; p. 333-345. ed.

6. Acha P, Szyfres B. 2003. Zoonoses and communicable diseases common to man and animals. Volume 2.Chlamydioses, rickettsioses, and viroses. 3rd ed.Washington DC: PAHO; 2003. Scientific and Technical Publication No. 580. Western equine encephalitis; p. 365-372. ed.

7. Giltner L, Shahan M 1933. The 1933 outbreak of infectious equine encephalomyelitis in the eastern states. North Am Vet 14:25.

8. Broeck GT, Merrill MH 1933. A serological difference between eastern and western equine encephalomyelitis virus. Proceedings of the Society for Experimental Biology and Medicine 31(2):217-220.

9. Prevention CfDCa 2016. Eastern Equine Encephalitis https://www.cdc.gov/easternequineencephalitis/ Accessed July 22, 2014.

10. Wolfe DN, Heppner DG, Gardner SN, Jaing C, Dupuy LC, Schmaljohn CS, Carlton K 2014. Current strategic thinking for the development of a trivalent alphavirus vaccine for human use. The American journal of tropical medicine and hygiene 91(3):442-450.

11. Sherman MB, Weaver SC 2010. Structure of the Recombinant Alphavirus Western Equine Encephalitis Virus Revealed by Cryoelectron Microscopy. Journal of Virology 84(19):9775-9782.

12. Paessler S, Weaver SC 2009. Vaccines for Venezuelan equine encephalitis. Vaccine 27S4:D80-D85.

13. Taylor K, Kolokoltsova O, Ronca SE, Estes M, Paessler S 2017. Live, Attenuated Venezuelan Equine Encephalitis Virus Vaccine (TC83) Causes Persistent Brain Infection in Mice with Non-functional αβ T-Cells. Frontiers in Microbiology 8:81.

14. Chang L-J, Dowd KA, Mendoza FH, Saunders JG, Sitar S, Plummer SH, Yamshchikov G, Sarwar UN, Hu Z, Enama ME, Bailer RT, Koup RA, Schwartz RM, Akahata W, Nabel GJ, Mascola JR, Pierson TC, Graham BS, Ledgerwood JE 2014. Safety and tolerability of chikungunya virus-like particle vaccine in healthy adults: a phase 1 dose-escalation trial. The Lancet 384(9959):2046-2052.

15. Kim JH, Iyer V, Joshi SB, Volkin DB, Middaugh CR 2012. Improved data visualization techniques for analyzing macromolecule structural changes. Protein Science 21(10):1540-1553.

16. Maddux NR, Joshi SB, Volkin DB, Ralston JP, Middaugh CR 2011. Multidimensional methods for the formulation of biopharmaceuticals and vaccines. Journal of Pharmaceutical Sciences 100(10):4171-4197.

17. Jones LS, Peek LJ, Power J, Markham A, Yazzie B, Middaugh CR 2005. Effects of Adsorption to Aluminum Salt Adjuvants on the Structure and Stability of Model Protein Antigens. Journal of Biological Chemistry 280(14):13406-13414.

18. Estey T, Vessely C, Randolph TW, Henderson I, Braun LJ, Nayar R, Carpenter JF Evaluation of chemical degradation of a trivalent recombinant protein vaccine against botulinum neurotoxin by LysC peptide mapping and MALDI-TOF mass spectrometry. Journal of Pharmaceutical Sciences 98(9):2994-3012.

19. Weaver SC, Ferro C, Barrera R, Boshell J, Navarro J-C 2003. VENEZUELAN EQUINE ENCEPHALITIS. Annual Review of Entomology 49(1):141-174.

20. 2009. APPENDIX 2. Transfusion 49:45S-233S.

21. Schmid F-X. 2001. Biological Macromolecules: UV-visible Spectrophotometry. eLS, ed.: John Wiley & Sons, Ltd.

22. Porterfield JZ, Zlotnick A 2010. A Simple and General Method for Determining the Protein and Nucleic Acid Content of Viruses by UV Absorbance. Virology 407(2):281-288.

23. Sambrook J, Russell DW. 2001. Molecular Cloning: A Laboratory Manual. ed.: Cold Spring Harbor Laboratory Press.

24. Warburg O 1941. Isolierung und kristallisation des garungsferments enolase. Biochem z 310:384-421.

25. Kim JH, Iyer V, Joshi SB, Volkin DB, Middaugh CR 2012. Improved data visualization techniques for analyzing macromolecule structural changes. Protein Sci 21(10):1540-1553.

26. Maddux NR, Joshi SB, Volkin DB, Ralston JP, Middaugh CR 2011. Multidimensional methods for the formulation of biopharmaceuticals and vaccines. J Pharm Sci 100(10):4171-4197.

27. Lua LHL, Connors NK, Sainsbury F, Chuan YP, Wibowo N, Middelberg APJ 2014. Bioengineering virus-like particles as vaccines. Biotechnology and bioengineering 111(3):425-440.

28. Roldão A, Mellado MCM, Castilho LR, Carrondo MJT, Alves PM 2010. Virus-like particles in vaccine development. Expert review of vaccines 9(10):1149-1176.

29. Zeltins A 2013. Construction and Characterization of Virus-Like Particles: A Review. Molecular Biotechnology 53(1):92-107.

30. Chirino AJ, Mire-Sluis A 2004. Characterizing biological products and assessing comparability following manufacturing changes. Nature Biotechnology 22:1383.

31. Federici M, Lubiniecki A, Manikwar P, Volkin DB 2013. Analytical lessons learned from selected therapeutic protein drug comparability studies. Biologicals 41(3):131-147.

32. Lubiniecki A, Volkin DB, Federici M, Bond MD, Nedved ML, Hendricks L, Mehndiratta P, Bruner M, Burman S, DalMonte P, Kline J, Ni A, Panek ME, Pikounis B, Powers G, Vafa O, Siegel R 2011. Comparability assessments of process and product changes made during development of two different monoclonal antibodies. Biologicals 39(1):9-22.

33. Zhao Q, Potter CS, Carragher B, Lander G, Sworen J, Towne V, Abraham D, Duncan P, Washabaugh MW, Sitrin RD 2014. Characterization of virus-like particles in GARDASIL® by cryo transmission electron microscopy. Human Vaccines & Immunotherapeutics 10(3):734-739.

34. Wang JW, Roden RBS 2013. Virus-like particles for the prevention of human papillomavirus-associated malignancies. Expert review of vaccines 12(2):10.1586/erv.1512.1151.

35. Baker TS, Newcomb WW, Olson NH, Cowsert LM, Olson C, Brown JC 1991. Structures of bovine and human papillomaviruses. Analysis by cryoelectron microscopy and three-dimensional image reconstruction. Biophysical Journal 60(6):1445-1456.

36. Diminsky D, Schirmbeck R, Reimann J, Barenholz Y 1997. Comparison between hepatitis B surface antigen (HBsAg) particles derived from mammalian cells (CHO) and yeast cells (Hansenula polymorpha): composition, structure and immunogenicity. Vaccine 15(6):637-647.

37. Gilbert RJC, Beales L, Blond D, Simon MN, Lin BY, Chisari FV, Stuart DI, Rowlands DJ 2005. Hepatitis B small surface antigen particles are octahedral. Proceedings of the National Academy of Sciences of the United States of America 102(41):14783-14788.

38. Toprani VM, Hickey JM, Sahni N, Toth RT, Robertson GA, Middaugh CR, Joshi SB, Volkin DB 2017. Structural characterization and physicochemical stability profile of a double mutant heat labile toxin (dmLT) protein based adjuvant. Journal of Pharmaceutical Sciences.

39. Qi W, Zeng Y, Orgel S, Francon A, Kim JH, Randolph TW, Carpenter JF, Russell Middaugh C 2014. Preformulation Study of Highly Purified Inactivated Polio Vaccine, Serotype 3. Journal of Pharmaceutical Sciences 103(1):140-151.

40. Jain NK, Sahni N, Kumru OS, Joshi SB, Volkin DB, Russell Middaugh C 2015. Formulation and stabilization of recombinant protein based virus-like particle vaccines. Advanced Drug Delivery Reviews 93:42-55.

41. Alsenaidy M, Jain NK, Kim J, Middaugh C, Volkin D 2014. Protein comparability assessments and potential applicability of high throughput biophysical methods and data visualization tools to compare physical stability profiles. Frontiers in Pharmacology 5(39).

42. More AS, Toprani VM, Okbazghi SZ, Kim JH, Joshi SB, Middaugh CR, Tolbert TJ, Volkin DB 2016. Correlating the Impact of Well-Defined Oligosaccharide Structures on Physical Stability Profiles of IgG1-Fc Glycoforms. Journal of Pharmaceutical Sciences 105(2):588-601.

43. Evans RK, Nawrocki DK, Isopi LA, Williams DM, Casimiro DR, Chin S, Chen M, Zhu D-M, Shiver JW, Volkin DB 2004. Development of stable liquid formulations for adenovirus-based vaccines. Journal of Pharmaceutical Sciences 93(10):2458-2475.

44. Peek LJ, Brey RN, Middaugh CR 2007. A Rapid, Three-Step Process for the Preformulation of aRecombinant Ricin Toxin A-Chain Vaccine. Journal of Pharmaceutical Sciences 96(1):44-60.

45. Pastorino B, Baronti C, Gould EA, Charrel RN, de Lamballerie X 2015. Effect of Chemical Stabilizers on the Thermostability and Infectivity of a Representative Panel of Freeze Dried Viruses. PloS one 10(4):e0118963.

46. Adebayo AA, Sim-Brandenburg JW, Emmel H, Olaleye DO, Niedrig M 1998. Stability of 17D Yellow Fever Virus Vaccine Using Different Stabilizers. Biologicals 26(4):309-316.

47. Wiggan ON, Livengood JA, Silengo SJ, Kinney RM, Osorio JE, Huang CYH, Stinchcomb DT 2011. Novel formulations enhance the thermal stability of live-attenuated flavivirus vaccines. Vaccine 29(43):7456-7462.

48. Ohtake S, Martin RA, Saxena A, Lechuga-Ballesteros D, Santiago AE, Barry EM, Truong-Le VU 2011. Formulation and Stabilization of Francisella tularensis Live Vaccine Strain. Journal of Pharmaceutical Sciences 100(8):3076-3087.

49. Bhatnagar BS, Bogner RH, Pikal MJ 2007. Protein Stability During Freezing: Separation of Stresses and Mechanisms of Protein Stabilization. Pharmaceutical Development and Technology 12(5):505-523.

50. Kumru OS, Joshi SB, Smith DE, Middaugh CR, Prusik T, Volkin DB 2014. Vaccine instability in the cold chain: Mechanisms, analysis and formulation strategies. Biologicals 42(5):237-259.

51. Diminsky D Physical, chemical and immunological stability of CHO-derived hepatitis B surface antigen (HBsAg) particles. Vaccine 18(1-2):3-17.

52. Kerwin BA, Heller MC, Levin SH, Randolph TW 1998. Effects of tween 80 and sucrose on acute short-term stability and long-term storage at −20 °C of a recombinant hemoglobin. Journal of Pharmaceutical Sciences 87(9):1062-1068.

53. Piedmonte DM, Summers C, McAuley A, Karamujic L, Ratnaswamy G 2007. Sorbitol Crystallization Can Lead to Protein Aggregation in Frozen Protein Formulations. Pharmaceutical Research 24(1):136-146.

54. Singh SK, Kolhe P, Mehta AP, Chico SC, Lary AL, Huang M 2011. Frozen State Storage Instability of a Monoclonal Antibody: Aggregation as a Consequence of Trehalose Crystallization and Protein Unfolding. Pharmaceutical Research 28(4):873-885.

55. Miller MA, Rodrigues MA, Glass MA, Singh SK, Johnston KP, Maynard JA 2013. Frozen-State Storage Stability of a Monoclonal Antibody: Aggregation is Impacted by Freezing Rate and Solute Distribution. Journal of Pharmaceutical Sciences 102(4):1194-1208.

56. Cavatur RK, Cavatur R 2002. Crystallization Behavior of Mannitol in Frozen Aqueous Solutions. Pharmaceutical research 19(6):894-900.

57. Wen J, Arthur K, Chemmalil L, Muzammil S, Gabrielson J, Jiang Y 2012. Applications of Differential Scanning Calorimetry for Thermal Stability Analysis of Proteins: Qualification of DSC. Journal of Pharmaceutical Sciences 101(3):955-964.

58. Johnson CM 2013. Differential scanning calorimetry as a tool for protein folding and stability. Archives of Biochemistry and Biophysics 531(1):100-109.

59. Kushnir N, Streatfield SJ, Yusibov V 2012. Virus-like particles as a highly efficient vaccine platform: Diversity of targets and production systems and advances in clinical development. Vaccine 31(1):58-83.

60. Thrane S, Janitzek CM, Agerbæk MØ, Ditlev SB, Resende M, Nielsen MA, Theander TG, Salanti A, Sander AF 2015. A Novel Virus-Like Particle Based Vaccine Platform Displaying the Placental Malaria Antigen VAR2CSA. PloS one 10(11):e0143071.

61. Caulfield MJ, Shi L, Wang S, Wang B, Tobery TW, Mach H, Ahl PL, Cannon JL, Cook JC, Heinrichs JH, Sitrin RD 2007. Effect of Alternative Aluminum Adjuvants on the Absorption and Immunogenicity of HPV16 L1 VLPs in Mice. Human Vaccines 3(4):139-145.

62. Deng Z-H, Hao Y-X, Yao L-H, Xie Z-P, Gao H-C, Xie L-Y, Zhong L-l, Zhang B, Cao Y-D, Duan Z-J 2014. Immunogenicity of recombinant human bocavirus-1,2 VP2 gene virus-like particles in mice. Immunology 142(1):58-66.

63. Fox CB, Kramer RM, Barnes V L, Dowling QM, Vedvick TS 2013. Working together: interactions between vaccine antigens and adjuvants. Therapeutic Advances in Vaccines 1(1):7-20.

64. Gupta RK 1998. Aluminum compounds as vaccine adjuvants. Advanced drug delivery reviews 32(3):155-172.

65. Al-Shakhshir RH, Regnier FE, White JL, Hem SL 1995. Contribution of electrostatic and hydrophobic interactions to the adsorption of proteins by aluminium-containing adjuvants. Vaccine 13(1):41-44.

66. Peek LJ, Martin TT, Elk Nation C, Pegram SA, Middaugh CR 2007. Effects of Stabilizers on the Destabilization of Proteins upon Adsorption to Aluminum Salt Adjuvants. Journal of Pharmaceutical Sciences 96(3):547-557.

67. Vessely C, Estey T, Randolph TW, Henderson I, Cooper J, Nayar R, Braun LJ, Carpenter JF 2009. Stability of a Trivalent Recombinant Protein Vaccine Formulation Against Botulinum Neurotoxin during Storage in Aqueous Solution. Journal of pharmaceutical sciences 98(9):2970-2993.

68. Wagner L, Verma A, Meade BD, Reiter K, Narum DL, Brady RA, Little SF, Burns DL 2012. Structural and Immunological Analysis of Anthrax Recombinant Protective Antigen Adsorbed to Aluminum Hydroxide Adjuvant. Clinical and Vaccine Immunology 19(9):1465-1473.

69. Dey AK, Malyala P, Singh M 2014. Physicochemical and functional characterization of vaccine antigens and adjuvants. Expert review of vaccines 13(5):671-685.

70. Rinella JV, Workman RF, Hermodson MA, White JL, Hem SL 1998. Elutability of Proteins from Aluminum-Containing Vaccine Adjuvants by Treatment with Surfactants. Journal of Colloid and Interface Science 197(1):48-56.

71. Iyer S, HogenEsch H, Hem SL 2003. Effect of the Degree of Phosphate Substitution in Aluminum Hydroxide Adjuvant on the Adsorption of Phosphorylated Proteins. Pharmaceutical development and technology 8(1):81-86.

72. Iyer S, Robinett RSR, HogenEsch H, Hem SL 2004. Mechanism of adsorption of hepatitis B surface antigen by aluminum hydroxide adjuvant. Vaccine 22(11):1475-1479.

73. Hem SL, HogenEsch H 2007. Relationship between physical and chemical properties of aluminum-containing adjuvants and immunopotentiation. Expert review of vaccines 6(5):685-698.

74. Shi Y, HogenEsch H, Hem SL 2001. Change in the degree of adsorption of proteins by aluminum-containing adjuvants following exposure to interstitial fluid: freshly prepared and aged model vaccines. Vaccine 20(1):80-85.

Chapter 5 Analytical Comparability Assessments of Five Recombinant CRM_{197} Proteins from Different Manufacturers and Expression Systems

5.1 Introduction

Polysaccharide vaccines have been used effectively since the 1970s to mitigate bacterially-associated diseases, such as pneumonia and meningitis, in adults[1]. The transient immune response elicited by polysaccharide vaccines limit efficacy in individuals with an immature (< 2 yrs) immune system[2]. Subsequently, conjugate vaccines, composed of bacterial polysaccharides chemically linked to a carrier protein, were developed to stimulate a more robust and sustained (T cell-dependent) immune response. While commercially available polysaccharide-protein conjugate vaccines (e.g., Prevnar®, Menveo®, VaxemHib®) have substantially decreased incident rates of bacterially associated diseases [3,4], their complex nature leads to costly production which currently is one major hurdle limiting vaccine coverage in developing countries[5,6].

Three carrier proteins have been used in a majority of commercial conjugate vaccines[7]. These immunogens consist of tetanus toxoid (TT), diphtheria toxoid (DT), and a single amino acid substitution of diphtheria toxin (G52E), termed cross-reactive material 197 or CRM_{197}. Conjugate vaccines employing these three proteins have proven to be safe and effective, and from the limited literature available, induce comparable immune responses to similar polysaccharide antigens. While the clinical efficacy of these proteins appears similar, inherent manufacturing requirements and challenges differentiate these three immunogens. TT and DT require detoxification prior to polysaccharide conjugation using formaldehyde treatment. Conversely, the amino acid substitution in CRM_{197} renders the protein non-toxic and therefore is more advantageous to manufacture than TT or DT since CRM_{197} does not require formaldehyde treatment (resulting in more lysine groups available in the carrier protein as potential polysaccharide conjugation sites. Production of CRM_{197} is hindered, however, by the strict growth requirements of the traditional expression system (*C. diphtheriae*) and generally lower

yields compared to other expression systems[8]. Given these challenges, evaluation of recombinant CRM_{197} expressed in multiple heterologous organisms (e.g. *E. coli*, *P. fluorescens*, *Bacillus subtilis*) is being pursued as alternative source of carrier protein[9].

Given the complex process of manufacturing conjugate vaccines[10], delineating the physicochemical properties of recombinant CRM_{197}, expressed in *C. diphtheriae* or a heterologous system, is essential to mitigate risk during manufacturing, including subsequent polysaccharide conjugation, to ensure the immunogenicity of the final drug product. CRM_{197} has a similar overall conformation to diphtheria toxin, however the crystal structure of CRM_{197} (PDB ID: 4AE0) elucidated subtle but functionally-important (i.e., lack of toxicity in CRM_{197}) differences between the two proteins[11]. CRM_{197} is translated as a 58 kDa polypeptide in *C. diphtheriae*, which can be cleaved by a trypsin-like protease into two subunits (fragments A and B) linked through a disulfide bond. During manufacturing of CRM_{197}, cleavage of the polypeptide, also known as "nicking", is controlled and generally limited to <5% of total CRM_{197}[12]. Following purification of CRM_{197}, polysaccharides are generally conjugated to primary amines on the carrier protein through either direct or indirect (linker molecule) methods [13]. In addition to multiple factors that can affect the immunogenicity of a vaccine during conjugation (e.g., polysaccharide composition, linker length, conjugation chemistry), the accessibility of specific side-chains in the carrier protein can affect polysaccharide conjugation [14]. Therefore ensuring the carrier protein is consistently manufactured and well-characterized prior to conjugation is critical.

In this study, five different recombinant CRM_{197} molecules from the traditional expression system (*C. diptheriae*) as well as two heterologous systems (*E. coli* and *P. fluorescens*) were analytically characterized and comprehensively compared in terms of structural integrity,

solubility and conformational stability using a wide variety of biochemical, biophysical and *in vitro* antigen binding assays. The results from this study provide baseline data sets of the key structural attributes of CRM_{197} to enable future comparisons of the physicochemical and immune-reactivity properties of recombinant CRM_{197} irrespective of expression system and/or production process.

5.2 Materials and Methods

5.2.1 Materials

The sample information for the five different CRM_{197} molecules examined in this study are summarized in Table 5.1. EcoCRM™ (Fina Biosolutions LLC, Rockville, MD), rCRM (Biological E. Limited, Hyderabad, Telangana, India), Pfenex CRM (Reagent Proteins, San Diego, CA), C7 CRM (List Biological Laboratories Inc., Campbell, CA) and VaxForm CRM (VaxForm LLC, Lehigh Valley, PA) were diluted to 2.0 mg/mL with their respective formulation buffers and then dialyzed against 10 mM sodium phosphate, 150 mM NaCl, pH 7.2 (PBS buffer) using 10 kDa molecular weight cutoff (MWCO) Slide-A-Lyzer Mini Dialysis devices (Thermo Scientific, Rockford, IL). The samples were dialyzed overnight at 4°C with three buffer changes at three hour intervals, and the concentration of each CRM_{197} sample was determined both pre and post centrifugation (13,000 rpm for 5 min). Each of the CRM_{197} samples were further diluted to 1.0 mg/mL with PBS buffer for all subsequent analyses. All other chemical and reagents were purchased from commercial sources.

5.2.2 Methods

5.2.2.1 UV-Visible Absorbance Spectroscopy

The UV-Visible absorption spectra of each CRM_{197} sample at 1.0 mg/ml was recorded using an HP-8453 photodiode array detector (Agilent Technologies, Santa Clara, CA) equipped

with Deuterium (D_2) and Tungsten (W) lamps. In addition, samples were centrifuged at 13,000 × g for 5 min and the UV-Visible absorption spectra of the resulting supernatant were recorded. The Beer-Lambert law was used to calculate the actual concentration given an extinction coefficient of a 0.1% solution of CRM (0.932 $mg/mL^{-1}cm^{-1}$) (calculated using http://web.expasy.org/protparam/). Spectra were collected from 190-1100 nm using a 0.5 s integration time and 1 cm path length quartz cuvettes. The instrument was first blanked using the buffer for each sample prior to measuring solutions containing protein. All UV-Visible absorbance spectra were mathematically corrected for light scattering using a technique included in the manufacturer's data analysis software (Chemstation UV-Vis analysis software, Agilent Technologies).

5.2.2.2 SDS-PAGE

For the reduced samples, 2.5 μg of each CRM_{197} sample was mixed with 4X LDS loading dye (Life Technologies, Grand Island, NY) containing 50 mM dithiothreitol (DTT, Invitrogen, Carlsbad, CA) and 100 mM iodoacetamide (Life Technologies), and incubated at room temperature for 30 min. The reduced CRM_{197} samples were then separated by sodium dodecyl sulfate polyacrylamide gel electrophoresis using NuPAGE 4-12% Bis-Tris (Life Technologies) gels and MES running buffer (Life Technologies). A similar procedure was followed for non-reduced CRM_{197} samples except the DTT was omitted during the incubation at room temperature for 30 min step. The NuPAGE gels were run for 60 min at 120 V. Protein bands were visualized by staining with Coomassie blue R250 (Teknova, Hollister, CA) and destained with a mixture of 40% methanol, 10% acetic acid, and 50% ultrapure water. Gels were digitized using an AlphaImager (Protein Simple, Santa Clara, CA) gel imaging system.

5.2.2.3 Intact Mass Spectroscopy

Each CRM sample in PBS (50 pmol) was injected into an 1200 series LC system (Agilent Technologies), bound to a C8 micro-trap (Michrom Bioresources Inc., Auburn, CA), desalted, and then subjected to electrospray ionization time-of-flight mass spectrometry (model 6220, Agilent Technologies). Mass spectra were acquired from 400 to 2000 m/z at a scan rate of one spectrum per sec. Protein MS spectra were deconvoluted using *MassHunter Quantitative Analysis* software (v B.07.00, Agilent Technologies).

5.2.2.4 LC-MS Peptide Mapping

Each CRM sample was incubated overnight at 37°C with 2 µg of trypsin. Trifluoroacetic acid (0.05%) was added to quench proteolysis and ~20 µg of each digested sample was subjected to LC-MS. The peptides from the digested protein solution were separated by a liquid chromatography system (Thermo Scientific, Waltham, MA) prior to analysis. Peptides were injected onto a C_{18} column (1.7µm, 2.1 x 150 mm, Waters) and a 55 min 5-50% B gradient (A: H_2O and 0.05% trifluoroacetic acid; B: ACN and 0.05% trifluoroacetic acid; 200 µl/min flow rate) for separation. MS was performed using a LTQ-XL ion trap (Thermo Scientific) and the Xcalibur *2.0* software (Thermo Scientific). The instrument was also tuned using a standard calibration peptide (Angiotensin II, Sigma, St. Louis, MO) for maximal sensitivity before running any experiments. The mass spectra were acquired in the LTQ over a mass range of m/z 350-1900. The ion selection threshold was 10,000 counts and the dynamic exclusion duration was 5 sec.

Raw experimental files were initially evaluated manually to determine if the ion counts and fragmentation of each peptide were sufficient for further analysis. The raw data files were then processed using *PepFinder* (v 2.0) software (Thermo Scientific). The database used for this

experiment consisted of the primary sequences of CRM and trypsin. Potential common post-translational modifications (e.g. Asn deamidation, Met oxidation, mixed disulfide bonds) were included during the analysis. Peptide assignments of MS/MS spectra were validated using a confidence score of ≥ 95% and disulfide-bonded peptide assignments were also manually verified.

5.2.2.5 Capillary Isoelectric Focusing (cIEF)

Electrophoretic separation by isoelectric point was performed using an ICE_{280} system (Protein Simple, Santa Carla, CA) equipped with a D_2 lamp (280 nm), a PrinCE micro-injector, and an auto-sampler. The FC coated cartridge was rinsed with ultrapure water before and after daily experiments. Separation efficiency and transfer time were determined by separation of a hemoglobin analytical standard. CRM samples were analyzed under the following conditions adapted from Rustandi *et.al*. (2014)[15] and Loughney *et.al.*(2017)[16]: Ampholytes: a mixture of pH 4-6.5 and pH 3-10 in a 2:1 ratio (GE Healthcare, Pittsburgh, PA), IEF markers (4.65, 7.05), additives (20% glycerol) and 1.0% methylcellulose (Protein Simple). The sample was resolved using the pre-focusing conditions of 1 min at 1500 V and a focusing condition of 8 min at 3000 V. Data analysis and peak integrations were performed using *ChromPerfect* software (Protein Simple).

5.2.2.6 Anion Exchange Chromatography (AEX)

AEX was performed on a Shimadzu Prominence UFLC HPLC system equipped with a diode array detector using a TSKgel BioAssist Q (4.6 mm × 5 cm, 10 µm) column (TOSOH Biosciences, King of Prussia, PA). 20 µg of each CRM_{197} sample was injected onto the column for each run, and the experiment was performed in triplicate. The column and auto-sampler temperatures were set at 30°C and 4°C, respectively. The mobile phases consisted of (A) 20 mM

sodium phosphate, pH 7.4; (B) 20 mM sodium phosphate, 1 M sodium chloride, pH 7.4. The flow rate was 0.7 mL/min and the gradient consisted of 0% B (5 min), 0-100% B (10 min), 100% B (3 min), 100-0% B (2 min), and 0% B (5 min). Protein peaks were monitored using the absorbance signal at 214 nm. In addition, the samples were subjected to AEX without the column attached to better determine if any fraction of the sample binds or cannot pass through the column (i.e., sample recovery). Data analysis was performed using LC solutions software (Shimadzu, Kyoto, Japan).

5.2.2.7 Far-UV Circular Dichrosim

Far-UV circular dichroism spectroscopy was performed using a Chirascan-plus CD spectrometer (Applied Photophysics Ltd, Leatherhead**,** UK) equipped with a 6-cuvette position Peltier temperature controller (Quantum Northwest, Liberty Lake, WA) and a high performance solid-state detector. The lamp (150 W air-cooled Xe arc*)* housing, monochromator and sample compartment were continuously purged with N_2 gas. The CD spectra of the protein samples at 0.2 mg/mL were collected in the range of 260-200 nm using 1 nm step size and a 0.5 sec sampling time. Quartz cuvettes (0.1 cm path length) sealed with a teflon stopper (Starna Cells Inc., Atascadero, CA) were used. The CD signal at 222 nm was monitored as a function of temperature from 10-90°C in 1.25°C intervals. The heating rate was 1°C/min, and the equilibration time at each temperature was 2 min. All data were subjected to a 5-point Savitzky-Golay smoothing filter using the *Chirascan* software (Applied Photophysics) and PBS buffer alone was subtracted from all measurements.

5.2.2.8 Intrinsic Tryptophan Fluorescence & Static Light Scattering

The intrinsic tryptophan fluorescence spectra of each CRM_{197} sample was measured in triplicate using a dual emission PTI QM-40 Spectrofluorometer (Photon Technology

International (PTI), Inc., Birmingham, NJ) equipped with a 4-position cell holder Peltier temperature control device, a high power continuous 75 W short-arc Xe lamp (Ushio), and a Hamamatsu R1527 photomultiplier tube. Data were collected using FelixGX software (PTI). Fluorescence emission spectra of 0.2 mg/mL CRM were recorded as a function of temperature (10-90°C) using an excitation wavelength of 295 nm (>95% Trp). Emission spectra were collected from 305-405 nm with a step size of 1 nm and an integration time of 1 sec. Static light scattering data were acquired concurrently with the fluorescence spectra by employing a second detector (90° to the incident light and 180° to the fluorescence detector) that collected light scattered signal at the excitation wavelength (295 nm) as a function of increasing temperature. The excitation and emission slits were both set such that the initial signal at 10°C had an emission maximum of ~800,000 counts per sec for fluorescence spectra and an emission maximum of ~20,000 counts per sec for light scattering spectra. The spectra were collected at 1.25°C intervals with a 2 min equilibration time at each temperature with samples in quartz cuvettes (1 cm path length). The position of the emission wavelength maximum was determined using a mean spectral center of mass method (MSM) executed using in-house software (*MiddaughSuite*) after formulation buffer subtraction. This analysis algorithm increases the signal to noise ratio, but the peak positions are generally red shifted by 5-10 nm from their experimental positions.

5.2.2.9 Extrinsic ANS Fluorescence

8-Anilino-1-naphthalene sulfonate (ANS) was used as an extrinsic fluorescence probe in the presence of CRM_{197} with the same instrument as described above. A dye to protein molar ratio of 25:1 was used for sample preparation. ANS was excited at 372 nm, and emission spectra of ANS was collected from 400-600 nm every 2 nm as a function of temperature from 10 to

90°C. The corresponding ANS in buffer spectrum was subtracted from ANS in the presence of protein spectrum prior to data analysis. The emission peak intensity was determined using a mean spectral center of mass method (MSM) executed in the in-house software. The T_{onset} values were determined by identifying the point at which the baseline deviated from linearity using Origin 8.0 software.

5.2.2.10 Differential Scanning Calorimetry

CRM_{197} samples were loaded in the autosampler tray held at 4°C and DSC was performed in triplicate using an Auto-VP capillary differential scanning calorimeter (MicroCal/GE Health Sciences, Pittsburgh, PA) equipped with Tantalum sample and reference cells. Scans were completed from 10-90°C using a scanning rate of 60°C/h. Reference subtraction and concentration normalization were performed using Origin (OriginLab, Northampton, MA). Data analysis was performed using the MicroCal LLC DSC plug-in for the Origin 7.0 software package. The results were fitted to a multistate model with two transitions to calculate the melting temperature (Tm) values. The onset melting temperature (Tonset) was determined by identifying the point where the heat capacity (Cp) value for the first thermal transition reached ≥500 cal mol^{-1} $°C^{-1}$.

5.2.2.11 Sedimentation Velocity Analytical Ultracentrifugation (SV-AUC)

SV-AUC experiments were performed on a Proteome Lab XL-I (Beckman Coulter, Fullerton, CA) analytical ultracentrifuge equipped with a scanning ultraviolet-visible optical system. All experiments were conducted at 20°C after ≥1 h of equilibration after the rotor reached the set temperature, at a rotor speed of 40,000 rpm and with detection at 280 nm. CRM_{197} samples and PBS alone were each loaded into Beckman charcoal-epon two sector cells with a 12 mm centerpiece and either sapphire or quartz windows.

The data were analyzed using *Sedfit* (Dr. Peter Schuck, NIH). A partial specific volume of 0.73 mL/g was calculated using *Sednterp* (Professor Thomas Laue, University of New Hampshire and BITC) based on amino acid sequence, and used in the analysis. The buffer density and viscosity used in the analysis, 1.0058 g/mL and 0.010195 Poise respectively, were calculated using *Sednterp* based on buffer composition. A continuous c(s) distribution was used with 200 scans. A range of 0 to 15 svedbergs was used, with a resolution of 300 points per distribution and a confidence level of 0.95. Baseline, radial independent noise, and time independent noise were fit, while the meniscus and bottom positions were set manually. Distributions were imported into *Origin* (OriginLab, Northampton, MA) before reporting.

5.2.2.12 Size Exclusion Chromatography (SEC)

A Shimadzu Prominence UFLC HPLC system equipped with a diode array detector (with absorbance detection at 214 nm) was used. Twenty micrograms of each CRM_{197} sample was injected onto a TSK-Gel BioAssist G2SWxl column (7.8 x 300 mm, TOSOH Biosciences) and the corresponding guard column (TOSOH Biosciences). The columns were operated at 30°C and equilibrated with at least 10 column volumes of mobile phase (10 mM sodium phosphate, 150 mM NaCl, pH 7.2) prior to sample injection. A flow rate of 0.7 mL/min was used with a 30 min run time. A gel filtration standard (Bio-Rad, Hercules, CA) was subjected to SEC before and after the CRM sample to ensure integrity of the column and HPLC system. In addition, the samples were subjected to SEC without the column attached to better determine if insoluble aggregates are present in the samples or if the sample binds to the column (i.e., sample recovery). *LC solutions* software (Shimadzu) was used for data analysis.

5.2.2.13 Resonant Mass Measurement (RMM)

An Archimedes Particle Metrology System (Malvern Instruments Ltd, United Kingdom) was used to quantify sub-micron sized particles (0.2-2μm). A Hi-Q micro-H sensor, calibrated using 1 μm polystyrene beads (Thermo Scientific), and a reference solution of 1:20 D_2O:H_2O was used for all measurements. Prior to daily measurements, the accuracy of the sensor was assessed by analysis of 1 μm polystyrene beads (Thermo Scientific). To achieve a clean baseline, the sensor and the tubing were rinsed with 20% Contrad-20 followed by ultrapure water. The sensor was then loaded with particle free water and two "sneeze" operations were performed. Each CRM_{197} sample at 1.0 mg/mL was loaded for 30 sec and a stop trigger of 300 particles was used. The total number and size distribution of sub-micron particles were analyzed in triplicate. The limit of detection was determined empirically (0.030 Hz) and used throughout the study. Data analysis was performed using ParticleLab software 1.9.30 (Malvern, UK).

5.2.2.14 Micro-Flow Imaging (MFI)

The concentration and size range of sub-visible particles (2-100 μm) were measured and quantified using a DPA-4200 flow microscope (Protein Simple) that was previously calibrated using 10 μm polystyrene particle standards (Thermo Scientific). The instrument was flushed with particle free water until a clean baseline was achieved. Each CRM_{197} sample at 0.2 mg/mL (1:5 dilution) was analyzed in triplicate experiments. The samples were carefully drawn up in a low protein binding, filter-tip pipette (Neptune Scientific, San Diego, CA) and analyzed using a flow rate of 0.2 mL/min. Data analysis was performed using MVSS software (Protein Simple)

5.2.2.15 PEG-Precipitation Assay

The protocol for the high throughput version of the PEG assay for assessing apparent solubility of CRM molecules was adopted from Gibson et al. (2011)[17] and Toprani et al. (2016)

[18]. Stock solutions of PBS pH 7.2 and PBS containing 40% w/v PEG-10,000 at pH 7.2 were mixed to prepare various concentrations of PEG solutions ranging from 0 to 40% w/v PEG. A volume of 200 µL of the various PEG-10,000 solutions was added to wells of a 96-well polystyrene filter plate (Corning Life Sciences, Corning, NY). Fifty microliters of each CRM sample in PBS pH 7.2 (1 mg/mL) was then added to each well to a final protein concentration of 0.2 mg/mL. The plates were incubated overnight at room temperature and then centrifuged at 3,500 rpm (1,233 rcf) for 15 min and the filtrate was collected in a clear 96 well collection plate (Greiner Bio-One North America Inc., Monroe, NC). Subsequently, 200 µL of filtrate was transferred into a 96 well UV Star microplate and the protein concentration in each filtrate was determined using a SpectraMax M5 UV-Visible plate reader. The % PEG_{midpt} and apparent solubility values (thermodynamic activity) were calculated as described previously [17].

5.2.2.16 Empirical Phase Diagrams/Radar Charts

Each of the five CRM_{197} samples were dialyzed against 10 mM sodium phosphate buffer containing sodium chloride at an ionic strength of 0.15 at pH 5.8, 6.3, 6.8, 7.2, 7.6, and 8.0 using Slide-A-Lyzer dialysis devices (10 kDa MWCO, Thermo Scientific). After four rounds of buffer exchange overnight at 4°C, each CRM_{197} sample was collected from the dialysis device and centrifuged at 13,000 × g at 4°C for 5 min. The biophysical stability of CRM_{197} molecules was determined using far-UV circular dichroism spectroscopy, intrinsic tryptophan fluorescence spectroscopy, static light scattering, and differential scanning calorimetry (as described above) for each protein sample at each pH as a function of temperature. EPDs and radar charts were constructed as data visualization tools to summarize the effect of pH and temperature on the physical stability profile of the CRM_{197} samples (using the biophysical stability data sets) as described in detail previously [19,20].

5.2.2.17 Enzyme-Linked Immunosorbent Assay (ELISA) using Polyclonal Antibodies

One hundred microliters of 0.5 µg/ml heparin-binding EGF-like growth factor (HB-EGF, Sigma) in PBS was added to each well of a 96-well plate. The plate was then incubated overnight at 4°C. The following day, the plate was washed three times with PBST (PBS with 0.05% Tween-20) and 200 µl of blocking buffer was added (PBS + 5% w/v fat-free milk). The plate was incubated for 1 hr at room temperature, and then the blocking solution was removed and the plate was washed three times with PBST. Each CRM sample in PBS pH 7.2 (at 2 mg/ml) was then diluted with PBST + 1% fat-free milk to 100 µg/ml. A 1:2 dilution series was performed with each CRM molecule in triplicate and 100 µl of each CRM solution was added to each well in the 96-well plate. The plate was incubated for 1 hr at 37°C, and then the CRM solutions were removed and the plate was washed three times with PBST. One hundred microliters of a rabbit anti-CRM polyclonal antibody (at 0.5 µg/ml in PBST, AIC LLC, Rockville, MD) was added to each well and the plate was incubated for 1 hr at 37°C. The primary antibody solution was removed and the plate was washed three times with PBST. One hundred microliters of a goat anti-rabbit antibody (at 0.25 µg/ml in PBST, Jackson ImmunoResearch, West Grove, PA) was added to each well and the plate was incubated for 1 hr at 37°C. The secondary antibody solution was removed and the plate was washed three times with PBST. One hundred microliters of SureBlue TMB peroxidase (SeraCare Life, Milford, MA) was added to each well and the plate was incubated for 1 hr at room temperature in the dark. One hundred microliters of 1N HCl was added to quench the reaction and the absorbance at 450 nm of each well was measured using a SpectralMax M5 plate reader (Molecular Devices, Sunnyvale, CA). Statistical analysis of the ELISA results was performed using Prism software (GraphPad Software Inc, La Jolla, CA). A asymmetrical (five parameter) dose-response (1) curve was fitted to each dataset [21].

(1) LogXb = LogEC50 + (1/HillSlope)*Log((2^(1/S))-1)

5.2.2.18 Enzyme-Linked Immunosorbent Assay (ELISA) using Monoclonal Antibodies

One hundred microliters of C7 CRM in PBS (1:1 serial dilutions from 10 to 0.005 mg/ml) was added to each well of a 96-well plate. The plate was then incubated overnight at 4°C. The following day, the plate was washed three times with PBST (PBS with 0.05% Tween-20) and 200 µl of blocking buffer was added (PBS + 5% w/v fat-free milk). The plate was incubated for 1 hr at room temperature, and then the blocking solution was removed and the plate was washed three times with PBST. The five monoclonal mouse CRM_{197} antibodies (AB8306, AB8307, AB8308, AB8310, and AB53827, Abcam, Cambridge, MA) were diluted 1:1000 with PBST + 0.1% w/v BSA and 100 µl of each antibody was added (individually) to the CRM_{197}-containing 96-well plate. The plate was incubated for 2 hr at room temperature, and then the antibody solutions were removed and the plate was washed three times with PBST. The goat anti-mouse antibody (Thermo Fisher) was diluted 1:4000 with PBST + 0.1% w/v BSA and 100 µl of the antibody was added to each well. The plate was incubated for 1 hr at room temperature and then, the secondary antibody solution was removed and the plate was washed five times with PBST. One hundred microliters of p-nitrophenyl phosphate-liquid substrate (Sigma) was added to each well and the plate was incubated for 1 hr at room temperature in the dark. One hundred microliters of 2N NaOH was added to quench the reaction and the absorbance at 405 and 490 nm of each well was measured using a SpectraMax M5 plate reader (Molecular Devices). The absorbance value at 490 nm was then subtracted from the 405 nm value.

5.2.2.19 BioLayer Inferometry

The binding kinetics of CRM with mAbs was evaluated using Octet Red 96 system (Pall Forte Bio LLC, Fremont, CA). Anti-mouse biosensors (Pall ForteBio LLC, Fremont, CA) were

hydrated for ~15-20 min in kinetics buffer (PBS pH 7.2 + 0.1% BSA), followed by preconditioning comprising of three rounds of 20 sec exposure each to regeneration buffer (10 mM glycine, pH 1.7) alternating with kinetics buffer. After the biosensor preconditioning, the kinetic assay comprised of five steps: (1) 300 sec equilibration with kinetics buffer; (2) 450 sec of antibody loading to capture CRM_{197}-mAb onto the biosensor; (3) 200 sec equilibration with kinetics buffer to obtain a stable baseline after Fc mAb immobilization; (4) 600 sec association with each of the five CRM_{197} samples individually; and (5) 600 sec dissociation with kinetics buffer. The biosensors were regenerated for up to 5 times by subjecting to alternating cycles of regeneration and kinetics buffer for 5 sec each. Kinetics assay were performed using 8 nM of each mAb and a range of CRM_{197} concentrations (0-200 nM). Data analysis were performed using *Octet Data Analysis* (v 8.2) software. After data processing, including reference subtraction using the 0 nM CRM_{197} concentration (buffer blank) trace, baseline alignment, and inter-step correction, the association and dissociation traces of the five CRM_{197} samples with each of the five mAbs individually were fit to a 1:1 binding model. K_D, k_a and k_{dis} values were extracted from the curve fitting analysis of the kinetic data.

5.3 Results

5.3.1 Protein Purity, Primary Structure and Post-translational Modification Analysis of Five CRM_{197} Molecules

Under non-reducing or reducing SDS-PAGE conditions, one band was primarily observed in each CRM_{197} sample (Figure 5.1A). The migration of the main band (between the 49 and 62 kDa molecular weight (MW) protein markers) was consistent with the theoretical MW of a CRM_{197} monomer (58.4 kDa). A small amount of lower MW species was observed in rCRM

and C7 CRM. Independent analysis of LC-MS peptide mapping confirmed these lower MW species were the A (~21 kDa) and B (~38 kDa) subunits of CRM_{197} (data not shown).

Intact mass spectrometry was used to elucidate and compare the molecular composition of the five CRM_{197} proteins. As shown in Figure 5.1B, a single species was observed in the deconvoluted mass spectra of rCRM, Pfenex CRM, and Vaxform CRM (58,541 ± 1 Da), which was consistent with the expected mass of an unmodified and non-reduced CRM_{197} monomer (Table 5.2). EcoCRM™ contained two species that differed in mass by ~131 Da. LC-MS peptide mapping confirmed these two species were the unmodified CRM_{197} monomer without (58,410 ± 1 Da) and with (58,541 ± 1 Da) an N-terminal Met residue (Figure 1C). In addition to the unmodified CRM_{197} monomer in C7 CRM, two additional higher MW species were observed (CRM_{197} MW + ~324 Da and CRM_{197} MW + ~648 Da), which may represent post-translational modifications involving disaccharides (e.g., potentially lactose glycations in the lyophilized samples).

The five different CRM_{197} molecules were also subjected to peptide mapping analysis to confirm their primary amino acid sequence. As shown in Figure 5.1C, the trypsin-digested reversed phase UPLC chromatograms of the five CRM_{197} samples were similar. MS/MS analysis of individual trypsin or GluC digests confirmed a similar amino acid composition of the five CRM_{197} proteins (Supplemental Figure 5.1). The two native disulfide bonds in CRM_{197} (Cys187-Cys201 & Cys462-Cys472) were identified in each CRM_{197} molecule, and no non-native disulfide bonds or free Cys residues were observed in any sample. Multiple smaller peaks were observed in C7 CRM, and while the identities of these peaks are unknown, they could potentially represent residual protein contaminants not completely removed by the purification process.

5.3.2 Charge Heterogeneity Analysis of Five CRM_{197} Molecules

Capillary isoelectric focusing (cIEF) and anion exchange chromatography (AEX) were utilized to assess the overall charge heterogeneity of each CRM_{197} protein. As shown in Figure 5.2A, the pI of the major peak in each CRM_{197} sample was ~5.7 as measured by cIEF, which was consistent with previously reported pI of CRM_{197}[15]. The EcoCRM™ and Vaxform CRM samples contained a small amount (4-7%) of a more acidic species (pI 5.5-5.6) relative to the main peak (Table 5.2), while the relative area of this species was more prominent in C7 CRM sample (~21%). The elution profile of each CRM_{197} protein through AEX was overall similar to their cIEF electropherograms profiles in which the retention time of the major peak was consistent across all five samples. In addition, EcoCRM™ and C7 CRM contained measurable acidic species, 8% and 24%, respectively, as measured by AEX. For Vaxform CRM sample, ~4% of the relatively more acidic species were observed through cIEF, but this species was found to be more prominent through AEX analysis (~17%).

5.3.3 Higher Order Structure (HOS) Analysis of Five CRM_{197} Molecules

Far-UV circular dichroism (CD) spectroscopy was used to assess the overall secondary structure of each CRM_{197} protein. As shown in Figure 5.3A, double minima at 208 and 222 nm were observed at 10˚C indicating a primarily α-helical secondary structure, consistent with the X-ray crystal structure of CRM_{197} (PDB ID:4AE0)[11]. Second derivative UV spectroscopy, intrinsic Trp fluorescence spectroscopy, and extrinsic ANS fluorescence spectroscopy analyses were performed to evaluate and compare the overall tertiary structures of the five CRM_{197} molecules at 10°C. Six major peaks were observed for each CRM_{197} sample by second derivative UV spectroscopy, which correspond to different local polarity environments of the three aromatic amino acids (phenylalanine (250-270 nm), tyrosine (250-290 nm) and tryptophan (250-

300 nm) in each protein (Figure 5.3B). The similar positions of these peaks between the five CRM_{197} proteins suggest a similar overall tertiary structure via a similar environment around the average aromatic acid residues. The intrinsic Trp and extrinsic ANS fluorescence spectra further support an overall similar tertiary structure across the five samples. As shown in Figure 5.3C, the intrinsic Trp fluorescence wavelength of maximum intensity (λ_{max}) was ~330 nm at 10˚C, which indicated a similar hydrophobic environment for the average Trp residue in each CRM_{197} molecule. Finally, the extrinsic ANS fluorescence emission peak maximum and peak intensity at 10˚C was not notably different between the five proteins (Figure 5.3D), which suggested a comparable overall surface hydrophobicity across the five proteins.

5.3.4 Size and Aggregate/Particle Analysis of Five CRM_{197} Molecules

The size analysis of monomer, aggregate and fragment species in each CRM_{197} sample was assessed under non-denaturing solution conditions by sedimentation velocity analytical ultracentrifugation (SV-AUC) and size exclusion chromatography (SEC). The sedimentation coefficient value of the major species in each CRM_{197} sample was 3.9 ± 0.1 S, consistent with a CRM_{197} monomer (Figure 5.4A). The relative area of this monomeric peak ranged from 68-99% of each sample's total peak area (Table 5.2). Furthermore, some larger species (e.g., dimer, trimer) with higher sedimentation values (~5-8 S) were observed in EcoCRM™, Vaxform CRM, and C7 CRM while smaller species (e.g., fragments), at ~1-3 S sedimentation values, were present in rCRM and C7 CRM samples. SEC analysis showed comparable size distributions of monomer, aggregate and fragment species in which EcoCRM™, rCRM, and Pfenex CRM were primarily monomeric (~97-100%) while Vaxform CRM and C7 CRM contained more abundant smaller fragment (1% and 14 %, respectively) and larger aggregate (28 % and 13 %, respectively) species (Figure 4B).

In addition to size analysis by SV-AUC and SEC, the presence of larger aggregates/particles were assessed through resonant mass measurements (RMM) and micro-flow imaging (MFI). RMM measures the concentration and size distribution of sub-micron (0.2-2 μm) particles, while MFI measures the same parameters for sub-visible (2-100 μm) particles. As reported in Table 5.2, a slightly higher number of sub-micron particles were present in Vaxform CRM and C7 CRM (~5 × 10^5 particles/mL) compared to EcoCRM™, rCRM and Pfenex CRM (~2 × 10^5 particles/mL). The majority of sub-micron particles were in the size range of 0.2-1.0 μm. MFI analysis indicated a low number of sub-visible particles in EcoCRM™, rCRM, Pfenex CRM, and Vaxform CRM (~100 particles/mL), while a slightly higher number of sub-visible particles were measured in C7 CRM (~450 particles/mL). The majority of sub-micron and sub-visible particles in all the five CRM_{197} samples were 0.2-1.0 μm and 2-5 μm, respectively.

5.3.5 Conformational Stability, Aggregation Propensity and Relative Solubility of Five CRM_{197} Molecules

The conformational stability of each CRM_{197} proteins' overall secondary structure was assessed through monitoring their molar ellipticity values at 222 nm as a function of temperature (10-90˚C) in PBS buffer, pH 7.2. As shown in Figure 5.5A, each of the CRM_{197} molecules (except C7 CRM) showed a sharp transition. The C7 CRM sample showed a biphasic transition between 55-75°C, which may be due to heterogeneity in the protein sample (as observed by SDS-PAGE and intact mass analysis; see Figures 5.1 and 5.2). The calculated apparent thermal melting temperature values (T_m) of EcoCRM™, rCRM, Pfenex CRM, and Vaxform CRM were ~58°C (Table 5.2). For C7 CRM, the broad and slightly biphasic nature of the transition prevented accurate calculation of an accurate values of T_m.

The conformational stability of each CRM_{197} proteins' overall tertiary structure vs. temperature was evaluated through both intrinsic and extrinsic fluorescence spectroscopy in PBS buffer, pH 7.2. A single transition (red shift) was observed in the intrinsic tryptophan fluorescence spectra peak position vs. temperature in all five samples with Tm values at ~42°C. The T_m values calculated from changes in ANS fluorescence emission peak intensity vs. temperature in the presence of the protein were also similar between the five CRM_{197} molecules (~41˚C). These results indicated a relative overall similar tertiary structure stability in terms of the average Trp residue and average surface hydrophobicity of the proteins, respectively. Furthermore, DSC was used to assess the overall conformational stability of each of the five CRM_{197} samples as a function of temperature in PBS buffer, pH 7.2. As shown in Figure 5.5D, one major and one minor endothermic peak was observed for all CRM_{197} molecules at ~40˚C and 50˚C, respectively. Overall, the DSC thermograms of rCRM, Pfenex CRM, and Vaxform CRM samples appeared similar but subtle differences were observed in EcoCRM™ (slightly lower stability of T_m1) and C7 CRM (slightly higher stability of T_m1)(Table 5.2).

The aggregation propensity and relative solubility of the five CRM_{197} samples was also studied by static light scattering vs temperature and PEG precipitation curves, respectively. The light scattered from each CRM_{197} sample was measured a function of temperature (10-65°C) in PBS buffer. As shown in Figure 5.5E, one sharp transition was observed in all samples that began (T_{onset}) at ~45°C. The relative apparent solubility (thermodynamic activity) profiles of the five CRM_{197} molecules were assessed using PEG precipitation assay as described previously[18]. As shown in Figure 5.5F, the shape of the PEG curves (concentration of protein, (mg/mL) vs. percentage (w/v) PEG-6,000 of Vaxform CRM appeared to have a shifted profile compared to the four other CRM_{197} samples (C7 CRM, rCRM, EcoCRM™ and Pfenex CRM). A possible

reason for the more rapid precipitation of Vaxform CRM as a function of PEG concentration is the relatively higher levels of aggregates present in the sample as observed by size exclusion chromatography and SV-AUC. From the PEG vs. protein concentration curves, two different relative solubility parameters (PEG_{midpt} and apparent solubility) were calculated. PEG_{midpt} value is a parameter to quickly and reliably compare datasets while the apparent solubility value is extrapolated from each precipitation curve and assumes no interaction between the PEG and protein, which is not necessarily the case for all proteins[17]. The PEG_{midpt} value was lowest for Vaxform CRM (~21.5%) while rCRM, EcoCRM™, Pfenex CRM and C7 CRM had similar PEG_{midpt} values (~23%)(Table 5.2). A comparison of the apparent solubility values of each of the proteins showed a similar trend as seen in the PEG_{midpt} values, in which Vaxform appeared to have a lower apparent solubility (~16 mg/mL) compared to C7 CRM, rCRM, EcoCRM™, and Pfenex CRM (~27-34 mg/mL) in PBS buffer, pH 7.2.

5.3.6 Physical Stability Profiles of Five CRM_{197} Molecules during pH/Temperature Stresses

The physical stability profiles of the five CRM_{197} molecules were evaluated in PBS buffer under a wide range of pH (pH 5.8-8.0) and temperature (10-90^{o}C) conditions. For each pH and temperature, the overall secondary and tertiary structural integrity, overall conformational stability and aggregation propensity of each CRM_{197} sample were measured using circular dichroism, intrinsic tryptophan fluorescence spectroscopy, differential scanning calorimetry and static light scattering, respectively. Representative data sets for C7 CRM in PBS buffer at different pH values from these different biophysical techniques are shown in Figure 5.6A (see Supplemental Figures 5.2-5.5 for the corresponding biophysical data sets for each of the five CRM_{197} proteins). The molar ellipticity at 222 nm vs. temperature of C7 CRM showed a

dramatic pH dependence with a single thermal transition event at pH values of s 5.8-7.2 (with Tm values ranging between ~37-62°C). At pH 7.6 and 8.0, however, a distinct thermal transition was not observed, which prevented accurate calculation of a T_m. Clear differences in the stability of the overall secondary structure were observed in the CRM_{197} samples (i.e., more stable pH ≥ 7.2 and less stable at pH 5.8-6.8). An increase in Trp fluorescence peak position of C7 CRM spectra was observed with increases in temperature for each pH, indicating a pH dependent alteration of the protein's overall tertiary structure. The observed T_m values were highest at pH 6.8-7.2 (42-44°C), slightly lower at pH 6.3, 7.6, or 8.0 (41-42°C), and distinctly lower at pH 5.8 (34°C) (Table 5.2). DSC results indicated the highest overall conformational stability of C7 CRM occurred at pH 6.8-7.2 and was slightly lower at the other solution pH conditions tested. Finally, the temperature at which C7 CRM began (T_{onset}) to scatter more light (i.e., aggregate) was lowest at pH 5.8 (29°C) and increased with an increasing solution pH (T_{onset} was 47°C at pH 8.0) as measured by static light scattering. Similar pH-dependent physical stability profiles were observed with EcoCRM™, rCRM, Pfenex CRM, and Vaxform CRM (See Supplementary Figures 5.2-5.5 and Supplemental Table 5.1).

Using the large biophysical datasets from the above four techniques, two data visualization tools were utilized, an empirical phase diagram (EPD) and a radar chart to better compare the overall physical stability profiles of each CRM_{197} protein as a function of pH and temperature [19,20]. The EPD displayed changes in the structural characteristics of each CRM as measured by the four different biophysical techniques (circular dichroism, intrinsic tryptophan fluorescence, static light scattering, and differential scanning calorimetry), as a function of temperature and pH. The EPD plots for all five CRM_{197} molecules indicated the presence of six distinct colored phases (designated as Regions I-VI) (Figure 5.6B and Supplemental Figure 5.6). Each color

represented regions with similar structural characteristics and changes in color reflected structural alterations in each CRM_{197} protein as measured by the biophysical measurements. In addition to the native-like region at low temperatures (Region I), five structurally altered protein states were observed both with EPD. Region II denotes an overall altered conformation of CRM_{197} molecule, Region III represents a structurally altered state beginning to aggregate, Region IV corresponds to an aggregated state of protein, Region V represents more extensively aggregated and structurally altered state, and Region VI shows substantial secondary structure alterations.

Radar plots were also constructed to visualize the same physical stability data sets for each of the five CRM_{197} proteins as a function of solution pH and temperature. A Radar plot displays the results of the different biophysical analyses in a polygon, in which each vertex is mapped to a particular biophysical technique and concentric circles represent the signal variation/strength. As shown in Figure 5.6C, the signals for each of the biophysical techniques (CD molar ellipticity, intrinsic tryptophan fluorescence, DSC, and static light scattering) were minimal in Region I, representing the native-like state for the CRM_{197} molecule. Region II represents CRM_{197} in an overall structurally altered conformation as indicated by increase in the DSC signal and alterations in the intrinsic tryptophan fluorescence peak position. Region III was assigned based on the loss of tertiary structure as monitored by intrinsic tryptophan fluorescence. Region IV represents CRM_{197} in aggregated state as indicated by increase in the light scattering signal. Region V corresponds to a more aggregated and structurally altered state as seen from notable changes in the signals from light scattering and CD, and lastly, Region VI reflects loss of secondary structure as measured by circular dichroism. Overall, a comparison of EPD and radar charts of multiple CRM_{197} molecules tested here indicated similar biophysical stability profiles

vs. pH and temperature. Additionally, the total area for the native-like state as a function of pH and temperature, Region I, was similar (35-37%) for all five CRM_{197} molecules.

5.3.7 In *vitro* Antigenicity Assessment of Five CRM_{197} Molecules

For comparing of the *in vitro* antigenicity of each CRM molecule, the steady-state and pre-steady state kinetics were measured through an ELISA (polyclonal anti-CRM_{197} antibodies) and bio-layer interferometry (individual measurements with five different monoclonal CRM_{197} antibodies), respectively. While a visual comparison of the binding curves of the CRM molecules to commercially available polyclonal CRM_{197} antibodies suggested subtle differences in antigenicity between the five CRM_{197} molecules (Figure 5.7A), a statistical analysis indicated, however, that the steady-state interactions of each CRM_{197} molecule with the polyclonal antibodies were not significantly ($p > 0.05$) different from each other (Table 5.2).

The pre-steady state kinetics of between each CRM_{197} and five monoclonal antibodies (mAbs) were measured using bio-layer interferometry (BLI). Prior to the BLI assay, the concentrations of each of the five mAbs required to monitor binding to C7 CRM was optimized with an ELISA. As shown in Figure 5.7B, affinity differences were observed between the five antibodies and C7 CRM as measured by the ELISA. The five mAbs were categorized into three groups, one higher-affinity mAb (AB53827), two intermediate affinity mAbs (AB8308 and AB8310), and two lower-affinity mAbs (AB8307 and AB8306). The pre-steady state kinetics (k_a, k_{dis}, and K_D) were then measured between each CRM_{197} molecule and mAb using BLI. A representative association and dissociation binding curve for C7 CRM and a lower-affinity mAb (AB8306) as measured by BLI is shown in Figure 4.7C. Similar to the ELISA results with C7 CRM and the two lower-affinity mAbs, the rate of association (3-5 x 10^5 M^{-1} s^{-1}), dissociation (1-2 x 10^{-3} s^{-1}), and binding affinity (3-6 nM) values measured by BLI with either mAb were

comparable between all the five CRM_{197} molecules (Table 5.2). For the three other mAbs (AB8308, AB8310, and AB53827), pre-steady state kinetics could not be accurately measured by this technique due to their strong affinity (K_D < nM) for each of the five CRM_{197} molecules.

5.4 Discussion

In this study, the physicochemical and immunological binding properties of recombinant CRM_{197} from the traditional expression system (*C. diptheriae*) as well as two heterologous systems (*E. coli* and *P. fluorescens*) were evaluated and compared as part of an analytical comparability assessment. A comprehensive suite of analytical techniques assessed numerous structural attributes including primary structure and post translational modifications, higher order structures, overall surface hydrophobicity and charge heterogeneity, and aggregate/particle formation from small multimers to larger sub-visible particles. Overall, the five CRM_{197} molecules exhibited overall highly similar physicochemical characteristics (with some exceptions in terms of subtle physicochemical differences as described below) in a common buffer (PBS, pH 7.2). These similarities were also conserved in terms of conformational stability under different stress conditions (pH/temperature changes) as well as for relative solubility (in the presence of molecular crowding agent, PEG). Finally, each CRM_{197} displayed essentially equivalent *in vitro* antigenicity in terms of binding to a series of antibodies (polyclonal and monoclonal mAbs specific for CRM_{197}). Together, these observations indicate the various expression systems produced generally comparable CRM_{197} molecules.

The largest differences noted between the CRM_{197} proteins were the presence of product-related variants/impurities. The nature of these species in some cases was determined, and in other cases, will require additional analysis. For example, N-terminal heterogeneity with a Met residue observed in EcoCRM™ was quantitatively described (~60% vs. 40% for CRM_{197} with

vs. without N-terminal Met) and was not necessarily unexpected given a lower catalytic efficiency of methionyl-aminopeptidase in some strains of *E. coli* [22,23]. Two low-abundant species in C7 CRM contained post-translational modifications with +324 and +648 Da, which were possibly caused by non-enzymatic glycation between a reducing sugar (lactose) within the formulation buffer and the protein, especially upon lyophilization, as has been observed with other freeze-dried proteins [24-26]. The C7 CRM sample also contained lower and higher molecular weight species that were observed by two different orthogonal sizing techniques (SV-AUC and SEC). The presence of these fragment and soluble aggregate species may have arisen during the bulk manufacturing process, lyophilization and/or subsequent storage. Analysis of material from each downstream processing step would be needed to identify the mechanism(s) that induced the formation of these species. In addition, the Vaxform CRM sample contained relatively elevated levels (~29% by SV-AUC) of higher molecular weight species, which could potentially be a consequence of the material's age and long-term storage (~11 yrs.). Furthermore, although speculative, the higher MW species in this sample may possibly be comprised of the observed acidic peak through AEX since the cIEF results indicated the levels of the acidic species in Vaxform CRM was greatly reduced. Unlike AEX, cIEF assess the overall charge (pI) of a generally unfolded molecule following migration through a pH gradient, therefore the larger (non-covalently associated) species in Vaxform CRM would likely dissociate during analysis. The more acidic species in C7 CRM however, were observed at a similar amount (21-24%) by both AEX and cIEF. This acidic peak in C7 CRM may represent CRM_{197} containing the lactose glycan(s) variants that were observed by intact mass analysis. Finally, the composition of the low abundant acidic species (7-8%) observed in EcoCRM™ through AEX and cIEF could represent chemically modified CRM_{197} (i.e., Asn deamidation), which has been suggested previously[15],

and determination of these species is suggested for future work. In addition, potential differences in process-related impurities (e.g. residual host cell proteins, residual DNA) between CRM_{197} from different manufacturers should also be examined as part of future comparability work.

In this work, we have implemented state-of-the-art analytical methods to comprehensively characterize the structural integrity, conformational stability and relative solubility of CRM_{197} bulk materials. Mass spectrometry analysis can rigorously define the primary structure and post translational of proteins ensuring the structural integrity and defining the presence of structural variants. A current technical challenge is the use of analytical tools to rigorously characterize the higher order structure of protein. This work did not utilize higher resolution methods such as X-ray crystallography or hydrogen deuterium exchange mass spectrometry since such methods are not commonly available, expensive and are relatively time consuming. Instead, the key structural attributes of the CRM_{197} molecule were monitored using commonly available analytical instruments. In addition, the biophysical techniques utilized in this work, combined with data visualization tools, can monitor the conformational stability of the CRM_{197} in a comprehensive manner as a function of stress conditions such as pH and temperature. The stability of protein structure can be a sensitive probe for the overall higher order structural integrity of proteins and it has been suggested such an approach is an important part of protein comparability studies and biosimilarity analyses [27-29]. In this work, the resulting empirical phase diagrams were similar overall for the five CRM_{197} molecules, indicating a similar structural integrity and conformational stability. Not surprisingly, all of the CRM_{197} molecules showed a notable decrease in the overall conformational stability profile as the solution pH was lowered from 6.8 to 5.8, a result which is consistent with the known

conformational change of diphtheria toxin at pH 5.0 related to insertion of the toxin into the endosomal membrane[30].

Interestingly, despite the noted structural heterogeneity differences noted between the five CRM_{197} samples, their binding reactivity to polyclonal or multiple individual monoclonal antibodies was equivalent. This result could be due to the low levels of these variants in the preparations and an associated lack of sensitivity to detect small differences in these types of binding assays. Future work would need to focus on the isolation of the variants and then a more direct comparison of their *in vitro* binding properties. Furthermore, the specific epitopes recognized by the five anti-CRM_{197} monoclonal antibodies described in this study are currently unknown, but in general, *in vitro* immunological binding assays are a critical probe of the overall structural integrity of biologicals. Due to the challenges in rigorously defining all aspects of higher order structure of proteins with current analytical technology (as described above), functional or potency assays are required to ensure to the overall structure/function of protein vaccine or drug candidates are maintained during development. To this end, biological potency assays (either *in vitro* assays or *in vivo* animal studies depending on the nature of the vaccine antigen) remain a cornerstone of the overall analytical strategy to ensure comparability and biosimilarity [31]. In the case of the carrier protein CRM_{197} for use in as polysaccharide conjugate vaccines, *in vitro* binding assays are a useful tool for probing the overall conformational integrity of the molecule as part of comparability assessments (especially using mAbs with known binding to specific epitopes to a reference with known *in vivo* activity as part of future work). Nonetheless, to directly compare the ability of the different CRM_{197} molecules to generate immune responses, an *in vivo* biological potency assay would be more suited for the final polysaccharide conjugated vaccine and not the carrier protein alone.

These findings lead to question if some or any of these subtle physiochemical differences/impurities observed in the bulk CRM_{197} have an effect (if any) on the preparation of the final drug product of conjugate vaccine. From the limited literature available, conjugate vaccines containing CRM_{197} from different expression systems elicit similar immune responses in animal models [5,31]. It is currently unknown which analytical readout(s) performed in this work could predict detrimental effects on subsequent conjugation of the protein to various polysaccharides and its effects on the safety and efficacy of the conjugate vaccine drug product. Furthermore, for industrial use of CRM_{197} as carrier protein in conjugate vaccines, the critical to quality (CTQ) parameters have to be established with prospective acceptance criteria to ensure that the carrier protein meets the quality requirements for robust and sustainable manufacturing. Typically this information would be available to the manufacturer in a pharmacopeia/WHO technical review series (TRS) monograph. Unfortunately, such a monograph does not currently exist for CRM_{197} carrier protein. It is also important for the industry to have this CTQ parameters quantified, so that these could be used for in-depth characterization, lot release and stability analysis. While additional studies are needed to determine if the observed subtle differences between different sources of commercially available CRM_{197} influence the development of conjugate vaccines, the presented results provide a basis to develop and establish specifications for this important carrier protein in the future.

Table 5.1. Summary of sample information for five different CRM197 molecules used in this study.

CRM Sample Name	Source	System for Recombinant CRM Expression	Lot Number (Manufacturing or Release Date)	Storage Temperature	Formulation Buffer	Reported Stock Concentration
EcoCRM™	Fina Biosolutions LLC	*Escherichia coli*	NO13p46 (Nov 2016)	-80°C (frozen liquid)	25mM HEPES, 10% glycerol, pH 7.2	5.0 mg/mL
rCRM	Biological E Limited	*Escherichia coli*	P/003/16 (Feb 2016)	-80°C (frozen liquid)	PBS, 5% Sucrose, pH 7.35	2.2 mg/mL
Pfenex CRM	Reagent Proteins	*Pseudomonas fluorescens*	162M4001 (May 2014)	4°C (Lyophilized)	250 mg sucrose, 1.1 mg sodium phosphate monobasic, 15 mg sodium phosphate dibasic, 0.275 mg polysorbate 80	20 mg/vial
Vaxform CRM	VaxForm LLC	*Corynebacterium diphtheriae*	Not provided (2006)	-20°C (frozen liquid)	10 mM sodium phosphate, 5% sucrose, pH 7.0	4.0 mg/mL
C7 CRM	List Biological Laboratories, Inc.	*Corynebacterium diphtheriae*	14936A1 (Feb 2015)	4°C (Lyophilized)	10 mM sodium phosphate, 5% lactose (when reconstituted with 0.25 ml water)	0.5 mg/vial

Table 5.2. Summary of the key structural attributes (physicochemical and *in vitro* antigenicity) of recombinant CRM_{197} proteins (in PBS pH 7.2) produced from three different expression systems and obtained from five different manufacturers.

Physicochemical Attribute	Analytical Method	Measurement		EcoCRM™	rCRM	Pfenex CRM	Vaxform CRM	C7 CRM
Primary Structure	Mass Spectrometry	Intact Protein Mass (Da)		58410 ± 1 58541 ± 1*	58410 ± 1	58410 ± 1	58410 ± 1	58410 ±1 58734 ± 1* 59058 ± 1*
		*Post-Translational Modification		N-terminal Met (+131 Da)	-	-	-	Glycation (+324, +648 Da)
Protein Charge Heterogeneity	Capillary Isoelectric Focusing	Main Peak (pI 5.6-5.7) (%)		92 ± 0	99 ± 0	99 ± 0	95 ± 0	79 ± 1
		Acidic species (pI 5.5-5.6) (%)		7 ± 0	0 ± 0	0 ± 0	4 ± 0	21 ± 1
		Basic species (pI 5.7-5.8) (%)		1 ± 0	1 ± 0	1 ± 0	1 ± 0	0 ± 1
	Anion Exchange Chromatography	Main Peak (%)		92 ± 0	100 ± 0	100 ± 0	83 ± 0	75 ± 1
		Acidic Species (%)		8 ± 0	0 ± 0	0 ± 0	17 ± 1	24 ± 1
Higher Order Structure	Circular Dichroism	Spectral minima at 10°C (nm)		208 & 222	208 & 222	208 & 222	208 & 222	208 & 222
		Tm (°C)		58.2 ± 1.0	57.9 ± 0.7	57.9 ± 0.3	59.6 ± 0.6	NA
	Intrinsic Trp Fluorescence	Peak emission maximum at 10°C (nm)		328 ± 1	329 ± 1	329 ± 1	330 ± 1	331 ± 1
		Tm (°C)		41.2 ± 0.3	42. 3± 0.3	42.3 ± 0.3	42.2 ± 0.6	43.2 ± 0.2
	Static Light Scattering	Tonset (°C)		43.0 ± 0.6	43.4 ± 0.2	43.6 ± 0.3	44.6 ± 0.5	45.2 ± 0.7
	Extrinsic ANS Fluorescence	Peak emission intensity (10^5 counts/s)		441 ± 7	441 ± 9	437 ± 8	443 ± 11	411 ± 16
		Tm (°C)		40.8 ± 0.5	41.5 ± 0.3	41.4 ± 0.5	41.3 ± 0.6	42.5 ± 0.2
	Differential Scanning Calorimetry	Tonset (°C)		32.7 ± 0.3	35.0 ± 0.2	34.8 ± 0.2	33.5 ± 0.2	35.2 ± 0.6
		Tm1 (°C)		42.0 ± 0.0	42.9 ± 0.0	42.8 ± 0.0	42.8 ± 0.2	44.0 ± 0.1
		Tm2 (°C)		51.3 ± 0.2	51.3 ± 0.1	51.1 ± 0.2	51.1 ± 0.3	51.7 ± 0.1
Aggregate/ Particle Analysis	Size Exclusion Chromatography	Monomer (%)		98 ± 0	99 ± 0	100 ± 0	71 ± 0	73 ± 1
		Aggregates (%)		1 ± 0	0 ± 0	0 ± 0	28 ± 0	13 ± 1
		Fragment (%)		2 ± 0	1 ± 0	0 ± 0	1 ± 0	14 ± 0
	Sedimentation Velocity Analytical Ultracentrifugation	Monomer (%)		99 ± 0	99 ± 0	100 ± 0	70 ± 0	68 ± 1
		Aggregates (%)		1 ± 0	0 ± 0	0 ± 0	30 ± 0	11 ± 1
		Fragment (%)		0 ± 0	0 ± 0	0 ± 0	0 ± 0	21 ± 0
	Resonant Mass Measurement (0.2-2 μm)	Total particles after dilution (number/mL x 10^5)		1.7 ± 0.4	2.3 ± 0.1	1.6 ± 1.2	4.6 ± 0.7	5.1 ± 0.4
	Micro-Flow Imaging (2-100 μm)	Total particles after dilution (number/mL)		85 ± 56	133 ± 19	84 ± 9	109 ± 16	453 ± 163
Apparent Solubility	PEG Precipitation Assay	PEGmidpt (%)		23.3 ± 0.2	23.0 ± 0.2	23.5 ± 0.1	21.5 ± 0.2	24.0 ± 0.2
		Apparent Solubility in PBS pH 7.2 (mg/mL)		30 ± 12	27 ± 9	31 ± 11	16 ± 10	34 ± 12
***In vitro* Immunological Activity**	ELISA	log EC_{50} (μg/mL)		1.6 ± 0.9	2.3 ± 0.9	1.8 ± 0.3	1.3 ± 0.3	1.3 ± 0.3
	Bio-layer Interferometry	Antibody ab8306	k_a (10^5 M^{-1} s^{-1})	4.2 ± 1.9	4.4 ± 0.8	5.0 ± 2.0	4.0 ± 0.9	2.9 ± 0.9
			k_{dis} (10^{-3} s^{-1})	1.3 ± 0.3	1.4 ± 0.5	1.5 ± 0.4	1.6 ± 0.9	1.7 ± 0.4
			K_D (nM)	3.4 ± 2.0	3.2 ± 1.3	3.3 ± 1.3	4.2 ± 2.6	6.1 ± 3.0
		Antibody	k_a (10^5 M^{-1} s^{-1})	4.4 ± 0.7	4.8 ± 0.8	5.4 ± 1.7	4.9 ± 1.0	3.5 ± 0.7

		ab8307	k_{dis} (10^{-3} s^{-1})	1.4 ± 0.4	1.3 ± 0.6	1.4 ± 0.4	1.6 ± 0.4	1.6 ± 1.0
			K_D (nM)	3.3 ± 1.5	2.9 ± 1.7	2.8 ± 1.5	3.4 ± 1.0	4.9 ± 2.9

***** Broad and slightly biphasic nature of the transition in C7 CRM prevented accurate calculation

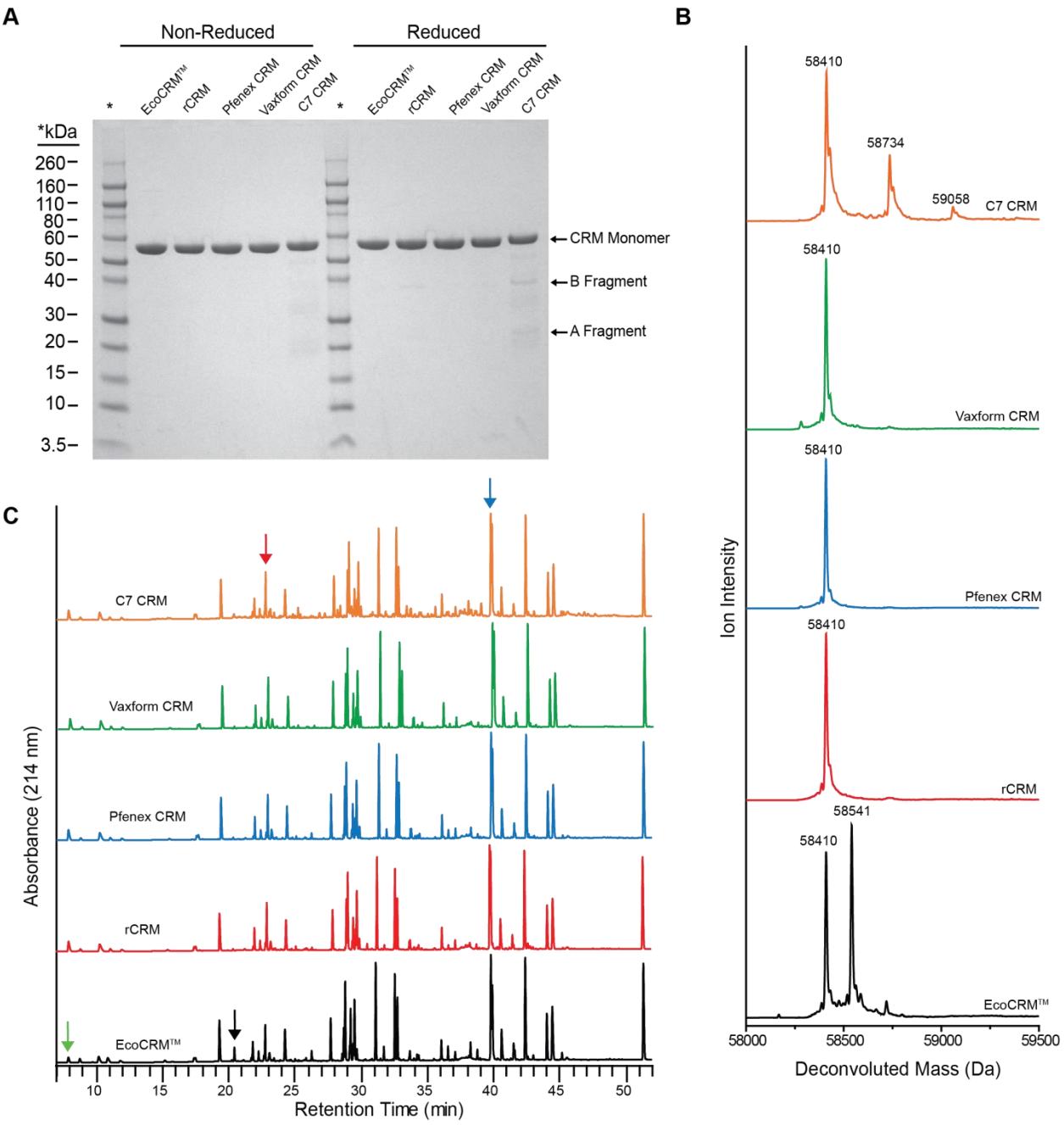

Figure 5.1. Primary Structure Analysis of Five CRM_{197} Molecules. (A) SDS-PAGE analysis of CRM_{197} molecules under non-reducing and reducing conditions. (B) Representative intact mass spectrometry analysis of the non-reduced CRM_{197} molecules. (C) Representative LC peptide mapping chromatograms of non-reduced trypsin-digested CRM_{197} samples. The red and blue arrows indicate the two peaks containing Cys^{461}-Cys^{273} and Cys^{186}-Cys^{200} bonded peptides, respectively. The black arrow indicates an N-terminal peptide with a Met residue.

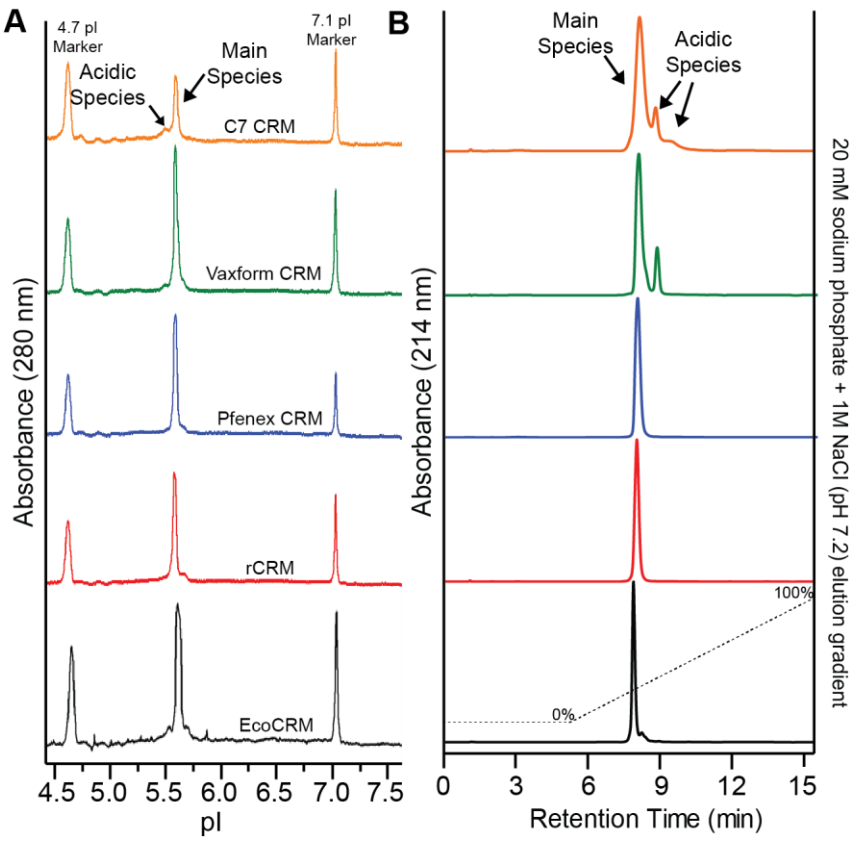

Figure 5.2. Charge Heterogeneity Analysis of Five CRM_{197} Molecules. The overall charge heterogeneity of the CRM_{197} samples were compared through both (A) capillary isoelectric focusing, and (B) anion-exchange chromatography. The migration of two pI markers (4.7 and 7.1) are indicated in the cIEF electropherogram for C7 CRM.

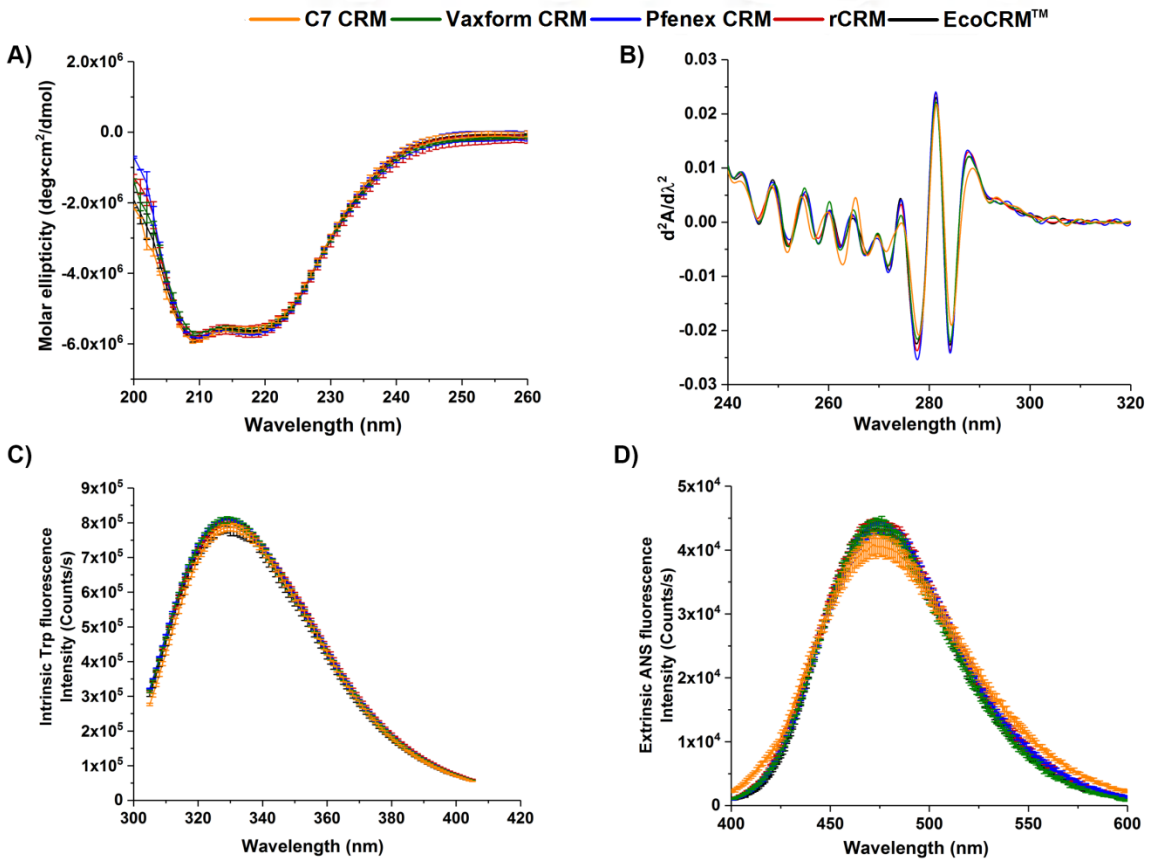

Figure 5.3. Higher Order Structure Analysis of Five CRM_{197} Molecules. (A) The overall secondary structures were evaluated by Far-UV circular dichroism spectra, (B) the overall tertiary structures were monitored by both (B) Second derivative UV absorbance spectra, and (C) Intrinsic tryptophan fluorescence emission spectra. (D) The overall surface hydrophobicity of the samples were determined by Extrinsic ANS fluorescence emission spectra. The five CRM_{197} samples were compared at 10˚C in PBS pH 7.2.

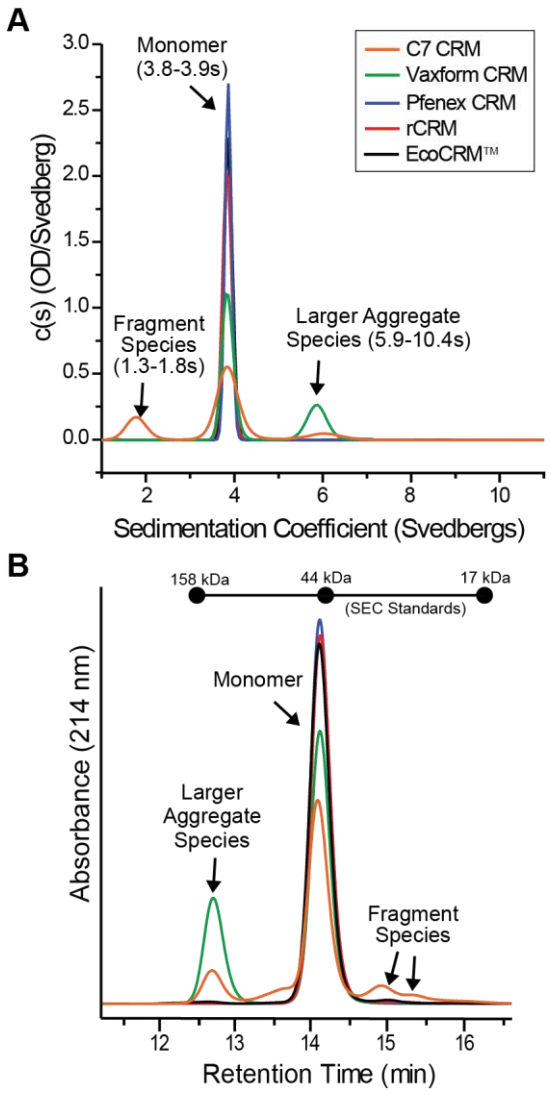

Figure 5.4. Size Analysis of Five CRM_{197} Molecules. The size and distribution of monomer, aggregate and fragment species in each of the CRM_{197} samples were compared through (A) sedimentation velocity analytical ultracentrifugation (SV-AUC), and (B) size exclusion chromatography (SEC). The elution times and molecular weight values of gel filtration standard proteins are shown above the SE chromatograms.

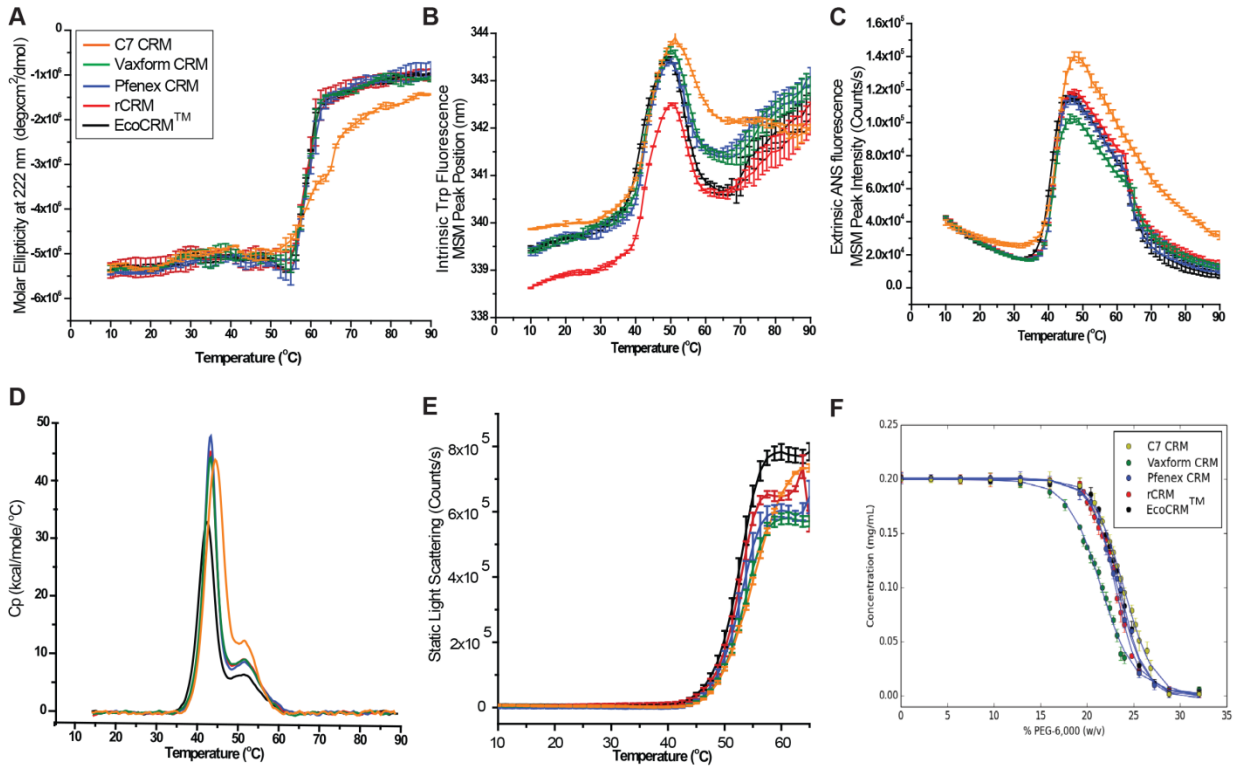

Figure 5.5. Conformational Stability, Aggregation Propensity, and Relative Solubility Analysis Five CRM_{197} Molecules. The conformational stability profiles of the CRM_{197} samples in PBS buffer (pH 7.2) were compared as a function of temperature (10-90˚C) through (A) far-UV circular dichroism, (B) intrinsic tryptophan fluorescence spectroscopy (MSM peak position), (C) extrinsic ANS peak intensity in the presence of each protein, and (D) differential scanning calorimetry. (E) The aggregation propensity of the CRM_{197} samples were compared through static light scattering as a function of temperature (10-90˚C). (F) The relative apparent solubility of the CRM_{197} samples were compared as a function of an increasing concentration (0-33% w/v) of a molecular crowding agent (PEG-6,000).

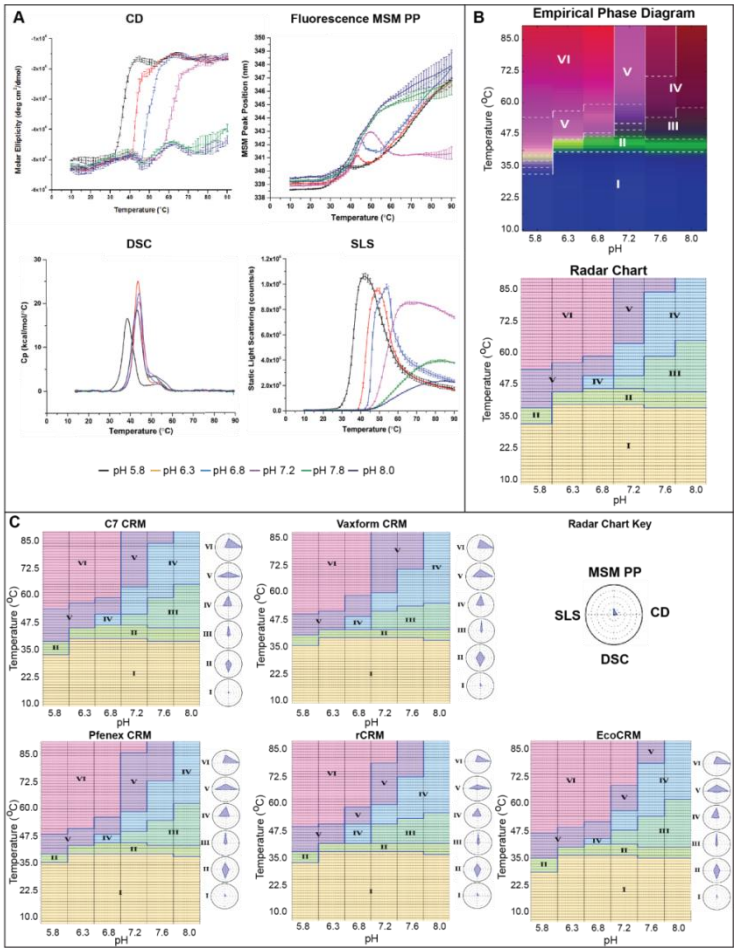

Figure 5.6. Physical Stability Analysis of the Five CRM_{197} Molecules as a Function of pH and Temperature. (A) The molar ellipticity at 222 nm, intrinsic Trp fluorescence MSM peak position, differential scanning calorimetry, and static light scattering at 295 nm for C7 CRM in PBS buffer at six different pH s (5.8, 6.3, 6.8, 7.2, 7.6, and 8.0) were measured as a function of temperature (10-90˚C). (B) An empirical phase diagram and radar chart for C7 CRM were generated from the data in panel A. Six distinct biophysical states of C7 CRM (regions I-VI) were observed as a function of pH and temperature (see *Results* section for more details). (C) Summary of calculated radar charts of each of the five CRM_{197} molecules. The contributions of each biophysical technique towards the different structural states of each CRM197 are indicated on each vertex in the key.

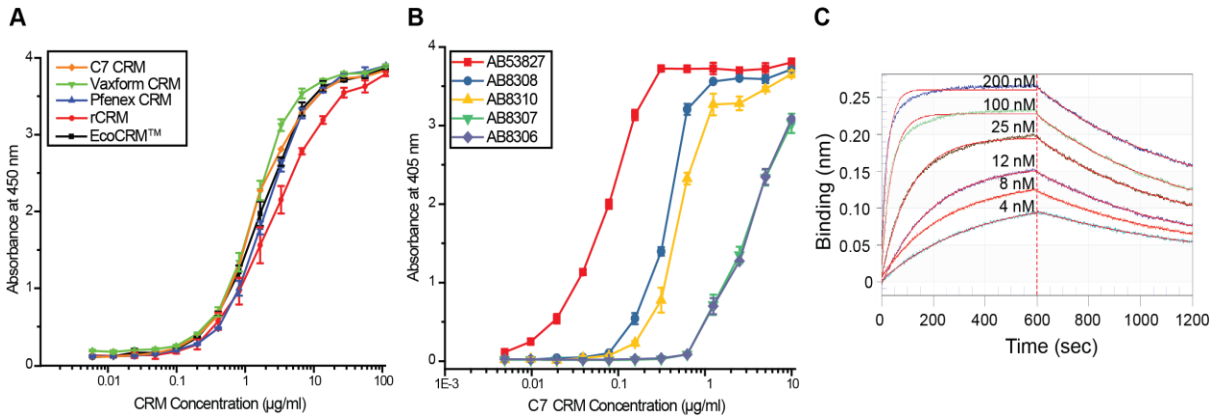

Figure 5.7. *In vitro* Antigenicity Analysis of the Five CRM197 Molecules. (A) ELISA reactivity of each CRM_{197} protein as a function of protein concentration (0.005-100 µg/mL) to a polyclonal CRM_{197} antibody. (B) ELISA reactivity of C7 CRM as a function of protein concentration (0.005-10 µg/mL) to five different monoclonal CRM_{197} antibodies. (C) Representative association and dissociation binding curves of six concentrations (4-200 nM) of C7 CRM to a monoclonal CRM_{197} antibody (AB8306) as measured by Octet analysis.

Supplemental Table 5.1. Thermal melting temperature (Tm) values of each CRM_{197} protein calculated from each biophysical technique in PBS buffer at pH 5.8, 6.3, 6.8, 7.2, 7.6, or 8.0 vs. temperature.

Technique	pH	EcoCRM™	rCRM	Pfenex CRM	Vaxform CRM	C7 CRM
Circular Dichroism at 222 nm (T_m)	**5.8**	33.8 ± 0.1	37.4 ± 0.0	37.4 ± 0.1	37.5 ± 0.1	36.5 ± 0.4
	6.3	41.1 ± 0.5	41.8 ± 0.6	41.7 ± 0.5	41.4 ± 0.4	42.9 ± 0.7
	6.8	45.8 ± 0.8	52.6 ± 0.2	49.1 ± 0.8	49.0 ± 0.2	47.9 ± 0.5
	7.2	59.6 ± 0.6	62.2 ± 0.4	61.9 ± 0.6	61.3 ± 0.1	59.0 ± 0.5
	7.6	*	*	*	*	*
	8.0	*	*	*	*	*
Intrinsic Tryptophan Fluorescence Peak Position (T_m)	**5.8**	32.3 ± 0.4	35.5 ± 0.7	36.0 ± 0.4	36.2 ± 0.3	34.4 ± 0.3
	6.3	39.4 ± 0.5	39.9 ± 0.2	39.9 ± 0.1	39.6 ± 0.5	41.0 ± 0.5
	6.8	41.3 ± 0.1	42.4 ± 0.2	42.3 ± 0.3	42.3 ± 0.2	42.7 ± 0.3
	7.2	41.5 ± 0.1	42.2 ± 0.2	42.5 ± 0.4	42.2 ± 0.2	43.5 ± 0.1
	7.6	40.1 ± 0.2	41.4 ± 0.0	41.3 ± 0.1	41.4 ± 0.0	42.2 ± 0.6
	8.0	39.9 ± 0.1	39.8 ± 0.2	40.5 ± 0.3	41.0 ± 0.2	41.7 ± 0.5
Differential Scanning Calorimetry (T_m^1)	**5.8**	36.7 ± 0.1	39.4 ± 0.0	39.3 ± 0.0	39.8 ± 0.0	38.9 ± 0.1
	6.3	41.7 ± 0.0	42.7 ± 0.0	42.6 ± 0.0	42.5 ± 0.0	43.6 ± 0.0
	6.8	42.3 ± 0.0	43.1 ± 0.0	43.1 ± 0.0	43.1 ± 0.0	44.2 ± 0.0
	7.2	42.2 ± 0.0	42.8 ± 0.1	42.9 ± 0.1	42.8 ± 0.0	44.1 ± 0.0
	7.6	41.3 ± 0.0	42.4 ± 0.0	42.4 ± 0.0	42.4 ± 0.0	43.4 ± 0.1
	8.0	41.2 ± 0.0	41.8 ± 0.0	41.9 ± 0.0	42.0 ± 0.0	43.0 ± 0.0
Static Light Scattering (T_{onset})	**5.8**	26.4 ± 0.1	28.2 ± 0.6	27.6 ± 0.2	27.8 ± 0.2	28.9 ± 0.2
	6.3	37.0 ± 0.1	35.0 ± 0.4	35.1 ± 0.2	34.1 ± 0.4	38.5 ± 0.1
	6.8	41.6 ± 0.1	40.4 ± 0.0	40.1 ± 0.0	40.2 ± 0.2	42.5 ± 0.2
	7.2	44.1 ± 0.1	42.5 ± 0.4	43.0 ± 0.1	42.1 ± 0.1	44.8 ± 0.6
	7.6	47.2 ± 0.2	43.3 ± 0.1	44.4 ± 0.1	43.9 ± 0.1	46.4 ± 0.6
	8.0	48.1 ± 0.1	43.6 ± 0.2	44.6 ± 0.1	44.2 ± 0.2	47.2 ± 0.1

*** T_m could not be calculated**

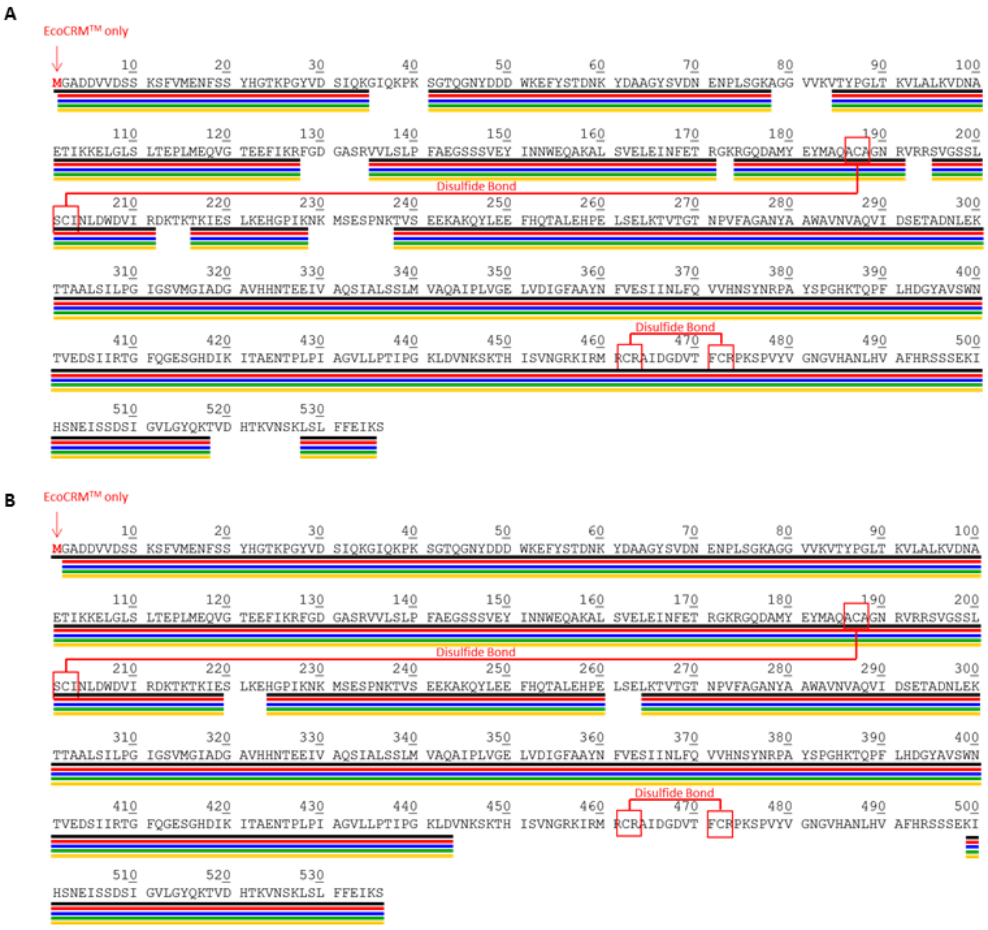

Supplemental Figure 5.1. Sequence coverage of the five CRM_{197} molecules from a non-reduced, A) trypsin-digestion or B) GluC-digested peptide mapping method. Black, red, blue, green, and orange bars indicate one or more peptides that were identified covering each region for EcoCRM™, rCRM, Pfenex CRM, Vaxform CRM, and C7 CRM, respectively. The two disulfide bonds within the protein are highlighted in red.

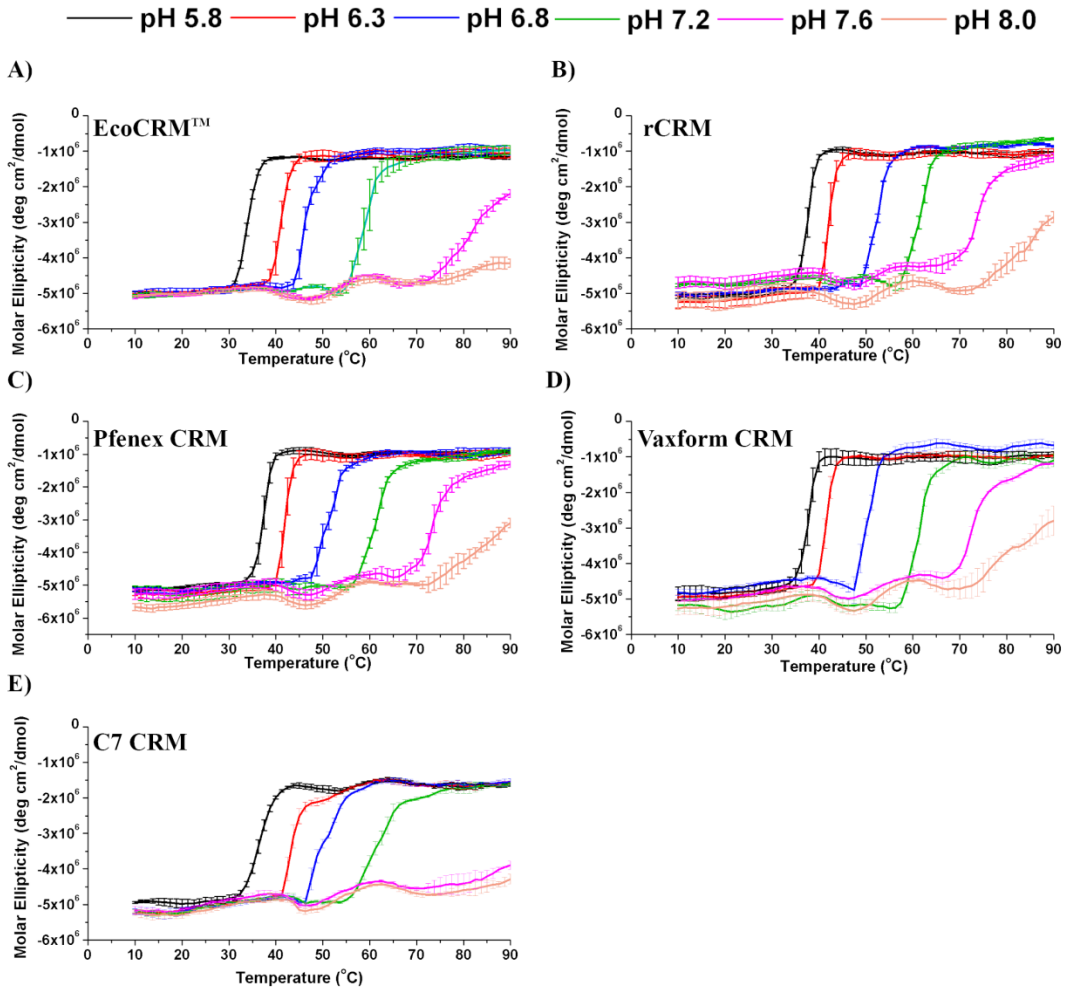

Supplemental Figure 5.2. Molar ellipticity values at 222 nm of each CRM_{197} protein in PBS buffer at pH 5.8, 6.3, 6.8, 7.2, 7.6, and 8.0 as a function of temperature (10-90˚C) as measured by Far-UV circular dichroism.

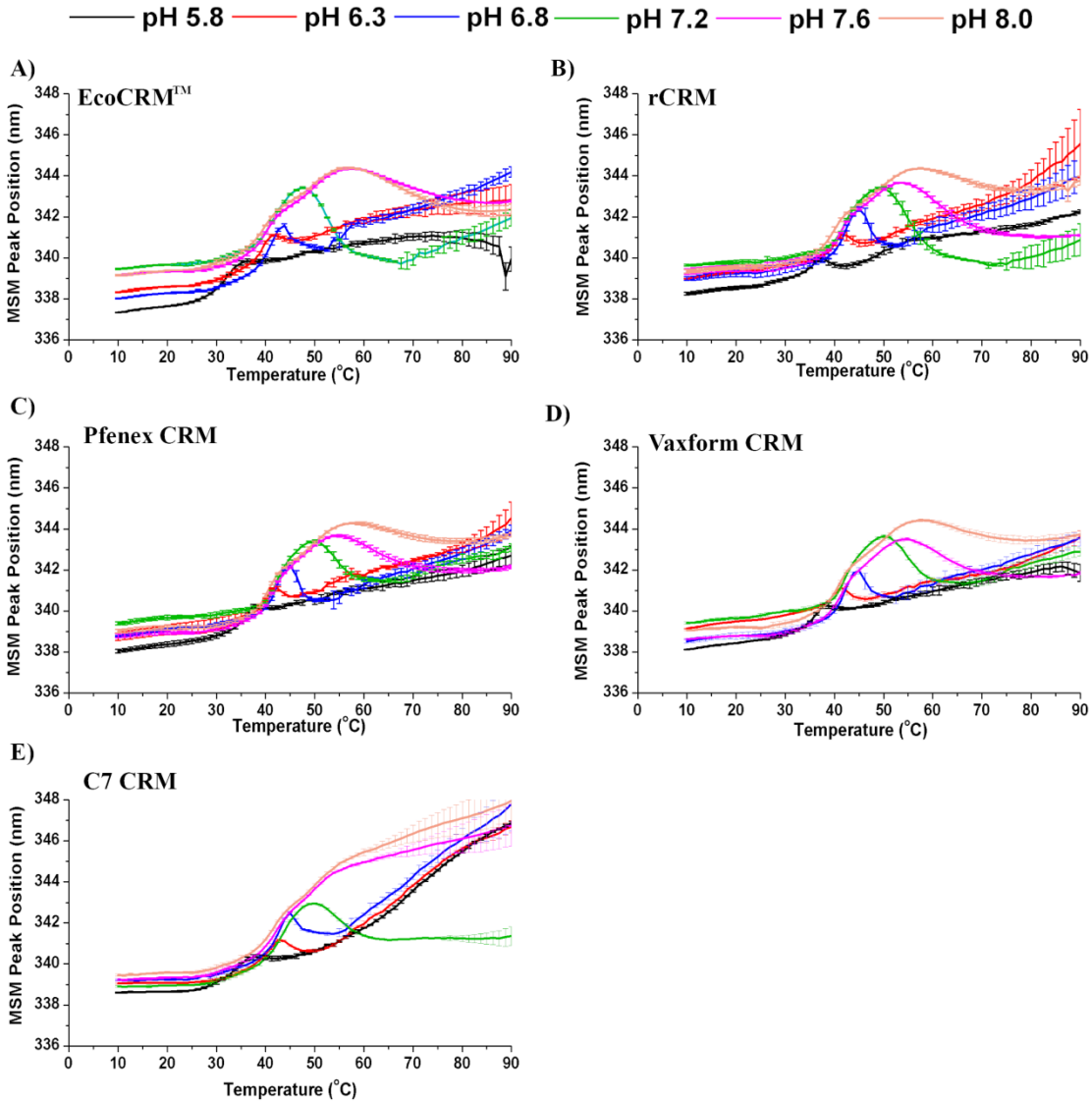

Supplemental Figure 5.3. Intrinsic Trp fluorescence spectroscopy MSM peak position values of each CRM_{197} protein in PBS buffer at pH 5.8, 6.3, 6.8, 7.2, 7.6, and 8.0 as a function of temperature (10-90˚C).

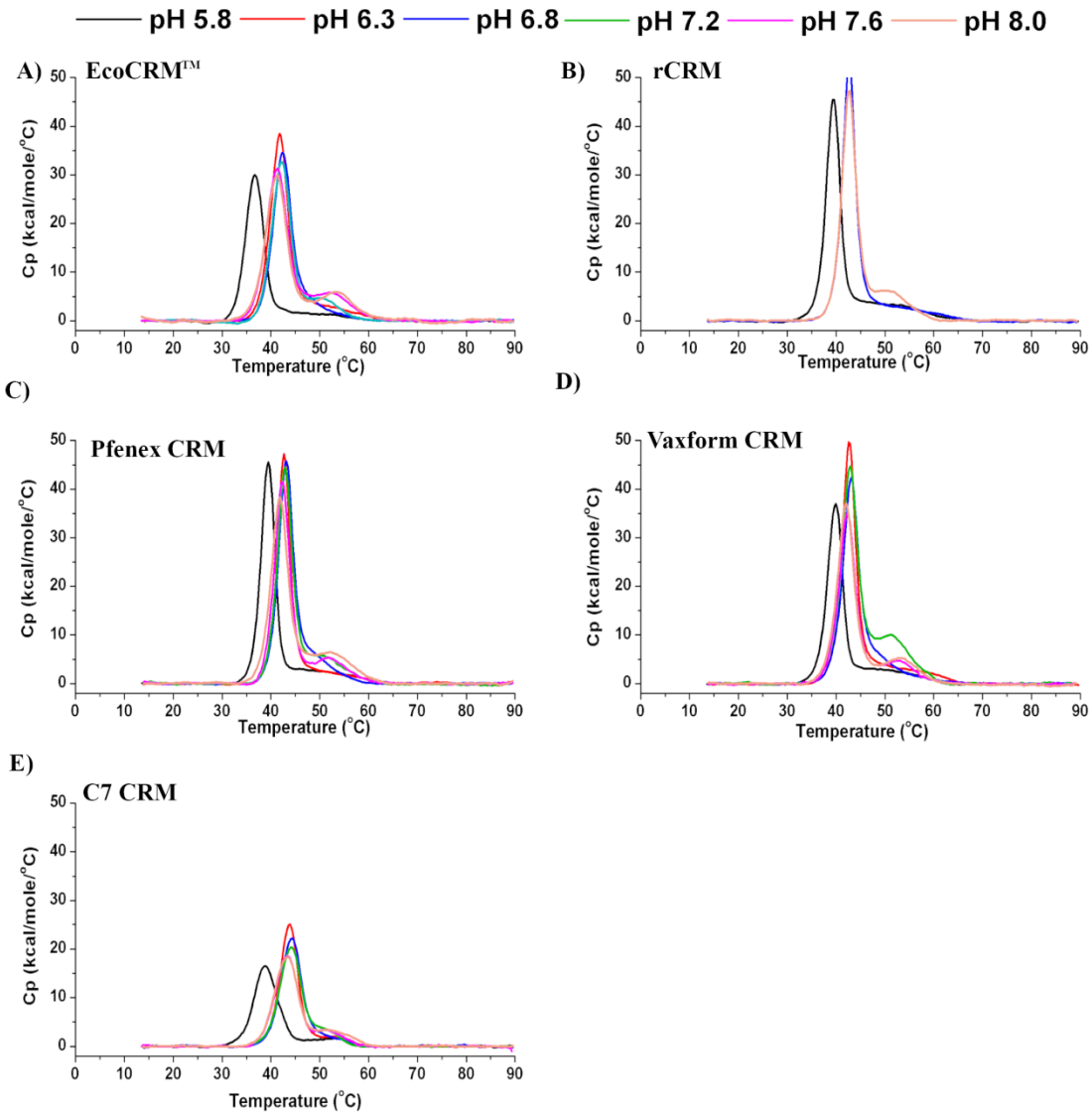

Supplemental Figure 5.4. Differential scanning calorimetry thermograms of each CRM_{197} protein in PBS buffer at pH 5.8, 6.3, 6.8, 7.2, 7.6, and 8.0 as a function of temperature (10-90˚C).

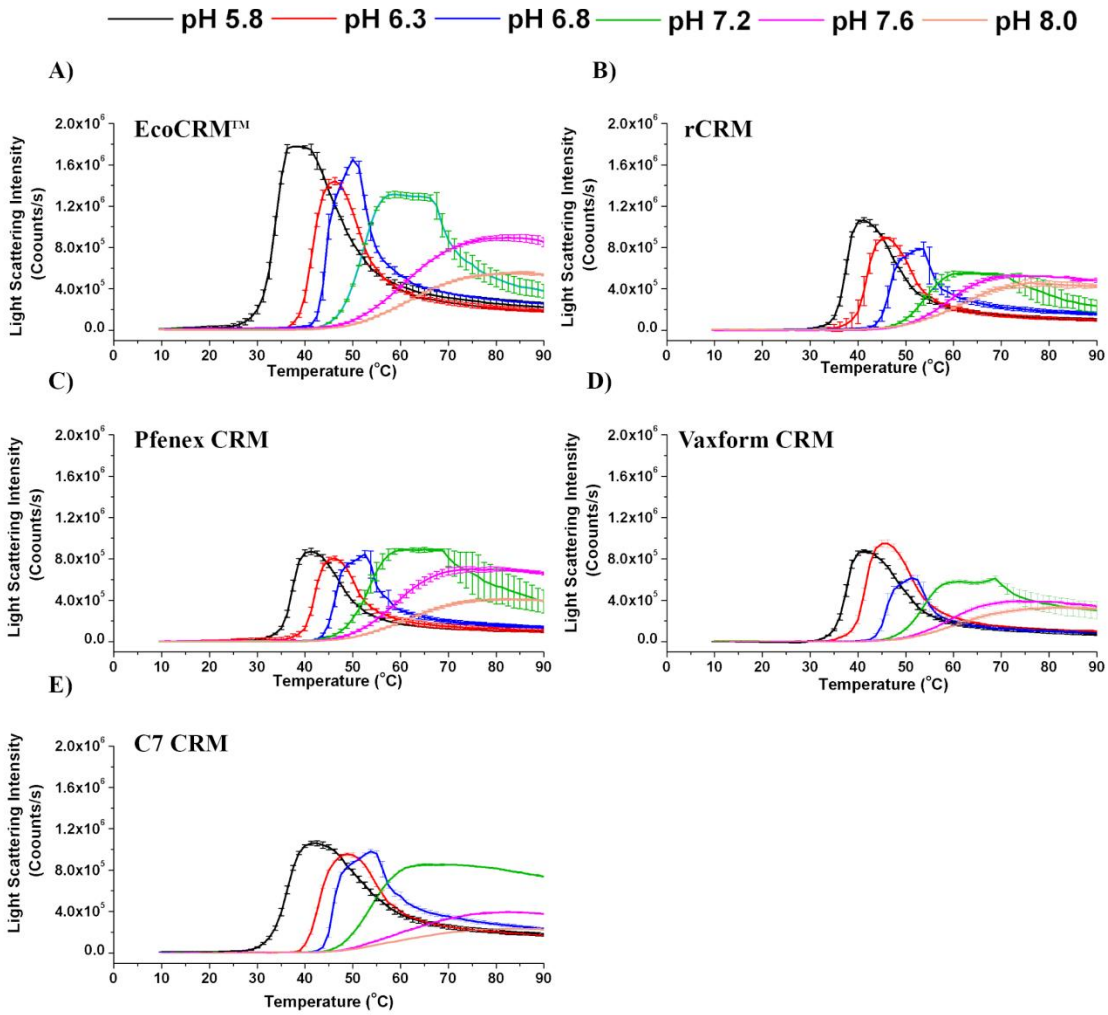

Supplemental Figure 5.5. Static light scattering signal of each CRM_{197} protein in PBS buffer at pH 5.8, 6.3, 6.8, 7.2, 7.6, and 8.0 as a function of temperature (10-90˚C).

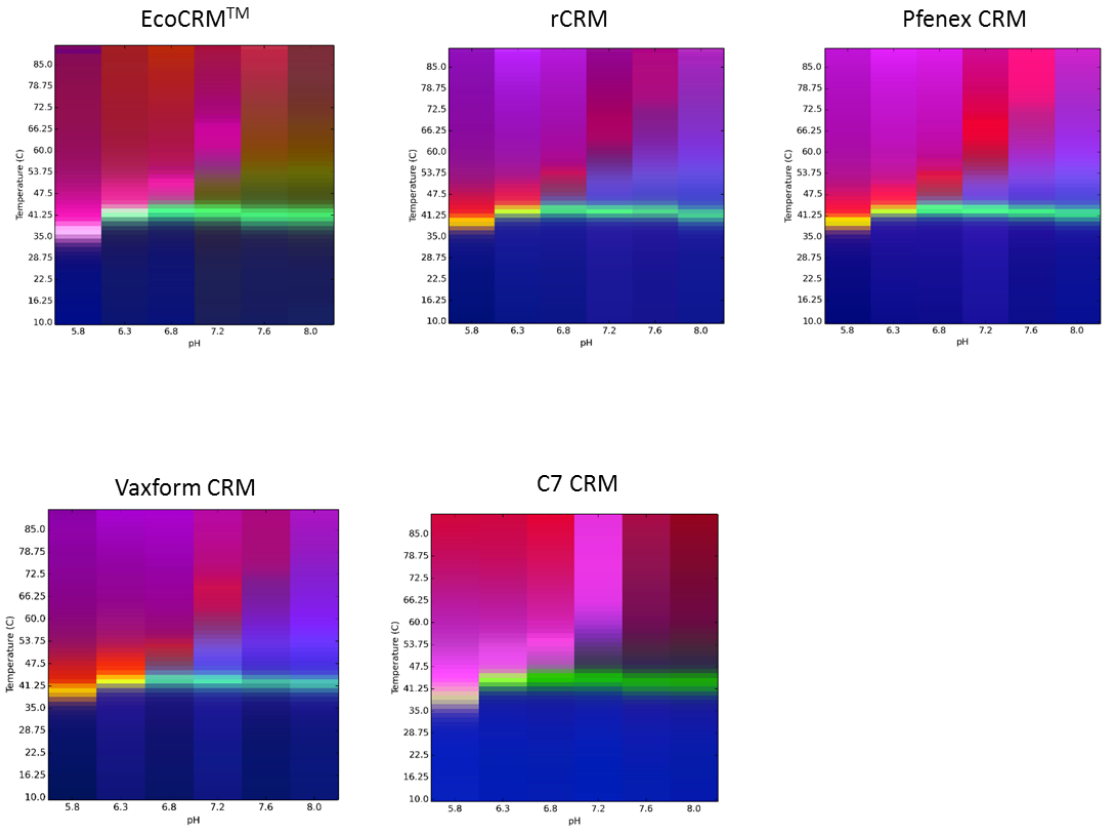

Supplemental Figure 5.6. Empirical phase diagram of each CRM_{197} protein in PBS buffer as a function of pH (5.8, 6.3, 6.8, 7.2, 7.6, and 8.0) and temperature (10-90˚C) as measured by circular dichroism, intrinsic tryptophan fluorescence, differential scanning calorimetry, and static light scattering.

5.5 References

1. Grabenstein JD, Klugman KP 2012. A century of pneumococcal vaccination research in humans. Clin Microbiol Infect 18 Suppl 5:15-24.

2. Strugnell R, Zepp F, Cunningham AL, Tantawhichien T. 2011. Understanding Modern Vaccines Perspectives in Vaccinology Vaccine Antigens, ed.

3. Shinefield HR 2010. Overview of the development and current use of CRM(197) conjugate vaccines for pediatric use. Vaccine 28(27):4335-4339.

4. Hickey JM, Sahni N, Toth RTt, Kumru OS, Joshi SB, Middaugh CR, Volkin DB 2016. Challenges and opportunities of using liquid chromatography and mass spectrometry methods to develop complex vaccine antigens as pharmaceutical dosage forms. J Chromatogr B Analyt Technol Biomed Life Sci 1032:23-38.

5. Brady C, Killeen K, Taylor W, Patkar A, Lees A 2012. Carrier Protein Outsourcing: A New Paradigm for Rapidly Translating Novel Conjugate Vaccines into the Clinic. BioProcess International 10(10):50-55.

6. Levine OS, Bloom DE, Cherian T, de Quadros C, Sow S, Wecker J, Duclos P, Greenwood B 2011. The future of immunisation policy, implementation, and financing. Lancet 378(9789):439-448.

7. Knuf M, Kowalzik F, Kieninger D 2011. Comparative effects of carrier proteins on vaccine-induced immune response. Vaccine 29(31):4881-4890.

8. Goffin P, Dewerchin M, De Rop P, Blais N, Dehottay P 2017. High-yield production of recombinant CRM197, a non-toxic mutant of diphtheria toxin, in the periplasm of Escherichia coli. Biotechnol J.

9. Zhou J, Petracca R 1999. Secretory expression of recombinant diphtheria toxin mutants in B. Subtilis. J Tongji Med Univ 19(4):253-256.

10. Broker M, Costantino P, DeTora L, McIntosh ED, Rappuoli R 2011. Biochemical and biological characteristics of cross-reacting material 197 CRM197, a non-toxic mutant of diphtheria toxin: use as a conjugation protein in vaccines and other potential clinical applications. Biologicals 39(4):195-204.

11. Malito E, Bursulaya B, Chen C, Lo Surdo P, Picchianti M, Balducci E, Biancucci M, Brock A, Berti F, Bottomley MJ, Nissum M, Costantino P, Rappuoli R, Spraggon G 2012. Structural basis for lack of toxicity of the diphtheria toxin mutant CRM197. Proc Natl Acad Sci U S A 109(14):5229-5234.

12. Chen RT, Shimabukuro TT, Martin DB, Zuber PLF, Weibel DM, Sturkenboom M 2015. Enhancing vaccine safety capacity globally: a lifecycle perspective. Vaccine 33(0 4):D46-D54.

13. Broker M, Berti F, Costantino P 2016. Factors contributing to the immunogenicity of meningococcal conjugate vaccines. Hum Vaccin Immunother 12(7):1808-1824.

14. Lockyer K, Gao F, Derrick JP, Bolgiano B 2015. Structural correlates of carrier protein recognition in tetanus toxoid-conjugated bacterial polysaccharide vaccines. Vaccine 33(11):1345-1352.

15. Rustandi RR, Peklansky B, Anderson CL 2014. Use of imaged capillary isoelectric focusing technique in development of diphtheria toxin mutant CRM197. Electrophoresis 35(7):1065-1071.

16. Loughney JW Quantitation of CRM197 using imaged capillary isoelectric focusing with fluorescence detection and capillary Western. Analytical biochemistry 534:19-23.

17. Gibson TJ, McCarty K, McFadyen IJ, Cash E, Dalmonte P, Hinds KD, Dinerman AA, Alvarez JC, Volkin DB 2011. Application of a high-throughput screening procedure with PEG-induced precipitation to compare relative protein solubility during formulation development with IgG1 monoclonal antibodies. J Pharm Sci 100(3):1009-1021.

18. Toprani VM, Joshi SB, Kueltzo LA, Schwartz RM, Middaugh CR, Volkin DB 2016. A Micro-Polyethylene Glycol Precipitation Assay as a Relative Solubility Screening Tool for Monoclonal Antibody Design and Formulation Development. J Pharm Sci 105(8):2319-2327.

19. Maddux NR, Joshi SB, Volkin DB, Ralston JP, Middaugh CR 2011. Multidimensional methods for the formulation of biopharmaceuticals and vaccines. J Pharm Sci 100(10):4171-4197.

20. Kim JH, Iyer V, Joshi SB, Volkin DB, Middaugh CR 2012. Improved data visualization techniques for analyzing macromolecule structural changes. Protein Sci 21(10):1540-1553.

21. Giraldo J, Vivas NM, Vila E, Badia A 2002. Assessing the (a)symmetry of concentration-effect curves: empirical versus mechanistic models. Pharmacol Ther 95(1):21-45.

22. Natarajan C, Jiang X, Fago A, Weber RE, Moriyama H, Storz JF 2011. Expression and purification of recombinant hemoglobin in Escherichia coli. PLoS One 6(5):e20176.

23. Liao YD, Jeng JC, Wang CF, Wang SC, Chang ST 2004. Removal of N-terminal methionine from recombinant proteins by engineered E. coli methionine aminopeptidase. Protein Sci 13(7):1802-1810.

24. Costantino HR, Carrasquillo KG, Cordero RA, Mumenthaler M, Hsu CC, Griebenow K 1998. Effect of excipients on the stability and structure of lyophilized recombinant human growth hormone. J Pharm Sci 87(11):1412-1420.

25. Zhang Q, Ames JM, Smith RD, Baynes JW, Metz TO 2009. A perspective on the Maillard reaction and the analysis of protein glycation by mass spectrometry: probing the pathogenesis of chronic disease. J Proteome Res 8(2):754-769.

26. Toprani VM, Hickey JM, Sahni N, Toth RTt, Robertson GA, Middaugh CR, Joshi SB, Volkin DB 2017. Structural characterization and physicochemical stability profile of a double mutant heat labile toxin (dmLT) protein based adjuvant. J Pharm Sci.

27. Alsenaidy MA, Jain NK, Kim JH, Middaugh CR, Volkin DB 2014. Protein comparability assessments and potential applicability of high throughput biophysical methods and data visualization tools to compare physical stability profiles. Frontiers in Pharmacology 5:39.

28. More AS, Toprani VM, Okbazghi SZ, Kim JH, Joshi SB, Middaugh CR, Tolbert TJ, Volkin DB 2016. Correlating the Impact of Well-Defined Oligosaccharide Structures on Physical Stability Profiles of IgG1-Fc Glycoforms. Journal of Pharmaceutical Sciences 105(2):588-601.

29. Kim JH, Joshi SB, Tolbert TJ, Middaugh CR, Volkin DB, Smalter Hall A 2016. Biosimilarity Assessments of Model IgG1-Fc Glycoforms Using a Machine Learning Approach. Journal of Pharmaceutical Sciences 105(2):602-612.

30. Leka O, Vallese F, Pirazzini M, Berto P, Montecucco C, Zanotti G 2014. Diphtheria toxin conformational switching at acidic pH. FEBS Journal 281(9):2115-2122.

31. Federici M, Lubiniecki A, Manikwar P, Volkin DB 2013. Analytical lessons learned from selected therapeutic protein drug comparability studies. Biologicals 41(3):131-147.

32. Lees A, Oganesyan N, Krauss I, Nguyen D. EcoCRM^{TM}: Affordable CRM_{197} Vaccine Carrier Protein Poster Presented at: Protein Engineering Summit, Boston, MA, U.S.A., May 1 2017.

Chapter 6 Summary, Conclusions and Future Work

6.1 Overview

The clinical development of a vaccine candidate includes several activities such as preclinical animal and human clinical testing, CMC (Chemistry, Manufacturing and Control) development and regulatory filings[1,2]. All of these activities result in a long, complex and costly process with an overall low chance of getting a regulatory approval[3,4]. Vaccines are considered the most complex products of biopharmaceutical industry (e.g., macromolecular antigens, adjuvants, excipients) and are among the most difficult to stabilize[5]. Proteins are structurally complex with fragile structures, and protein based vaccines are very sensitive to environmental stresses that can lead to physical or chemical instabilities which in turn can affect potency and efficacy[6]. Thus, it is critical to ensure that the protein maintains its stability during all stages of CMC development including manufacturing, long term storage, transportation and eventual administration to patients[5,7]. There is an ongoing need for better and more sensitive analytical tools and robust formulation development approaches to monitor a protein's key structural and biological properties to ensure the stability and potency of the final drug product over the desired shelf life[8]. In an effort to better understand the interrelationships between physicochemical stability of a protein vaccine with critical functional attributes (such as potency), key focus areas of this thesis work included the development of analytical stability-indicating tools and formulation development strategies for different protein-based subunit vaccine candidates.

This dissertation further demonstrated the importance of developing analytics and its utility in characterizing the structural integrity and stability profiles for dmLT, a protein-based adjuvant (Chapter 3) and three equine encephalitis virus-like particle (EEV VLPs) vaccine antigens (Chapter 4). Furthermore, analytical stability indicating methods were developed and used to identify stabilizing excipients for a development of stable candidate formulations for the bulk

storage of VLPs antigens and dmLT adjuvant candidate. Additionally, a micro-PEG precipitation assay was developed to determine the apparent solubility of multiple proteins using less than a milligram of material (Chapter 2) and also used in determining the apparent solubility profiles of CRM_{197} molecules (Chapter 5). In addition to analytical characterization and formulation development, comparability assessment exercises are also essential to determine the structural integrity and stability of a protein containing vaccine candidate due to both product and process related manufacturing changes[9,10]. An extensive set of analytical tools was utilized to compare the physicochemical properties, physical stability profiles and *in vitro* antigenic properties of five recombinant CRM_{197} molecules from different expression systems and manufacturers (Chapter 5).

6.2 Chapter summaries and future work

6.2.1 Chapter 2

A micro PEG assay was successfully developed to estimate the apparent solubility of various mAbs against HIV-1 virus. The optimized assay utilizes only about 1 mg of protein, as developed using the VRC01-WT mAb including determining the assay's accuracy and precision for various readouts. Relative protein apparent solubility profiles of a series of broadly neutralizing mAbs to HIV-1 envelope were determined using micro PEG assay including evaluating the curve shape (%PEG vs. protein concentrations), %PEG midpoint numbers, and extrapolated apparent solubility values.

The PEG-assay was then successfully utilized to a) rank ordering via evaluation of PEG_{curves}, PEG_{midpt}, and apparent solubility values of different mAbs compared to VRC01-WT and b) screen numerous formulation conditions (buffers, salt, pH and arginine) to evaluate the

relative protein apparent solubility profiles of VRC01-WT. The PEG_{midpt} values were found to decrease as the solution pH increased over the range of pH 5.0 - 8.0 using phosphate buffer. The apparent solubility values also decrease as the pH increased from 5.0 to 8.0. The relative apparent solubility profiles of VRC01-WT mAb varied under different formulation conditions. Both salt and arginine increased the relative apparent solubility of VRC01-WT as is evident by their effect on the PEG_{curves}, PEG_{midpt} and apparent solubility values. A final optimization of the micro-PEG assay established that protein amounts as low as 0.1-0.2 mg can be used. Thus, this high throughput assay developed in this study can be very useful in early candidate selection and assessing apparent solubility of mAbs where only limited amounts of material are available. Further, it can also be used to screen various solution conditions as a part of preformulation studies.

As part of future work, experiments to study the effect of different combinations and concentrations of commonly used pharmaceutical excipients (such as polysorbate-80 and sucrose) in presence of PEG and their effect on the apparent solubility of various mAbs and/or model proteins can be explored. Such studies would provide a data base of excipient effects on protein solubility and correlations to other physical properties (such as protein-protein interaction) could be established from a formulation development point of view. It would also be interesting to examine the utility of micro-PEG assay to determine the relative apparent solubility of combination protein drug products (e.g., multiple mAbs coformulated). This work will help in better understanding the utility of this tool during protein formulation development and its applicability to study novel combination therapeutics.

6.2.2 Chapter 3

This chapter employed a wide variety of analytical techniques to comprehensively evaluate the physicochemical properties of a lyophilized sample of dmLT (a protein based adjuvant) and develop a stable frozen liquid formulation for its bulk storage and subsequent use with a wide variety of vaccine antigens in a drug product. LC-MS peptide mapping confirmed with primary amino acid sequence of the protein and a glycated Lys84 residue was identified as a post- translational modification. A combination of size analysis by SV-AUC and HIC determinations showed the dmLT sample consists of a mixture of free B chain and AB_5 complex. The physicochemical degradation pathways of dmLT included protein aggregation, glycation and oxidation By identifying the physicochemical degradation pathways of dmLT using newly developed stability-indicating analytical methods, a more stable candidate bulk formulation of dmLT was developed that protected dmLT against conformational destabilization, freeze-thaw stress, aggregation/particle formation and chemical degradation. By developing a new frozen liquid stable bulk formulation, lyophilization and reconstitution of dmLT for use in preclinical and clinical studies will no longer be required. Removing the lyophilization unit operation should not only reduce costs, but also simplify future patient administration procedures with dmLT adjuvant. HIC was able to separate out free B chain from AB_5 complex and can potentially be used in the future as a process control and/or QC assay for dmLT.

As a part of future work, the isolation of degradants (e.g., forced oxidation or deamidation products) and determining their potency as an adjuvant will be useful to identify CMC challenges and potential CQA's of dmLT. For further pharmaceutical development of dmLT adjuvant stored in the candidate bulk formulation, compatibility testing with different vaccine antigens in a final drug product, and finally immunogenicity studies to evaluate adjuvant

activity will be needed. Another part of future work includes analytical comparability studies of physicochemical properties of two dmLT molecules made by different host organisms using the analytical stability indicating assays developed from this work. For such a study, freeze-thaw stability of dmLT at two protein concentrations (1 and 10 mg/mL) and real-time/accelerated stability of the same samples at different temperatures (-80,-20, 4 and 37 ^{o}C) could be evaluated. Furthermore the storage stability comparisons of dmLT material from different host systems at 1 mg/mL and stored at 4, 15, 25, 30, 37 and 45˚C will be executed to develop Arrhenius plot. Such plots will be useful to predict the degradation rates at storage temperatures and estimate the shelf life of the protein.

6.2.3 Chapter 4

Chapter 4 of this dissertation examined the structural integrity of three equine encephalitis virus-like particles (VLP) based vaccine candidates (EEE, WEE and VEE) using various biophysical methods. Initial characterization studies showed the VLPs were uniform in size, ~70 nm and contained some nucleic acid impurities. The physical stability profile of the three VLPs was assessed over a wide range of pH (6.5-8.5 with 0.5 unit increments) and temperature conditions (from 10°C-90°C with 2.5°C increments). We observed that the physical stability of EEE and WEE VLPs was higher than VEE VLP. Various stabilizing excipients were identified for developing six monovalent candidate bulk formulations. The final candidate formulation showed a good maintenance of stability at all storage stability conditions except when stored at minus 20^{o}C. Both the monovalent and trivalent VLPs formulated in the candidate formulation were also found to be stable and compatible with Alhydrogel® adjuvant, and this will enable future pharmaceutical drug product development of the vaccine using common formulation conditions.

For future work, some additional steps or improvements to the existing steps during the downstream processing of these VLPs can be implemented to remove the nucleic acid impurity from the VLPs. The possible ways include adding DNAase and RNAase enzymes during purification or using ion exchange chromatography to remove the nucleic acids. Additionally, by correlating the physicochemical data from this work with immunological potency assays to monitor key protective epitopes (e.g., *in vitro* binding or animal potency assays); a structure-function relationship can be established. Such studies will help to identify CQA's of the three VLPs and help in better understanding of product and processes parameters as these VLPs further advance into clinical development. Furthermore, long term storage stability studies of both the adjuvanted monovalent and trivalent drug products along with immunogenicity studies in animal models should be performed.

6.2.4 Chapter 5

In this chapter, an analytical comparison of recombinant CRM_{197} expressed in the natural host source (*C. diptheriae*) as well as in non-natural sources (i.e., *E. coli* and *P. fluorescens*) was executed. A wide variety of analytical techniques were employed to: analytically compare the physicochemical properties of the five CRM_{197} molecules; evaluate the relative solubility of the five CRM_{197} molecules using polyethylene glycol (PEG) and compare the physical stability profile of each CRM molecule as a function of pH and temperature using data visualization tools (Empirical Phase Diagram (EPD) and Radar Chart). Finally, *in vitro* antigenic reactivity of each CRM_{197} molecule were assessed through two methods, ELISA containing polyclonal anti-CRM antibodies; and bio-layer interferometry measuring association/dissociation rates with five monoclonal anti-CRM antibodies.

Overall, this work indicated that recombinant CRM_{197} molecules expressed in non-natural systems were very similar (if not better) to those expressed in the natural host system in terms of primary sequence, higher-order structural conformation, apparent solubility, physical stability profile as a function of pH and temperature, as well as *in vitro* immune-reactivity. Therefore, the analytical similarity between the tested CRM_{197} molecules suggest that recombinant CRM_{197} expressed in the non-natural sources (i.e., *E. coli* and *P. fluorescens*) could be used instead of CRM_{197} expressed in the natural host (*C. diphtheria*) to develop lost cost CRM bulk protein and eventually low-cost conjugate vaccines.

In terms of future work, these physicochemical assays could complement standard QC and potency assays and should be useful for future formulation development work, comparability assessments, stability analyses, and process validation studies (e.g., consistency of manufacturing). Future analytical comparison of these five CRMs from different manufacturers and expression systems should focus on measuring the extent of polysaccharide conjugation with each protein. Furthermore, the immunological activity of conjugate vaccines composed of these CRM_{197} proteins from these different sources should be tested in an animal model to evaluate if the polysaccharide-carrier protein conjugates using CRM_{197} from different sources are similar *in vivo*.

6.3 References

1. Singh M, Srivastava IK, Srivastava IK. 2011. Development of Vaccines: From Discovery to Clinical Testing. ed., Hoboken, UNITED STATES: Wiley.

2. Han S 2015. Clinical vaccine development. Clinical and Experimental Vaccine Research 4(1):46-53.

3. Struck M-M 1996. Vaccine R&D success rates and development times. Nature Biotechnology 14:591.

4. Pronker ES, Weenen TC, Commandeur H, Claassen EHJHM, Osterhaus ADME 2013. Risk in Vaccine Research and Development Quantified. PloS one 8(3):e57755.

5. Ohtake S, Lechuga-Ballesteros D, Truong-Le V, Patzer EJ, P. Wen E, Ellis R, S. Pujar N. 2014. Strategies for Heat-Stable Vaccines. Vaccine Development and Manufacturing, ed.: John Wiley & Sons, Inc. p 287-318.

6. Brandau DT, Jones LS, Wiethoff CM, Rexroad J, Middaugh CR 2003. Thermal stability of vaccines. J Pharm Sci 92(2):218-231.

7. Kumru OS, Joshi SB, Smith DE, Middaugh CR, Prusik T, Volkin DB 2014. Vaccine instability in the cold chain: mechanisms, analysis and formulation strategies. Biologicals 42(5):237-259.

8. Dey AK, Malyala P, Singh M 2014. Physicochemical and functional characterization of vaccine antigens and adjuvants. Expert review of vaccines 13(5):671-685.

9. Federici M, Lubiniecki A, Manikwar P, Volkin DB 2013. Analytical lessons learned from selected therapeutic protein drug comparability studies. Biologicals 41(3):131-147.

10. Lubiniecki A, Volkin DB, Federici M, Bond MD, Nedved ML, Hendricks L, Mehndiratta P, Bruner M, Burman S, DalMonte P, Kline J, Ni A, Panek ME, Pikounis B, Powers G, Vafa O, Siegel R 2011. Comparability assessments of process and product changes made during development of two different monoclonal antibodies. Biologicals 39(1):9-22.